THERMODYNAMIC ANALYSIS OF INTEGRATED RENEWABLE ENERGY

SYSTEMS FOR SUSTAINABLE BUILDING OPERATION

by

Emaduddin Iqbal

A Thesis Presented to the Faculty of the
American University of Sharjah
College of Engineering
in Partial Fulfillment
of the Requirements
for the Degree of

Master of Science in
Mechanical Engineering

Sharjah, United Arab Emirates

September 2014

Approval Signatures

We, the undersigned, approve the Master's Thesis of Emaduddin Iqbal.

Thesis Title: Thermodynamic Analysis of Integrated Renewable Energy Systems for Sustainable Building Operation

Signature   **Date of Signature**

_____   _____
Dr. Mohamed Gadalla
Professor, Department of Mechanical Engineering
Thesis Advisor

_____   _____
Dr. Essam Wahba
Associate Professor, Department of Mechanical Engineering
Thesis Committee Member

_____   _____
Dr. Zarook M. Shareefdeen
Associate Professor, Department of Chemical Engineering
Thesis Committee Member

_____   _____
Dr. Essam Wahba
Interim Head, Department of Mechanical Engineering

_____   _____
Dr. Mohamed El-Tarhuni
Associate Dean, College of Engineering

_____   _____
Dr. Leland Blank
Dean, College of Engineering

_____   _____
Dr. Khaled Assaleh
Director of Graduate Studies

Acknowledgements

It is with deep gratitude that I acknowledge the help and support of my thesis advisor Professor Mohamed Gadalla, whose guidance and feedback was vital to this accomplishment. I would like to thank him for his patience and understanding throughout the course of my study.

I would also like to express my gratitude to my thesis committee members Dr. Essam M. Wahba and Dr. Zarook M. Shareefdeen for reviewing my thesis and providing useful feedback on the same.

Furthermore, I would like to thank my friends and colleagues for their constant encouragement and assistance which helped me to complete my thesis.

I am particularly grateful to Dr. Tahir Ratlamwala and Mr. Taha Shafeeq for their valuable inputs to this work.

And lastly, I would like to express my utmost appreciation and gratitude to my parents, and my sister, for their unlimited support, guidance and belief in me. Without them, this undertaking would have been impossible at the least.

Dedication

To my Lord, Allah, who made this happen, and the people I love, my parents and sister, who are everything to me, my grandparents and relatives, who helped make me who I am today, my friends, who are like family to me, and my late best friend, Ebrahim R. P., who I miss sorely in taking on the world.

Abstract

Increasing demands for energy, depleting hydrocarbon reserves, and accelerated climate change drive the need to look for alternative sources of energy. The residential housing sector is one of the main consumers of electrical power worldwide. This thesis aims to contribute to future conservation strategies by focusing on the feasibility and analysis of the integration of renewable energy systems, namely solar and wind power, with cooling and storage equipment, into tri-generation systems. These systems are to provide uninterrupted electrical power, heat and air-conditioning to residential units (villas) in the U.A.E., thus ensuring sustainable, grid-independent operation of the villas. Individual sub-systems are first modeled, verified and analyzed quantitatively and qualitatively through energetic and exergetic analyses respectively, after which three integrated system configurations are also analyzed and present worth analysis is conducted to determine which integrated system is most economical. It must be noted that results presented in this thesis cannot be generalized to all systems as they are for specific operating conditions and for the meteorological conditions of the chosen site in the U.A.E. From the results it can be seen that the integrated PV/T-WT system performs best during March when wind speeds are highest, the integrated PTSC-TEAS system performs better than the PTSC-DEAS system for daytime cooling, and the highest energetic and exergetic COPs, 1.77 and 1.7 respectively, are recorded for the combined PTSC-TEAS system during July when average energetic efficiency for the combined PV/T-CGVCS system is also seen to be highest. The CGVCS is found to be a better thermal storage system than the HTS, its highest COP is obtained for a mass ratio of 2.5 and a maximum mass of 1980.2 kgs of clathrate is required for daily nighttime cooling during August. Lastly, the most feasible overall integrated option studied allows the villas to be completely independent of the grid, has maximum energetic and exergetic efficiencies of 0.38 and 0.201, and offers savings of AED 168,657 over the lifetime of the integrated system. The methods used and the results presented shall prove useful for researchers and decision-makers looking to investigate sustainable building operation options in hot and humid climates.

Search terms: Absorption, PTSC, PV/T, wind turbine, clathrate, COP, exergy.

Table of Contents

List of Figures

11

13

List of Tables

Nomenclature

A	Area, m^2
A_c	Area of PTSC glass cover, m^2
b	Breadth of the PV module, m
Col_r	Number of PTSC collector rows
$C_{p,r,i}$	Specific heat capacity of water at inlet to receiver, $J.kg^{-1}K^{-1}$
$C_{p,r,o}$	Specific heat capacity of water at outlet of receiver, $J.kg^{-1}K^{-1}$
D	Diameter, m
$D_{c,o}$	Glass cover outer diameter, m
$D_{r,i}$	Receiver inner diameter, m
$D_{r,o}$	Receiver outer diameter, m
Eff	Effectiveness, dimensionless
F	Solar heat gain coefficient, dimensionless
F_1	PTSC collector efficiency factor, dimensionless
F_r	Heat removal factor of PTSC, dimensionless
G_b	Global solar irradiation, $W.m^{-2}$
H	Height, m
h_{ba}	Heat transfer coefficient from black surface of PV to air, $W.m^{-2}.K^{-1}$
$h_{c,ca}$	Convection heat coefficient between PTSC cover & ambient, $W.m^{-2}.K^{-1}$
$h_{c,r,in}$	Convective heat transfer coefficient, PTSC receiver inlet, $W.m^{-2}.K^{-1}$
h_i	Combined heat transfer coefficient for inner window pane, $W.m^{-2}.K^{-1}$
$h_{p,2}$	Penalty factor due to the presence of the black surface below PV, dimensionless
h_o	Combined heat transfer coefficient for outer window pane, $W.m^{-2}.K^{-1}$
$h_{r,ca}$	Radiation heat coefficient between PTSC cover & ambient, $W.m^{-2}.K^{-1}$
$h_{r,cr}$	Radiation heat coefficient between PTSC cover & receiver, $W.m^{-2}.K^{-1}$
h_s	Heat transfer coefficient of space between two window panes, $W.m^{-2}.K^{-1}$
h_t	Heat transfer coefficient from the bottom surface of PV to air, through the glass, $W.m^{-2}.K^{-1}$

I	Solar irradiance, $W.m^{-2}$
k	Conductivity of wall material, $W.m^{-1}.K^{-1}$
k_{air}	Thermal conductivity of air at T_0, $W.m^{-1}.K^{-1}$
K	Heat transfer coefficient, $W.K^{-1}$
k_r	Receiver tube thermal conductivity, $W.m^{-1}.K^{-1}$
L	Length, m
$\dot{m}$	Mass flow rate, $kg.s^{-1}$
Nom	Number of PV modules
Nu	Nusselt number, dimensionless
P	Pressure, kPa
$\dot{P}$	Power, kW
$\dot{Q}$	Heat transfer rate, kW
R	Air Gas Constant, $kJ.kg^{-1}.K^{-1}$
Re	Reynold's number, dimensionless
S	Solar radiation absorbed by the receiver, $W.m^{-2}$
T	Temperature, ^0C, K or ^oF
T_c	Glass cover temperature, ^0C
U	Conductance of villa wall material, $W.m^{-2}.K^{-1}$
U_b	Overall heat transfer coefficient between the bottom of the PV panel to the ambient, $W.m^{-2}.K^{-1}$
U_L	Overall heat loss coefficient of PTSC, $W.m^{-2}.K^{-1}$
U_0	Overall heat transfer coefficient of PTSC, $W.m^{-2}.K^{-1}$
U_t	Overall heat transfer coefficient from solar cell to the ambient through the PV glass cover, $W.m^{-2}.K^{-1}$
V	Velocity, $m.s^{-1}$
V_w	Wind velocity, $m.s^{-1}$
w	Width of PTSC collector aperture, m
$\dot{W}$	Rate of work, kW
$\dot{X}$	Rate of exergy, kW

Abbreviations

AC	Alternating Current
ADWEC	Abu Dhabi Water and Electricity Company
AHU	Air Handling Unit
ASHRAE	American Society of Heating, Refrigerating, and Air-conditioning Engineers
CGVCS	Clathrate Generation Vapor Compression System
CHS	Clathrate Hydrate Slurry
COP	Coefficient Of Performance
C.S.E.M.	Centre Suisse d' Electronique et de Microtechnique
DC	Direct Current
G.E.	General Electric
HCFC	Hydro-Chloro-Fluoro-Carbons
HFC	Hydro-Fluoro-Carbon
H.G.	High Generator
H.S.X.	High Solution Heat Exchanger
HTF	Heat Transfer Fluid
HTS	Hot Thermocline Storage
HVAC	Heating Ventilation and Air-Conditioning
HVDC	High Voltage Direct Current
LiBr	Lithium Bromide
L.G.	Low Generator
LHSCS	Latent Heat Storage Clathrate System
LHTESS	Latent Heat Thermal Energy Storage Systems
MIG	Million Gallons
M.G.	Medium Generator
MPCMS	Microencapsulated Phase Change Material Slurry
M.R.	Mass ratio of clathrate, i.e. ratio of water to refrigerant in clathrate
MRF	Maximum Residence Factor
M.S.X	Medium Solution Heat Exchanger
PCM	Phase Change Material
PCME	Phase Change Material Emulsions

PCS	Phase Change material Slurry
PTSC	Parabolic Trough Solar Collector
PV	Photo-Voltaic
PV/T	Photo-Voltaic/Thermal
R&D	Research and Development
R.E.	Renewable Energy
R.E.S.	Renewable Energy Systems
SC	Shading coefficient
s.h.c.	Specific heat capacity
S.H.G.F.	Solar Heat Gain Factor
SPCMS	Shape-stabilized PCM Slurries
TEAS	Triple Effect Absorption System
TES	Thermal Energy Storage
TR	Tons of Refrigeration
TW	Terawatts
VCC	Vapor Compression Cycle
WFES	World Future Energy Summit

Subscripts:

0	Atmospheric/ambient
1	Inlet, initial
2	Outlet, final
a	Air, ambient
abs	Absorber
ap	Aperture
appl	Appliances
av	Average
atm	Atmospheric
b	Black surface
bs	Back surface of PV module
c	Condenser, cooling
cell	Solar cell

cond	Conduction
cvr	PTSC glass cover
d	Desorber/generator
e	Evaporator
el	Electric
EN	Energetic
EX	Exergetic
exch	Air exchanges by infiltration
F	Degrees Fahrenheit
g	Generator/desorber
HTF	Heat Transfer Fluid
HTG	High Temperature Generator
i	Inlet
inf	Infiltration
K	Kinetic
ℓ	Low
m	Medium
mph	Miles per hour
o	Outlet
ov	Overall
p	Pump
Ph	Physical
Ppl	People
PV	Photovoltaic
r	PTSC receiver
Re	Reynold's number
ref	Reference
s	Isentropic state
shx	Solution heat exchanger
sol	Solar
th	Thermal
w	Wind

w.ch	Wind chill
win	Window
WT	Wind Turbine

Greek Letters:

α	Absorptivity
β_c	PV solar cell packing factor
ϵ_{cv}	Glass cover emissivity/emittance
ϵ_r	Receiver emissivity
η	Efficiency
η_r	Receiver efficiency
η_{II}	Second law efficiency
ρ	Density, kg.m^{-3}
μ	Viscosity, N.s.m^{-2}
σ	Stefan-Boltzmann constant, W.m^{-2}.K^{-4}
τ_g	Transitivity of the PV glass cover

Chapter 1: Introduction

1.1   Problem Statement

Energy demands throughout the world are increasing on a daily basis. With dwindling natural resources such as coal and oil, and rising costs, both, in terms of prices and environmental footprint, it is imperative that a substitute be found to reduce our dependency on these limited fuels and find a green, sustainable and efficient alternative to meet the future needs of our carbon based-economies. Thus renewable energy sources play an important part in reducing this dependency, and solar and wind energy has been put into use to the same effect. Systems such as Parabolic Trough Solar Collectors (PTSCs) and Wind Turbines (WTs) that harness these abundant, free energies can be used in conjunction with existing systems or independently to power and cool our communities in an eco-friendly and efficient way.

In hot climates, a large fraction of the total energy consumption can be attributed to meeting space cooling requirements [1]. This fraction for Abu Dhabi, the capital of the United Arab Emirates (U.A.E), according to a study conducted as part of the Abu Dhabi Municipality's Energy Efficiency Program by Schneider Electric, a global specialist in energy management, amounts to 57.5 % for a typical building [2], as shown in Figure 1.

Given that most space cooling around the world is accomplished through the employment of compressor driven technologies, this is understandable since compressing gases consumes a lot of power. In order to alleviate these problems of diminishing natural resources and the carbon footprint associated with their rising generation and consumption, it makes ever more sense to use renewable energies to power and cool spaces efficiently so as to reduce both, our reliance on conventional sources of fuel, and the emissions associated with their consumption.

Companies and individuals who have realized this need and the potential benefits of implementing renewable energies for efficient power and cooling, have taken steps towards the advancement of this area.

Many systems such as those investigated in [3-9] have been developed that use renewable energy sources such as geothermal, solar and wind power to power

facilities, and use solar power or waste heat from turbines to drive heat driven technology such as absorption systems to cool and heat spaces [3, 10].
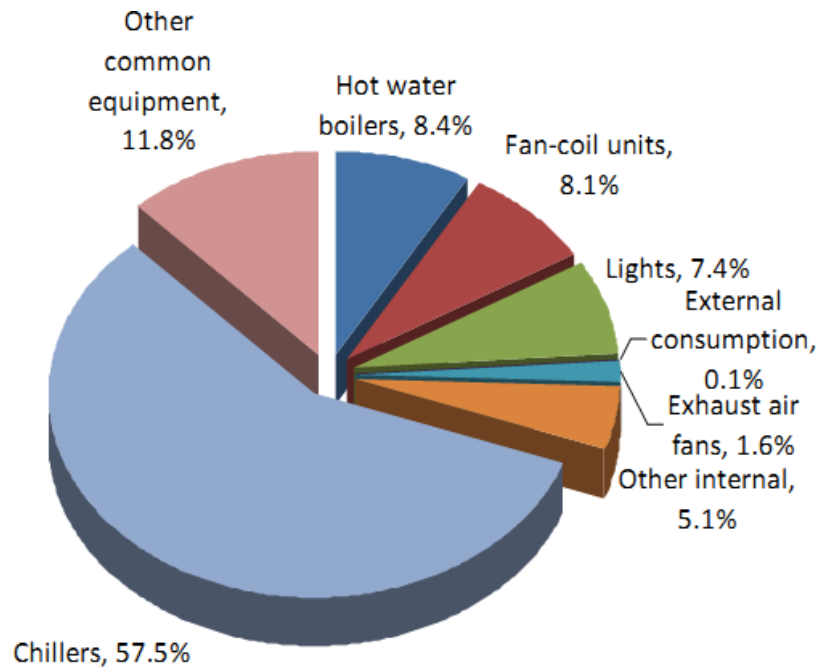
Figure 1: Electricity consumption for a typical consumer building, U.A.E. [2]

However, to date, most of the current integrated systems meant for supplying power and cooling to individual residential units are either too small to benefit from economies of scale due to prohibitive initial costs, or are not efficient enough to meet the requirements, particularly those of cooling in hot climates, completely. The Coefficient Of Performance (COP) is a quantity used to measure the performance of a heating or cooling system, and is defined as the ratio of the output of the system to its input.

For a cooling system, the output is the cooling produced, whereas the input could be whatever energy is provided to run the system. In an attempt to increase the COP of existing cooling systems [11], there has been plenty of research in the area of absorption systems driven by solar technology, with mostly double [12-16] and some triple effect systems [1, 17, 18] developed theoretically and by industry. However,

current absorption technology is still not good or feasible enough to compete with conventional vapor compression systems [19].

Double effect absorption systems have not been able to deliver COPs that are good enough to compete with vapor compression systems, although triple effect systems offer more promise. According to the literature review, very few studies have been conducted on integrating triple effect systems with thermal storage systems, solar technology and wind to provide a completely grid-independent system for domestic purposes. Moreover, none have been done on the integration of wind with solar to provide energy and cooling, with most existing literature [20-22] pertaining to hybrid technology involving Photo-Voltaics (PVs) and wind for power generation for various purposes.

This research focuses on developing a co-generation system that, using renewable energies, shall be able to satisfy the electricity and the Heating, Ventilation and Air Conditioning (HVAC) needs of a group of households, thus making them independent of the grid. It involves selecting technologies based on their performance characteristics and their environmental impact, and investigating and integrating them to develop hybrid systems for co-generation.

The hybrid systems investigated comprise a Parabolic Trough Solar Collector (PTSC), Solar Photo-Voltaic/Thermal (Solar PV/T), a Triple Effect Absorption Cooling System (TEACS), a Wind Turbine (WT), Phase Change Materials (PCMs) and a Vapor-Compression Cycle (VCC). Each of these systems shall be modeled independently at first and the models validated, after which the various models of the renewable energy systems shall be integrated with those of the absorption system.

The resulting system shall be integrated with each of the storage systems in turn and parametric studies shall be conducted on the overall systems. The economic and thermodynamic study of these systems and their performance shall offer an insight into the role of renewable energy technologies in contributing to an efficient, environmentally friendly and sustainable future for building operations.

The main objectives of this research are:
- To design the best system using an analytical model to meet the electricity and cooling needs of a group of households in hot climates

24

- Use only renewable energy technology to make the households standalone and thus independent of the grid.
- Use a storage system that will allow the households to run even in the absence of these renewable energy technologies.

- To develop a triple effect absorption chiller in an effort to make an improvement over the COP of current systems in the market.

- Integration of solar, wind and absorption technologies for trigeneration i.e. combined cooling-heating-power generation purposes and thus sustainable building operation. This work shall demonstrate the feasibility of this integration and shall pave the way for further studies in this area.

- To conduct a performance evaluation of the overall system
  - Conduct energetic and exergetic analyses
  - Evaluate individual subsystem performance using measures such as COP, energetic and exergetic efficiencies for various changes in parameters.
  - Evaluate steady state integrated system performance in a building at full load
  - Provide for appropriate storage systems to ensure uninterrupted operation.
  - Identify the most cost-effective integrated option.

1.2 Significance of the Research

Technology, life and society are driven by energy. Individuals and societies use energy resources as a means of obtaining wealth and improving living standards, and thus aiding their development. Furthermore, development that is sustainable requires, among other factors, access to energy resources. This makes energy a key aspect of discussions of sustainable development. Sustainable development has been defined in many ways, including "development that meets the needs of the present without compromising the ability of future generations to meet their own needs". It is affected by a number of factors, among them being the supply of energy resources. A secure supply of the latter is generally necessary but does not suffice societal development.

Sustainable societal development, however, requires a sustainable supply of energy resources, i.e. a secure supply that is readily and sustainably available in the long term at reasonable cost and that can be utilized for all required tasks without causing negative societal impacts. Effective and efficient utilization of energy

25

resources can also contribute to sustainable development [23]. The harnessing of renewable energy sources and their use in Renewable Energy Systems (R.E.S.) ensures such a secure supply of energy resources as is needed for societal development. Renewable Energy (R.E.) can be used to meet electricity and cooling needs of a society, and this concept has been explored in theory and practice before because of rising costs, both, in terms of fuel prices and the environmental footprint.

1.2.1 Global needs for renewable energy systems deployment

In May 2011, General Electric (G.E.), at the Alternative Energy, Utilities and Power Conference held in New York, projected that global electricity demand was set to double by 2030, and at current growth rates the world's population would stand at 8 billion. They believe that these statistics, along with the heightened security situation in many countries, were bringing about changing energy needs which in turn were driving new opportunities [24] for sustainable development.

Other prominent reasons for the global community to adopt R.E. follow [23, 25]. Their disproportionate reliance on certain energy resources is one such reason. Developed societies would be left crippled were there an interruption in the supply of energy from resources[23] such oil, gas and coal, all of which are being naturally exhausted. An example of this is the multi-day blackout across parts of Canada and the US in 2003 which resulted in loss of access to vital everyday facilities such as lighting, computers, elevators, HVAC and healthcare.

Secondly, the environmental impact of energy processes will have a deleterious effect on the future, causing environmental problems such as global climate change, acid precipitation, stratospheric ozone depletion, emissions of a wide range of pollutants including radioactive and toxic substances, and loss of forests and arable land[25, 26].

Third, R.E.S. deployment is still limited compared to the scale at which it can and should be employed. R.E. resources are plentiful and need to be cultivated. It is estimated that the world wind potential is on the order of 55 TeraWatts (TW). Therefore it can be concluded that, purely on a theoretical basis, and disregarding the mismatch between supply and demand, the wind alone could, theoretically, supply an amount of electrical energy equal to the present world electricity demand [27]. By

taking into consideration engineering practicality, reliability, applicability, economics and public acceptability, appropriate uses and means for harnessing sustainable and renewable energy resources can be found, which could promote interest in making R.E.S. more readily available to the end-user.

Fourth, energy pricing that does not reflect actual societal costs [23] such as the cost to the environment and people's health. Lastly, the global disparity in energy use with wealthy industrialized economies containing 25% of the world's population using 75% of the world's energy supply [23].

1.2.2 Global commitment to renewable energy.

But though distribution of conventional energy fuel consumption is disproportionate, nations lagging behind can catch up by investing in the capture and utilization of R.E. which is abundant and more or less evenly distributed around the globe.

Technologies used to acquire R.E. are established enough to provide complete security of energy supply [28]. Nations the world over, both in the developed world and otherwise, have realized their potential for exploiting R.E. and are implementing R.E.S.s to tap into these free, sustainable and environmentally friendly sources of energy.

Proof of this lies in the fact that over 40 countries have added R.E. targets in the last 5 years and 85 countries have renewable portfolio targets [24]. From countries in the far-east such as China, a leading wind-turbine producer, Australia, Egypt and Algeria in Africa in the southern hemisphere, Pakistan and India in south-east Asia, Turkey and Europe, to the US, Canada, Brazil and Argentina in the west, there are nations on nearly every continent that are taking part in the renewable energy revolution.

And they have ample reason to do so. Worldwide installed capacity for wind and solar installations has increased nearly 10 times in the past 12 years due to increased reliability and efficiency of technology. Moreover, the cost of wind and installations has dropped by 80% over the last 25 years while the cost of solar installations has dropped by 70% in just the past 3 years.

However, solar and wind energy market penetration still stands at 4%, showing there's significant potential for growth. Just a 1% increase in renewables penetration would mean 40,000 more wind turbines and 600 million more solar modules need to be installed [24]. By targeting the housing sector, R.E. targets can be achieved with far more ease and can have a significant impact on the world's fuel resources and its environment.

Another concern is that few countries have made the attempt to make R.E. available to individual consumers in terms of R.E.Ss and policy making, with even fewer making it possible for individual consumers in remote areas to become completely stand-alone and thus become grid-independent, though there's research suggesting that connecting to the grid in remote applications is often more impractical than installing R.E.S.s [29-35].

1.2.3 Industrial commitment to renewable energy.

Countries aren't the only ones experimenting with R.E. Many industrial giants, Siemens, G.E. and Schneider Electric to name a few, are leading this initiative already. G.E. alone has a fleet of over 17,000+ wind turbines with a total output of more than 27GW with an energy capture rate of more than 40%.

They have invested $250 million in solar R&D with more than 300 dedicated solar employees and 250 scientists, of which 100 are Ph.Ds, and have a 30MegaWatt (MW) pilot manufacturing line for solar panels[24]. The result is that they boast the highest recorded thin film solar efficiencies and have announced a 400 MW U.S. solar factory.

Siemens, another big player, is not only one of world's leading suppliers of on- and offshore wind power solutions, but also offers solutions in Small Hydro-Power and Tidal Power, as well as solar solutions ranging from components to turn-key solar power plants, with it set to acquire the solar thermal power company Solel Solar Systems Ltd, one of the world´s two leading suppliers of parabolic trough power plants with a combined delivered capacity of 750 MW [36].

Schneider Electric was recently awarded the prestigious Zayed Future Energy Prize for its work on clean-tech projects, which go beyond the company's core business. Such initiatives included their BipBop program which aims to develop

access to reliable, affordable and clean energy for poor countries with limited or no access to electricity.

Schneider Electric also participated in the Fifth World Future Energy Summit where they showcased their revolutionary 'SmartCity' range of critical infrastructure management tools which was a holistic software integrating 'SmartGrid' solutions for electricity demands and renewable energy with their other products [37].

The fact that such major institutions are investing heavily in R.E.S.s is evidence that the shift from a carbon-based economy to one reliant on R.E. resources is inevitable, and that any research in this area will only serve to preserve the future for coming generations.

1.2.4 Cost of R.E.S. and global deployment statistics.

The global community can only move away from conventional energy resources when R.E. offers a feasible solution, financially and otherwise, to its energy requirements. The implementation of R.E.S.s faces no hurdles when it comes to being environmentally friendly whereas it is a well-known fact that conventional carbon-based energy sources cause widespread environmental problems and are considered a primary source of global warming. What is less-known, is that when considering all the costs associated with conventional fuels, R.E. is cheaper.

Research has shown that the least expensive energy sources worldwide are currently wind and solar power. One kilowatt hour (kWh) of electricity produced by wind power stations on the coast or in the countryside currently costs an average of 0.07 euro (about $0.09).

Electricity produced from new solar energy plants in central and southern Europe costs a mere average of 0.14 euro per kWh whereas in Germany, the cost is about 0.18 euro when using rooftop solar panels, and in southern European solar parks it costs about 0.10 euro per kWh.

On the other hand, electricity produced from new coal plants costs twice as much as wind, and about the same as solar power. By 2020, wind and solar power will become the most economical way to generate power due to the combination of rising energy costs and innovation in the energy sector [26].

1.2.5   Necessity for energy management, the case of the U.A.E.

R.E. may offer a cheap source of energy, but the U.A.E. is rich in carbon-based resources and only recently saw reason to cultivate its R.E. potential when the growth of the U.A.E.'s demand for electricity started showing signs of overtaking the growth of supply. This growth of energy demand and consumption has been as result of a number of factors, prime amongst which is economic growth and the demographic pressures of a growing population. But equally important are other factors.

The U.A.E., being located close to the equator, has a hot and humid climate, and as mentioned before, 57.5 % of the total energy consumption can be attributed to meeting space cooling requirements for a typical building due to electricity driven – vapor-compression technologies [1]. Heavy subsidies on the domestic energy market encourage overconsumption of electricity, and the removal of these subsidies would see increases in cost of electricity for expatriates and local Emiratis of 40% and 80% respectively.

Domestic water use is also heavily subsidized, and together, the water and electricity subsidies play a major role in the growth of energy use [38]. The U.A.E. has limited water resources, and as a result as to resort to desalination to supply its residents with water for agricultural or consumption purposes. The desalination process is energy-intensive, with a power requirement standing at 1 MW for every million gallons (MIG) of water produced.

With the U.A.E.'s water demand set to increase at a rate of 5% per annum, similar increases in desalination capacity can be expected and hence supply needs to increase to match this demand. Moreover, this problem of demand-supply mismatch has already been encountered in certain parts of the U.A.E with the capital, Abu Dhabi, headed for a similar fate.

According to the Abu Dhabi Water and Electricity Company (ADWEC) Global Peak Electricity Demand Forecast for 2010-2020, the UAE is home to the world's fifth-largest gas reserves at 6.4 trillion cubic meters (Tcm), with Abu Dhabi, the capital, alone holding 5.62 Tcm.

However, as illustrated in Figures 2 and 3, the emirate has attained a point where demand for natural gas has exceeded production and continues its increase beyond the break-even point.
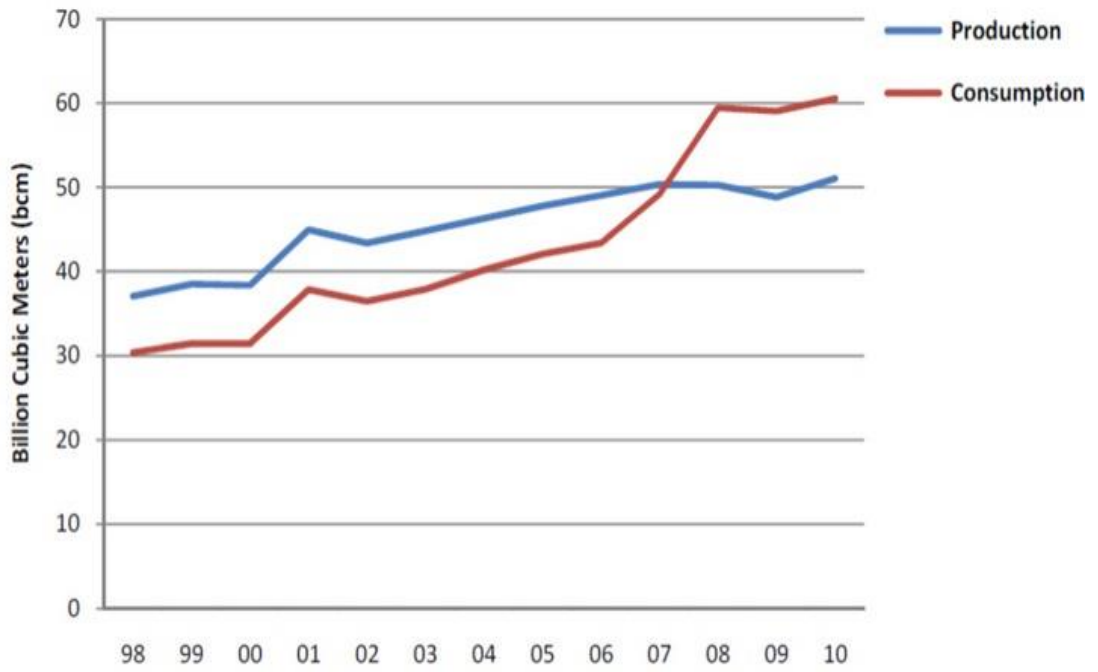
Figure 2: UAE Natural Gas Production and Consumption [38]
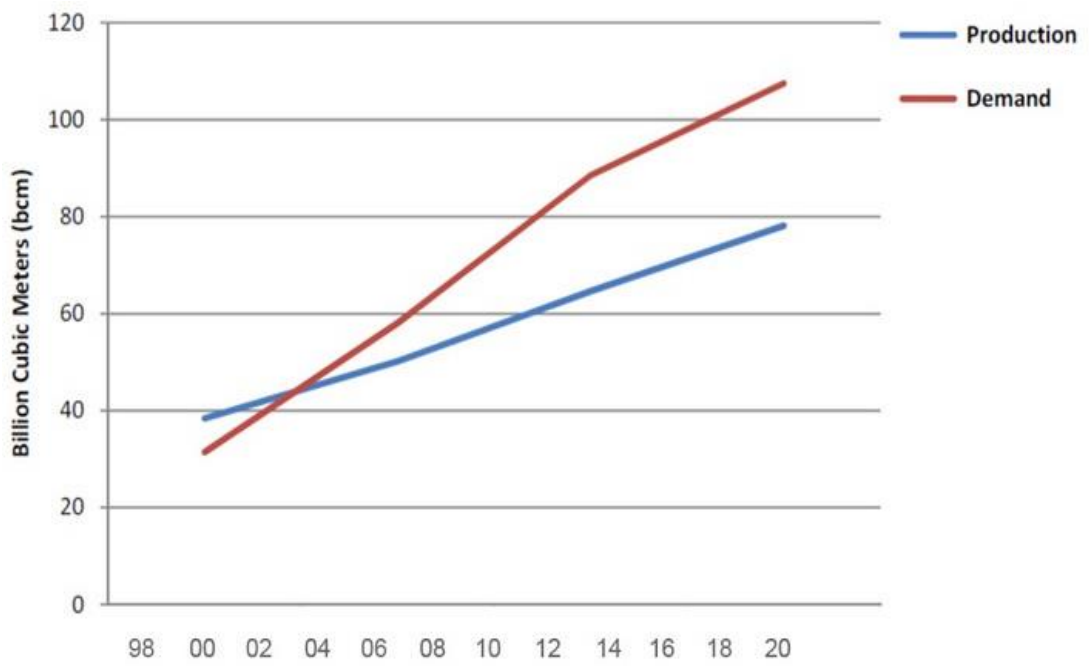
Figure 3: UAE Natural Gas Production and Demand 2000-2020 [38]
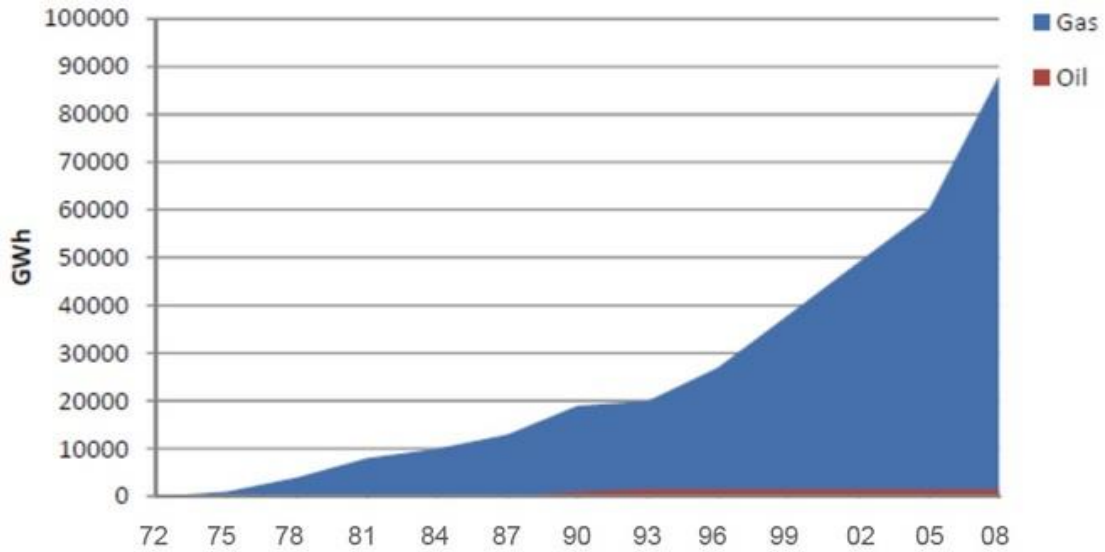
Figure 4: Total electricity production by generation type 1972-2008 [38]

Despite this, at current rates, Abu Dhabi, which uses mainly gas and steam turbines to generate electricity (see Figure 4), will not be able to provide enough natural gas to meet the 7%-10% yearly growth in electricity demand continuing up to 2020.

These reasons suggest that while there may be sufficient oil resources to meet future demand, the U.A.E., along with other gulf countries, may be facing an energy crisis due to its dependence on natural gas as its primary fuel to generate electricity. ADWEC has forecasted that Abu Dhabi alone will need to meet 28,188MW of electricity demand by 2020, whereas supplies of fuel are only adequate for 20,000-25,000 MW of power generation capacity by 2020. This means that a mere 71%-89% of electricity demand can be met [38].

Also, even if this demand can be met, there is the issue of environmental impact. In the U.A.E., per capita emissions of CO_2 rose from 26.44 tons/pop in 2005 to 32.19 in 2008, a growth rate of 7% being achieved per annum.

Though per capita emissions decreased by one percent to 31.97% in 2009 following the global economic downturn, at a national level, total CO_2 emissions were rising at an annual growth of 9% between 2005 and 2009, registering 147 million tons in 2009, 39% of which was attributed to the electricity and heat production sector.

These figures register among the highest worldwide, second only to Qatar, and are set for further increases in light of economic and energy development [39].

The Abu Dhabi government has noted these disturbing issues, and has recently begun taking steps to diversify its economy and energy mix from a sole dependency on fossil fuels, but these measures, some of which are mentioned below, are still in their initial stages, showing great potential for improvement and expansion.

1.2.6   R.E. Developments in the Middle East and the U.A.E.

At the World Future Energy Summit (WFES), Goktug Gur, Country President for the UAE & Oman, Schneider Electric Gulf, said that the event highlighted "the growing role of the UAE and Abu Dhabi in promoting innovation and investment opportunities in renewable energy and clean technologies." [37]

This might be seen in the U.A.E.'s recent adoption of nuclear energy to meet the U.A.E.s growing power demands. However, studies show that external costs due to risks not covered by power plants operators affect the total cost of nuclear energy, such as the chance of a nuclear accident. It's estimated that Fukushima and Chernobyl have cost many hundreds of billions of euros, and that society has paid most of the damages [26].

These additional risks raise the cost of nuclear energy to between 0.11 and 0.34 euros per kWh. If these costs were added to electricity costs, a kWh of electricity generated by a new nuclear power plant would cost between 0.31 and 0.54 euros and, if produced by an old plant, between 0.13 and 0.36 euros.

This shows that wind and solar energy would still be more feasible and safer options with costs of 0.07 euro and 0.10 euro per kWh respectively [26]. The U.A.E. has already taken measures in the solar direction, but has not actively exploited its wind resources.

Solar energy on the scale of 550 W/m^2 on average is available for more than 11 hours daily throughout the year. This holds enormous potential for both power production and cooling, where solar driven systems are fed with energy trapped with photovoltaic solar cells or solar thermal systems.

Numerous solar thermal technologies are available, with a worldwide capacity installed capacity standing at 102 GigaWatt (GW) in 2013, according to the Emirates Solar Industry Association (ESIA).

Electrical power can be produced through thermal power plants, some of the most widely used technologies including PTSCs, solar towers, and solar dishes. The most established systems of these are the PTSCs which have been used in large power plants since the 1980s.

Moreover, several thermal solar power plants, mostly based on PTSC, are under currently under construction or have recently been completed, some of the most recent ones being in the U.A.E such as those at Shams 1 in Abu Dhabi and the Centre Suisse d' Electronique et de Microtechnique -U.A.E. (CSEM-U.A.E.) in Ras Al Kheimah.

At Shams 1, 100 MW at a cost of $600 million (AED 2.2 billion) are to be installed in one of the largest projects of its kind in the world with 768 PTSCs spread over an area of 2.2 km^2 [50].

At CSEM - UAE, there is ongoing research in other solar-related areas as well such as passive cooling, adapting existing PV technology to local conditions, energy efficient buildings, solar tracking and solar assisted cooling, desalination and power generation [52].

Another solar project coming up soon in the U.A.E. will be the Mohammad Bin Rashid Al Maktoum Solar Park which, at a cost of Dh12 billion upon completion, will produce upto 1 GW of power over a 48km^2 area [51]. Hence it can be seen that the U.A.E. is at the forefront of new solar projects as part of plans to tap into this enormous free resource. It has numerous reasons to do so- one of them is falling solar technology prices. In 2004 it cost 120 fils to produce a kilowatt of electricity using solar technology, and now the cost is 70 fils.

Major global players such as G.E., Siemens and Schneider Electric are actively involved in pushing development in the U.A.E. in the renewable energy and sustainability sector.

Also, trapping of solar energy will reduce emissions, enable the UAE to meet its own internal and domestic power demand, as well as benefit from the opportunity cost of fuels by exporting oil saved due to the use of solar power to the world market,

and possibly, in the future, export excess power generated from solar onto the Middle East grid or even to foreign markets.

But solar energy isn't the only renewable resource the U.A.E. is rich in. Wind speeds around the U.A.E. go up to an average of 6.7 m/s [40] and 7.5 m/s along some shorelines in some areas [39]. Maximum gust speeds range between 8m/s and 14 m/s [41]. But despite all these resources, there's considerable potential for development using Wind Turbine (WT) systems in terms of policy making and installed capacity.

Since any one source is not sufficient to provide all of earth's energy needs, hybrid systems tapping into two or more sources such as solar and wind, have the potential to provide a feasible alternative to conventional energy sources and suffice the world's energy requirements [42].

Siemens acknowledges this; being a participant in the Desertec initiative, a program encompassing wind farms, solar thermal power plants and transnational power highways (High Voltage Direct Current, i.e. HVDC transmission) and smart grids to efficiently carry clean electricity generated in the Middle East and North Africa to Europe's load centers [53].

Nevertheless, though there's incentive for R.E.S.s deployment in the U.A.E, it can be seen that majority of the existing mechanisms in place look to simply enhance power production rather than curtail or discourage consumption.

Proactive measures on the part of the Abu Dhabi government such as the Estidama program seek to enforce energy efficient building codes, a semi-mandatory green building system as well as a national requirement for energy labeling of appliances. These represent a major effort to reduce building's demand for cooling, heating, and lighting by encouraging more efficient designs [38].

However, there is insufficient proof that enough is being done to incorporate R.E.S.s on a more individual scale which would allow the U.A.E. government to lower the ecological footprint of the country's biggest contributor, its households, who contribute 57 % due to their water and electricity consumption [43]. Moreover, most renewable energy systems that have been looked at either cater to only power production or only cooling, but none that provide both.

This research looks to explore the area of combined cooling and power generation by integrating solar, wind and absorption technologies, to make individual

households completely independent of the grid and thus reduce their ecological footprint.

Given that in hot climates such as those of the U.A.E, a large portion of the overall electrical consumption goes towards cooling using conventional existing vapor-compression systems [1], it makes sense to explore higher regimes of performance in technology driven by renewable resources so as to enable this technology to enter the market and thus reduce the load on the grid.

Furthermore, in the literature studied, there is little information on triple effect absorption systems, and if the absorption systems are to contend with vapour-compression technology in the future for sustainable building operation, they will need to provide higher levels of performance [19], and the development of a novel triple effect absorption system in this research helps to contribute to that effort.

Lastly, the rapid growth in the number of residential and commercial buildings in a vibrant economy such as the U.A.E.s, coupled with ever-increasing energy prices, will quite possibly lead to energy shortages, with local suppliers unable to match the increasing demand, resulting in a considerable number properties awaiting connection to the grid.

The implementation of co-generation and tri-generation that can be efficiently, and more importantly, locally deployed to meet individual or multiple building power and cooling needs can greatly relieve power suppliers of the increased burden, and with appropriate policy making, will perhaps allow these independent units to feed power back to the grid.

This research focuses on the development of such co-generation (cooling-power generation) systems that will allow individual building units to become independent, and thus the results of this work can go towards developing systems and further research in this area, subsequently contributing to this inevitable route.

1.3   Literature Review

Many hybrid renewable energy systems have been explored in the literature to produce both energy and cooling. Among the systems studied are the following.

1.3.1 Absorption cooling system.

Absorption cooling machines are driven by heat instead of electric power delivered to a shaft, and hence can provide reliable and quiet cooling where power in unavailable or expensive, or where waste, geothermal or solar heat is available in sufficient quality and abundance. The basis behind their operation is, as their name suggests, 'absorption'.

Absorption is the process of attracting and retaining moisture by substances called desiccants. Desiccants are materials which attract and hold other gases or liquids that have a particular affinity for water. The characteristic of desiccants which allows them to bind to moisture makes them very useful in chemical separation process such as the one employed in absorption systems [27].

Absorption cooling cycles are similar to conventional vapor compression cooling cycles, with one exception: compression work is avoided in an absorption system through modifying the pressurization stage(s). This is done by using a suitable working pair comprising a refrigerant, and an absorbent, i.e. a solution that can absorb this refrigerant.

An absorbent on the low pressure side absorbs evaporating refrigerant in a direct contact heat exchanger called the 'absorber', then flows to the high pressure end of the cycle where it is heated up in a 'generator', and releases the refrigerant again as a consequence.

The hot refrigerant loses heat in a 'condenser' and undergoes expansion in an 'expansion valve', changing state and losing energy before entering the evaporator at its coldest point in the cycle.

This cycle is depicted in Figure 5, which shows a single-stage absorption cooling system. The number of stages can be increased up to a certain limit by adding more pressure levels and successively higher temperatures in more generators, and by changing system configurations.

The most common working fluid pairs are Lithium bromide-water (LiBr-H_2O), where water is the refrigerant, and ammonia water (NH_3-H_2O), where the refrigerant is ammonia. Since this thesis is based on the LiBr-H_2O working pair, the refrigerant vapor in Figure 5 will be water-vapor.
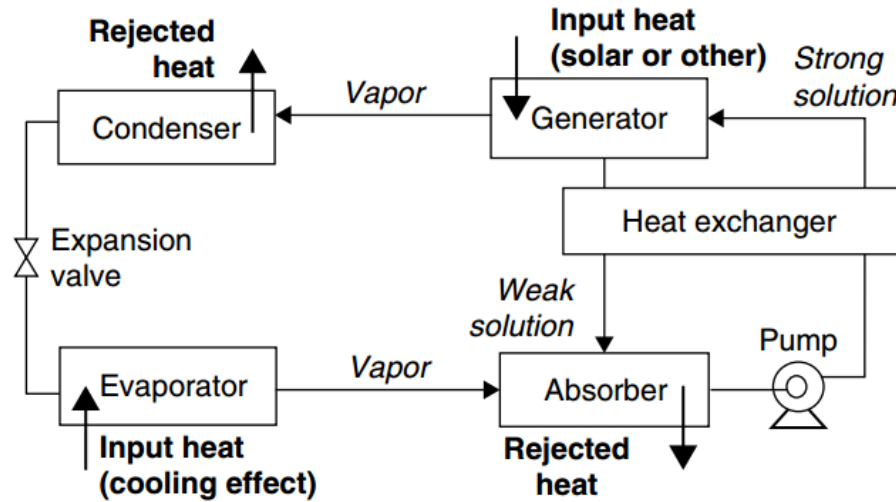
Figure 5: Single stage absorption cooling system [44]

Numerous studies on absorption systems coupled with varied sub-systems have been made in the past. One such study [1] makes use of an PV/T integrated with an absorption system for cooling and hydrogen production. The study analyses the effect of various parameters on the power generated, rate of heat production, energetic and exergetic efficiencies and hydrogen production.

The results show that the overall energetic and exergetic efficiency varies greatly depending on which month it is because of the variation of solar radiation during that time of year and the number of day-lit hours, with maximum achieved values of 15.6% and 7.9% respectively, both occurring during March.

The amount of hydrogen production however, is seen to depend on both, the number of day-lit hours and the solar irradiation intensity, with a maximum of 9.7 kg produced during August, when the solar irradiation is high and is available for almost 13 h daily. The maximum energetic and exergetic COPs are found to occur in June, solar radiation is high for the specified cooling load of 15 kW, with calculated values reaching 2.28 and 2.145 respectively.

Various configurations have been explored to increase the efficiency of the standard parallel double effect absorption system. From an energy conservation point of view, J.I. Yoon et al. experimentally study the benefit of waste heat recovery where the weak absorbent solution heading from the absorber to the low-temperature

generator is pre-heated by exhaust gases from the burner of the high-temperature generator.

The experiments range across cooling and heating cycles, and include testing a feature that reduces the time taken for switching from a heating to a cooling mode. They observe that waste heat utilization results in higher COPs than those possible with a conventional system for a wide range of inlet coolant temperatures and reduces the energy consumption in the high temperature generator by 2.8% and 5.1% for cooling and heating processes, respectively. Also, the 'starting-time shortened' feature enhances the efficiency of the process by raising the temperature of the waste-heat gas [10].

Other recent studies on absorption systems include that by Lizarte et al. [45] who study an innovative directly air-cooled absorber-condenser absorption chiller experimentally from the standpoint of the external fluids for a residential application.

The chiller is powered by vacuum flat-plate solar collectors with a total aperture area of 42.2 m^2 and a storage tank of 1.5 m^3 capacity. They discovered that no solution crystallization problems arose inside the prototype even when the temperature of the input stream to the generator reached 109^0C.

Paurine et al. [46] modeled, designed, manufactured and tested a novel packed bed regenerative solution heat exchanger for a single stage LiBr-$H_2$0 absorption system that minimized risks of crystallization, was more compact and cheaper than conventional solution heat exchangers for absorption systems, and had the potential to save energy by up to 30%.

Avanessian and Ameri [47] assess and compare the performance of three types of absorption refrigeration systems from an energetic, chemical exergetic and economic standpoint. They discovered that direct-fired chillers have a higher energy utilization factor and second law efficiency that those powered by hot water. They also determined that CO_2 emissions of the single effect system is about 1.9 and 1.7 times higher than those for the direct fired and hot water double effect chillers respectively.

Ketjoy et al. [48] evaluate the performance of a evacuated-tube-collector-driven absorption system of 35 kW_c capacity with a gas backup system. They found the average COP of the system to be 0.33 while and maximum and minimum values

for the same were 0.5 and 0.17 respectively for a solar fraction of 0.55 and an ambient temperature of 32^0C.

The performance of a LiBr absorption system was studied using flow ratio and first and second law considerations by Wonchala et al. [49]. They determined that simultaneous increase of the condenser and absorber temperatures was seen to result in a severe deterioration of both the circulation ratio and first law coefficient of performance, while the second law performance indicator improved significantly.

The circulation ratio and the coefficient of performance were seen to improve as the temperature of the heat source increased, while the second law performance deteriorated. The same qualitative responses were obtained when the temperature of the refrigerated environment was increased.

1.3.2 Parabolic trough solar collectors.

Parabolic Trough Solar Collectors (PTSCs) are high performance solar collectors that are used to efficiently produce temperatures in the range of 50^0C to 400^0C. They are relatively low cost and can have light structures, ranging in size from 25 m to 150 m in length.

They primarily comprise a sheet of reflective material bended into a parabolic shape, and a receiver comprising a black metal tube concentric with an outer glass tube placed along the focal line of the parabolic sheets.

Directing the parabolic reflector at the sun results in the sun's parallel rays incident on the reflector to be reflected and concentrated onto the receiver, the black tube helping to absorb heat while the glass tube helps to retain the heat absorbed and prevent convective loss.

The surface of the inner tube is typically plated with a selective coating that has high absorptivity for solar radiation but low emissivity for thermal radiation loss, while the glass cover tube usually has an anti-reflective coating to improve transmissivity else light passing through the glass incurs a transmittance loss of approximately 0.9 when the glass is clean [44]. Figure 6 shows a typical industrial scale PTSC.

Figure 6: Industrial scale PTSC

The radiation concentrated by this process heats up the Heat Transfer Fluid (HTF) circulating through the receiver tube, and the HTF can then be used for various solar powered applications such as solar water heaters and powering absorption systems such as the one studied in this thesis and by Sulaiman et al. [5], where the performance of a tri-generation system that makes use of parabolic trough solar collectors (PTSCs) and an Organic Rankine cycle (ORC) is modeled using exergetic analysis.

Cooling, in the latter study, is produced using a single-effect absorption chiller whereas heating is made possible through a heat exchanger. Three modes of operation, a solar mode during the low-solar radiation time of the day, solar and storage mode during the high-solar radiation time of the day, and storage mode during night time are assessed using four different methods of exergetic analysis, namely, electrical-power, cooling-cogeneration, heating-cogeneration, and tri-generation. Variation of the ORC evaporator pinch point temperature, ORC pump inlet temperature, and turbine inlet pressure allow for obtaining varying values of the exergetic efficiencies and exergy destruction rates.

The results shows that the values of exergy efficiency using the tri-generation approach are higher than those obtained using the values of maximum electrical-exergy efficiency for the different modes of operation. While electrical-exergy efficiency values obtained for the solar mode, the solar and storage mode, and the storage mode are 7%, 3.5% and 3% respectively, the maximum trigeneration-exergy efficiencies are 20%, 8%, and 7%. The results of the study also show that the main sources of exergy destruction are the solar collectors and ORC evaporators, and that the ORC turbine can be run on low inlet pressures with insignificant drops in output to allow for savings.

Although there is a large amount of literature on absorption systems, very little is available on integrating them with PTSCs to develop system that satisfy the cooling needs of individual households. Among the researchers who have made inroads in this direction are Mazloumi et al. [6]. They model a single effect lithium bromide–water absorption cooling system driven by solar energy absorbed by a PTSC (oriented N-S) and stored in an insulated thermal storage tank. The study determines whether this system satisfies the cooling needs for a house with a floor area of 120 m^2 and a maximum cooling load of 17.5 kW (5 TR) in ambient temperatures of up to 50 ^{0}C. The results of the study show that the collector mass flow rate has a negligible effect on the minimum required collector area (found to be 59.8 m^2 for a collector mass flow rate of 1800 kg/hr with the initial temperature of the storage tank equal to ambient temperature during daytime, and 57.6 m^2 when the initial temperature of the storage tank was about 71^{0}C, which resulted from the storage water temperature at the end of each day of operation).

However it is discovered that the collector mass flow rate has a significant effect on the optimum required capacity of the storage tank. The smallest storage tank capacity is obtained for the time of the year when the cooling loads are matched by the available solar radiations during September, and when operation of the system continues after sunset through use of the storage system.

Similarly, the design, installation and modeling of a multipurpose solar thermal cooling and heating system at Carnegie Mellon University, the smallest high temperature cooling system in the world, was performed [7]. A 16 kW double effect parallel, LiBr-water absorption machine with heat recovery heat exchanger was

connected to 52 m^2 of linear parabolic trough solar collectors, and system performance models were developed in the TRaNsient SYstem Simulation program (TRNSYS) to investigate physical and control measures of improving the performance of the overall system. Among the physical measures that were used were variation of the solar collectors' area and orientation, the use of thermal storage in the system, and variation of diameter and length of interconnected pipes. It was found that this solar thermal system had the potential to supply 39% of cooling and 20% of heating energy for this building space in Pittsburgh, PA, if it included a properly sized storage tank and short, low diameter connecting pipes with PTSCs oriented in a N-S direction. This would result in annual savings during the cooling and heating seasons of 100 kWh/m^2 and 34 kWh/m^2, whereas for an E-W orientation, savings of 74 kWh/m^2 and 61 kWh/m^2 could be made and 37% of cooling needs and 29 % of heating needs can be met annually.

Many recommendations were made for further optimization, including decreasing the Heat transfer fluid pipe length in the solar sub-system loop to reduce losses, maintaining constant temperature control to reduce time and energy required to circulate HTF, and inclusion of a drain back tank and storage tank to conserve excess energy accumulated during the day and use it or prevent it from being lost during the night respectively [7].

1.3.3 Photovoltaic thermal technology.

Hybrid photovoltaic/thermal (PV/T) systems allow the effective conversion of absorbed solar radiation into electricity and heat without the emission of greenhouse or any other gases. This makes them an environmentally friendly means of harnessing renewable energy, and a better option than plain PV modules, in that they have a larger energy output. They are reliable and can be built in virtually any size, ranging from milliwatt to megawatt of electrical output because of their modular nature, i.e. output can easily be increased by the addition of more units. PV/T systems are often set up as stand-alone systems, particularly in areas remote from utility grids. This is because PV/Ts make cost effective solutions when the supply of power from conventional sources is impractical or costly. They also provide good value when connected to the grid because of their ability to produce electricity during periods of peak demand, thereby reducing the need for costly extra conventional capacity to cover peak

demand. Moreover, most PV electricity is generated where it is consumed, thus diminishing transmission and distribution losses and enhancing system reliability.

In PV/T systems, electricity is generated by PV cells comprising two or more thin layers of semi-conducting material such as silicon. When light falls on the silicon, electrical charges are generated in the latter which can be conducted away by metal contacts as direct current. Since the electrical output of an individual cell is small, multiple cells are connected and encapsulated to form a PV module. For thermal generation in a PV/T, heat extraction systems are coupled to PV modules. An HTF, usually air or water, is heated in the heat extraction system by the hot PV panels, thus also serving to cool the PV modules and increase their electrical efficiency. PV/T systems are space and cost effective compared to separate PV and thermal units of the same total aperture surface area because of the additional thermal output produced by the thermal extraction device of the PV/T. In PV/T system applications, the main priority is the generation of electricity, and thus it is more effective to operate the PV modules at a low temperature to keep PV cell electrical efficiency at a sufficient level. Water-cooled PV/T systems are very practical and quite commonplace, as they can contribute to cover both electrical and thermal loads for a variety of applications, particularly those solar related.

In terms of construction, the electrical sub-system of a PV/T system comprises a series of PV panels, a battery bank, and an inverter, whereas the thermal sub-system consists of a prime mover, a differential thermostat, and a thermal storage device. In the case of flat PV/T systems, the assembly usually consists of a transparent cover to protect the PV module beneath, a PV module made of amorphous or crystalline silicon to absorb the solar radiation and convert it to electricity, a dark base for the PV modules to absorb remaining solar radiation and the heat from the PV, and a heat extraction system comprising a duct or ducts placed directly underneath the base.

As solar radiation falls on the assembly, heat is transferred from the base to the HTF fluid through the duct. The prime mover could be a pump in the case of a liquid such as water, or a blower or fan in the case of a gas, usually air. The thermal storage device could be for storing sensible or latent heat, depending on the application.

With the exception of the prime mover or a tracking system, PV/T systems have no moving parts. They are thus silent, require minimal maintenance, and are

hence reliable and long-lasting. With ever-decreasing PV costs, they make good candidates for powering stand-alone housing applications [44].

PV/T technology has thus become the subject of numerous studies. Joshi et al. [50] have studied the thermal performance of a hybrid PV/T air collector system for a composite climate in India with two different types of PV module bases, namely glass and Tedlar. They found that the system with a glass base offered better overall performance in terms of thermal efficiency. Dubey et al. [51] designed and tested a glass-glass PV/T integrated with a solar water heater. They derived and experimentally validated the characteristic equation of the PV/T for various configurations, and found good agreement between the theoretical and experimental results. They found that an increase in glazing area, i.e. a decrease in the collector area covered by the PV, led to an increase in instantaneous efficiency.

Joshi et al. [52] compare the thermodynamic performance characteristics of a PV and a PV/T system based on their energy and exergy efficiencies. Values of fill factor are determined for the two systems and its effect on their efficiencies was investigated for a semi-tropical climate. They found that while the energy efficiency varies from a minimum of 33% to a maximum of 45% for both systems, the exergetic efficiency was higher for the PV/T system, varying from 11.3% to 16% whereas that for the PV varied from 7.8% to 13.8%. Saloux et al. [53] develop electrical and thermal models for PV and PVT systems and use them to anticipate the effect on performance of different solar intensities and ambient temperatures. They determine the irreversibilities, define current and voltage reduction factors and determine and graphically portray the locations and causes of exergy destruction for both systems. They also study the performance of the PV/T system under cold climatic conditions, and compare their results for the above with those of Dubey et al. [54] who conduct a similar to study to Joshi et al. [50], but also study the effect of the presence of ducts on the performance on the PV/T.

1.3.4 Wind turbine.

While solar energy can be used to meet cooling loads, wind energy can be used to meet electrical loads. Wind energy systems, when used in tandem with solar systems; provide an especially attractive solution to meeting energy needs as they can

provide a virtually uninterrupted supply of power for installations not connected to the grid. One study that investigates such a system is that of Calderon et al. [8] A system comprising a hybrid wind/solar generator with means for generating, storing and utilizing hydrogen to generate electricity is designed, tested and assessed using energy balances and calculating energy conversion efficiencies. The values of overall conversion efficiency of surplus solar and wind energy into electrical energy delivered to the load when using hydrogen as an energy vector were found to be very low. However, it was noted that this surplus energy would otherwise go unused, and that the system fulfills the primary purpose of providing an uninterrupted power supply for a stand-alone facility. Li et al. [55] also study a hybrid system utilizing wind turbines in conjunction with solar power technology. Their paper describes a rooftop wind solar hybrid heat pump system that is used to satisfy hot water, heating and cooling loads for a building. The paper presents energy and exergy analyses as well as an environmental benefit assessment of the system, which comprises a shrouded wind-lens turbine subsystem, a flat-plate solar thermal subsystem and a water/air source heat pump subsystem, where the wind and solar subsystems are compactly installed on the rooftop. The solar collector heats water for supplying domestic hot water and increasing the heat pump evaporation temperature for room heating. The study found that the solar-thermal subsystem is not feasible from an exergetic efficiency point of view and that a better design of the solar collector can improve the system exergy efficiency. Other results showed that wind power can provide 7.6% of the yearly heat pump power demand to satisfy the thermal loads of a 198 m^2 residential building in Beijing, and that use of the system offers a reduction of 31.3% in carbon dioxide emissions compared to conventional energy systems.

Wind turbines can also be used in tandem with conventional power sources to enhance overall power output. A combined Brayton-Reheat Rankine cycle coupled with a WT is studied by Rabbani et al. [56]. The required input power for the compressor in the Brayton (gas turbine) cycle and the pump in the Rankine cycle is provided by the WT, in order to increase the overall power output. In addition, their analysis of three different configurations of the system shows that increasing the combustion temperature reduces the critical velocity and mass flow rate, and that increases in wind speed reduce both, the first and second law efficiency of the overall

46

system. In the case of a low electricity demand and high penetration configuration, extra wind power is used to compress air which can then be used in the low penetration configuration. During a high load demand, all the wind power is used to drive the pump and compressor and if required additional compressed air is supplied by a storage unit.

Buhagiar et al. [57] propose a system that uses offshore wind energy to simultaneously generate electricity and extract thermal energy by using the WT to drive a hydraulic pump that supplies deep seawater under high pressure to a land based plant consisting of a hydroelectric power generation unit and heat exchanger. Through adequate parameter selection, the results of their steady-state system model show that the total rate of energy output for such a system, consisting of both electricity and thermal energy, is shown to increase by as much as 84%, when compared to a conventional wind turbine having an identical rotor diameter but which supplies only electrical energy.

Wind turbines are primarily of two types, those with a horizontal axis of rotation and those with a vertical axis. Of the two, horizontal axis turbines are more commonly found. Both types are studied by Hadhrami [58] for an off-grid application in the middle-east, and the study, which covered sixteen HAWTs and 8 VAWTs over power categories ranging from 1 to 80 KW, revealed that horizontal axis wind turbines (HAWTs) were generally found to be more efficient that their vertical axis counterparts. The study evaluated the energy output and plant capacity factors of the wind turbines, and results showed that the highest percentage change in annual energy yield (AEY) was obtained for an increase in hub height from 20m to 30m.

For the U.A.E., the region of Fujairah experiences average monthly offshore wind speeds in the range of 2.3 m/s to 6.5 m/s suggesting that the winds have magnitudes sufficient for them to be exploited for power generation purposes at certain times of the year. Redha et al. [40] investigated the energetic and exergetic efficiencies of wind energy conversion systems in UAE, as well as the thermodynamics of wind for different months during the year. The results, show that there are noticeable differences between energetic and exergetic efficiencies and that for moderate wind speeds, the power generated is maximized by using a wind turbine with a low cut-in speed to make as much use as possible of the available wind power.

It was noted that the power production during March was about 17% higher than the month of February and 6.6% higher than January.

1.3.5 Thermal energy storage.

Thermal energy storage (TES) systems have been used to store heat or have been used as cold storage in applications where heat or cooling cannot be produced continuously and the demand for these needs to be met. Thus TES is a technology that has a high potential for usage in various thermal applications, particularly those involving closing the gap between demand and supply of energy [59]. It can contribute significantly to meeting society's needs for more efficient, environmentally benign energy use. Savings, particularly in the design and operation of energy conversion systems, can result if a means of storing thermal energy is arranged for.

Criteria for selecting appropriate TES include the storage period required, i.e. diurnal or seasonal, economic viability, operating conditions, etc. whereas the types of TES that can be implemented vary. Finally, TES can be achieved in three ways: by using sensible (e.g. water, rock, oil), latent (e.g. water/ice and salt hydrates), and thermochemical (e.g. inorganic substances) means of storing heat [60].

1.3.5.1.   Sensible heat storage.

In a sensible TES system, the temperature of the storage medium is changed to store energy. This temperature change ($\Delta T = T_2 - T_1$) is application specific and is limited by the heat source and by the storage system. In order to calculate the sensible heat stored in any storage medium, the following equation can be used [59] :

$$Q_{sensible} = \int_{T_1}^{T_2} c_p \cdot dT$$

where $Q_{sensible}$ is the amount of sensible heat stored, c_p is the specific heat of the material and dT is the differential change in temperature. The specific heat capacity and temperature changes are thus used to determine the energy storage density in sensible heat storage. Studies have been conducted on the use of many different mediums for sensible heat storage, most of which employ commonly available materials such as water , rock beds [61-64] , oil [5], bricks, sand and soil, with various reviews on the applicability of different mediums to applications [65].

In order to allow for night-time cooling of the villas, and to compare between sensible and latent heat storage, a hot thermal storage is decided upon as a means to store sensible heat to allow us to run the absorption systems at night. The sensible heat in this case can either come from the HTF loop that is heated by the PTSC, or from the air loop that is heated by the PV/T array which provides power to the villas. In either case, the heating loop coils heats up the tank during the daytime. The sensible heat thus stored is later used during periods of low sunlight or nighttime to run the absorption systems which in turn provide cooling.

The storage itself comprises a Thermocline tank, which is essentially a single tank with temperature stratification. The storage medium, water, contained in the tank, is usually warmer towards the top and cooler towards the bottom because of both natural convection and buoyancy effects [66], i.e. differences in density due to temperature. In general, liquid at a higher temperature is usually less dense and moves towards the top of the container while cooler liquid tends to move towards the bottom because it has a higher density.

In our Thermocline tank, a secondary piping circuit containing high temperature HTF or hot air enters through the top, heating the water in this region, coils through the height of the tank, and leaves through the bottom.

As the water cools, convection currents cause it to flow to the bottom, creating two different temperature regions with a connecting space between them over which temperature gradually changes. This thermal stratification is known as a temperature gradient or 'thermocline'.

Thermocline tanks are a cheaper option than the more commonly found two-tank configuration, one hot and one cold, and are thus being explored actively. While the two-tank configuration is mostly used in concentrated solar power plants as solar heat storage, it has a higher unit investment cost and operating cost than thermoclines because of a larger amount of container material and HTF and higher high-temperature management expense than thermoclines [67].

While costs of thermocline tanks are comparatively lower, they can be further reduced by replacing a large bulk of the HTF in the tank by a filler material such as concrete that can store the sensible heat [66, 68, 69]. Storage efficiency can be further increased by replacing the sensible heat-storing filler material by a filler material such

as PCM that can store latent heat, hence leading to further size reductions and improved heat storage density.

In our case, the thermocline tank is filled entirely with water and no filler material is present. This is because the use of a filler material reduces the efficiency of heat delivery due to poor contact between the filler material and the piping containing the HTF [69]. The thermocline tank is heated by the HTF circuit looping through the tank, hence having a higher efficiency than the use of a heat exchanger to achieve the same purpose.

1.3.5.2.   Latent heat storage.

Although sensible heat storage systems are quite efficient, Latent Heat Thermal Energy Storage Systems (LHTESS), offer advantages over them by making use of latent heat present within the mass of the storage medium to store energy. LHTESS are among the most promising due to their ability to provide high-energy storage per unit mass in quasi-isothermal processes [59] as well as uniform storage temperature and compactness of size [70].

In order to make an improvement on the energy storage density of sensible storage, some LHTESS make use of a phase change that takes place within the temperature range experienced by the storage. Such storage mediums which undergo a phase change within the desired temperature range are termed Phase Change Materials (PCMs). In order to determine the amount of heat stored in a PCM, we consider the temperature interval over which the storage operates: $\Delta T = T_2 - T_1$

$$Q_{latent} = \int_{T_1}^{T_{PC}} c_s \cdot dT + \int_{T_{PC}}^{T_2} c_l \cdot dT + \Delta H_{ls}$$

where Q_{latent} is the summation of the integrals which represent the sensible and latent heat stored respectively and the heat of fusion ΔH_{ls} of the PCM at the phase change temperature T_{PC}.

A large quantity of energy can thus be stored by PCMs by making use of the solid-liquid phase change process they undergo. PCMs can cater to a wide range of temperatures and provide higher storage capacity and more isothermal behavior during charging and discharging compared to systems storing sensible heat. This is because

latent heat storage systems have a higher energy storage density than sensible heat storage systems.

They can be both, organic or inorganic in nature, with paraffin and fatty acids being examples of the former, and aqueous salt solutions and gas hydrates serving as examples of inorganic PCMs. Both, organic and inorganic PCMs show a single melting temperature when they are pure and a melting range when they are mixtures, whereas a high specific heat is desired to provide additional significant sensible heat storage [59].

Numerous studies such as [71, 72] have been done on the analysis of these PCMs in order to address different aspects of their properties. Attempts have been made to improve on the PCMs by enhancing desirable characteristics such as high energy storage density, high latent heat of fusion per unit volume, high power capacity, high thermal conductivity of both solid and liquid phases and low segregation of the PCM molecules [59].

Moreover, PCM should also have a melting/freezing temperature that lies in the practical range of operation, should be chemically stable and should melt/freeze congruently with minimum sub-cooling, and should be cost-effective, non-toxic and non-corrosive.

Extensive literature is also available for the use of PCM in various applications, both domestic and industrial. Domestic applications include use in hot water tanks [73] and space heating or cooling of buildings [60, 74-76], peak load shifting [77, 78], solar energy applications and seasonal storage [73, 79-84] as well as cold TES applications such as food storage and transportation [85-87].

Many reviews have also been written on the subject [59, 88-92]. Industrial applications include transportation of waste heat [93] and temperature sensitive materials [94] as well as biomedical [94], electronic [95] and solar applications [96]. Out of the above mentioned applications, among the most common uses of PCM is that of passive space heating and cooling [97].

In the latter, PCM is used in many ways, one of them involving the use of PCM as construction or filling material in walls of buildings and housing where it provides high latent heat thermal energy storage over the narrow range of temperatures typically encountered in buildings [98], thus serving to increase the thermal inertia of

the structure's envelope and subsequently improving the energy performance of the structure [84].

 Zhang et al [98] find that by using suitable PCMs and suitable methods of incorporating them into building material, LHTESSs can be economically efficient for heating and cooling buildings, although several problems need to be addressed before reliable and practical application of the same.

1.3.5.2.1   PCM implementation as energy storage in buildings.

- Incorporation into the envelope:

One of the ways of implementing PCM includes incorporation of PCM into the building envelope to increase the thermal mass of the lightweight construction materials. This allows for radiant heating and cooling of PCM over large surface areas since the PCM is part of the building structure. Incorporation of PCM into the building envelope can be done in various ways, the most promising ones being direct incorporation, immersion, encapsulation and lamination of the PCM boards [98].

- Direct incorporation:

This entails mixing powdered or liquid PCM with construction materials such as concrete or gypsum during production of the latter. This is probably the most economical method of using PCM as passive thermal storage since it requires little additional process complexity [98].

- Immersion:

Like its namesake, the process involves immersion of a porous building material such as a gypsum board, brick or concrete block, into hot melted PCM. This causes the PCM to diffuse into the pores. The building material is then removed from the liquid PCM and cooled, the PCM remaining in the pores. This process is convenient as it allows the conversion of ordinary wallboard into PCM wallboard as, when and where required. However, it's impractical if the wallboard is to be used over many years, as extended usage leads to PCM leakage [98].

- Encapsulation:

This is usually done to avoid the negative effects of PCM on construction material. It is of primarily two types, macro-encapsulation and micro-encapsulation.

Macro-encapsulation involves packaging the PCM into containers which are then integrated into the building material. The containers can be of various forms and sizes, including tubes, pouches, spheres, etc. PCM macro-encapsulated structures result in considerably reduced heat fluxes, but also have disadvantages. .

Drawbacks include necessity of protection from destruction, poor heat transfer coefficients of PCM when it is in the solid state, as well as high cost due to difficulty in integrating macro-encapsulation into building products.

To improve the heat transfer coefficient, micro-encapsulation is used because of the increased heat transfer area and the protection against destruction it provides. Micro-encapsulation involves enclosing small PCM particles in a thin, high-molecular weight polymeric film compatible with both, the PCM and the construction material. Its drawback however is that it might affect the mechanical strength of the structure and still doesn't offer as much surface area for heat transfer as would be provided by immersed and directly incorporated PCM [99, 100].

- Lamination of the PCM boards:

This is done by laminating the PCM onto a single layer or area of the envelope, such as an inside wall lining. Many studies such as [101] have been conducted on the development and analysis of PCM laminated boards Darkwa et al. [101] analytically and experimentally analyzed two gypsum-based PCM-integrated systems.

In these randomly mixed and laminated PCM systems, they found that the thermal performance of the laminated PCM system was about 18% better than the randomly mixed type. However, their study was limited to narrow boundary conditions and assumptions, and in a later study, they simulated both types again in a model room designed for passive thermal performance.

This later study, which also assessed the effect of three phase-change zones (narrow, intermediate and wide), found that the laminated PCM type had a much better overall thermal performance than the randomly mixed PCM type, strengthening their previous results.

More specifically, the laminated PCM type was found to be capable of increasing the minimum room temperature by about 17% more than the randomly mixed type [102].

- Packed bed:

Figure 7 shows an example of a ventilated PCM packed bed [98]. Cooling the PCM using forced and/or natural ventilation at night provides a lost-cost method to store thermal energy at off-peak periods, thus reducing peak loads. The cooled PCM then absorbs heat the following day, providing comfort by reducing both the indoor air and wall temperature. This method, though not very feasible for summer seasons in the middle-east where even nighttime conditions rarely coincide with comfort levels, is applicable during cooler months where it can help to shift day-time loads.
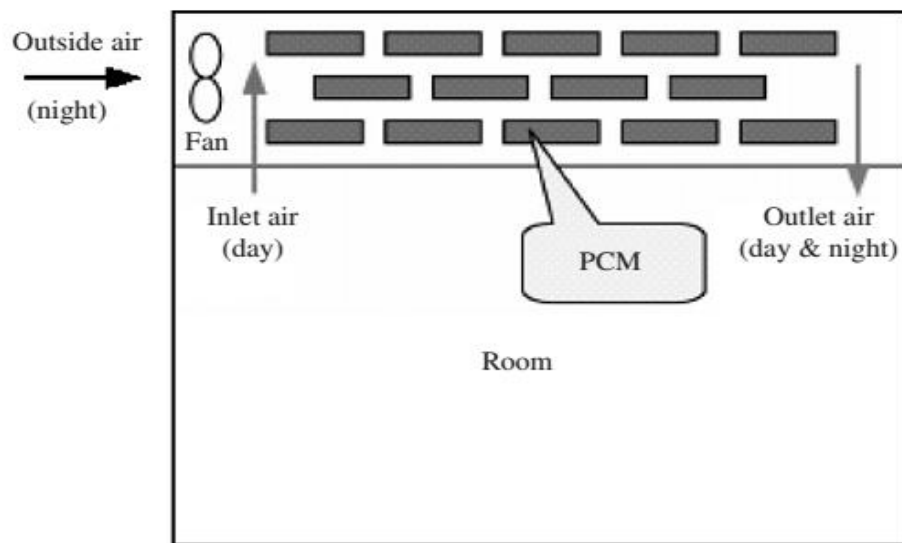
Figure 7: Radiant cooling using PCM

Activation of the latent heat storage in the all of the incorporative methods is due to passive activation, i.e. the construction material that makes up the thermal mass is heated or cooled only due to indoor temperature fluctuations that were not caused by any additional means of mechanical cooling or heating.

All of them help to shift peak loads and can also be used for passive solar applications etc. However, for a hot climate such as the U.A.E.'s, passive cooling, though effective to some extent is not very feasible. This is because though peak loads will be shifted, spaces still need to be cooled during the evening and nighttime for most parts of the year.

This means that though lesser cooling might be required during the daytime if passive cooling is implemented, then cooling loads will be higher at later parts of the day.
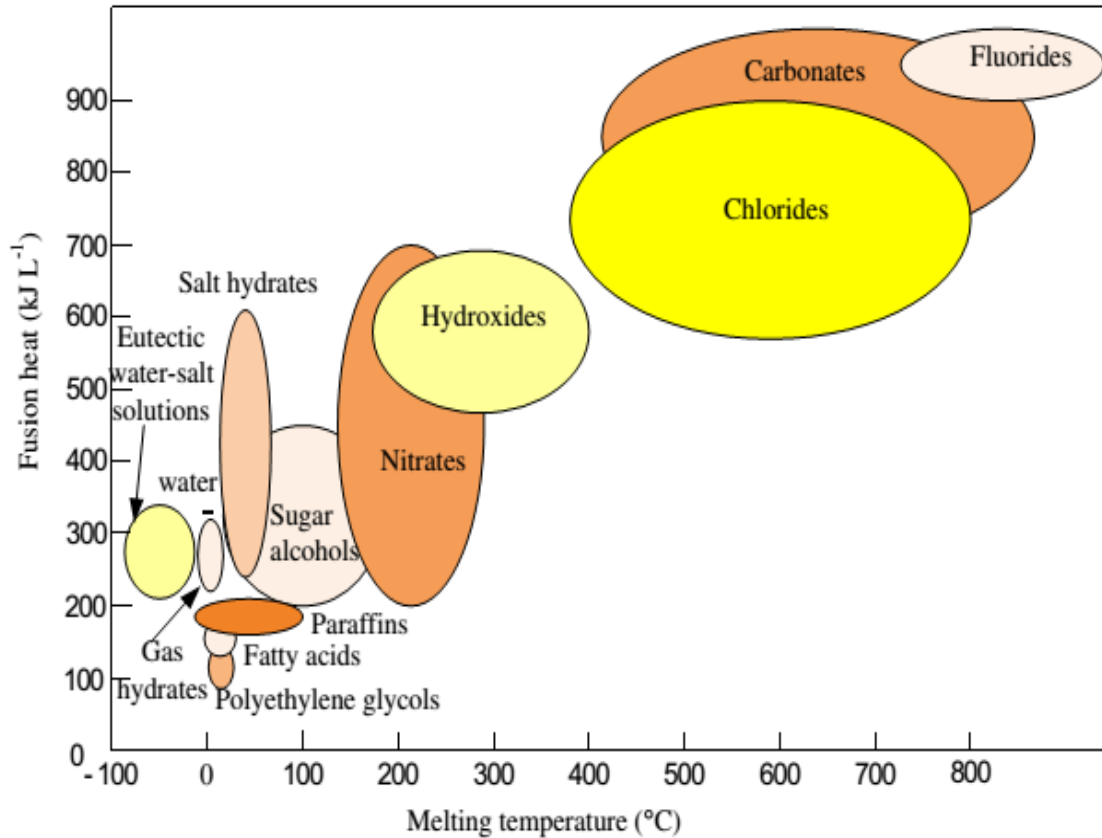
Figure 8: Melting temperature and fusion heat of existing PCMs [103]

Moreover, with equal tariffs during peak and off-peak hours, there is little incentive to the end-user to shift peak loads, although the benefits to the grid would be considerable if there were widespread implementation of passive cooling.

Hence from the end-user's perspective, it would make more sense to install an active cooling system instead of a passive cooling system.

In this work, the active cooling is provided through the use of the absorption system during the daytime.

This leaves the determination of a suitable cooling system for the nighttime. Since the overall system has to be as sustainable as possible, this leaves only a few suitable options.

For this system, cold PCM generated during the daytime was chosen as the preferred option. This PCM would be then used to cool a stream of water that would then be fed to the air handling units.

Determination of a suitable PCM for application depended on the temperatures that would be encountered during the cooling process.

A vapor compression chiller (VCC) was to be used to produce the PCM, and accordingly a PCM with a melting temperature in the range of -5^0C to 12^0C was to be utilized.

From Figure 8, it can be seen that the PCM families that would cater to the temperature range under question would include, in order of decreasing temperature, paraffin waxes, salt hydrates, polyethylene glycols, fatty acids, gas hydrates, water-ice and eutectic water-salt solutions.

While all of these have their advantages and disadvantages, refrigerant gas hydrates have been mainly known to be suited for air-conditioning applications [103].

This may be because they offer the highest overall performance among the options mentioned above.

As can be seen in Figure 9, they have high fusion heat by volume, thermal conductivity and density compared to the paraffin, salt hydrates, eutectics and fatty acids.

They also have minimal corrosion and phase-separation problems, and the super-cooling effect can be easily dealt with using mechanical agitation [103, 104], by the inclusion of additives [105] or even by using a magnetic field or ultrasonic waves [103].

Hence clathrate was chosen as the PCM on the basis of its small volume, high temperature density, slow melting characteristics and simplicity of employment.

1.3.5.2.2   Clathrate.

The PCM clathrate was chosen as an alternative form of thermal storage to the the hot thermal storage tanks in order that the villas can be cooled during periods of non-availability of solar power. While the hot thermal storage, i.e. the thermocline tank, stores sensible heat to allow us to run the absorption system at night, clathrate

can allow us to provide direct cooling to the villas without the need to run the absorption system.

Clathrate hydrates are essentially a form of PCM that characterize a certain class of crystalline solid compounds where a thermodynamically unstable lattice structure with cavities is formed using water molecules ("host" molecules) linked through hydrogen bonding.
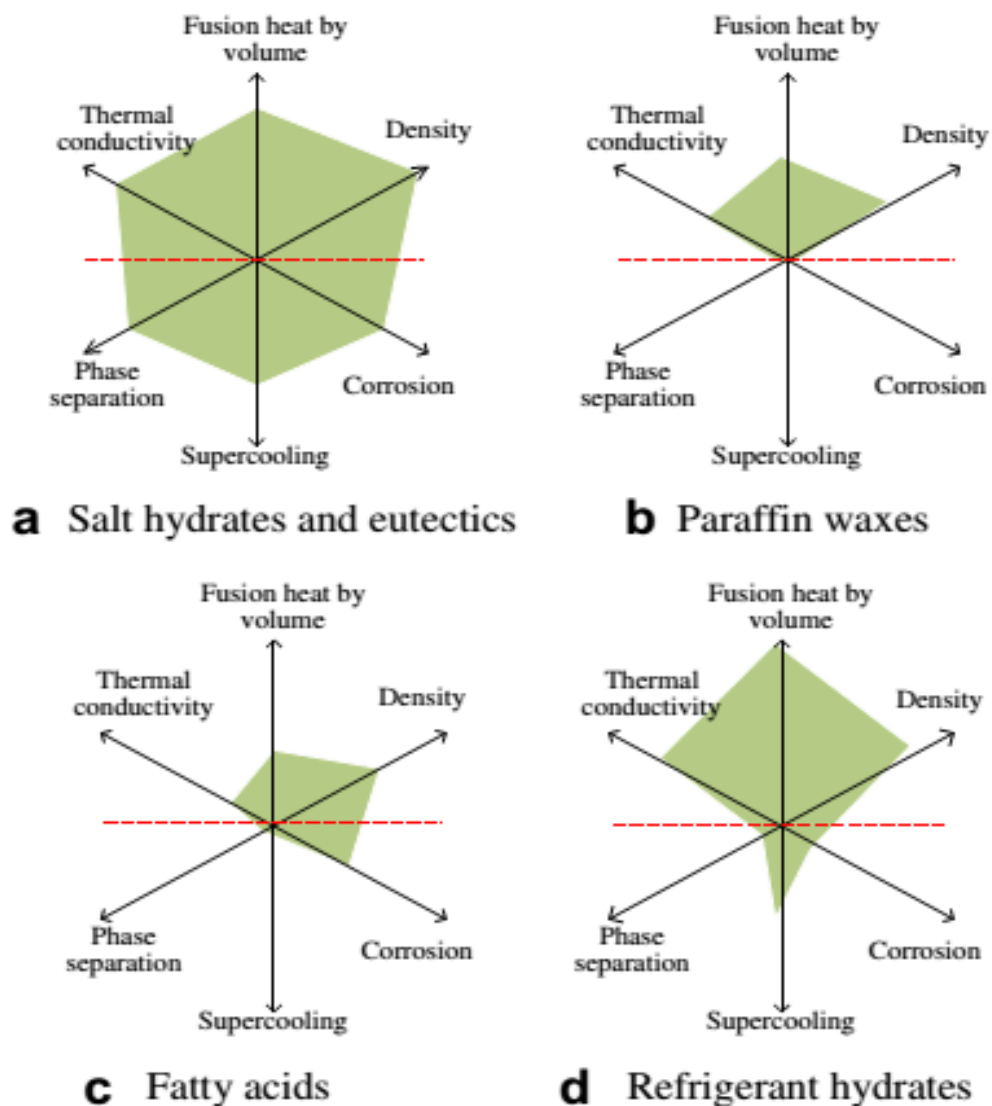
Figure 9: Comparison of properties of different PCMs [103]

This lattice structure can be stabilized under suitable temperatures and pressures and by filling the cavities with "guest" molecules of some species other than

57

water. The "guest-in-cavity" structure that results from this filling procedure is known as a clathrate hydrate or a gas hydrate [91].

Clathrate hydrates have been increasingly employed in various technological aspects of energy utilization by human beings, examples of which include the formation and storage of clathrate hydrates as cool storage media for air conditioning, refrigeration and freezing applications, the prediction and prevention of plugging due to hydrate formation in natural gas pipelines, and disposal into the ocean of waste liquefied carbon dioxide harnessed at fossil-fuel-fired power plants [91, 106, 107]. For refrigeration systems particularly, for hydrate-based systems to become suitable alternatives to conventional systems, the guests substances used in the former are required to be non-toxic, non or slightly-flammable, non-explosive, non-corrosive, environmentally friendly, and inexpensive [108].

The use of clathrates for these applications has led to many studies of both, experimental and theoretical nature. Sugaya et al. [109] conducted observational studies on a water-HydroFluoroCarbon (HFC)-134a refrigeration system to reveal the mechanism of growth of the clathrate hydrate phase at the boundary of water in the liquid state, and the fluorocarbon in the liquid or vapor state. They observed that the surface morphology of the hydrate layer depended strongly on the degree of saturation of the water with the fluorocarbon, but did not vary much with the state of the fluorocarbon. They also expected that the surface morphology would be significantly affected by hydrodynamic conditions such as the solubility of the guest species in liquid water, the water-guest reaction at the interface, and the diffusive transport of the heat of hydrate formation away from the interface, and observed the same. Another observational study by

In [108], Ogawa et al. attempt a novel hydrate-based refrigeration system to show the potential advantages of the same over a conventional refrigeration system. They performed thermodynamic analysis, simulations and constructed a laboratory scale refrigeration system. The thermodynamic analysis and simulations were on a scenario where HFC-32 and cyclo-pentane were simultaneously used as the hydrate-guest substances, and revealed that if the hydrate formation temperature, i.e. the temperature at which heat is discharged from the system, and the hydrate dissociating temperature, i.e. the temperature at which cool energy is supplied from the system are

adjusted to 25.5^0C and 5^0C respectively, then the COP of the refrigeration system could be as high as 8.0, suggesting that hydrate-based refrigeration performance can exceed that of conventional refrigeration.

Furthermore, the experimental setup involving HydroChloroFluoroCarbon (HCFC-22) as the hydrate-guest substance showed that the system could operate steadily with no sign of internal blocking by the formed hydrate.

They suggested selecting more suitable hydrate-guest substances (for eg. with hydrate-forming temperatures sufficiently higher than the temperature of the heat reservoir to which the heat is being rejected), improving the design of the hydrate-forming/dissociating reactors, the multi-phase compressor, etc., and optimizing the operating conditions to improve the performance of the overall system.

Wijeysundera et al. [110] studied the effect of the location of the coolant nozzle in a direct-contact heat transfer system to determine the best location to avoid clogging due to freezing of water. They used Fluoroinert FC-84 as the hydrate guest gas and obtained an ice-fraction of 40% when a jet was directed upwards into the ice slurry tank using a nozzle located at the bottom of the tank.

They found that the ice formation rate depended on the nozzle position and on the spray pattern, with nozzles with an axis-symmetric, inclined spray pattern having a faster clathrate-production rate than the vertical spray nozzle.

Computational models based on the experimental setup were then used to determine the heat transfer coefficients between the coolant drops and the water; the coefficients calculated using single-sphere correlations were found to be larger than the experimental ones.

Tajima et al. [104] used static mixing for clathrate formation in an experimental set-up. They used HFC-134a as the guest hydrate gas, and observed clathrate formation of two types: plug-like hydrate and hydrate slurry comprising agglomerated HFC-134a bubbles covered with hydrate, and small hydrate particles dispersed in water, respectively.

The hydrate formation pattern was determined by a balance between hydrate formation kinetics and mixing by a static mixer, i.e. the number and structure of the mixing elements, and the gas flow rate.

Also, high pressure differences between the HFC-134a vapor pressure and the water pressure result in plug-like hydrate formation whereas slurry formation was found to take place due to slower hydrate formation under small pressure differences.

A similar experimental was conducted by Xie et al. [111] who studied various means to enhance hydration, and found that mechanical blending was the best option.

Adding a heat exchanger with vertical fins, use of an additive-Sodium dodecyl benzene sulfonate of 0.04% concentration, increasing the coolant flow rate and decreasing the coolant temperature were found to be less effective methods, but also suitable means of significantly enhancing hydration.

Other studies include the following. Bi et al. [112] constructed thermodynamic optimization models using entropy generation minimization as the optimization objective.

They found that the optimal operating conditions of the clathrate storage system can be achieved by keeping the phase change rates uniform. Ohmura et al. [113] demonstrated the suitability of an interferometry technique for in situ measurements of polycrystalline hydrate film thickness. They compared the effect of using water pre-saturated with R-134a to using pure water, and observed and reported the differences in clathrate surface morphology at the planar interface between the liquid HFC and liquid water (pure or pre-saturated).

Wu and Wang [114] tried to enhance the cooling potential of R-134a hydrate through the means of alcohol additives. Their work indicated that adding alcohol into the overall solution was essential for stable and smooth operation and that an indirect contact configuration in the storage tank was industrially applicable. Another enhancement technique studied by Li et al. [105] was conducting the formation and dissociation of the HFC 134a hydrate in a nano-copper suspension of different mass fractions. Their experimental results indicated that the greater the addition of nano-copper, the more improved the hydrate formation.

Gas hydrates can also fall under the category of phase change slurries (PCS) which are basically PCMs in slurry form. PCS can be used as thermal storage and heat transfer fluids, and thus can play an important part in enhancing the efficiency of air-conditioning and refrigeration applications.

In addition, use of PCS also helps to reduce the quantity of thermal fluids required for the aforementioned applications. In addition to the numerous theoretical and experimental studies conducted to explore and enhance these PCS, many reviews of those studies have been conducted.

Zhang et al. [115, 116] look at generation and storage methodologies as well as performance and application cases for various PCS employed as storage media and secondary refrigerants in refrigeration and air-conditioning systems, including ice slurries, microencapsulated PCS (MPCS) and clathrate hydrate slurries (CHS).

The flow and heat transfer characteristics of PCS in both, tubes and heat exchangers summarized to some extent. Li et al. [103] recently review a wide range of cold storage media for air conditioning applications, including water and ice, salt hydrates and eutectics, paraffin waxes, refrigerant hydrates, MPCS, etc. and summarize thermal, hydraulics and physiochemical properties of different PCMs, particularly clathrate slurries and MPCS.

In addition, they look at the problems associated with use of these mediums, such as phase separation, super-cooling and corrosion as well as previous works pertaining to these issues. Finally, Li et al. [103] summarized the efficiency and reliability of ice-slurry generation, reviewed sorption techniques for cold storage, and provided some perspectives on the commercialization of various storage materials.

Youssef et al. [117], in a more or less concurrent review as Li's, take a more focused approach, concentrating on the formation, thermo-physical, rheological, flow and heat transfer properties and applications of four PCS systems: Clathrate hydrate slurry (CHS), Microencapsulated Phase Change Materials Slurry (MPCMS), shape-stabilized PCM slurries (SPCMSs) and Phase Change Material Emulsions (PCMEs).

Moreover, they also provide the advantages and disadvantages of the different PCS media, hence providing insight on their viability for laboratory and industrial applications.

1.3.5.2.3   *Advantages of clathrate.*

Clathrate hydrates are an attractive technology, particularly for cold storage applications. They offer a high cold storage density and have a higher phase change temperature compared to water, and have smaller pumping requirements to produce

the same cooling. They offer better heat transfer properties and improved cyclic stability compared to eutectic salts [118] . In addition, they offer comparable fusion heat by volume and thermal conductivity to salt hydrates and eutectics, which are their closest competitors, while experiencing minimal drawbacks normally associated with salt hydrates and eutectics, such as corrosion, super-cooling and phase separation. and the super-cooling effect can be easily dealt with using mechanical agitation [103, 104], by the inclusion of additives [105] or even by using a magnetic field or ultrasonic waves [103].

Moreover, clathrates have a small volume, high temperature density, slow melting characteristics and are simple to use. They also are non-toxic, non or slightly-flammable, non-explosive, non-corrosive, environmentally friendly, and inexpensive.

In comparison to the hot thermal storage, the space taken up by a clathrate generation system (CGVCS) is much lesser than that occupied by the thermocline tank, and the charging time is lesser, meaning that multiple units can be charged simultaneously and can subsequently be used to offset peak loads during daytime as well as provide night-time cooling, while this would not be possible with the thermocline tank.

In spite of the large volume of work done on the subject of clathrates, to the author's knowledge, none has been conducted on the integration of clathrates into real-life refrigeration/air-conditioning applications as part of a sustainable system. For this reason, the use of clathrates in a sustainable housing scenario needed to be explored, as is done in this thesis.

1.4   Research Results and Summary of Key Findings

This research was conducted to design an environmentally benign system that was powered entirely by renewable energy sources and that helped to curb the environmental footprint left by the housing sector.

Three different integrated systems are studied, and the technologies that were integrated to form the different configurations are a wind turbine, solar PTSC, solar PV/T, clathrate storage and an absorption cooling cycle, and were chosen based on their merits of eco-friendliness, safety of use, cost-effectiveness, efficiency and sustainability.

To recap, the primary motivations and objectives of this research were as follows:

- To use renewable energy resources for co-generation of power and cooling as an alternative to using power from the grid.

- Development of a unique triple effect absorption system for performance gain over existing designs.

- Integration of solar, wind and absorption technologies to result in an environmentally friendly, sustainable solution.

- Energetic and exergetic performance analysis of the integrated system to determine the optimum solution under different operating conditions.

Thermodynamic models of the integration between the individual systems give us various insights into the operating characteristics and the feasibility of using such an integrated system as a solution to the energy strains and global warming of today's world.

Some of the most prominent insights gleaned are as follows. The highest energetic and exergetic COPs are recorded for the month of July for the integrated PTSC-TEAS system even though exergetic efficiency of the PTSC is lowest during the same month.

The exergetic efficiency of the wind turbine is seen to increase with wind speed but is also affected by air temperature, and thus is highest for the month of January rather than March when wind speeds, and subsequently power production and flow exergies, are highest. The power and heat production of the PV/T increase with irradiation intensity and daytime outdoor temperature, and are highest during the month of August when these two meteorological quantities peak, and thus effectively help to meet the demand for night-time cooling, although thermal efficiency is seen to be highest is July and electrical and exergetic efficiencies are seen to peak in January when ambient temperatures are lower and thus help the solar cells to function more efficiently.

For night-time cooling, the clathrate-generation system is seen to have the highest charging COP at a mass ratio of 2.5 and while cooling is provided by the integrated PTSC-TEAS system during the daytime and the integrated PV/T-clathrate system during the night. The PV/T and the WT together produce all the electrical power required by the villas, with their combined energetic efficiency achieving a

maximum during July and their combined exergetic efficiency being highest during August. Lastly, the economic analysis shows that this sustainable solution is economically viable at the current electricity cost to the consumer.

These results and more show that this integrated system would be a viable alternative to conventional power and cooling sources for the residential sector in the U.A.E., thus reducing the environmental footprint of the region, and can be used as a base for further studies and solutions to global warming for similar climates.

1.5   Thesis Organization

This chapter gives an insight into the scope of and motivations behind this work as well as what the author aims to accomplish. Background information is presented on the sub-systems that make up the three integrated systems studied and the main findings of this project are summarized.

Chapter two describes and details the operating principles of the three integrated systems. System diagrams are provided to aid visualization of the systems. Chapter two then delves into the methodologies implemented to analyze the different sub-systems both individually as well as holistically as integrated systems.

Accordingly, the energy and exergy relations that are used to evaluate the qualitative and quantitative merits of the sub-systems and the integrated systems are detailed here.

Results of the thermodynamic analyses conducted on the three mutually different integrated systems are given in chapter three. A thorough investigation of the behavioral aspects of the individual sub-systems and the integrated systems in response to parametric modifications is provided.

Lastly, chapter four comprises the principal conclusions drawn from this study and recommendations for further work in this area.

Chapter 2: System Description and Modeling

2.1   System Description of Case 1: Fully Standalone Power and Cooling with Redundancy and DEAS-PTSC Daytime Cooling

In this section, a detailed elaboration of the first of the integrated tri-generation systems is provided, with the system being shown in Figure 10. In order to provide cooling to the villas, the parabolic trough solar collector (PTSC) works in conjunction with the LiBr Double Effect Absorption System (DEAS). The sun's rays hit the reflectors/mirrors of the PTSC, thus being concentrated on the central absorber/receiver tube that lies along the focal length of the mirrors. Pressurized hot water being pumped through the receiver tube gets heated up as a result of the concentrated heat, and the hot water thus produced in the PTSC is fed into the high generator (H.G.) of the DEAS to sufficiently power the latter throughout the year.

Refrigerant-rich (dilute) solution pre-heated in the high solution heat exchanger (H.S.X.) enters the H.G. at state 13, and is further heated to the highest temperature in the cycle by the incoming hot water from the PTSC. Some of the refrigerant (water vapor) dissociates from the dilute mixture and leaves the H.G. at state 17 whereas the remaining mixture, now concentrated and very hot, leaves the H.G. through a separate route at state 14. This concentrated solution then passes through the H.S.X. to pre-heat the incoming stream (state 12) from the low generator (L.G.), and thus reduces the amount of heat required to be supplied to the high generator.

Both streams exiting the H.G. then enter the relatively lower pressure L.G. to generate more vapor. However, while the hot water vapor at state 17 enters the L.G. to provide heat to the dilute solution in the L.G., the relatively cooler concentrated stream at state 15 enters the L.G. to mix with the dilute solution entering at state 3. The additional vapor generated in the L.G. leaves at state 7 to mix with the vapor used to heat the L.G., which now cooler, leaves at state 18. In this way, the L.G. acts as a condenser for the stream at state 17, and the heat supplied in the highest generator is used twice to generate vapor, hence the term 'double-effect'.

The stream at state 18 passes through an expansion valve to allow its pressure to drop to the pressure of the L.G. and mixes with the newly generated vapor at state 7 to form a stream at state 7'. The dilute solution in the L.G., after losing water vapor,
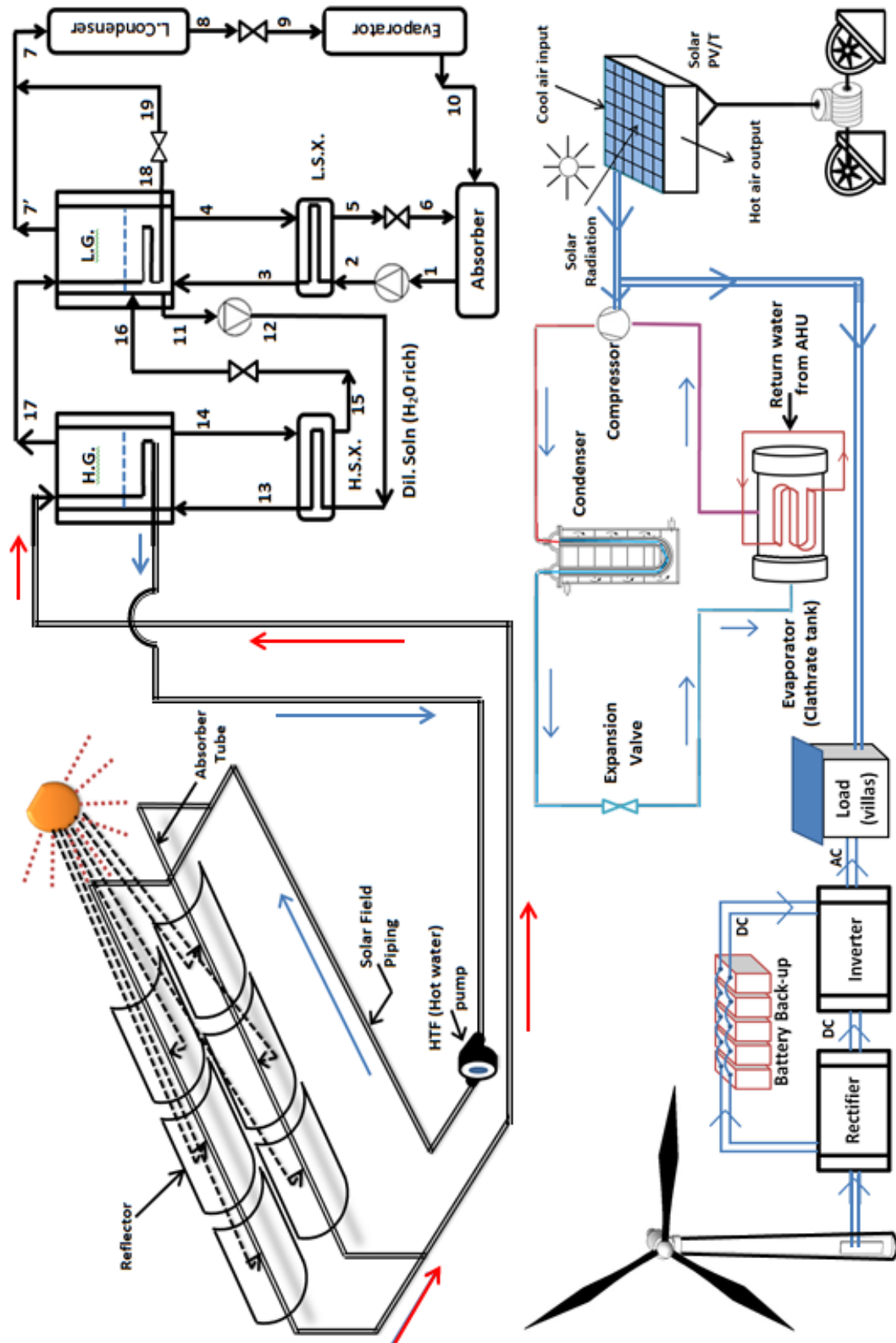
Figure 10: Case 1 integrated system diagram

exits the L.G. in concentrated form at state 4 and reaches a cooler state 5 by losing heat to the low solution heat exchanger (L.S.X.) to pre-heat the dilute stream at state 2 coming from the absorber. The vapor stream generated in the L.G. at state 7' then enters the condenser. Here, it loses heat, leaving at state 8, and gets throttled and further cooled to the coldest point in the cycle at state 9 before entering the evaporator where it absorbs heat and passes to the absorber at state 10. The dilute solution in the L.G., after releasing water vapor in the L.G., leaves the latter at a concentrated state 4 to enter the low solution heat exchanger where it releases heat and cools to state 5. It then passes through an expansion valve, getting throttled and cooled to state 6, and thus enters the absorber where it mixes with the incoming vapor at state 10 to once again get diluted and pumped at state 1 to the cycle.

Night-time cooling is achieved through the use of cold thermal storage in the form of clathrate. The clathrate is generated during the daytime using a vapor compression cycle (VCC) that is powered by a PV/T array. Excess power produced by the PV/T array is fed to the villas. The total PV/T area required is 390m^2. The clathrate is generated and stored, and when needed, warm chilled-water which is returning from the air handling units (AHUs) is circulated through the clathrate and is subsequently cooled and pumped off to the AHUs again. Sufficient clathrate is generated during the day to meet the night-time cooling needs of the villas during any season.

While the above systems provide cooling, the electrical load of the villas is met by the wind turbine and the PV/T. Since the output of the wind turbine is unstable alternating current (AC), it needs to be passed through a rectifier to convert it to direct current (DC) and then an inverter to convert it to AC which can then be used by the villas. All systems are sized such that the electrical and cooling needs of the villas are more than met throughout the year solely through the use of renewable energy. Hence excess electricity generated is stored in batteries which have the capacity to store charge for 7 days, whereas the heat produced by the PV/T and any excess heat produced by the PTSC, can be stored to run the DEAS at night, provide hot water for the households, and provide heating during colder months. The heat produced by the PV/T could be stored in a hot thermal storage tank, i.e. a Thermocline tank, to run the absorption system at times of insufficient/absent sunlight, but as will be seen later, the R-134a-water CGVCS serves as a better night-time cooling storage option than a

Thermocline tank, and hence is chosen to be the preferred storage system to be integrated into the overall system.

2.2 System Description of Case 2: TEAS Integrated with PTSC, PV/T and WT for Partial Load Satisfaction

This system is similar to the one in Case 1, but differs in the cooling system used to cool the villas. Unlike Case 1, instead of using a DEAS, the parabolic trough solar collector (PTSC) works in conjunction with a triple effect LiBr absorption system (TEAS) in Case 2. Also, while in Case 1 only the PTSC is used to provide heat to the DEAS, here, the heat generated by the PV/T is also used to power the absorption system. Moreover, the PTSC and PV/T are sized such that together they produce just enough heat to power the absorption system, as a result of which capital costs for the PTSC and PV/T are smaller.

However, there is a trade-off, because a smaller PV/T array means not enough electricity is generated to power both, the villas and the Clathrate Generation Vapor Compression System (CGVCS). The system can be seen in Figure 11 and operates in the following manner.

Sunlight falling on the PTSC is concentrated onto the central absorber/receiver tube that lies along the focal length of the mirrors of the PTSC. Pressurized hot water being pumped through the receiver tube gets heated up as a result of the concentrated heat, and the hot water thus produced in the PTSC is fed into the high generator of the TEAS (H.G.) to power the triple effect LiBr absorption system (TEAS). At the same time, air heated up by passing through the ducting under the PV panels, also enters the H.G. of the TEAS.

Refrigerant-rich (dilute) solution pre-heated in the high solution heat exchanger (H.S.X.) enters the H.G. at state 23, and is further heated to the highest temperature in the cycle by the incoming hot water from the PTSC and hot air of the PV/T. Some of the refrigerant (water vapor) dissociates from the dilute mixture and leaves the H.G. at state 27 whereas the remaining mixture, now concentrated and very hot, leaves the H.G. through a separate route at state 24.

This concentrated solution then passes through the H.S.X. to pre-heat the incoming stream (state 22) from the medium generator (M.G.), and thus reduces the

Figure 11: Case 2 integrated system diagram

amount of heat required to be supplied to the high generator. The air supplied by the PV/T, now cooler, exits to the environment while the stream of water from the PTSC returns to the latter to be reheated. The stream of water vapor generated in the H.G. as well as the concentrated LiBr solution exiting the H.G. then enters the relatively lower pressure M.G. to generate more vapor through different mechanisms.

While the hot water vapor at state 27 enters the M.G. to provide heat to the dilute solution in the M.G., the relatively cooler concentrated stream at state 25 enters the M.G. to mix with the dilute solution entering at state 13. The additional vapor generated in the M.G. leaves at state 17 to mix with the vapor used to heat the M.G., which now cooler, leaves at state 28. In this way, the M.G. acts as a condenser for the stream at state 27.

The stream at state 28 passes through an expansion valve to allow its pressure to drop to the pressure of the M.G. and mixes with the newly generated vapor to form a stream at state 17'. The dilute solution in the M.G., after losing water vapor, exits the M.G. in concentrated form at state 14 and reaches a cooler state 15 by losing heat to the medium solution heat exchanger (M.S.X.) to pre-heat the incoming dilute stream from the low generator (L.G.) which is at state 12. The concentrated solution at state 15 experiences throttling through an expansion valve, and its pressure drops to that of the L.G. before it enters the L.G. to mix with the dilute solution there. The vapor at state 17' enters the L.G. for heating purposes so that more vapor is generated. In this way, the heat supplied in the highest generator is used thrice to generate vapor, hence the term 'triple-effect'.

Vapor generated in the L.G. at state 7 then mixes with the used vapor stream at state 18 after the latter gets throttled to state 19, and forms a vapor stream at state 7' which enters the condenser. Here, it loses heat, leaving at state 8, and gets throttled and further cooled to the coldest point in the cycle at state 9 before entering the evaporator where it absorbs heat and passes to the absorber at state 10.

On the other hand, the dilute solution in the L.G., after releasing water vapor in the L.G., leaves the latter at a concentrated state 4 to enter the low solution heat exchanger where it releases heat and cools to state 5. It then passes through an expansion valve, getting throttled and cooled to state 6, and thus enters the absorber

where it mixes with the incoming vapor at state 10 to once again get diluted and pumped at state 1 to the cycle.

Night-time cooling is achieved through the use of cold thermal storage in the form of clathrate. The clathrate is generated during the daytime using a vapor compression cycle (VCC) that is powered by a 16.5 m^2 PV/T array. Any excess power produced by the PV/T array is fed to the villas.

The clathrate is generated and stored, and when needed, warm chilled-water which is returning from the air handling units (AHUs) is circulated through the clathrate and is subsequently cooled and pumped off to the AHUs again. However, because of the limited electrical supply from the PV/T, this system generates insufficient clathrate during the day to meet the night-time cooling needs of the villas.

While the above systems provide cooling, the electrical load of the villas is met by the wind turbine and the PV/T, albeit partially. Since the output of the wind turbine is unstable alternating current (AC), it needs to be passed through a rectifier to convert it to direct current (DC) and then an inverter to convert it to AC which can then be used by the villas.

2.3   System Description of Case 3: Fully Standalone Power and Cooling with Redundancy and TEAS-PTSC Daytime Cooling

In this configuration, as shown in Figure 12, in order to provide cooling to the villas, the parabolic trough solar collector (PTSC) works in conjunction with the triple effect absorption system (TEAS). The sun's rays hit the reflectors/mirrors of the PTSC, thus being concentrated on the central absorber/receiver tube that lies along the focal length of the mirrors. Pressurized hot water being pumped through the receiver tube gets heated up as a result of the concentrated heat, and the hot water thus produced in the PTSC is fed into the high generator of the TEAS (H.G.) to power the triple effect LiBr absorption system (TEAS).

Refrigerant-rich (dilute) solution pre-heated in the high solution heat exchanger (H.S.X.) enters the H.G. at state 23, and is further heated to the highest temperature in the cycle by the incoming hot water from the PTSC. Some of the refrigerant (water vapor) dissociates from the dilute mixture and leaves the H.G. at state 27 whereas the remaining mixture, now concentrated and very hot, leaves the H.G. through a separate route at state 24.
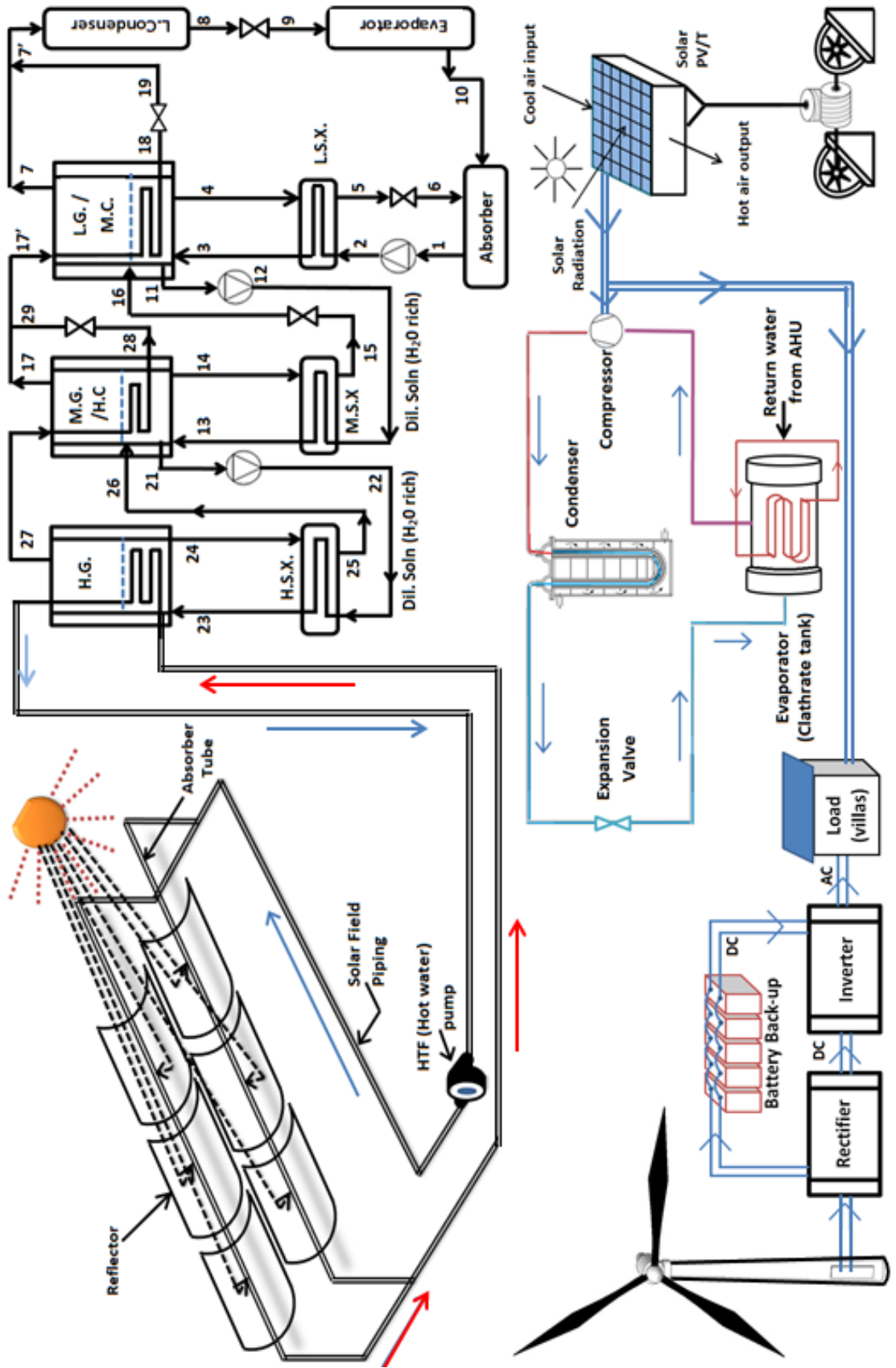
Figure 12: Case 3 integrated system diagram

This concentrated solution then passes through the H.S.X. to pre-heat the incoming stream (state 22) from the medium generator (M.G.), and thus reduces the amount of heat required to be supplied to the high generator.
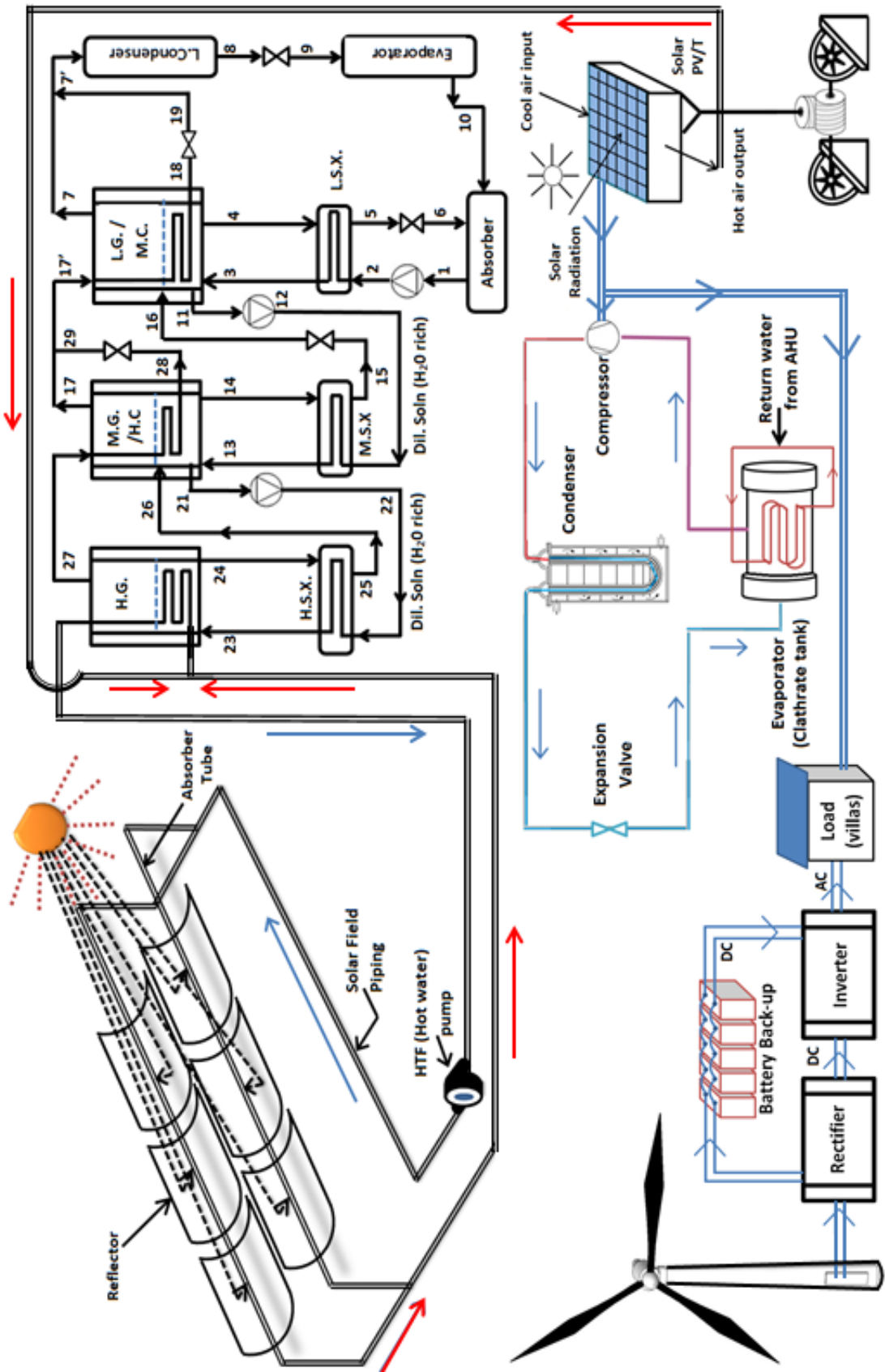
Both streams exiting the H.G. then enter the relatively lower pressure M.G. to generate more vapors. However, while the hot water vapor at state 27 enters the M.G. to provide heat to the dilute solution in the M.G., the relatively cooler concentrated stream at state 25 enters the M.G. to mix with the dilute solution entering at state 13. The additional vapor generated in the M.G. leaves at state 17 to mix with the vapor used to heat the M.G., which now cooler, leaves at state 28. In this way, the M.G. acts as a condenser for the stream at state 27.

The stream at state 28 passes through an expansion valve to allow its pressure to drop to the pressure of the M.G. and mixes with the newly generated vapor to form a stream at state 17'. The dilute solution in the M.G., after losing water vapor, exits the M.G. in concentrated form at state 14 and reaches a cooler state 15 by losing heat to the medium solution heat exchanger (M.S.X.) to pre-heat the incoming dilute stream from the low generator (L.G.) which is at state 12. The concentrated solution at state 15 experiences throttling through an expansion valve, and its pressure drops to that of the L.G. before it enters the L.G. to mix with the dilute solution there.

The vapor at state 17' enters the L.G. for heating purposes so that more vapor is generated. In this way, the heat supplied in the highest generator is used thrice to generate vapor, hence the term 'triple-effect'. Vapor generated in the L.G. at state 7 then mixes with the used vapor stream at state 18 after the latter gets throttled to state 19, and forms a vapor stream at state 7' which enters the condenser.

Here, it loses heat, leaving at state 8, and gets throttled and further cooled to the coldest point in the cycle at state 9 before entering the evaporator where it absorbs heat and passes to the absorber at state 10.

On the other hand, the dilute solution in the L.G., after releasing water vapor in the L.G., leaves the latter at a concentrated state 4 to enter the low solution heat exchanger where it releases heat and cools to state 5. It then passes through an expansion valve, getting throttled and cooled to state 6, and thus enters the absorber where it mixes with the incoming vapor at state 10 to once again get diluted and pumped at state 1 to the cycle.

Night-time cooling is achieved through the use of cold thermal storage in the form of clathrate. The clathrate is generated during the daytime using a vapor compression cycle (VCC) that is powered by a PV/T array. Any excess power produced by the PV/T array is fed to the villas. The total PV/T area required is 390m^2. The clathrate is generated and stored, and when needed, warm chilled-water which is returning from the air handling units (AHUs) is circulated through the clathrate and is cooled and pumped off to the AHUs again. Sufficient clathrate is generated during the day to meet the night-time cooling needs of the villas during any season.

While the above systems provide cooling, the electrical load of the villas is met by the wind turbine and the PV/T. Since the output of the wind turbine is unstable alternating current (AC), it needs to be passed through a rectifier to convert it to direct current (DC) and then an inverter to convert it to AC which can then be used by the villas. All systems are sized such that the electrical and cooling needs of the villas are more than met throughout the year solely through the use of renewable energy. Excess heat and power generated is stored in the same way as in Case 1.

2.4   Modeling: Triple Effect Absorption System

The equations required to develop the triple effect absorption system model are given below, starting with those modeling the absorber in order to adhere to the numbering system applied to the various state-points. Assumptions for the cycle inputs and parameters are given in Table 1 whereas the state points can be seen in the Duhring-schematic of the system in Figure 13.

Table 1: Inputs for the triple effect absorption cooling system model

Parameter and unit	Symbol	Value
Mass flow rate of dilute (refrigerant rich) solution out of absorber (kg/s)	$\dot{m}_1$	0.49
Temperature of condenser [a] (^{0}C)	T_c	30

Table 1: Inputs for the triple effect absorption cooling system model (cont.)

Parameter and unit	Symbol	Value
Temperature of evaporator [b] (^0C)	T_e	5
Temperature of high generator [c] (^0C)	T_g	180
Effectiveness of solution heat exchangers	ϵ_{shx}	0.5
Pinch point temperature difference between condensers and generators (^0C)	ΔT	5
Cooling load [d] (kW_{cool})	$\dot{Q}e$	112.544

a. $T_c = T_8 = T_1$
b. $T_e = T_{10}$
c. $T_g = T_{24}$
d. 8 T.R. per villa
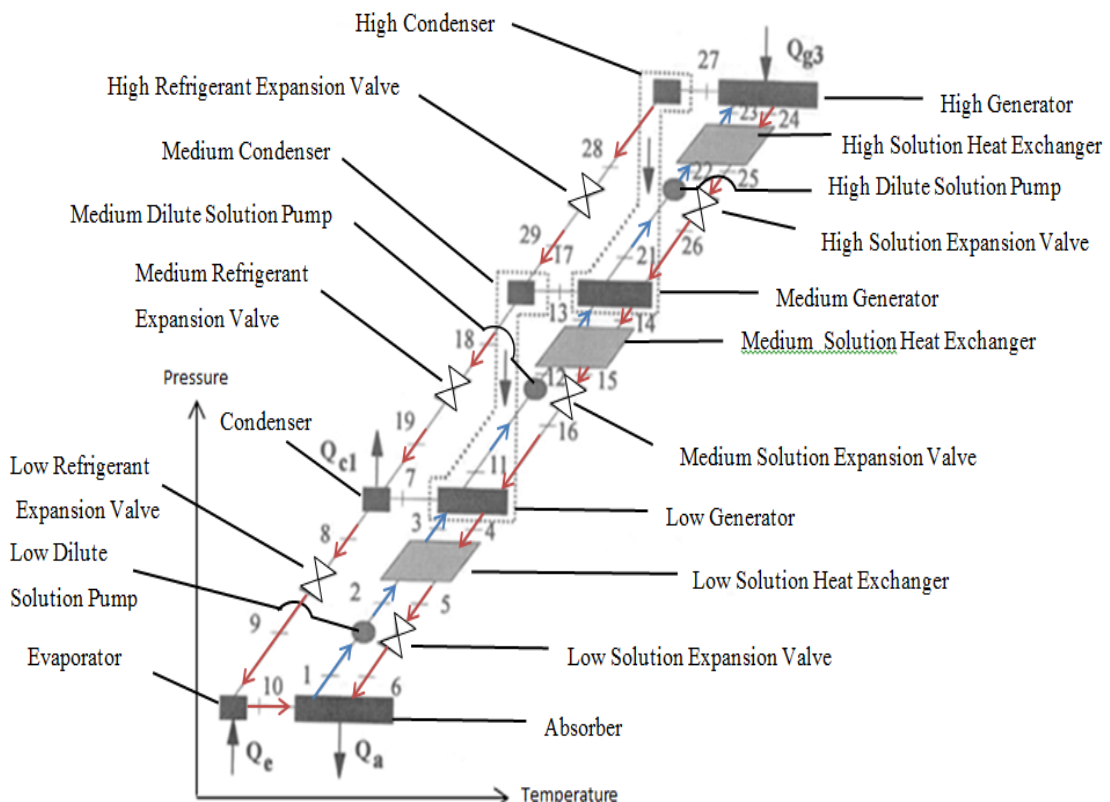
Figure 13 : Schematic of a triple effect, parallel flow, LiBr-H_2O system

The mass and energy balance equations respectively, for the absorber, are as follows:

- Absorber

$$\dot{m}_1 = \dot{m}_6 + \dot{m}_{10} \tag{2.1}$$

$$\dot{m}_1 \cdot h_1 + \dot{Q}_{abs} = \dot{m}_6 \cdot h_6 + \dot{m}_{10} \cdot h_{10} \tag{2.2}$$

where $\dot{Q}_{abs}$ is the rate of heat rejected by the absorber.

- Pump

The below equations are for the low pressure pump. Similar equations are used for the pumps at the two other pressure levels (medium and high pressure). The mass balance equation for the low pressure pump is:

$$\dot{m}_2 = \dot{m}_1 \tag{2.3}$$

Similarly, the concentration balance is:

$$x_2 = x_1 \tag{2.4}$$

The power consumed by the pump, in kW, is found from the below equations:

$$\dot{W}_{l,P} = \dot{m}_1 \cdot v_1 \cdot \left(\frac{P_m - P_l}{1000} \right) \tag{2.5}$$

where v_1 is the specific volume of the weak (refrigerant rich) solution leaving the absorber. Then, the power is also calculated by:

$$\dot{W}_{l,P} = \dot{m}_1 (h_2 - h_1) \tag{2.6}$$

- Solution heat exchanger

The equations presented below are for the low solution heat exchanger. Similar analysis can be expected for the medium and high level solution heat exchangers. The solution heat exchanger allows the pre-heating of the dilute solution using the heat from the stream returning from the generator. The mass balances governing the operation of the solution heat exchanger are:

$$\dot{m}_3 = \dot{m}_2 \tag{2.7}$$

$$\dot{m}_5 = \dot{m}_4 \tag{2.8}$$

The following equations give the concentration balances for the mass flows:

$$x_2 = x_3 \tag{2.9}$$

$$x_5 = x_4 \tag{2.10}$$

The rate of heat exchanged in the low solution heat exchanger between the dilute and the concentrated (refrigerant poor) streams can be found using:

$$\dot{Q}_{shx,1} = \dot{m}_1 \cdot (h_3 - h_2) \tag{2.11}$$

$$\dot{Q}_{shx,1} = \dot{m}_4 \cdot (h_4 - h_5) \tag{2.12}$$

Accordingly, the effectiveness of the solution heat exchanger taken to be 0.5 and is expressed by:

$$Eff_{shx,1} = \frac{T_4 - T_5}{T_4 - T_2} \tag{2.13}$$

- Solution expansion valve

The solution expansion valves are located on the concentrated stream returning from the solution heat exchanger to the absorber, or, at higher pressure levels, from the solution heat exchanger to the low and medium pressure generators. When located before the absorber, they allow the pre-cooling of the solution before it enters the absorber, thus reducing the amount of heat needed to be rejected from the absorber. The modeling is identical for the valves on all three pressure levels, and the analysis is presented for the valve at the lowest pressure level before the absorber. The mass balance and the concentration balance respectively, are:

$$\dot{m}_5 = \dot{m}_6 \tag{2.14}$$

$$x_5 = x_6 \tag{2.15}$$

It is to be noted that though the concentration remains the same before and after the expansion valve, the quality of the solution changes as some of the liquid flashes to vapor on passing through the valve.

- Generator

The equations developed for the generator are given below. They are identical for the low and medium temperature generators, but slightly differ for the highest generator because of the absence of streams leaving to and entering from higher pressure levels. This is because the highest generator is at the highest pressure level. In the TEAS, the low and medium generators serve as mixing chambers for all the streams entering them. Since concentrated streams returning from higher generators may not have released all their water vapor, this mixing in the medium and low

generators allows more vapor to be generated from the concentrated streams. The below equations define the mass balances for the streams associated with the low temperature generator, with the analysis for the medium temperature generator being identical:

$$\dot{m}_3 + \dot{m}_{16} = \dot{m}_4 + \dot{m}_{11} + \dot{m}_7 \tag{2.16}$$

where $\dot{m}_{16}$ is the stream returning from the medium solution expansion valve, $\dot{m}_{11}$ is the stream supplied to the medium pressure level pump, $\dot{m}_7$ is the water vapor generated, $\dot{m}_3$ and $\dot{m}_4$ are the streams coming from and returning to the low solution heat exchanger respectively. The mass balance for the high temperature generator is as given below:

$$\dot{m}_{23} = \dot{m}_{27} + \dot{m}_{24} \tag{2.17}$$

The concentration balances for the model ensure the direction of mass flows in the model is correct. For the low generator, they are as follows:

$$\dot{m}_3 \cdot x_3 + \dot{m}_{16} \cdot x_{16} = \dot{m}_4 \cdot x_4 + \dot{m}_{11} \cdot x_{11} \tag{2.18}$$

$$x_{11} = x_3 \tag{2.19}$$

$$x_4 = x_{16} \tag{2.20}$$

The previous analysis is adopted for the medium generator. Note that the concentrated (refrigerant poor) return streams from all generators have the same concentration. Thus, the concentration balance for the high generator is:

$$\dot{m}_{23} \cdot x_{23} = \dot{m}_{24} \cdot x_{24} \tag{2.21}$$

Some temperature constraints have been applied to the model and are given below. The constraints ensure that the vapor that is generated in and leaving the generators is at the same temperature as the dilute (refrigerant rich) streams leaving the low and medium generators towards the higher parts of the cycle. This is supposed to represent the physical temperature stratification that takes place within the low and medium generator-condenser.

$$T_{11} = T_7 \tag{2.22}$$

$$T_{21} = T_{17} \tag{2.23}$$

The temperature constraints given below serve a different purpose from the ones above. They implement the pinch-point temperature differences which ensure that the high temperature vapor streams which supply heat to their respective

generators are at a sufficiently higher temperature than the generators they supply at all times. This subsequently guarantees that vapor will always be generated in every generator.

$$T_{18} = T_4 + \Delta T_1 \tag{2.24}$$

$$T_{28} = T_{14} + \Delta T_2 \tag{2.25}$$

Enthalpy relations are also implemented to allow calculation of the heat generated in every generator. In the low and medium temperature generators, the heat is generated from the vapor coming from higher pressure levels.

Stream 17 generated in the medium generator is routed through the low generator, loses heat which is used to drive more vapor from the low generator in the form of stream 7, and as a result is cooled.

Hence the low temperature generator acts as a condenser for stream 17 and a generator for stream 7. The same principle applies to stream 27 generated in the high generator, and cooled in medium generator, producing stream 17 as a result.

This process exemplifies the concept of the 'effects' in a double or triple effect absorption system where vapor generated at higher pressure and temperature levels is used to generate vapor at lower levels.

The relations below allow the determination of the rate of heat transferred from stream 17 to the low temperature generator; relations for stream 27 transferring heat to the medium generator are similar:

$$\dot{Q}d_1 = \dot{m}_4 \cdot h_4 + \dot{m}_{11} \cdot h_{11} + \dot{m}_7 \cdot h_7 -$$
$$\dot{m}_3 \cdot h_3 - \dot{m}_{16} \cdot h_{16} \tag{2.26}$$

where $\dot{Q}d_1$ is the heat transferred to the low generator from stream 17 leaving the medium generator. For the high generator, heat is supplied from an external loop heated by the HTF of the PTSC, and can be determined by an energy balance on the generator:

$$\dot{Q}d_3 = \dot{m}_{27} \cdot h_{27} + \dot{m}_{24} \cdot h_{24} - \dot{m}_{23} \cdot h_{23} \tag{2.27}$$

- Condenser

In a triple effect absorption system, there is only one true condenser, which is the low condenser. The mass balance for the low condenser is given by:

$$\dot{m}_8 = \dot{m}_7 + \dot{m}_{19} \tag{2.28}$$

The energy balance of the low pressure condenser is given by:

$$\dot{Q}c_1 = \dot{m}_7 \cdot h_7 + \dot{m}_{19} \cdot h_{19} - \dot{m}_8 \cdot h_8 \tag{2.29}$$

where $\dot{Q}c_1$ is the rate of heat rejected by the condenser to the environment.

The other two condensers are the medium and high pressure condensers. The medium condenser and the low generator are essentially the same component to facilitate heat transfer between the vapor stream supplying heat and the solution to be heated.

Stream 17 leaving the medium pressure generator enters the low generator and releases heat, getting cooled as a process.

Hence the low generator also acts as the medium condenser. Therefore the heat released in the medium condenser is identical to the heat rate required/generated in the low generator:

$$\dot{Q}c_2 = \dot{Q}d_1 \tag{2.30}$$

and can also be calculated by:

$$\dot{Q}c_2 = \dot{m}_{17} \cdot h_{17} - \dot{m}_{18} \cdot h_{18} + \dot{m}_{29} \cdot h_{29} \tag{2.31}$$

Similarly, the heat released in the high pressure condenser is identical to the heat required/ generated in the medium generator:

$$\dot{Q}c_3 = \dot{Q}d_2 \tag{2.32}$$

and can also be calculated by:

$$\dot{Q}c_3 = \dot{m}_{27} \cdot h_{27} - \dot{m}_{28} \cdot h_{28} \tag{2.33}$$

The mass balances for the medium and high pressure condenser are as follows:

$$\dot{m}_{18} = \dot{m}_{17} + \dot{m}_{29} \tag{2.34}$$

$$\dot{m}_{28} = \dot{m}_{27} \tag{2.35}$$

- Refrigerant expansion valve

The equations below are used to model the refrigerant expansion valves located after the condensers in the triple effect absorption system. The analysis is identical for all of them, with the equations being presented for the lowest refrigerant expansion valve just before the evaporator.

The mass balance is:

$$\dot{m}_8 = \dot{m}_9 \tag{2.36}$$

The enthalpy across the expansion valve remains constant as:

$$h_8 = h_9 \tag{2.37}$$

- Evaporator

The following straightforward analysis is used to model the evaporator which receives the refrigerant, i.e. water vapor, from the low expansion valve. The mass balance for the evaporator is:

$$\dot{m}_{10} = \dot{m}_9 \tag{2.38}$$

Whereas the energy balance is given by:

$$\dot{Q}e = \dot{m}_9 \cdot (h_{10} - h_9) \tag{2.39}$$

- COP

The energetic COP of the system can be found by:

$$COP = \frac{\dot{Q}e}{\dot{Q}d_3} \tag{2.40}$$

Whereas the exergetic COP can be found using:

$$COP_{EX} = \dot{X}_{eva,th} / \dot{X}_{HTG,th} \tag{2.41}$$

where

$$\dot{X}_{evap,th} = \left(1 - \frac{T_0}{T_{evap}}\right) \cdot \dot{Q}e \tag{2.42}$$

and

$$\dot{X}_{HTG,th} = \left(1 - \frac{T_0}{T_{d,3}}\right) \cdot \dot{Q}d_3 \tag{2.43}$$

In the above expression, $T_{d,3}$ is the temperature of the highest generator, given by:

$$T_{d,3} = \frac{T_{23} + T_{24} + T_{27}}{3} + 273 \tag{2.44}$$

where T_{23} is the temperature of the dilute solution entering the highest generator, T_{24} is the temperature of the concentrated solution returning from the generator, and T_{27} is the temperature of the stream of water vapor generated in the highest generator.

2.5   Modeling: Parabolic Trough Collector

The analysis of the PTSC was carried out based on the model developed by Suleiman et al. in [5], with some parameters also adopted from [44]. A 55m PTSC was designed for a HTF (hot water) flow rate of 2.222 kg/s. The outlet temperature of the HTF that is required from the PTSC is 463 K (190^{0}C), which is slightly higher than the temperature required in driving the vapor from the highest generator of the triple effect

absorption system. The return temperature from the absorption system is 183^0C, which is 456 K, and which is also the temperature of the HTF input to the PTSC. The specific heat of the HTF varies slightly from 4.45 kJ/kg.K at the inlet of the PTSC inlet to 4.46 kJ/kg.K at the exit of the PTSC. Other values of the various parameters governing the performance of the PTSC are given in Table 2, with most values being derived from [44] unless otherwise mentioned.

Table 2: Input data for solar PTSC sub-system

Parameter and unit	Symbol	Value
Receiver inlet temperature (^{0}C)	$T_{r,i}$	190
Receiver outlet temperature (^{0}C)	$T_{r,o}$	183
Absorbed solar radiation (W/m^2)	G_b	653
S.h.c.[a] of inlet water to receiver (J/kg.K)	$C_{p,r,i}$	4450
S.h.c. of outlet water from receiver (J/kg.K)	$C_{p,r,o}$	4460
Length of collector (m)	L	55
Aperture width (m)	W	3.5
Glass cover outer diameter (m)	$D_{c,o}$	0.09
Receiver outer diameter (m)	$D_{r,o}$	0.05
Receiver inner diameter (m)	$D_{r,i}$	0.04

Table 2: Input data for solar PTSC sub-system (continued)

Parameter and unit	Symbol	Value
Receiver efficiency	η_r	0.765 [5]
Receiver tube thermal conductivity (W/m.K)	k_r	15
Stefan-Boltzmann constant ($(W/m^2.K^4)$)	σ	$5.67 \cdot 10^{-8}$
Glass cover emissivity	ϵ_{cv}	0.87
Receiver emissivity	ϵ_r	0.92
Convective heat transfer coefficient inside receiver (W/m^2.K)	$h_{c,r,in}$	330
Glass cover temperature (^{0}C)	T_{cvr}	320
Wind velocity (m/s)	V_w	5
Number of collector rows	Col_r	1
Thermal conductivity of air at T_0 (W/m.K)	k_{air}	0.0276

a.   S.h.c is an abbreviation for specific heat capacity

In order to maintain constant temperatures at the outlet and inlet of the PTSC, a certain amount of heat must be constantly added to the HTF as it travels along the receiver pipe. This heat must be equal or greater than the amount of heat delivered to the highest generator of the absorption system. Since the state of the HTF does not change between the outlet and the inlet of the receiver, the rate of heat added is mostly sensible, and is hence calculated using the following equation:

$$\dot{Q}_g = \dot{m}_r \cdot c_{p,r} \cdot (T_{r,o} - T_{r,i}) \tag{2.45}$$

For our analysis, it is assumed there is not heat loss from the HTF between the exit of the receiver and the inlet to the generator. The rate of heat transferred from PTSC to the HTF is thus also the rate of heat transferred from HTF to the generator, given by:

$$\dot{Q}_g = F_r \cdot (S \cdot A_{ap} - A_r \cdot U_L \cdot (T_{r,i} - T_{r,o})) \tag{2.46}$$

where F_r is the heat removal factor, S is the solar radiation absorbed by the receiver, A_{ap} is the collector aperture area, A_r is the receiver area, and U_L is the overall heat loss coefficient of the PTSC. The area of the aperture A_{ap} is given by:

$$A_{ap} = (w - D_{c,o}) \cdot L \tag{2.47}$$

The total surface area of the receiver available to capture heat is:

$$A_r = \pi \cdot D_{r,o} \cdot L \tag{2.48}$$

Whereas the area of the receiver cover as given by [5] and known as A_g in [44] is:

$$A_{cvr} = \pi \cdot D_{c,o} \cdot L \tag{2.49}$$

The solar radiation absorbed by the receiver 'S' is a fraction of the total incident radiation G_b in W/m²:

$$S = G_b \cdot \eta_r \tag{2.50}$$

where η_r is the efficiency of the receiver. The heat removal factor F_r is given by:

$$F_r = \frac{\dot{m}_r \cdot c_{p,r}}{A_r \cdot U_L} \cdot \left(1 - \exp\left(-\frac{A_r \cdot U_L \cdot F_1}{\dot{m}_r \cdot c_{p,r}}\right)\right) \tag{2.51}$$

and the average $c_{p,r}$ of the HTF along the receiver is:

$$C_{p,r} = (C_{p,r,i} + C_{p,r,o})/2 \tag{2.52}$$

The collector efficiency factor F_1 in the expression for F_r is:

$$F_1 = \frac{U_0}{U_L} \tag{2.53}$$

where the overall heat transfer coefficient U_0 is:

$$U_0 = \left(\frac{1}{U_L} + \frac{D_{r,o}}{h_{c,r,in} \cdot D_{r,i}} + \left(\frac{D_{r,o}}{2 \cdot k_r} \cdot \ln(D_{r,o}/D_{r,i})\right)\right)^{-1} \tag{2.54}$$

The collector heat loss coefficient U_L in Equation 2.54 is expressed as:

$$U_L = \left(\frac{A_r}{(h_{c,ca} + h_{r,ca}) \cdot A_{cvr}} + \frac{1}{h_{r,cr}}\right)^{-1} \tag{2.55}$$

Whereas the convection heat coefficient $h_{c,r,in}$ for the inlet side of the receiver, in the expression for U_0 in Equation 2.54, is defined as:

$$h_{c,r,in} = (Nus_r \cdot k_{air} / D_{r,i})\tag{2.56}$$

where the subscript r indicates the receiver, and $h_{c,r,in}$ is also referred to as $h_{\emptyset}$ in [44]. The convection heat coefficient $h_{c,ca}$ between the cover and the ambient is defined as:

$$h_{c,ca} = (Nus \cdot k_{air} / D_{c,o})\tag{2.57}$$

where Nus, k_{air} and $D_{c,o}$ are the Nusselt number, thermal conductivity of the air and the outer diameter of the cover respectively. The radiation heat coefficient $h_{r,ca}$ in the expression for U_L is defined as :

$$h_{r,ca} = \left(\epsilon_{cv} \cdot \sigma \cdot (T_{cvr} + T_a) \cdot (T_{cvr}^2 + T_a^2)\right)\tag{2.58}$$

The radiation heat coefficient between the cover and the receiver can be calculated as:

$$h_{r,cr} = \left(\frac{\sigma \cdot (T_{cvr} + T_{r,av}) \cdot (T_{cvr}^2 + T_{r,av}^2)}{1/\epsilon_r + \frac{A_r}{A_{cvr}} \cdot \left(\frac{1}{\epsilon_{cv}} - 1\right)}\right)\tag{2.59}$$

where ϵ_{cv} and σ are the emittance and the Stefan-Boltzmann constant respectively. The average temperature of the HTF inside the receiver is the mean of the inlet and outlet temperatures:

$$T_{r,av} = \frac{T_{r,i} + T_{r,o}}{2}\tag{2.60}$$

and the temperature used to find the Reynold's number for the HTF is:

$$T_{Re} = \frac{T_0 + T_{cvr}}{2}\tag{2.61}$$

where the assumed temperature of the cover (T_{cvr}) in the expressions above is:

$$T_{cvr} = \left(\frac{h_{r,cr} \cdot T_{r,av} + (A_{cvr}/A_r) \cdot (h_{c,ca} + h_{r,ca}) \cdot T_0}{h_{r,cr} + (A_{cvr}/A_r) \cdot (h_{c,ca} + h_{r,ca})}\right)\tag{2.62}$$

and T_{cvr} is referred to as T_g in [27] and is taken to be 337 K. The Reynold's number is given by the expression:

$$Re = \frac{\rho_{HTF} V_{HTF} D_{c,o}}{\mu}\tag{2.63}$$

The expression used for the Nusselt number is that used in [27] for Reynold's numbers between 1000 and 50,000 is:

$$Nus = 0.3\,(Re)^{0.6} \tag{2.64}$$

The rate of heat produced by the PTSC, in kW is:

$$\dot{Q}_{PTSC} = \dot{Q}_g/1000 \tag{2.65}$$

Whereas the rate of heat obtained by the PTSC from the sun is given by:

$$\dot{Q}_{solar} = (F_r \cdot A_{ap} \cdot S \cdot Col_r)/1000 \tag{2.66}$$

The energetic efficiency of the PTSC is thus given by:

$$\eta_{PTSC} = (\dot{Q}_{PTSC}/\dot{Q}_{solar}) \cdot 100 \tag{2.67}$$

The exergy of the PTSC is given by the below expression taken from [119]:

$$\dot{X}_{PTSC} = A_{ap} \cdot G_b \cdot \left(1 + \frac{1}{3} \cdot \left(\frac{T_0}{T_{sol}}\right)^4 - \left(\frac{4}{3}\right) \cdot \left(\frac{T_0}{T_{sol}}\right) \right)/1000 \tag{2.68}$$

where T_{sol} is the temperature of the sun, equaling 6000 K.

Whereas the exergy rate of the heat produced by the PTSC is given by:

$$\dot{X}_{prod} = \dot{Q}_{PTSC} \cdot \left(1 - \frac{T_0}{T_{prod}} \right) \tag{2.69}$$

where T_{prod} is given by:

$$T_{prod} = \left(\frac{2 \cdot T_{r,o} + T_{cvr,avg}}{3} \right) \tag{2.70}$$

and the average cover temperature $T_{c,avg}$ is given by:

$$T_{cvr_{avg}} = \frac{\left((h_{r_{cr}}) \cdot (T_{r_{av}}) + \left(\frac{A_{cvr}}{A_r}\right) \cdot (h_{c_{ca}} + h_{r_{ca}}) \cdot (T_0) \right)}{\left(h_{r_{cr}} + \left(\frac{A_{cvr}}{A_r}\right) \cdot (h_{c_{ca}} + h_{r_{ca}}) \right)} \tag{2.71}$$

The exergetic efficiency of the PTSC then becomes:

$$\dot{\varepsilon}_{PTSC} = (\dot{X}_{prod}/\dot{X}_{PTSC}) \cdot 100 \tag{2.72}$$

2.6   Modeling: Wind Turbine

As mentioned earlier, the wind turbine model is developed based on the model presented by Gadalla et al. in [40]. Input parameters to the model are given in Table 3. The below equation defines what speed the wind is reduced to after the turbine. This ratio is specific to the turbine under study and is unique for every wind turbine:

$$\frac{V_{2,w}}{V_{1,w}} = 0.76517 \tag{2.73}$$

The swept area of the wind turbine is given by:

$$A_{WT} = \frac{\pi D_{WT}^{2}}{4} \tag{2.74}$$

The mass flow rate of the wind through the turbine blades is:

$$\dot{m}_w = \rho A_{WT} V_{1,w} \tag{2.75}$$

where $V_{1,W}$ is the speed of wind prior to passing through the turbine.

Table 3: Input parameters to the wind turbine model

Parameter and unit	Symbol	Value
Turbine diameter (m)	D_{WT}	21
Density of air at 15^0C and 35^0C respectively (kg/m^3)	ρ_{air}	1.225 and 1.161
Specific heat capacity of air (0^0C-40^0C) (kJ/kg.K)	$C_{p,a}$	1.005
Air gas constant (kJ/kg.K)	R	0.287
Atmospheric pressure (kPa)	P_{atm}	101.325

The electric power generated by the wind turbine is given by equation 2.76.

$$\dot{P}_w = \left[\frac{1}{2}\dot{m}_w\left(V_{1,w}^2 - V_{2,w}^2\right)\right]/1000 \tag{2.76}$$

To find the energetic efficiency of the wind turbine:

$$\eta_w = \frac{\dot{P}_w}{\dot{W}_w} \tag{2.77}$$

where $\dot{W}_w$ is the rate of energy input to the wind turbine by the wind and is given by:

$$\dot{W}_w = \left[\frac{1}{2}\rho A_{WT}V_{1,w}^3\right]/1000 \tag{2.78}$$

For the analysis of the wind turbine from an exergetic point of view, we need to calculate the wind chill temperatures, i.e. the cooling effect experienced by the wind immediately before and after the turbine due to suction and discharge effects respectively.

Rather than assuming the wind chill temperatures, we calculate them. Calculation of the wind chill temperatures requires us to obtain the wind speed in miles per hour (mph). The below conversion allows us to convert from meters per second (mps) to mph.

$$V_{1,w,mph} = (2.23693629) \times V_{1,w} \tag{2.79}$$

$$V_{2,w,mph} = (2.23693629) \times V_{2,w} \tag{2.80}$$

The wind chill temperatures are calculated using the relations developed in [120]. These relations, which are given below, use ambient temperatures in ^{0}F.

$$T_{w.ch,1} = 35.74 + (0.6215) \times T_{0,F} - (35.75) \times V_{1,w,mph}^{0.16}$$
$$+ (0.4274) \times T_{0,F} \times V_{1,w,mph}^{0.16} \tag{2.81}$$

$$T_{w.ch,2} = 35.74 + (0.6215) \times T_{0,F} - (35.75) \times V_{2,w,mph}^{0.16} +$$
$$(0.4274) \times T_{0,F} \times V_{2,w,mph}^{0.16} \tag{2.82}$$

Since the above calculated wind-chill temperatures are in ^{0}F, they need to be converted to degrees Kelvin so that they can be used in the exergetic relations. This is done by the following equations, where $T_{1,w}$ and $T_{2,w}$ are the wind chilled temperatures in Kelvin before and after the turbine respectively.

$$T_{1,w} = \frac{5}{9} \times \left(T_{w.ch,1} - 32\right) + 273 \tag{2.83}$$

$$T_{2,w} = \frac{5}{9} \times \left(T_{w.ch,2} - 32\right) + 273 \tag{2.84}$$

Also required for the exergetic analysis is the average temperature of the wind stream as it flows through the turbine and the wind pressures before and after the turbine. The average temperature is obtained by simply taking the arithmetic mean of the wind-chilled temperatures.

$$T_{w,avg} = \frac{\left(T_{1,w} + T_{2,w}\right)}{2} \tag{2.85}$$

The wind pressure before and after the wind turbine can be calculated as follows:

$$P_{1,w} = P_{atm} + \frac{\rho \dfrac{V_{1,w}^2}{2}}{1000} \tag{2.86}$$

$$P_{2,w} = P_{atm} + \frac{\rho \dfrac{V_{2,w}^2}{2}}{1000} \tag{2.87}$$

The exergetic analysis is conducted by finding the different components of the wind's flow exergy, namely the physical exergy, $\dot{X}_{Ph}$, and the kinetic exergy, $\dot{X}_K$.

The physical exergy is the exergy of the flow that is due to its sensible heat, and that which is left after irreversibility due to temperature difference between the ambient and the wind have been taken into consideration.

The kinetic exergy is the exergy that the flow contains due to its velocity, and is thus the exergy transferred to the turbine is the form of mechanical work produced in the turbine, i.e. rotation of the blades.

$$\dot{X}_{w,flow} = \dot{X}_{Ph} + \dot{X}_K \tag{2.88}$$

The physical exergy rate can further be expressed by Equation 2.89.

$$\dot{X}_{Ph} = \dot{m}_w [c_{p,a}\left(T_{2,w} - T_{1,w}\right) + T_0[c_{p,a}\left(ln\left(T_{2,w}\right) - ln\left(T_{1,w}\right)\right)$$
$$- Rln\left(P_{2,w}/P_{1,w}\right) - c_{p,a}\frac{\left(T_0 - T_{w,avg}\right)}{T_0}]]/1000 \tag{2.89}$$

Whereas the kinetic exergy is also taken to equal the work done by the wind:

$$\dot{X}_K = \dot{W}_w \tag{2.90}$$

Lastly, the exergetic efficiency of the wind turbine is given by:

$$\eta_{II,W} = \frac{\dot{P}_w}{\dot{X}_{w,flow}} \tag{2.91}$$

2.7   Modeling: Photo-Voltaic Thermal

The equations used to model the PV/T have been adopted from the models in [121], [50] and [1]. Numerical values of constants used in the analysis are listed in Table 4. Depending on which integration option the PV/T is sized for, electricity generated by the PV/T can be used for the houses and the compressor of the CGVCS.

While 21 kW has to be generated for the integrated options Cases 1 and 3, 1.5 kW is needed for Case 2. However, the PV/T model is first developed for a building block array that can produce 0.5 kW, and later the number of building blocks required is determined. The necessary number of PV modules required to make up the building block is defined as:

$$Nom = \frac{A_{PV}}{0.605} \tag{2.92}$$

where 0.605 m^2 is the area of one module. The overall heat transfer coefficient from the solar panel to the ambient through the top and bottom surfaces of the insulation is:

$$U_L = U_b + U_t \tag{2.93}$$

where U_b the overall is heat transfer coefficient from the bottom of the panel to the ambient, and U_t is the overall heat transfer coefficient from solar cell to the ambient through the glass cover. The heat transfer coefficient from black surface to air, h_{ba} is assumed to be equal to the heat transfer coefficient from the bottom surface to air through the glass, h_t.

$$h_{ba} = h_t \tag{2.94}$$

The power generated by the PV, in kW, is determined from the expression:

$$\dot{P}_{PV} = (\eta_{cell} \cdot I \cdot \beta_c \cdot \tau_g \cdot A_{PV})/1000 \tag{2.95}$$

where η_{cell} is the solar cell efficiency, I is the irradiance in W/m^2, β_c is the solar cell packing factor, τ_g is the transitivity of the glass and A_{PV} is the area of the array. The rate of heat produced by the PV/T is determined from the relation:

$$\dot{Q}_{PVT} = \frac{\dot{m}_a c_{p,a}}{U_L} \left[h_{p,2} \cdot z \cdot I - U_L \left(T_{a,i} - T_0 \right) \right] \cdot \left(1 - \exp \frac{(-b \cdot U_L \cdot L)}{\dot{m}_a c_{p,a}} \right) \qquad (2.96)$$

where $h_{p,2}$ is the penalty factor due to the presence of the black surface and z is further defined as:

$$z = \alpha_b \cdot \tau_g^2 \cdot (1 - \beta_c) + h_{p,1} \cdot (\tau_g \cdot \beta_c \cdot (\alpha_{cell} - \eta_{cell})) \qquad (2.97)$$

where $h_{p,1}$ is the penalty factor due to the presence of solar cell material, glass and EVA (Ethyl Vinyl Acrylate) for a glass to glass PV/T system. The heat produced by the PVT is also given by the relation:

$$\dot{Q}_{PVT} = \dot{m}_a \cdot \left(T_{a,o} - T_{a,i} \right) \qquad (2.98)$$

Table 4: Inputs and constants for the solar PV/T model

Parameter and unit	*Symbol*	*Value*
Area of building block PV module (m^2)	A_{PVT}	11
Breadth of building block PV module (m)	b	0.45
Penalty factor due to the presence of solar panel materials (solar cell material, glass and EVA for this glass-glass PV/T.	$h_{p,1}$	0.9782
Penalty factor due to the presence of interface between glass and working fluid through absorber plate for this glass-glass PV/T.	$h_{p,2}$	0.1890
Intensity of solar radiation (W/ m^2)	I	variable

Table 4: Inputs and constants for the solar PV/T model (continued)

Parameter and unit	Symbol	Value
Heat transfer coefficient from back surface to air through glass (W/ m^2.K)	h_t	6.5
Length of PV module (m)	L	1.2
Atmospheric pressure (kPa)	P_0	101
Atmospheric temperature (^{0}C)	T_0	25
Inlet temperature of air (^{0}C)	$T_{a,i}$	32
Surface temperature of the sun (^{0}C)	T_{sun}	5777
Overall heat transfer coefficient from bottom to ambient (W/ m^2.K)	U_b	0.62
Overall heat transfer coefficient from solar cell to ambient through glass cover (W/ m^2.K)	U_t	2.8
Overall heat transfer coefficient from glass to black surface through solar cell (W/ m^2.K)	U_{tb}	8.11
Absorptivity of black surface	α_b	1
Absorptivity of solar cell	α_{cell}	0.9
Packing factor of solar cell	β_c	0.83
Solar cell efficiency	η_{cell}	0.12
Transitivity of glass	τ_g	0.95

The exergy rate of the heat from the sun can be determined by:

$$\dot{X}_{solar} = (1 - (T_0 + 273.15)/T_{sun}) \cdot I \cdot A_{PV} \tag{2.99}$$

The first law thermal efficiency of the PVT is given by the expression:

$$\eta_{th,PVT} = (\dot{Q}_{PVT} \cdot 1000)/(I \cdot b \cdot L) \tag{2.100}$$

Whereas the first law electrical efficiency, which is temperature dependent, is given by the relation used by [51]:

$$\eta_{el,PVT} = \eta_c \cdot (1 - 0.0045 \cdot (T_c - 25)) \cdot 100 \tag{2.101}$$

where T_c is given by the relation:

$$T_c = \frac{\left[\tau_g \cdot \beta_c \cdot I \cdot (\alpha_{cell} - \eta_{cell}) + U_t \cdot T_0 + h_t \cdot T_{bs}\right]}{(U_t + h_t)} \tag{2.102}$$

The back surface temperature of a PV module T_{bs} in the above relation is given by:

$$T_{bs} = \frac{\left[z \cdot I + T_0 \cdot (U_b + U_{tb}) + h_{ba} \cdot T_{a,avg}\right]}{(h_{ba} + U_b + U_{tb})} \tag{2.103}$$

Whereas the expression for $T_{a,avg}$ is given by:

$$
\begin{aligned}
T_{a,avg} = \left[T_0 + \frac{h_{p,2} \cdot z \cdot I}{(U_L)}\right] \cdot \left(1 - \exp\left(-bU_L L/\dot{m}_a c_{p,a}\right)\right) \\
+ T_{a,i} \cdot \exp\left(-bU_L L/\dot{m}_a c_{p,a}\right)
\end{aligned} \tag{2.104}
$$

The overall exergetic efficiency of the PVT covers both, the thermal and the electrical aspect, as expressed by [121], is:

$$
\begin{aligned}
\varepsilon_{PVT} = \frac{\left[(\eta_{el,PVT}) \cdot (1 - \beta \cdot \Delta T) \cdot I \cdot A_{PV}\right]}{I \cdot A_{PV}} + \\
\frac{\dot{Q}_{PVT}\left(1 - \dfrac{T_0 + 273}{T_0 + 273 + \Delta t}\right)}{I \cdot A_{PV}}
\end{aligned} \tag{2.105}
$$

where β and ΔT are given by:

$$\Delta T = T_{a,o} - T_0 \tag{2.106}$$

$$\beta = 0.0045 \,^0C \tag{2.107}$$

2.8   Modeling: Clathrate Latent Heat Storage System

In order to calculate the amount of clathrate required to cool the houses over the year, the average length of the night in hours was calculated for every month. This was then multiplied by the peak load during the night and a factor of 0.75 to account for drops in temperature during the night. This in turn predicts the total amount of cooling in kJ required from the clathrate. The procedure that allowed us to calculate the total household cooling loads is as follows. The cooling loads are mainly due to the following five sources of sensible and latent heat:

- electrical lighting and household appliances
- people
- air exchanges through the villa envelope
- conduction
- solar heat gain

Heat loads experienced due to the floor are negligible and ignored [122].

2.8.1. Electrical lighting and household appliances.

Lighting was assumed to be of two types, 100 W incandescent bulbs and tube-light arrays of 4 tube-lights/array, with each array consuming 4x15W=60W. Each room then had appliances accounted for. Distribution of lighting and appliances resulted in a total wattage consumption $\dot{Q}_{appl}$ of 3390 W for each house. It was then assumed that for each watt of electricity consumed, one watt of heat was released.

2.8.2. Heat gains due to people.

These resulted from the 6 residents and 3 visitors that were approximated to be living/frequenting each house. A maximum residence factor (M.R.F.) was applied to account for people entering and leaving the house, with the factor equaling 0.8.

Thus, the final load that needed to be handled by the HVAC unit would be the load due to 6+3=9 people, multiplied by this factor. Each person was assumed to emit 75 W and 70 W of sensible and latent heat, respectively.

These figures are commonly used by the HVAC industry to calculate sensible and latent loads due to persons. The total average sensible ($\dot{Q}_{ppl}$) and latent loads due to people thus worked out to 540 W and 504 W respectively for each villa.

2.8.3. Heat gains due to air exchanges through the villa envelope.

These were calculated based on ASHRAE conditions for acceptable indoor air quality. Fresh air requirements as per ASHRAE Standard 62-87 guidelines amount to 7.5 liters/second/person [122] which equals 0.054m^3/s/villa after considering the MFR.

Thus, fresh hot or cold air is exchanged with the ambient either through the HVAC system or through infiltration which affects the cooling load. Based on the fresh air requirements, the infiltration heat transfer coefficient for the envelope is calculated:

$$K_{exch} = (\rho C_p)_a \dot{V}_{a,exch} \tag{2.108}$$

2.8.4. Heat gains due to conduction.

Since the outdoor weather conditions are rarely identical to the indoor condition, there almost always exists a temperature difference between the two which results in a temperature gradient in the outermost walls, i.e. the envelope. As a result, conduction takes place down this temperature gradient and affects the indoor condition.

At higher surroundings temperature, more heat will be conducted into the houses and vice versa. In order to determine the amount of heat transferred by conduction, it is necessary to obtain the conductive heat transmission coefficient K_{cond} for the walls and roof.

This is done using the following equations:

$$U = k/\Delta x \tag{2.109}$$

$$K_{cond} = U \cdot A \tag{2.110}$$

where k is the conductivity of the wall material in W/m.K which can be concrete or glass with glazing for the windows, Δx is the average thickness of the wall material, U is the conductance of the material, and A is the area covered by the wall material. The different parameters used to determine the K_{cond} values for an individual villa are given in Table 5.

The overall heat transfer coefficient K_{ov} is then determined to be:

$$K_{ov} = K_{cond} + K_{exch} \tag{2.111}$$

This overall heat transfer coefficient is then used to determine the total heat gain due to temperature difference between the environment and the envelope.

For the cooler months, it is seen that heat is lost to the environment whereas for the warmer months there is a net flow of heat into the envelope as expected. The heat gain due to temperature difference is then calculated to be:

$$\dot{Q}_{\Delta T} = K_{ov} \cdot (T_{in} - T_{out}) \qquad (2.112)$$

The sensible load that thus needed to be met by the clathrate system is the summation of the heat gain due to air exchanges and conduction across the envelope, and the heat gains due to the occupants and the lighting and appliances, i.e.

$$\dot{Q}_{clath} = \dot{Q}_{appl} + \dot{Q}_{ppl} + \dot{Q}_{\Delta T} \qquad (2.113)$$

Table 5: Parameters for heat gains due to conduction

Parameter and unit	Symbol	Value
Average height of external wall (m)	H_{wall}	2.5
Average height of double glazed window (m)	H_{win}	1.5
Thickness of wall (m)	Δx	0.2
Conductivity of wall concrete (W/m.K)	k	0.72
Conductance of wall concrete (W/m^2.K)	U_{wall}	3.6
Conductance of glazed window (W/m^2.K)	U_{win}	3
Conductive heat transmission coefficient (dependent on area)	K_{cond}	Variable

It is assumed that the cooling using the clathrate would take place immediately after sunset, as up-to that point the PTSC would be supplying the necessary heat to the absorption system to provide cooling (we assume that there is a storage tank that stores the hot water which supplies enough heat until sunset to run the absorption in case there is a lack of solar irradiation to heat the water sufficiently).

The clathrate system was designed for a mass ratio of 2.23, i.e.

$$M.R. = \frac{mass\ of\ H_20}{mass\ of\ refrigerant} \qquad (2.114)$$

In the thermal energy storage system, the refrigerant used is R-134a. It is to be noted that 2.23 is the ratio in which the clathrate always forms, and hence this ratio was decided upon for the system.

Since we are concerned with how much power the compressor of the vapor compression cycle forming the clathrate would consume, only the charging process, i.e., that of forming the clathrate, is of interest to us.

The change in temperature for this charging process is seen to follow a decreasing path with decelerating pace. This, from intuition, can be attributed to the decreasing amounts of sensible and latent heat available in the reactants as the clathrate forms.

Data points previously plotted for the temperature trend for different mass ratios were extracted and plotted, and six-degree polynomials fitted through them. These were then used to determine the temperature trend for a mass ratio of 2.23, the polynomial for which is below:

$T_{2.23}$ = 23.3960703 - 1.90281729· (t) + 0.102141777·(t^2) –

$\qquad$ 0.00281201365·(t^3) + 0.000040061903· (t^4) – $\qquad\qquad$ (2.115)

$\qquad$ 2.82912333· (10^{-7}) · (t^5) + 7.82569077 · (10^{-10}) · (t^6)

Plots of power were also produced for the mass ratio of 2.23 based on enthalpy based calculations and on V.I calculations. However, due to the nature of the curve, it was impossible to fit a curve through it, and hence plots were approximated using the 65th rule.

2.8.5. Heat gains due to solar radiation.

Exposure to solar radiation results in solar heat gain. Since the walls and roofs of the villas are exposed to sunlight, a large amount of heat is accumulated within the building material, with considerable heat being transferred into the envelope for as long as a temperature gradient exists between the ambient and the inside of the villas. This is one of the primary reasons we need cooling in a hot climate such as the U.A.E.s, and thus naturally, it puts a huge strain on the cooling apparatus. However, more heat is transferred into the envelope through clear surfaces such as windows and skylights rather than walls, so much so that solar heat gain through walls is negligible if the window area is considerable [122]. The heat gain through the windows is calculated using the expression:

$$\dot{Q}_{sol,win} = A_{win} \cdot SC \cdot SHGF \tag{2.116}$$

where $\dot{Q}_{sol,win}$ is the solar heat gain through the windows, A_{win} is the total area covered by windows for each villa, SC is the shading coefficient of the window panes, and $SHGF$ is the Solar Heat Gain Factor. SHGF is the solar heat gain through DSA (double standard sheet) glass and is taken to be equal to the product of $F \cdot I$. The solar heat gain coefficient F is a constant of proportionality taken to be 0.58. For double glazing as is used in our case, F is given by:

$$F = \tau + \alpha_0 \cdot \frac{U}{h_0} + \alpha_i \cdot U \cdot \left(\frac{1}{h_s} + \frac{1}{h_0}\right) \quad with \quad \frac{1}{U} = \frac{1}{h_i} + \frac{1}{h_s} + \frac{1}{h_0} \tag{2.117}$$

where τ is the transmissivity, α_0 and α_i are the absorptivities of the inner and outer panes respectively, h_s is the heat transfer coefficient of the space between the two panes and is the sum of the radiation and convection terms for transfer across one air-space, and h_i and h_0 are the overall (combined for radiation and conduction/convection) heat transfer coefficients of the inner and outer panes respectively. The shading coefficient SC is the ratio of F for the glazing being considered to the F for the reference glazing, taking DSA as the reference glazing, where DSA has a F value equaling 0.87, i.e.:

$$SC = \frac{F_{glazing}}{F_{refer}} \tag{2.118}$$

The solar heat gain through the windows and walls is calculated for every month. Walls are less susceptible to solar heat gain, with typical values being approximately a fifth of the solar heat gain through windows.

Also, total wall area exposed to the sun is found to be 2.5 times the window area. This information is used to calculate the heat gain through the walls, which is thus approximately half the heat gain through the windows:

$$\dot{Q}_{sol,wall} = \dot{Q}_{sol,win} * 2.5 * 1/5 \tag{2.119}$$

The sensible heat load to be met by the absorption system during the daytime is the summation of the heat load to be met by the clathrate system and the heat gain due to solar radiation. However, since the component of the heat gain through the windows due to solar radiation already accounts for conduction, the separate calculation of K_{cond} is omitted in the calculation of the sensible heat load met by the absorption system (for the daytime hours). The evaporator load then becomes:

$$\dot{Q}e = \dot{Q}_{sol,win} + \dot{Q}_{sol,wall} + \dot{Q}_{clath} \tag{2.120}$$

The cooling capacity in kW, when it is multiplied by the number of hours for which cooling is needed during the day, gives us the daily amount of cooling required from the clathrate in kJ. This figure, divided by the latent heat of clathrate, which is taken to be 358 kJ/kg, estimates the mass of clathrate required to be generated on average daily for that particular month.

2.9 Modeling: Hot Thermocline Storage

In order to make the generation of heat using solar energy attractive, thermal energy storage needs to be employed. Solar energy has some primary characteristics such as low energy density and an intermittent and dynamic supply, which result in the solar energy being gathered exhibiting non-continuous and non-steady state features, and as a result necessitate the use of thermal storage. Hot water thermocline storage tanks are one such form of storage, and have been included in this thesis as a form of thermal storage to store sensible heat that will allow us to run the absorption system in the absence of sunlight. The use of a hot water storage tank as TES necessitates the determination of suitable dimensions for the tank, as well as arrangement for an appropriate energy input source. Hence the PTSC needs to be resized so that it suffices

both the tank charging requirements as well as the day-time heat requirements of the absorption system. Moreover, to gain insight into the feasibility of such a storage system, it is beneficial to obtain its charging efficiency on both, a daily and monthly basis.

In order for the determination of the size of the tank required to be conducted, we first determine the amount of heat to be stored in kWh. This is a four step process. The initial step is to calculate the average length of time for which the storage is to be used. This includes hours of night-time as well as the number of hours that sunlight is insufficient to run the absorption systems, such as dusk and dawn. This is done for every month.

Next, the cooling requirement for the average length of is determined using the monthly ambient conditions. These are subsequently used to calculate, monthly, the average daily heating requirement in kWh during non-availability of daylight.

The highest of these values is then converted into kJ and incremented by the amount of heat required for heating the tank up from the lowest temperature reached during nighttime to the desired tank temperature of 192.5^0C, and the result is used as the design value for the amount of heat to be stored by the tank.

It shall be seen later that the size of the tank is not affected by heat losses from the tank as these are negligible.

Based on the calculations, it is seen that the month with the most amount of heat required on average, is August, when 119.9 kWh of heat are required to run the absorption system during hours of insufficient/absent sunlight. Since we know the amount of heat to be delivered, we can determine the volume of the tank. The volume of the tank is found using a known quantity - the density of water, and an unknown quantity - the mass of water.

The mass of water is determined using the specific heat capacity of water and the amount of heat needed to be stored. The mass is determined to be 103,177 kg for an average C_p of 4.187 kJ/kg.K. Thus, for a tank height of 5m, the radius is determined to be 2.563m, i.e. the diameter of the tank is 5.126m.

$$mass = \frac{119.9 \; kWh * 3600 \frac{kJ}{kWh}}{4.187 \frac{kJ}{kg.K}} \qquad (2.121)$$

Accordingly, the volume is found to be:

$$volume = \frac{mass}{density} = \frac{103177\ kg}{1000\ \frac{kg}{m^3}} = 103.177\ m^3 \tag{2.122}$$

Next, it is to be noted that heat loss from a thermal storage tank is inevitable. After the tanks size being decided, it's necessary to estimate the heat loss to see if sufficient heat can be stored after accounting for heat losses.

To compensate for the heat loss, a larger volume of the heat storage tank and a longer heat charge period may be needed. Li et al. [123] propose that a simple way of refining the design is to increase both the heat charge time and tank size with a percentage equal to the ratio of heat loss versus the projected heat delivery.

In order to do this, the losses have to be calculated first, and are determined as follows.

$$\dot{Q}_{l,hst} = U \cdot A_h(T_{hst} - T_0) \tag{2.123}$$

where

$$A_h = 2\pi r h + 2\pi r^2 \tag{2.124}$$

$$U = 0.00016 \frac{kW}{m^2 \cdot K}$$

The value for U is taken to be the recommended U value for hot water storage tanks given in [44] and A_h is the area of a cylinder. Based on the above equations, the area A_h is calculated to be 121.79m^2.

The hourly charging efficiency of the tank is defined as:

$$\eta_{ch,HTS} = Q_e/Q_{PTSC} \tag{2.125}$$

Whereas the COP of the charging process, which allows us to compare the performance of the HTS-TEAS system to that of the CGVCS as a night-time cooling system, is:

$$COP_{HTS,TEAS} = Q_e/Q_{HTS} \tag{2.126}$$

where Q_{HTS} is the net heat added to the HTS, i.e. the amount of heat added to the HTS minus the losses to the surroundings.

2.10 Modeling: Battery Storage

The last sub-system to be considered for integration is the battery storage. Deep cycle batteries were chosen based on their merit of holding charge for long periods of time, and the battery rating was calculated by the following expression:

$$Battery\ charge\ (kAh) = \frac{[\dot{P}_{out}\ (kW) * (\#\ hours) * (\#\ days)]}{Voltage\ (V)} \tag{2.127}$$

2.11 Modeling: Integrated Options

The methodologies used to evaluate the three different integrated options are given in this section.

Since the daytime cooling aspect of the sustainable system is handled by the triple effect absorption system and the PTSC working in conjunction, it is necessary to develop a parameter to gauge the performance of the combined system integrating the two technologies.

These parameters were the overall energetic and exergetic COPs. Two different expressions for the overall energetic COP of the PTSC-TEAS were used. The monthly overall energetic COP was obtained using both expressions and the results plotted.

The first formulation uses the outputs from the PTSC and the TEAS to define the COP whereas the second uses a product of the performance parameters, i.e. efficiency and COP of the PTSC and the TEAS. The expressions are defined as below:

$$COP_{EN,PTSC-TEAS,1} = (\dot{Q}e/\dot{Q}_{PTSC}) \tag{2.128}$$

$$COP_{EN,PTSC-TEAS,2} = \eta_{PTSC} \cdot COP \tag{2.129}$$

For the overall exergetic COP, the term 'efficiency' is used instead of 'COP' because the values obtained had a magnitude less than 1. The overall exergetic efficiency of the PTSC-TEAS system can be defined as:

$$\varepsilon_{PTSC-TEAS} = \dot{X}_{\dot{Q}e}/\dot{X}_{\dot{Q}_{PTSC}} \tag{2.130}$$

With the villas being cooled during the daytime using the PTSC-TEAS integrated system, night-time cooling is achieved through the use of the integrated solar PVT-LHSCS.

The overall energetic efficiency of this solar PVT-LHSCS integrated system is:

$$\eta_{PVT-LHSCS} = \frac{\dot{Q}_{LHSCS} + \dot{Q}_{PVT}}{I \cdot b \cdot L} \tag{2.131}$$

For the case where both wind and PVT are used to provide electricity to the household, the overall energetic efficiency of the WTS-PVT system becomes:

$$\eta_{PVT-WTS} = \left(\frac{\dot{P}_{PVT} + \dot{Q}_{PVT} + \dot{P}_W}{\dot{W}_W + I \cdot b \cdot L} \right) \tag{2.132}$$

And the overall exergetic efficiency is:

$$\varepsilon_{PVT-WT} = \left(\frac{\dot{P}_{PVT} + \dot{X}_{PVT} + \dot{P}_W}{\dot{X}_{w,flow} + I \cdot A_{PV}} \right) \tag{2.133}$$

where

$$\dot{X}_{PVT} = \left(1 - \frac{T_0}{T_{a,o}} \right) \cdot \dot{Q}_{PVT} \tag{2.134}$$

For calculating the overall energetic and exergetic efficiencies of the complete integrated system cases 1,2 and 3, the following expressions are used:

$$\eta_{Case\ 1,2,3} = \left(\frac{\dot{P}_{PVT} + \dot{Q}_{PVT} + \dot{P}_W + \dot{Q}_e}{\dot{W}_W + I \cdot b \cdot L + I \cdot A_{ap}} \right) \tag{2.135}$$

$$\varepsilon_{Case\ 1,2,3} = \left(\frac{\dot{P}_{PVT} + \dot{X}_{PVT} + \dot{P}_W + \dot{X}_{\dot{Q}e}}{\dot{X}_{w,flow} + I \cdot A_{PV} + I \cdot A_{ap}} \right) \tag{2.136}$$

Chapter 3: Results

In this chapter, the results of the thermodynamic analysis of the integrated systems studied in this thesis are presented. Modification of the various parameters that govern the performance of the individual subsystems and the overall system give us an insight into the factors that affect the performance most significantly. First, the individual subsystems are studied, & then different integration options are analyzed.

3.1   Solar and Wind Potential Determination

In order to determine the feasibility of the use of solar and wind systems, it was imperative to initially conduct a Solar and wind potential assessment, site selection and weather data assessment. This was a crucial step because though the middle-east's potential for solar power is relatively common knowledge, knowledge about the Middle East's wind energy potential is not as the mainstream. Moreover, literature on the U.A.E.'s wind potential is quite scarce. This necessitates a more thorough investigation which will give us an insight into the potential for the region's power production using wind.

Accordingly, Fujairah was selected as the site for WT installation for two main reasons. This is because it is a coastal town with the one of the best wind regimes because of its geographical location. Previous studies by both, academics and industry, have shown that average wind speeds of up-to 7.5 m/s are experienced at this site, thus demonstrating reasonable wind –generation potential.

A well-established Spanish wind energy company by the name of Energia Hidroelectrica de Navarra (EHN), in collaboration with the Fujairah Department of Industry and Economics and the UAE University, found, after 18 months of data collection and economic analysis, that Fujairah has a power generation capacity of 130-200 MW [39].

In order to determine the annual performance of a wind turbine, it was necessary to gather data for every month that would allow us to do a monthly analysis of the wind turbine's performance. Based on the results of these previous studies, the wind turbine was initially planned on being considered the primary source of power for the villas considered in this study.

104

However, wind potential assessment of the site of Fujairah revealed otherwise. The wind turbine sized and selected for this study, the Northern Power 100 WT is one of the newest and most efficient in the market.

Having said that, it will only start to produce power at a cut-in speed of 4 m/s, and will only produce enough power to meet the 4 villas' electricity needs of 15 kW, or 350 kWh daily, at wind speeds above 5.6 m/s. Hourly data collection for the year 2012 shows us this would only be possible during the month of March when average wind speeds are around 6.5 m/s. The rest of the year, wind speeds are below even 5 m/s, with the exception of February, when average wind speeds are 5.1 m/s. Figure 14 shows this monthly wind speed distribution.
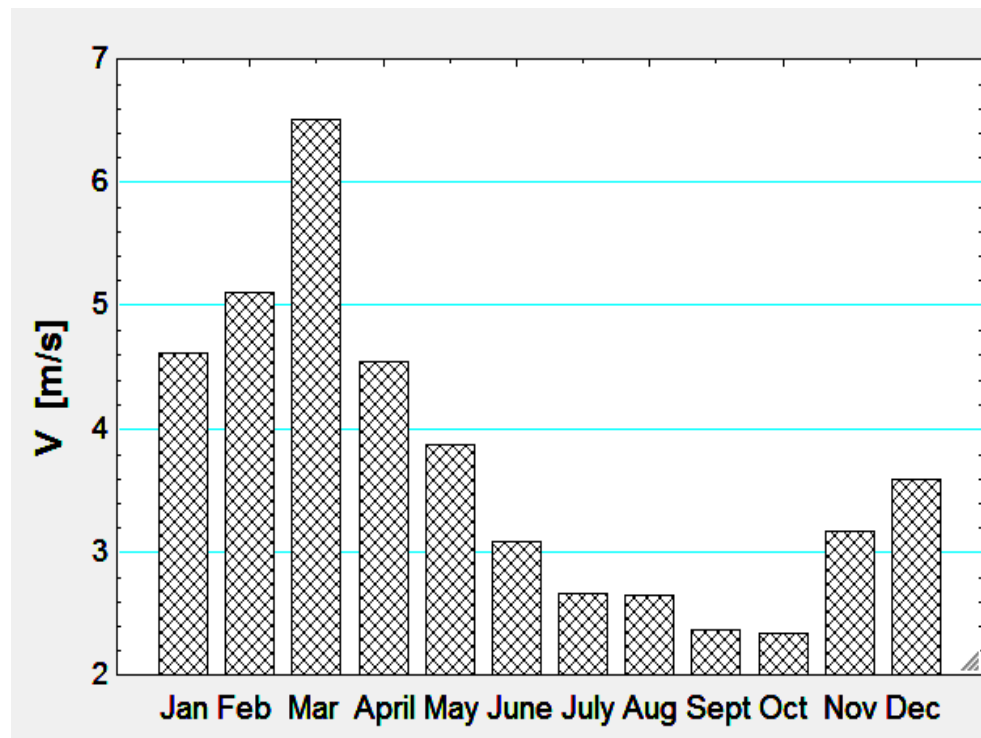

Figure 14 : Average monthly wind speeds for Fujairah, 2012

It is to be noted however, that these wind speed readings have been obtained from a site offshore, and may not be representative of the wind speeds encountered at the shore, which are often higher. Nevertheless, these average wind speeds will be the basis of the calculations in this work to determine the performance of a wind turbine

placed offshore. As for solar prospective, installed solar technology capacity in the U.A.E. will exceed 1.1 GW in the near future. This stands testament to the abundance of solar resources in the country. With an average of 500 W/m^2 available for utilization for many hours a day, solar power can be considered a viable alternative energy option. The solar technologies that are decided upon to be used to trap this ample free and green energy are PVT and PTSC, whereas a horizontal axis wind turbine is assumed to be used to harness wind energy. Solar technologies are just as vital as wind, if not more, given the lackluster potential of the above mentioned wind speeds, and will play an important role in making homes in the gulf sustainable and independent of the grid in the near future.

3.2   Outdoor Conditions and HVAC Selection

In order to determine what air-conditioning loads will be handled by any HVAC system and to design the latter accordingly, it is necessary to know what outdoor conditions are likely to be encountered so that comfort levels can be maintained indoors even in the most severe conditions, that is, appropriate cooling is established. Accordingly, the site weather conditions for the east coast (Fujairah) of the U.A.E. are taken to be the 2% evaporation design ASHRAE 2009 standards for Abu Dhabi: a wet bulb temperature of 29.2^0C and mean coincident dry bulb temperature of 34.1^0C [124]. Monthly average dry-bulb temperatures for the daytime and night-time needed for this work are given below. In order to design for the worst case scenario, daytime averages are calculated by averaging maximum temperatures reached over the year 2012. Figure 15 illustrates this. For night-time averages, the average temperature encountered over the whole day, and the average of this latter value for each month, is listed by ASHRAE.

In order for the analysis to consider the worst case scenario, these temperatures are taken to be the average monthly night-time temperatures, and are given in Figure 16. In order to brave the severe hot climate of the U.A.E., air-conditioning is imperative. In this study, the large air-conditioning loads encountered in the U.A.E. will be handled by absorption systems which will be modeled and integrated into the final overall system.
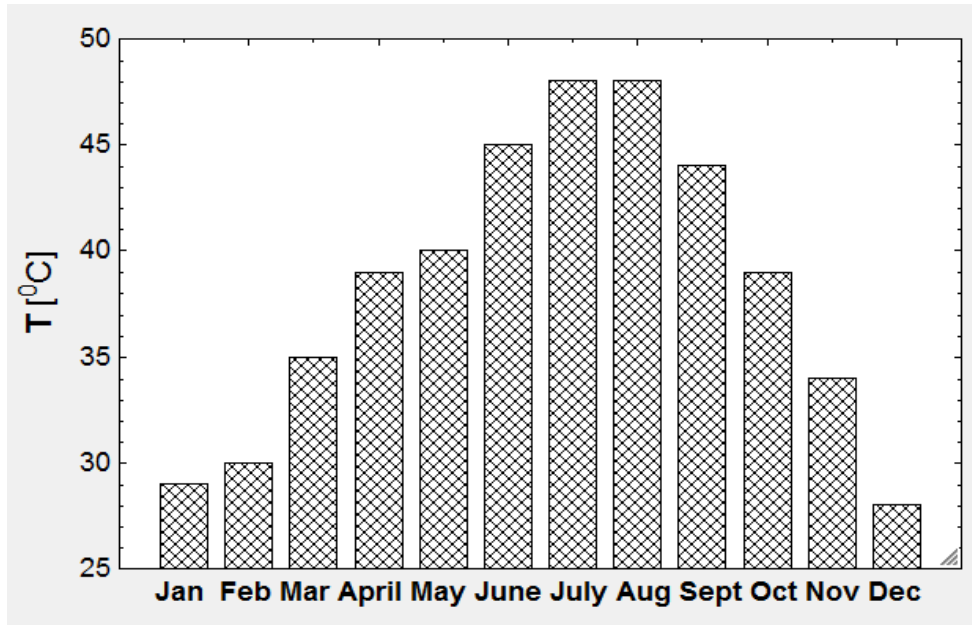
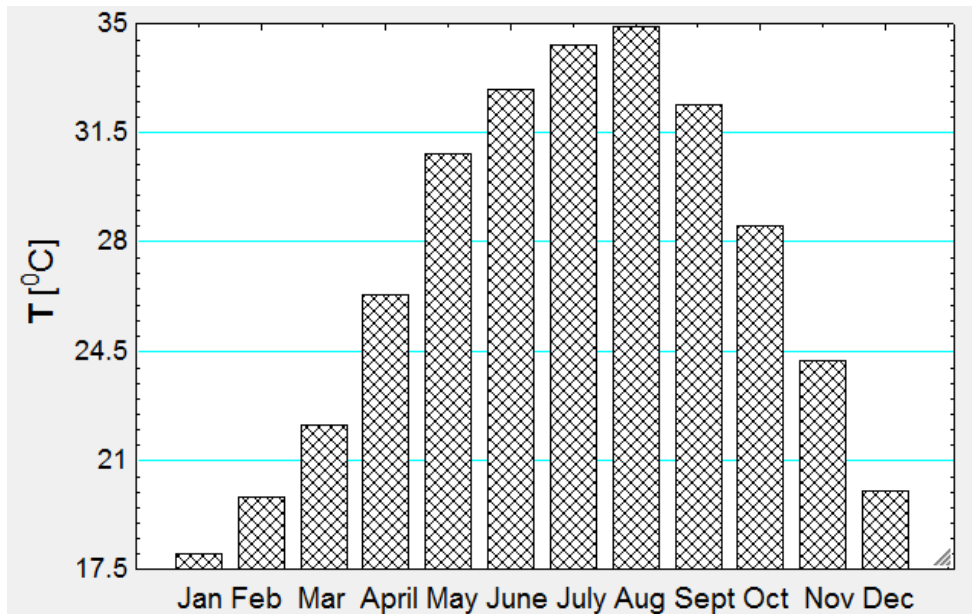Figure 15: Monthly day-time average for the U.A.E.

Figure 16: Monthly night-time temperatures for the U.A.E.

This will allow the villas to be standalone and thus reduce the load on the national grid as well as the power needed to be produced for the community. As a result, environmentally–unfriendly emissions will also be lowered.

3.3   Absorption System

The absorption system that is integrated into the overall system is a triple effect parallel flow machine using LiBr-H$_2$0 as the working fluid. However, to ensure that this was modeled correctly, it was necessary to first model simpler machines with lower effects. The term 'effect' refers to the number of times the input energy is utilized within the machine.

Thus, more effects imply more input energy utilization, consequently, less energy wasted and thus more efficient cycles. Lower effect cycles, namely half, single and double effect cycles, though many in industry and literature, have relatively low COPs, but when modeling multiple-effect cycles, it is necessary to use these lower effect cycles as building blocks to allow comparison of performance at every stage of modeling as 'effects' are added.

3.3.1   Single effect absorption system.

In this work, a single effect, parallel flow absorption cycle was first modeled and the results compared with those by Herold et al.[19].
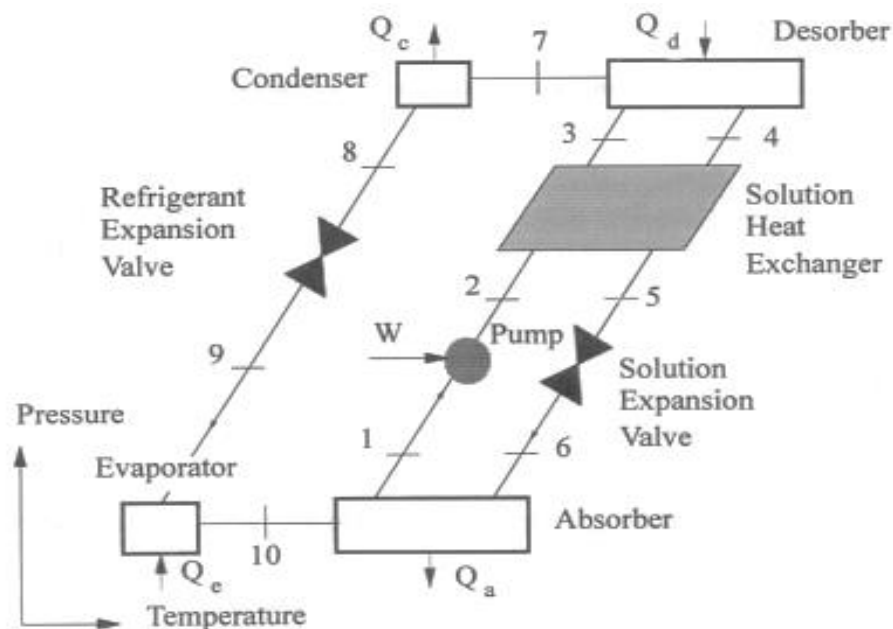

Figure 17: Schematic of a single effect, parallel flow, LiBr-H$_2$0 system

A schematic of a single effect cycle is given in Figure 17, while a comparison of the enthalpies obtained at every state of the base model, is given in Table 6. The similarity between the results obtained from the developed model and that of Herold et.al demonstrates the accuracy of the model. For an absorber mass flow rate of 0.05 kg/s, the COP obtained for our model was 0.714 whereas the model by Herold et al. [19] produced a COP of 0.72. Cycle inputs are identical to those used by Herold et al.

Table 6: Specific enthalpy comparison between single-effect system by Herold et al. [19] and that developed for this study

Herold et al. Enthalpy (kJ/kg)	State	Current Model Enthalpy (kJ/kg)
85.2409	1	86.82
85.2451	2	86.82
159.3	3	147.8
222.5	4	226.1
141.0	5	159
141.0	6	159
2645.0	7	2644
168.2	8	168.3
168.2	9	168.3
2503.1	10	2503

3.3.2 Double effect absorption system.

The single effect cycle is then further developed to a double effect one to enhance the COP. Again, the system is modeled in EES and the results compared with the model of Herold et al. [19] for the same inputs used by the latter in [19]. A schematic of the double effect system can be seen in Figure 18. For an absorber mass flow rate of 1.0 kg/s and various identical system parameters (such as vapor quality, mass fractions, mass flow rates, temperatures, pressures, evaporator load, pump power inputs and heat exchanger effectiveness values), the COP obtained for our model was 1.574 whereas the baseline model by Herold et al. [19] produced a COP of 1.325. The

similarity of the results to that of the reference model again proves the accuracy of the developed model, as seen in Table 7.
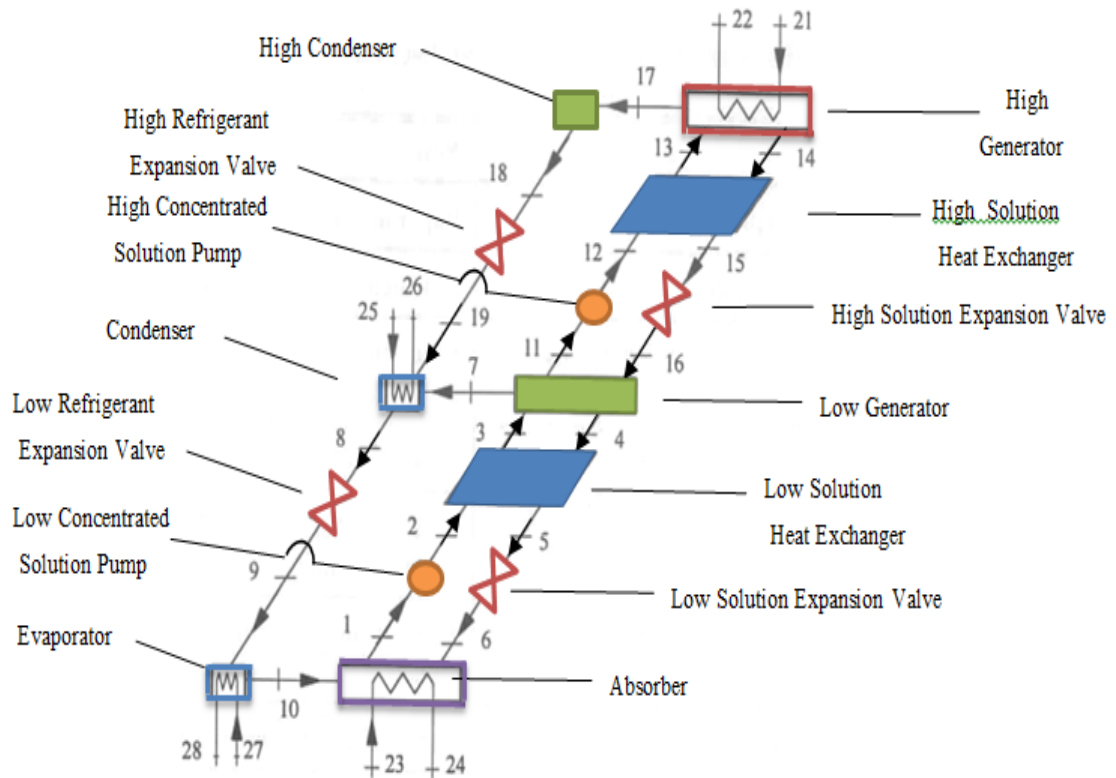

Figure 18: Schematic of a parallel flow, LiBr-H$_2$0 DEAS

Table 7: Specific enthalpy comparison between double-effect system by Herold et al. [19] and that developed for this study

Herold et al. Enthalpy (kJ/kg)	State	Current Model Enthalpy (kJ/kg)
65.59	1	66.78
65.59	2	66.78
102.7	3	111.1
195.0	4	197.8
151.4	5	146.1
151.4	6	146.1
2608.7	7	2608

Table 7: Specific enthalpy comparison between double-effect system by Herold et al. [19] and that developed for this study (continued)

Herold et al. Enthalpy (kJ/kg)	State	Current Model Enthalpy (kJ/kg)
124.5	8	124.5
124.5	9	124.5
2511.0	10	2629
124.28	11	124.7
124.32	12	124.8
194.1	13	228.7
323.3	14	329.6
241.4	15	207.4
241.4	16	207.4
2726.2	17	2726
367.2	18	367.4
367.2	19	367.4

3.3.3   Triple effect absorption system.

Conventional modern vapor-refrigeration systems have an average COP of around 3. Therefore, for absorption systems to compete with this well-established technology, significant performance increases are required. Hence, multiple effect systems have been investigated in literature with very few being commissioned in practice. To gain a performance increase over the double-effect system, a triple-effect system was modeled, and again the results compared to those by Herold et al. [19].

The COP obtained by Herold et al. [19] was found to be 1.645, identical to the COP obtained when running this model. Additional slight modifications to the system and inputs resulted in a COP of 1.943. Table 8 shows the results of the comparison, for the same input conditions given in [19], between the model by Herold et al. and the developed model, the schematic of which is shown in Figure 19.

Table 8: Specific enthalpy comparison between triple-effect model by Herold et al. [19] and that developed for this study

Herold et al. Enthalpy (kJ/kg)	State	Current Model Enthalpy (kJ/kg)
66.4	1	66.4
66.4	2	66.4
101.4	3	101.4
166.8	4	166.8
128.0	5	127.9
128.0	6	127.9
2609.9	7	2608.4
125.6	8	125.7
125.6	9	125.7
2510.7	10	2509.7
126.0	11	126.0
126.0	12	126.0
181.8	13	181.8
268.0	14	268.0
206.2	15	206.2
206.2	16	206.2
2700.6	17	2699.6
311.5	18	311.8
311.5	19	311.8
232.8	21	232.8
232.9	22	233.0
296.8	23	298.1
384.9	24	387.6
314.0	25	315.4
314.0	26	315.4
2799.4	27	2798.8
528.2	28	528.6
528.2	29	528.6
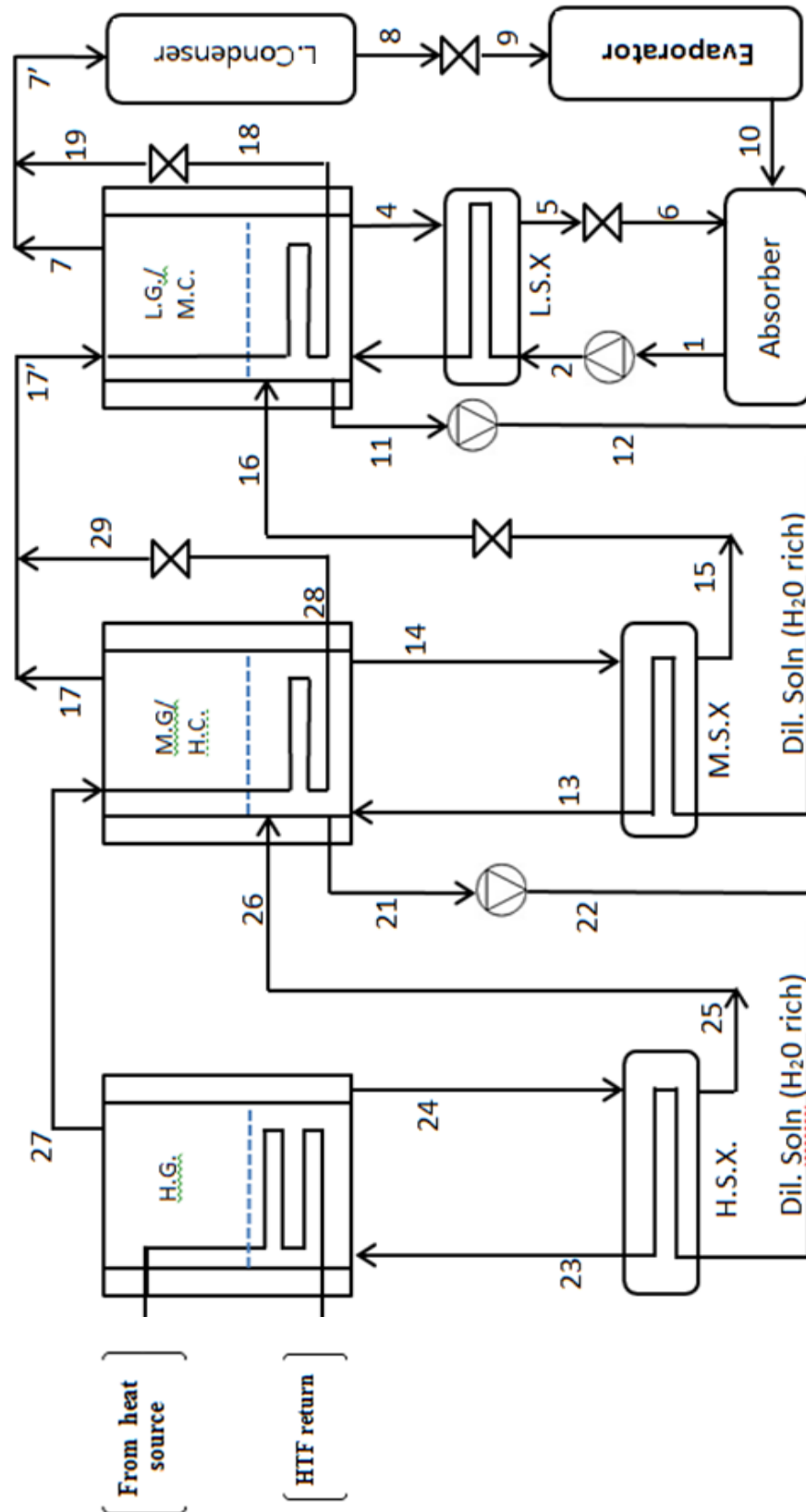
Figure 19 : Schematic of the modeled triple effect, parallel flow, LiBr-H$_2$0 absorption system

Once the triple effect system was modeled and verified, the effects of cycle parameters on the performance of the system were studied. Cycle performance was studied with variation of evaporator temperature, the generator temperature and the condenser temperature, as well as the temperature difference governing heat transfer between the intermediate condenser-generator, while cycle input parameters that remain constant are taken from [19].

Component temperatures were chosen to be the varied parameters as the cycle is most strongly affected by changes in temperatures at its different levels [19]. Performance indicators are the energetic and exergetic COPs of the cycle, which allow us to determine the loss of efficiency due to irreversibilities which cannot be detected otherwise from only an energetic analysis. Also conducted was a monthly analysis of the system where, keeping all other parameters constant, the mass flow rates were altered to meet the cooling loads as they varied from month to month. Figure 20 gives us an idea of the evaporator loads required and produced for the whole year. Input conditions are identical to those in [19], whereas the condenser temperature is assumed to be maintained constantly at 25^0C.

The monthly cooling loads shown in Figure 20 were produced for the input parameters in [19], with variations in evaporator load being brought about by varying the primary flow rate of weak solution from the absorber to the low generator. Figure 21 displays the various mass flow rates needed to achieve the monthly cooling targets.

Once the cooling loads were determined, parametric studies on the absorption system were carried out. The first parameter to be varied was the evaporator temperature T_{evap}. An increase in evaporator temperature results in a sharp increase in the capacity of the evaporator $\dot{Q}_e$ as can be seen in Figure 22. This is because the increase in temperature causes an increase in the evaporator pressure, which in turn increases heat transfer potential.

Also can be seen is an increase in the heat required by the highest desorber (generator) $\dot{Q}_{d,3}$. This can be attributed to the increased pressure in the evaporator, which in turn causes an increase in the pressure in the absorber. The increased absorber pressure causes the mass fraction of the weak (water-rich) solution being sent to the low generator to decrease. This means that the mass of water in the mixture decreases.
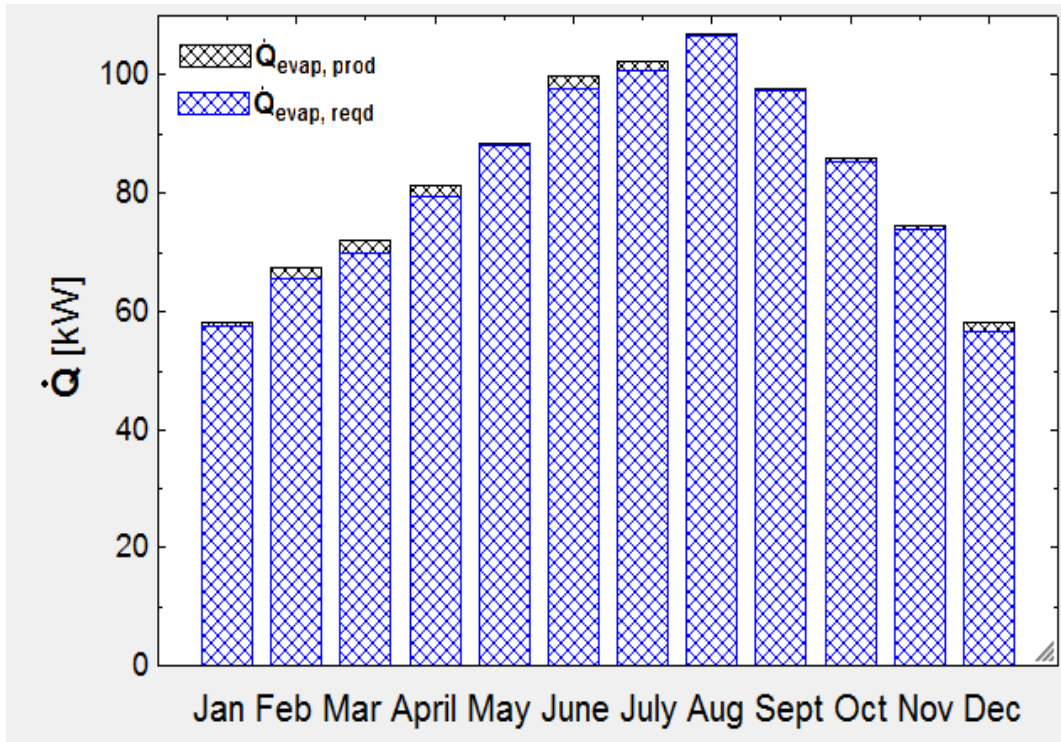
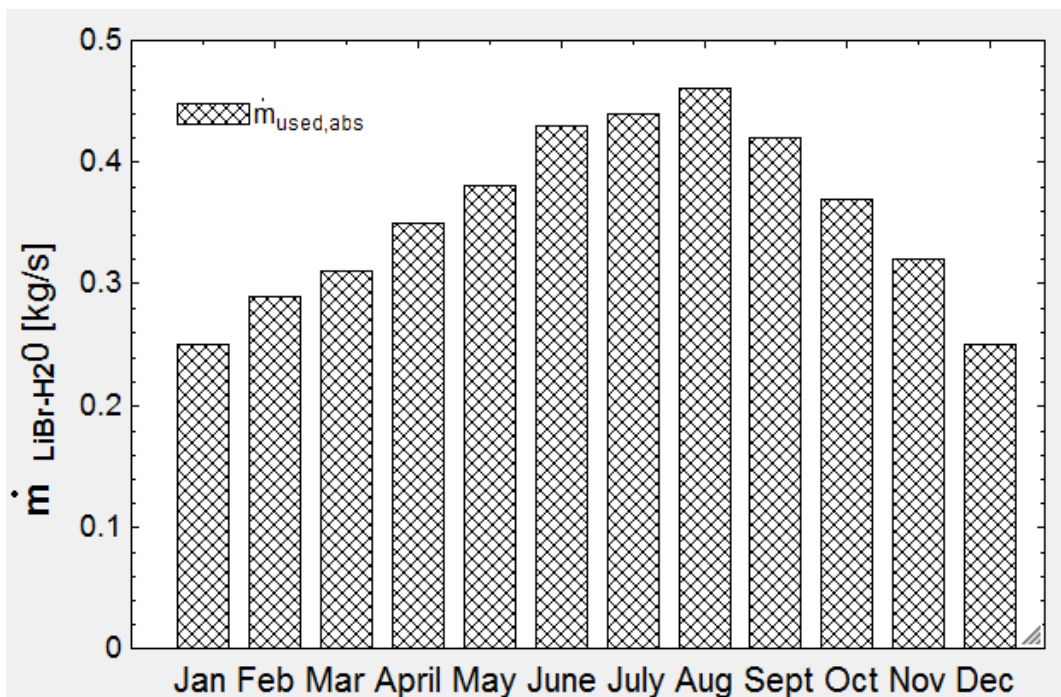Figure 20: Monthly cooling loads and evaporator loads produced

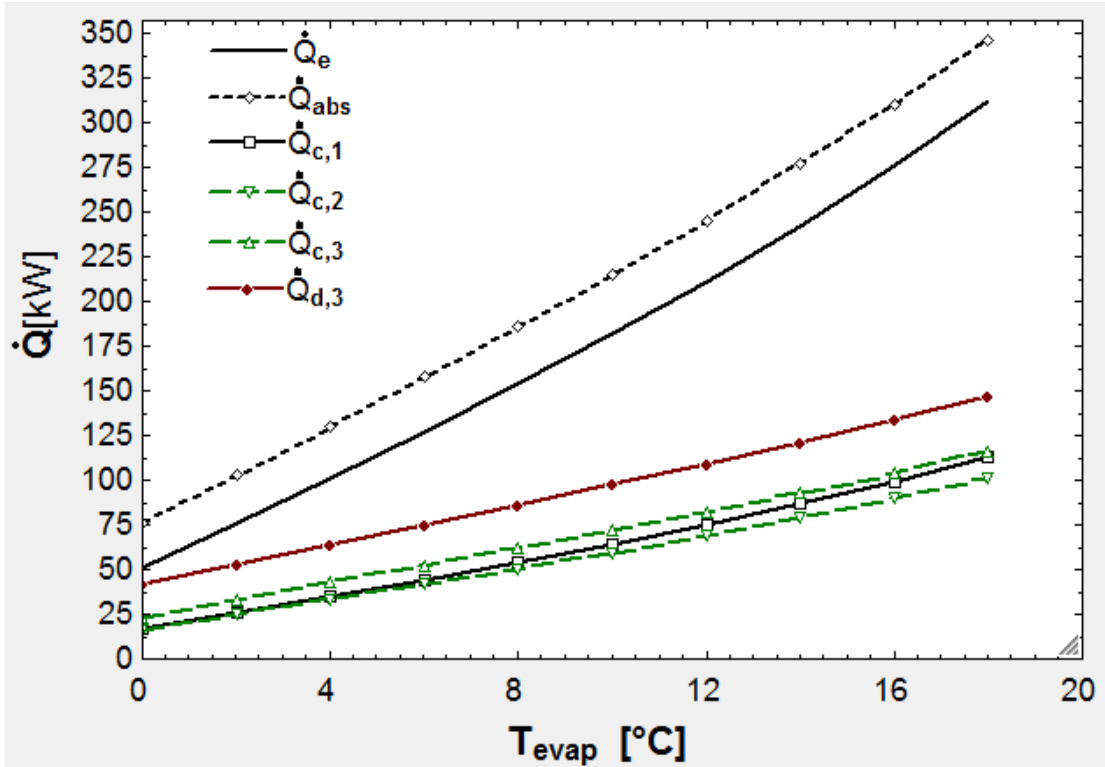Figure 21: Monthly mass flow rates needed to produce required cooling

Figure 22: Variation of cycle conditions with evaporator temperature

Thus, consequently, more heat is required to generate the same amount of vapor to be sent to the evaporator. The increased demand at the lower generator is replicated at the higher generators and eventually causes the increased load seen in the curve.

The increase in the temperature of the return streams from the generators and the evaporator also causes a steep increase in the absorber temperature, hence increasing its heat rejection rate $\dot{Q}_{abs}$, as well as an increase in condenser temperatures throughout the cycle, which explains the increasing trends in the figure of $\dot{Q}_{c,1}, \dot{Q}_{c,2}$ and $\dot{Q}_{c,3}$.

The effect of the increased evaporator temperature is to overall cause an increase in the energetic and exergetic COPs of the system. This can be seen in Figure 23. The energetic COP increases because the increase in evaporator temperature has a more pronounced effect on the evaporator load than on the highest generator, thus making the evaporator load higher than the required generator heat input.
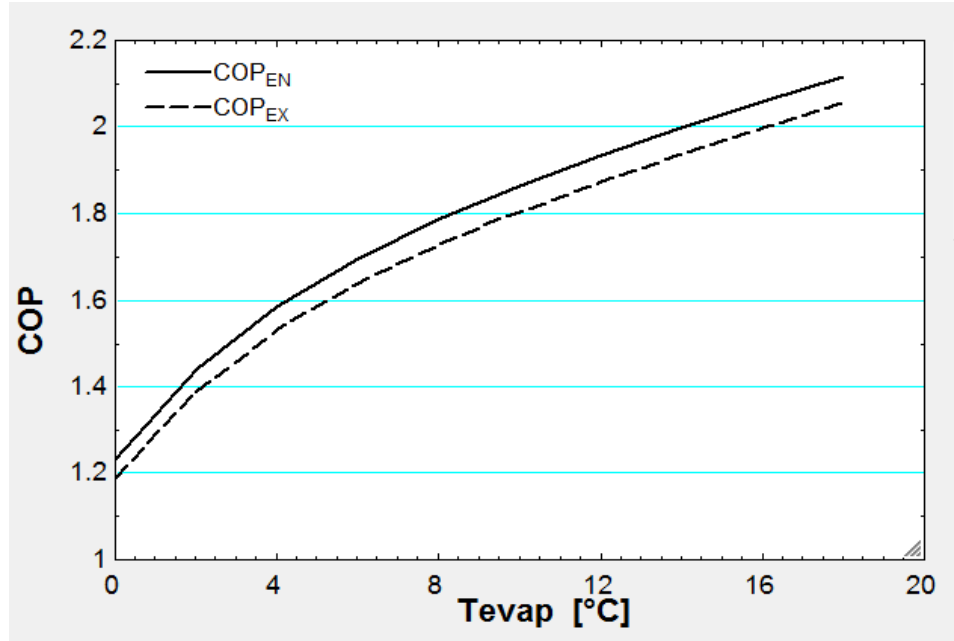
Figure 23: Variation in COP with evaporator temperature

The increase in exergetic COP is linked to the increase in energetic COP in that it is intrinsically linked to the temperatures of the exit streams of the evaporator and the absorber, which are directly affected by the temperatures and heat loads inside the components.

The gradually decreasing rate in Figure 23 is attributed to the heat exchanger duties which increase with increasing heat transferred, hence causing the irreversibilities to increase faster than the increase in heat rate, and thus effectively preventing a linear relationship between temperature and heat transferred.

The next parameter to be varied was the temperature of the highest generator T_{gen}. Once again the evaporator load $\dot{Q}_e$ experiences a greater increase than the heat input rate to the generator, $\dot{Q}_{d,3}$, as can be seen in Figure 24.

This is primarily because a larger $\dot{Q}_{d,3}$ results in a larger amount of water vapor generated, which ultimately results in a larger evaporator cooling capacity $\dot{Q}_e$. The higher temperatures at the generator are also cascaded to the lower temperature levels, hence resulting in the increasing trend in heat rejection from the condenser $\dot{Q}_{c,1}$.
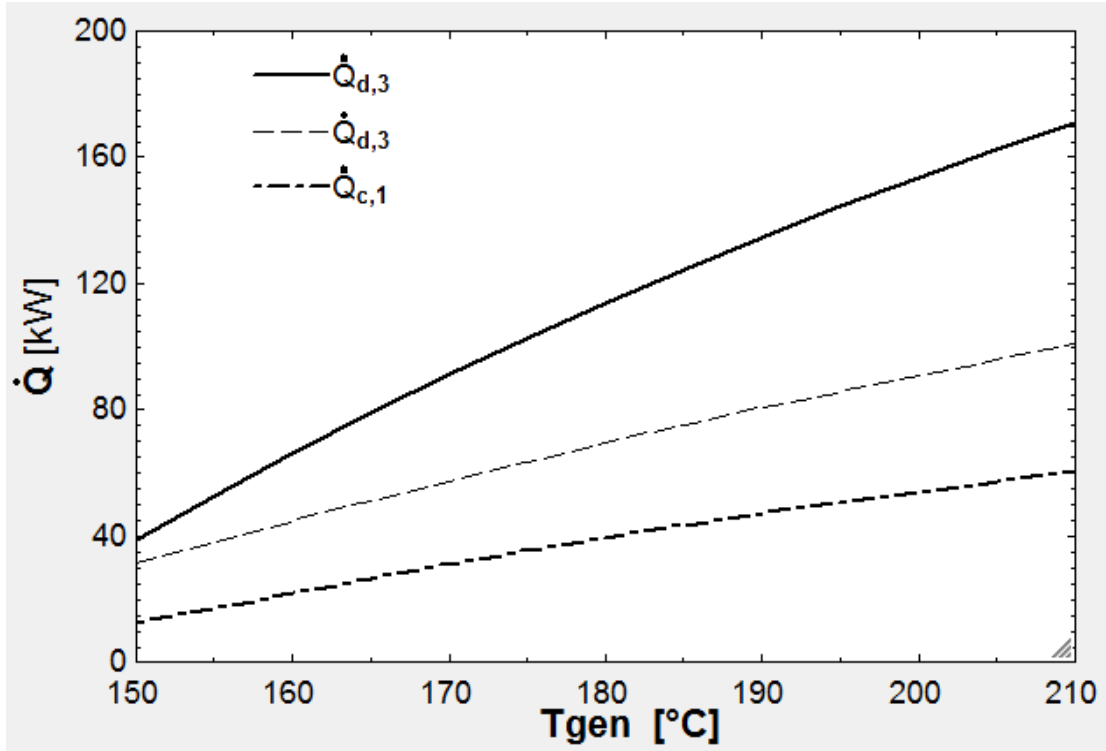
Figure 24: Variation of heat rates with temperature T_{gen} at the highest generator

Similar trends in COP can be seen with increasing generator temperatures as were observed with increase evaporator temperatures. COPs, both energetic and exergetic increase with T_{gen}, but the rate of increase is dampened by the increasing irreversibilities within all the heat exchangers, i.e. the components and the intermediate heat exchangers.

The trends discussed herein can be observed in Figure 25. The faster rate of damping in comparison to that in the case of varying T_{evap} suggests a higher T_{gen} causes more irreversibilities than does a higher T_{evap}.

To be also noted, however, is that for operation within reasonable limits, i.e. T_{evap} up to 9^0C, COPs are more or less identical for both increasing T_{gen} or T_{evap} , with values in the range of 1.7 to 1.8 for the energetic COP and 1.6 to 1.7 for its exergetic counterpart. Figure 25 shows how the energetic and exergetic COPs vary with T_{gen} while the results of investigating the variation of cycle parameters with condenser temperature T_c, can be seen in Figure 26.
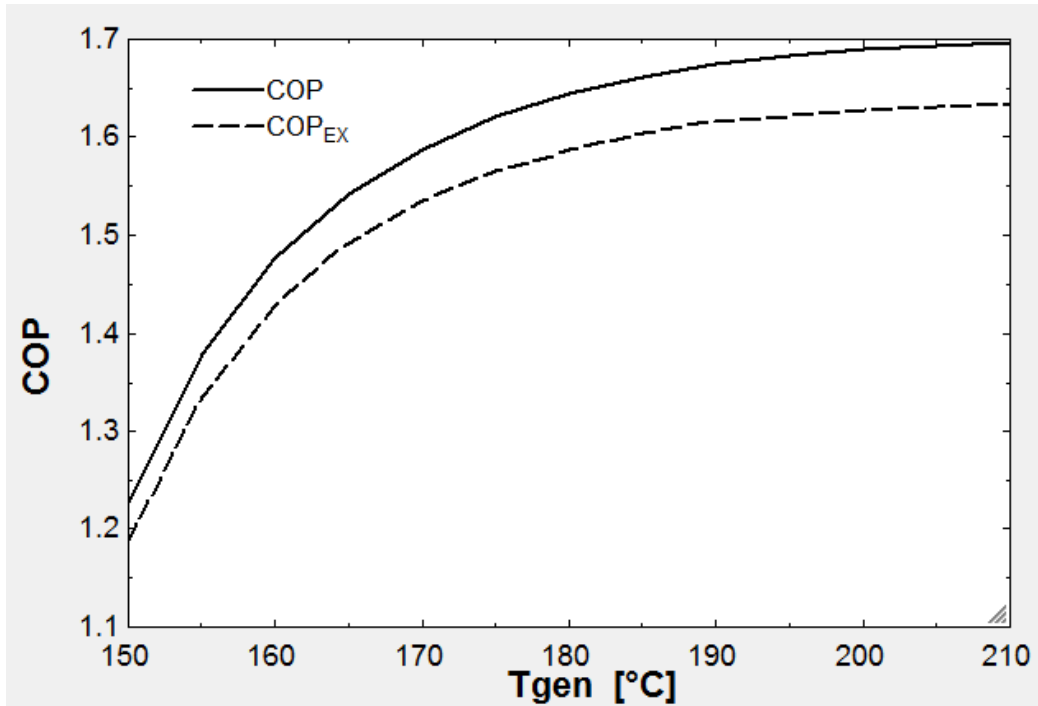
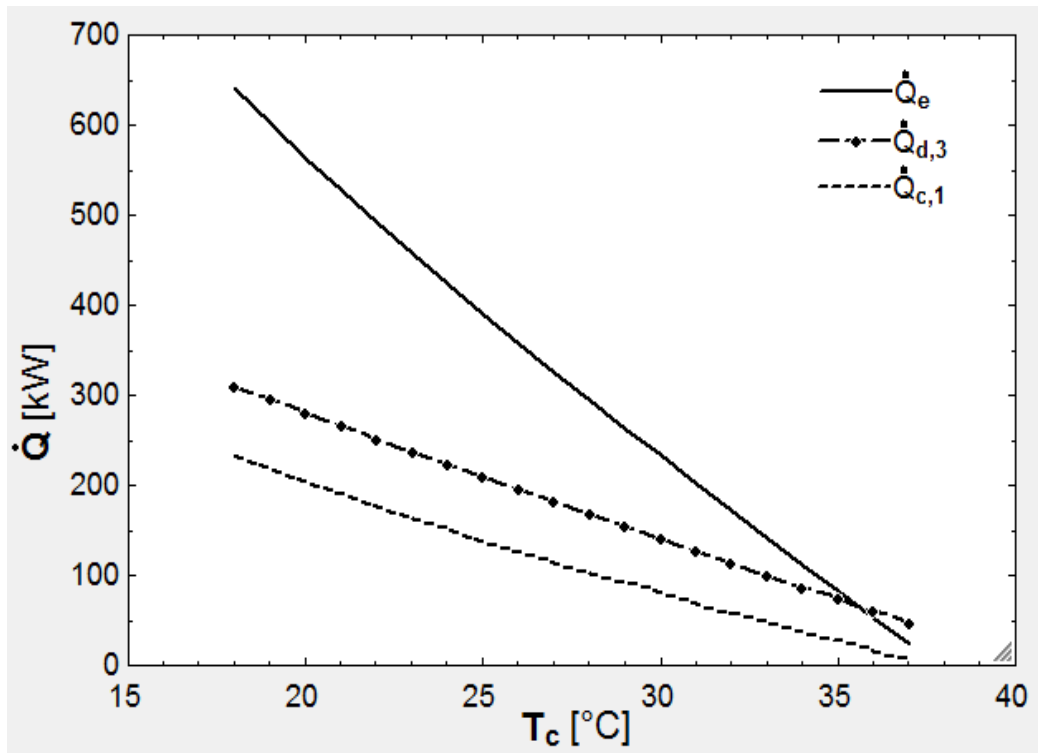Figure 25: Variation of COP with temperature T_{gen} at the highest generator

Figure 26: Variation of heat rates with condenser temperature T_c

Increasing the condenser temperatures has a severely adverse effect on the performance of the triple effect absorption cycle, which seems to be more sensitive to changes in the condenser temperature than those in evaporator temperature. The primary reason behind this is that higher condenser temperatures result in higher condenser exit temperatures which in turn result in the refrigerant being of a higher quality when it enters the evaporator for a fixed evaporator and generator temperature. This reduces the ability of the refrigerant to uptake heat from the chilled water stream and effectively reduces the cooling capacity $\dot{Q}_e$.

As can be seen from Figure 26, the effects of this lower capacity are cascaded to other parts of the absorption system, with lower pressures and hence lower temperatures within the generator and the absorber, which consequently result in lower heat transfer rates within the same.

Figure 27 shows the effect on the COPs of increasing condenser temperatures. The overall effect is that of negatively affecting the COPs, with the evaporator load dropping faster than the generator as can also be seen in Figure 26.
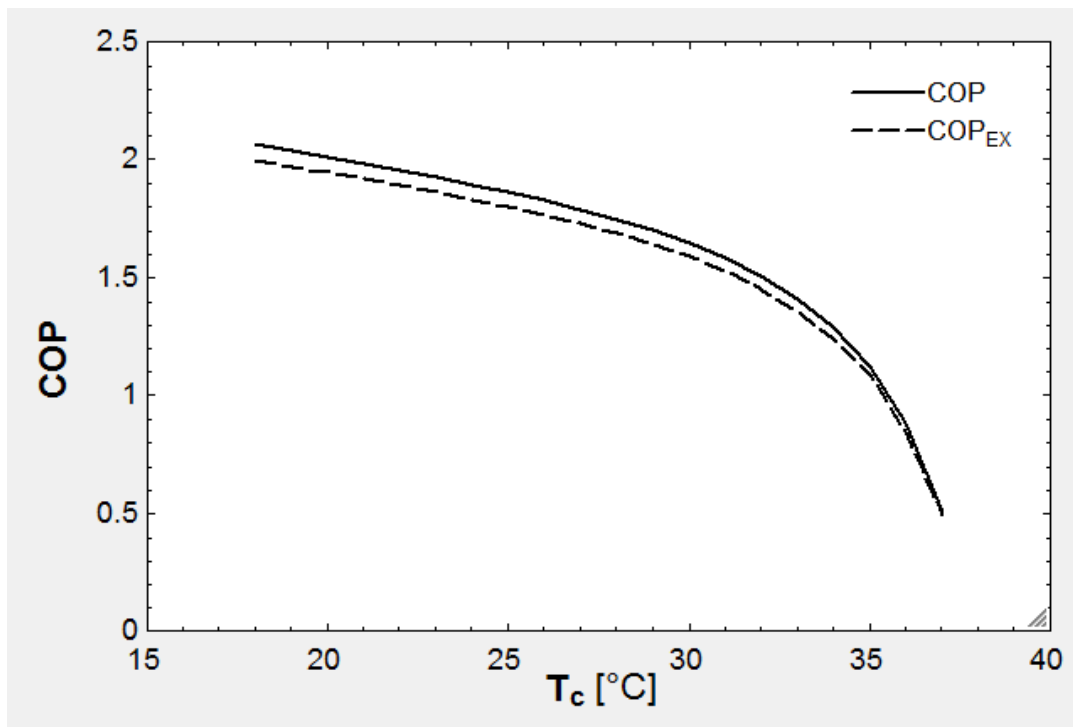

Figure 27: Variation of COP with condenser temperature T_c

3.4 Solar Parabolic Trough Collector

In order to supply the absorption system with the heat it requires for operation, a heat source is necessary. Keeping in line with the aim of making the villas completely standalone whilst employing a sustainable and eco-friendly solution, solar energy is used to supply the necessary heat. Figure 28 gives us the average solar irradiation values for the whole year on a monthly basis in W/m^2.
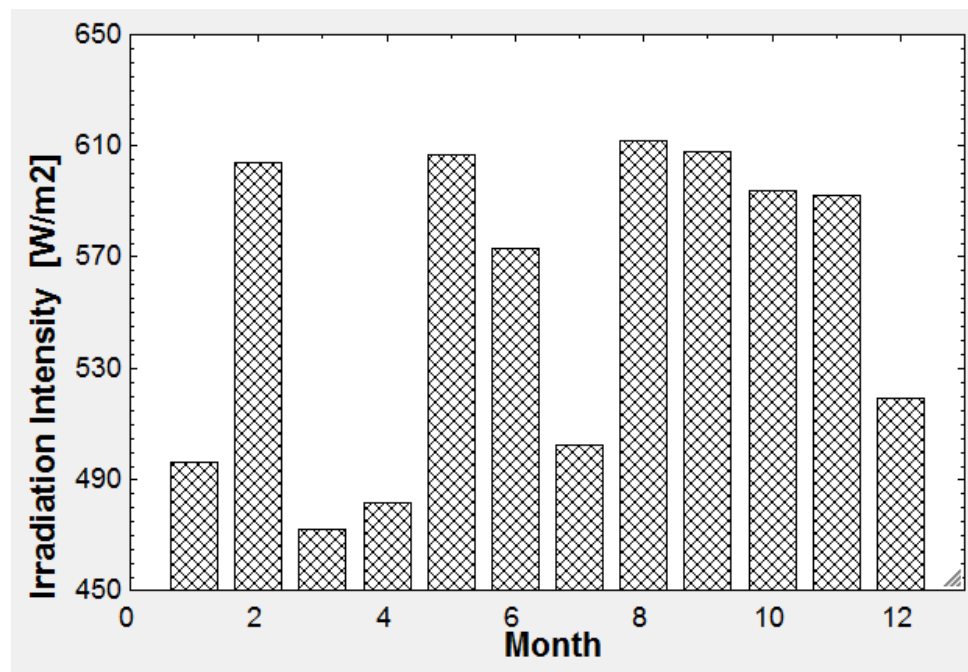

Figure 28: Monthly solar irradiation values for the U.A.E.

This solar energy, as already mentioned, is supplied by a solar PTC, which is modeled using the equations developed by Sulaiman et al. in [5] and [27] and the model is verified with an example problem in [44] which considers a collector which is 20m in length. Figure 29 gives a schematic of such a parabolic trough solar collector.

The quantities to be determined in the example problem were useful heat produced and the outlet temperature of the HTF from the receiver. The values were determined to be 23.01 kW and 273.3 ^{0}C. The model developed for this study

produced values of 23.04 kW and 273.5 ^{0}C, thus confirming the accuracy of the model. The model was then tailored to meet the absorption system's generator input requirements.
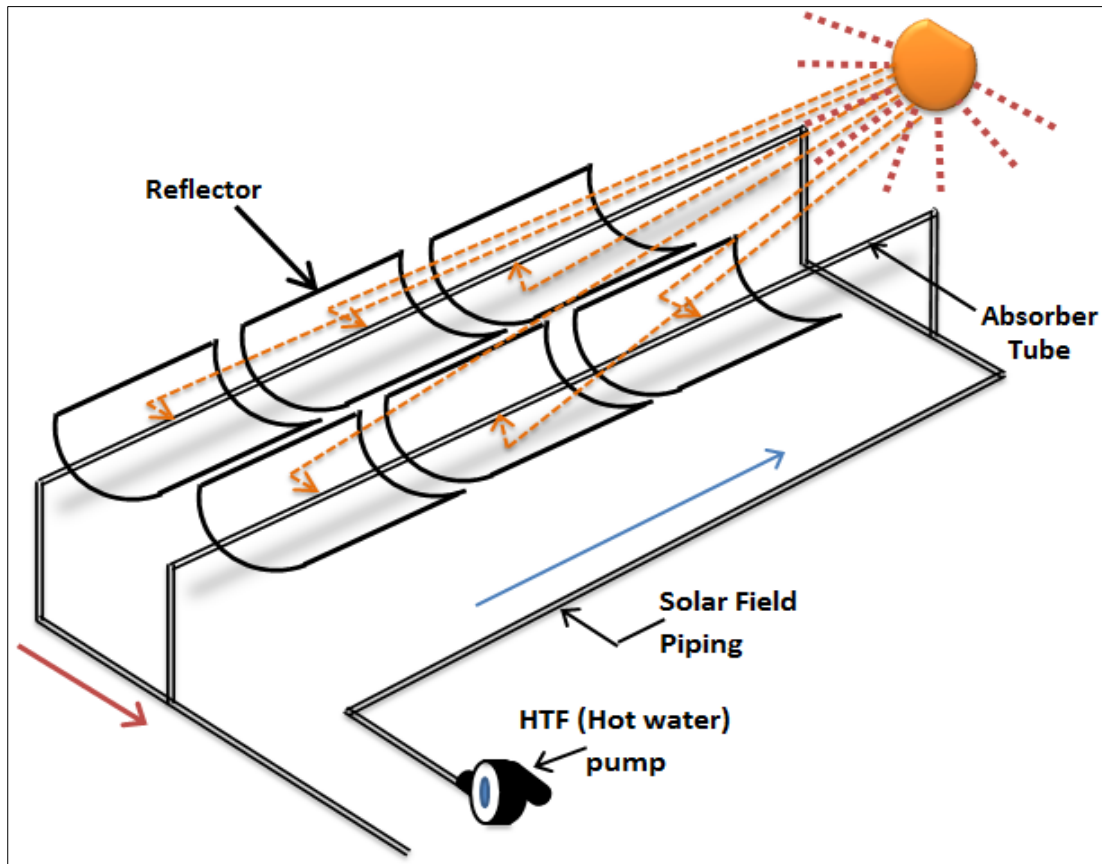

Figure 29: Schematic for Parabolic Trough Solar Collector

In order to fix an appropriate length for the PTSC, it was decided that the minimum length required to satisfy the absorption system's highest generator's heat requirements, was to be found. This was to be done by finding the length that would provide sufficient heat for the absorption system to function satisfactorily even at the lowest experienced solar irradiation values, i.e. those in the range of 450 W/m^2.

Hence, the peak cooling loads that would be handled by the absorption system each month, were determined. This was necessary as the corresponding heat inputs to the absorption generator were needed to be found for each month, and these heat requirements were to be satisfied by the solar PTSC.

Thus, the length of PTSC that would provide this heat was calculated, and it was deliberated that a 55 m collector would be sufficient, although since the absorption requires an input temperature of 190^0C at all times, the minimum length of PTSC required to be able to supply a stream of hot water at 190^0C at a minimum solar irradiation of 450W/m^2 is 80m.

The length decided upon (55m) is mainly because ambient temperatures make up for low solar irradiation values to some extent, as will be seen later, and the average temperature throughout the year in the U.A.E. is relatively high, thus allowing a higher output from the PTSC in general.

Various parametric studies were carried out on the PTSC to study how the latter's performance varied with changes in solar irradiation, receiver mass flow rate and ambient temperatures. Figure 30 relays how the outlet temperature of the heat transfer fluid (HTF) varies with mass flow rate with Therminol-66 as the HTF.
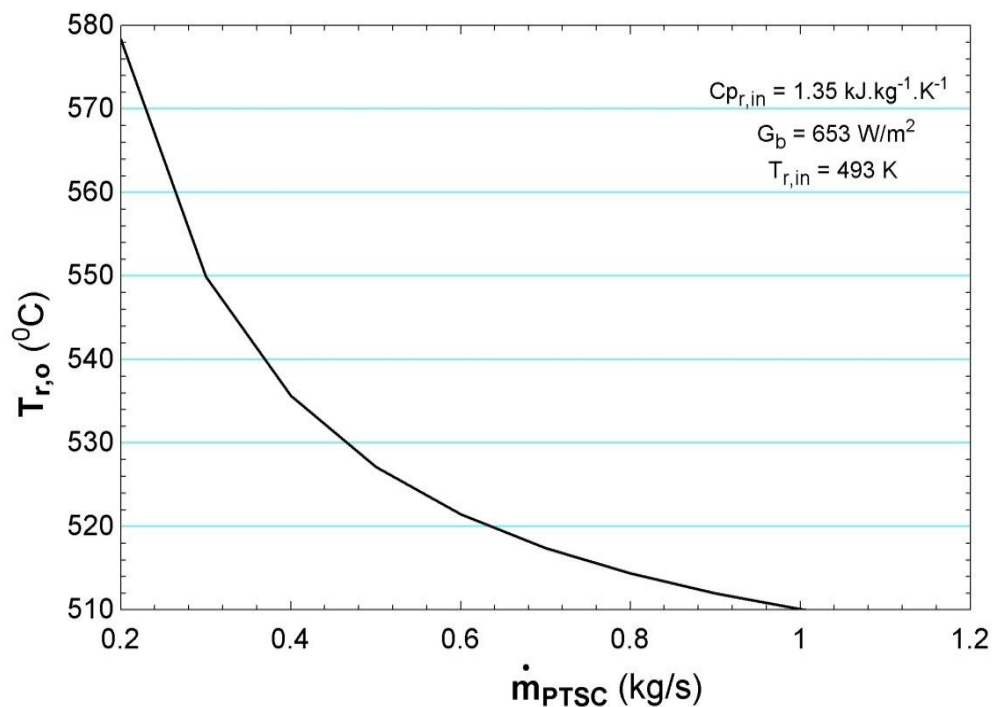

Figure 30: Variation of receiver outlet temperature with mass flow rate

As can be seen from Figure 30, the outlet temperature decreases with increasing mass flow rate; this agrees with intuition in that a larger flow rate will allow

the HTF to spend less time in the PTSC receiver and subsequently receive less heat, thus resulting in its lower outlet temperature.

Another design factor which significantly affects PTSC performance is its length. In order to visualize the output temperature and heat rate produced by the PTSC, a plot of length versus these quantities is produced (with HTF as water henceforth). The same is shown in Figure 31. It can be seen that both, the outlet temperature and the heat produced by the PTSC increase at a decreasing rate with an increase in length. This increase, as can be understood from intuition, is due to the HTF spending more time inside the receiver for a longer length, thus allowing more heat to be added, which subsequently results in a higher outlet temperature.
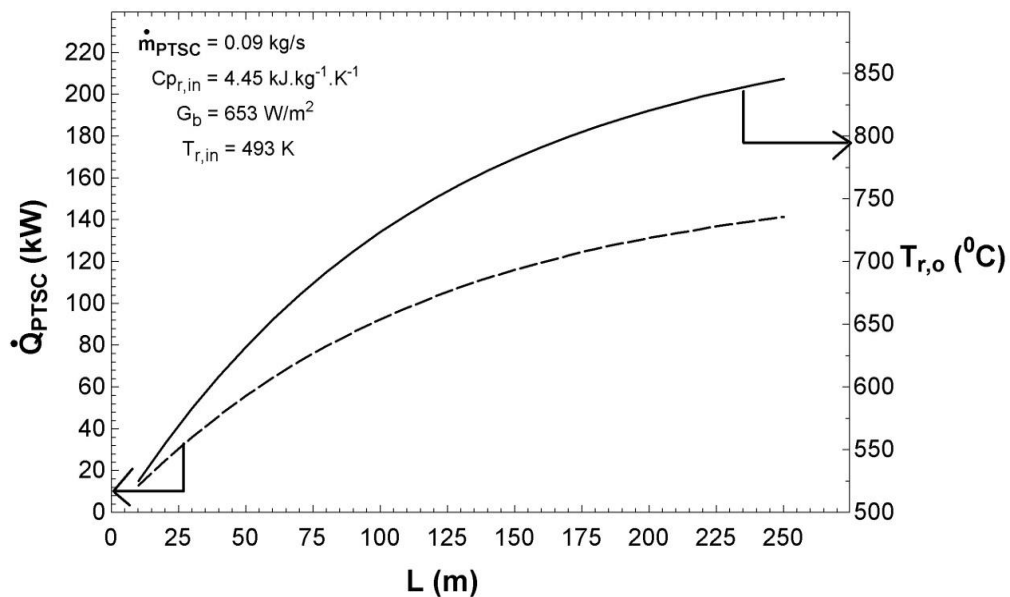

Figure 31: Variation of output and HTF outlet temperature with length

Also studied was the variation of PTSC energetic and exergetic efficiencies with length as can be seen in Figure 32. As can be inferred from Figure 32, first law efficiency, η_I, decreases with increasing PTSC length. This is because longer lengths mean larger collector areas and more potential for losses by convection and radiation. Since longer tubes mean higher outlet temperatures, the higher temperatures result in higher heat transfer coefficients which in turn result in more losses to the environment.
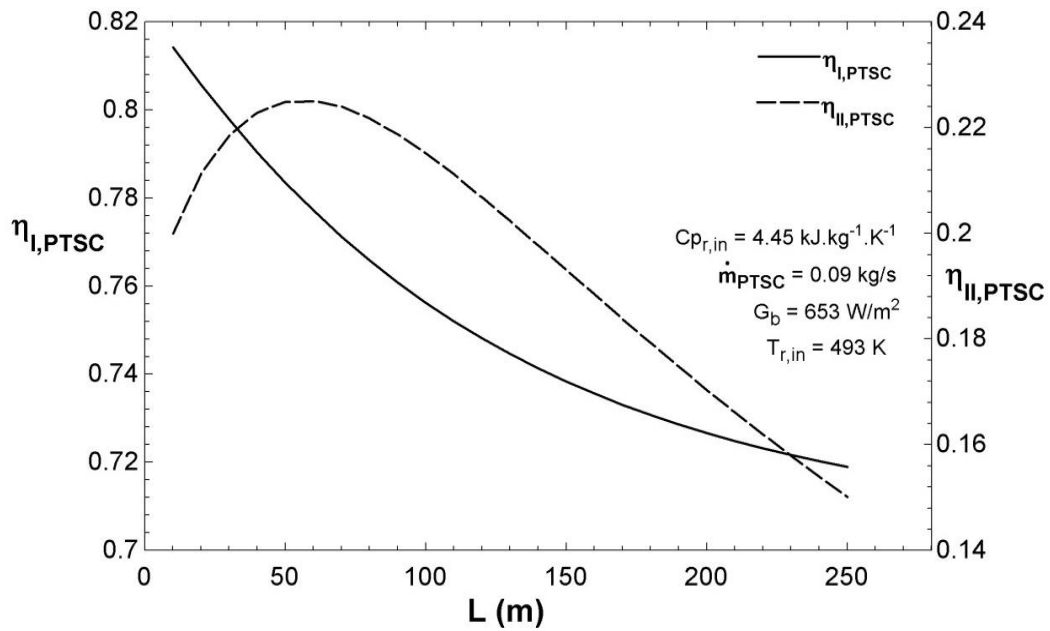
Figure 32: Variation of energetic and exergetic efficiency with PTSC length

As for exergetic efficiency, the trend in Figure 32 is observed because up-to 60m, the exergy transfer between the sunlight and the HTF overcomes the irreversibilities that occur due to heat losses due to temperature difference between the temperature inside the receiver and the ambient, due to the mass flow rate, and due to friction within the receiver tube. With increase in length over 60m, the rate of increase of these irreversibilities overcomes the exergy transfer rate, serving to slow it down. This is one of the reasons why a length of 60m is chosen for the PTSC as will be seen later. Since PTSC is a solar technology, it's natural that its performance will also be highly dependent on the strength of solar irradiation falling on it. Figure 33 shows the relation between solar irradiation and PTSC output and between the rate of energy collected by the PTSC and the rate of energy transfer to the circulating HTF. It is seen that for the average solar irradiation range of 450-650 W/m^2 experienced in the U.A.E., the PTSC collects between 61.72 and 89.16 kW of heat, and produces between 48.66 and 76.09 kW of heat correspondingly. Since the variation of both, the outputs and the inputs of the PTSC with irradiation is defined, it's possible to plot the associated energetic and exergetic efficiencies of the system. Figure 34, obtained using the same conditions as Figure 33, shows that both efficiencies increase with increasing

irradiation. This is because the rate at which energy is taken up with increasing irradiation is much higher than that at which energy is lost to the surroundings, hence resulting in the trend observed in Figure 34.
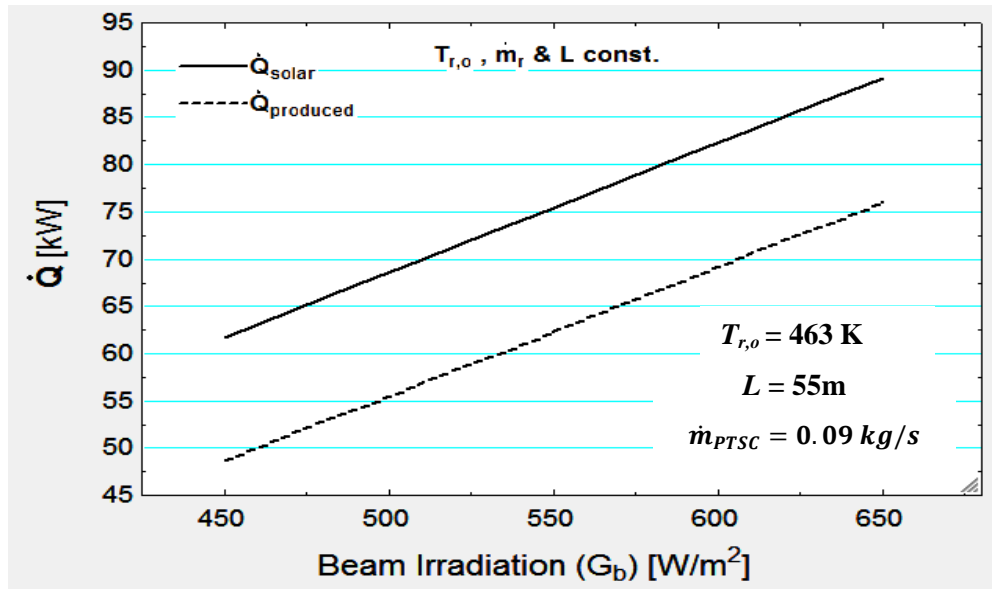

Figure 33: Variation of solar power with solar irradiation in the U.A.E.
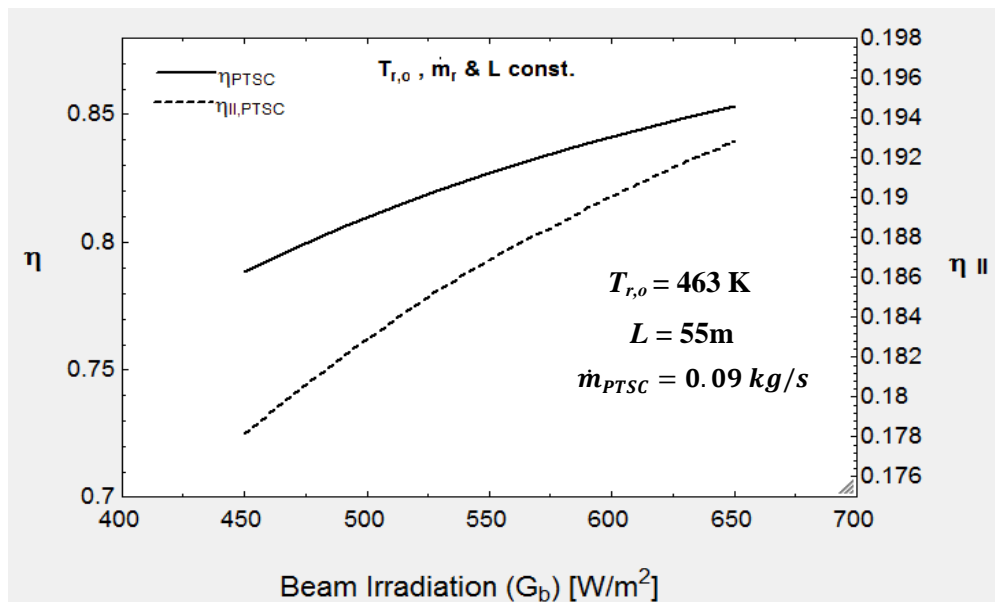

Figure 34: Variation of PTSC efficiencies with solar irradiation

In order to determine how the efficiencies of the PTSC fluctuated throughout the year, Figure 35 was produced. It is seen that despite the considerable fluctuation in irradiation from month to month, very little of this deviation is reflected in the monthly performance of the PTSC, with energetic and exergetic efficiencies remaining relatively constant throughout the year at approximately 0.8 and 0.19 respectively for values of $T_{r,o}, \dot{m}_r$ and L fixed at 463 K, 0.09 kg/s and 55m.

This is because ambient temperatures play some role in determining the performance of the PTSC, and were taken into consideration alongside monthly irradiation values in drawing up Figure 35.

High ambient temperatures make up for low irradiation intensities during the month of July and April, and the result is that energetic efficiencies vary very little, from 0.8108 in March to 0.8668 in August for the energetic efficiency, and from 0.1613 in July to 0.1852 in February for the exergetic efficiency.

Since the absorption system had already been sized according to the monthly cooling loads experience by the U.A.E., it was possible to determine the heat loads required by the generator on a monthly basis.
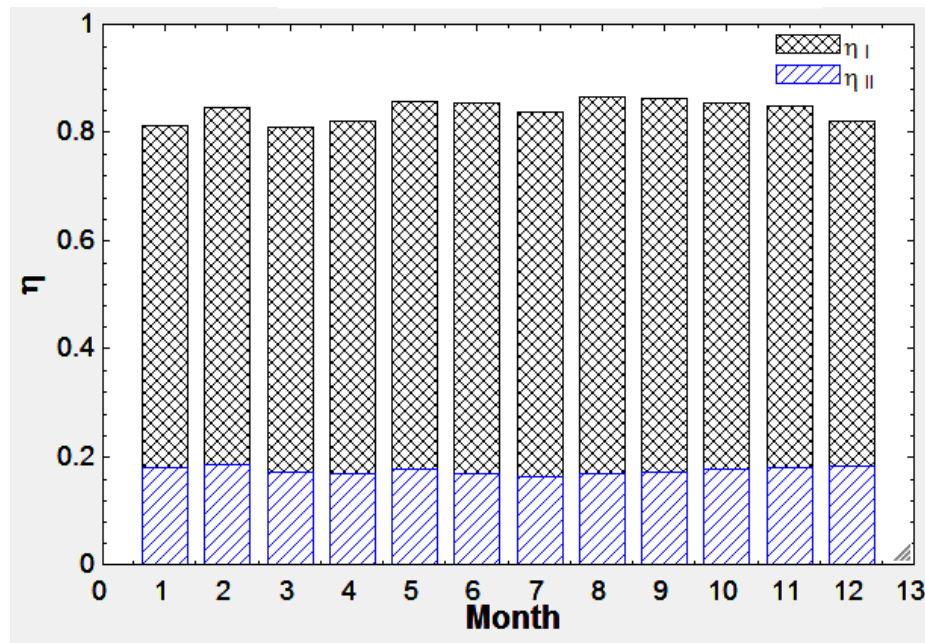

Figure 35: Monthly PTSC energetic and exergetic efficiencies

3.5 Integrated PTSC-DEAS System Results For Case 1

Given in Figure 36 are the monthly generator input requirements and the corresponding heating power produced by the PTSC for Case 1. As can be seen from Figure 36, the PTSC of length 75m that was modeled using EES, consistently exceeded the input requirements of the highest generator of the DEAS throughout the year, thus showing that the PTSC was sufficiently sized for the application.
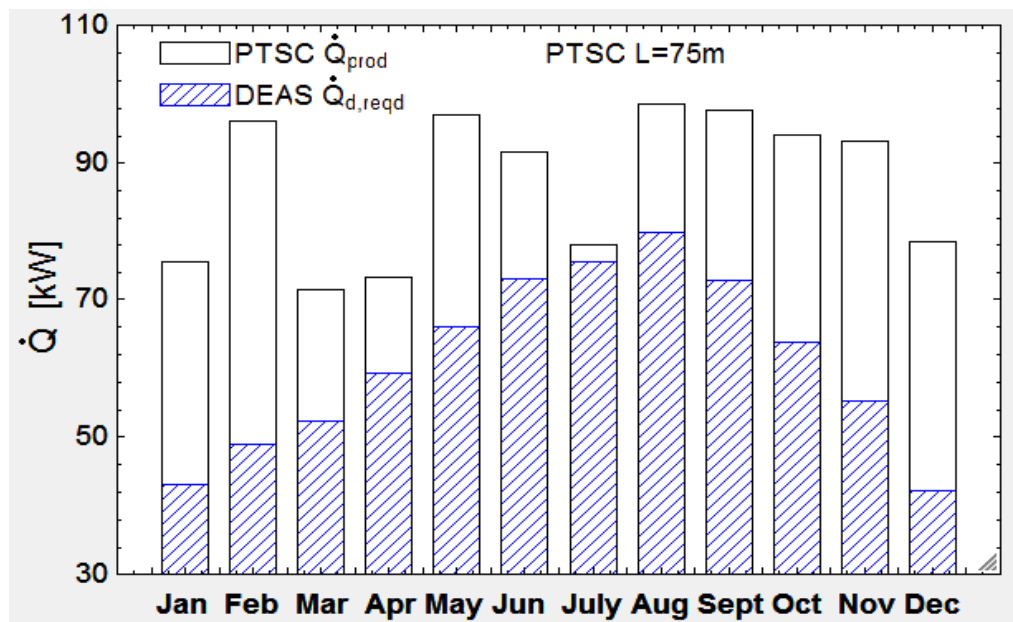
Figure 36: $\dot{Q}$ required by DEAS generator and produced by the PTSC

Figure 37 shows us the COP produced monthly by the PTSC integrated with the double effect absorption system. As can be seen from Figure 37, the highest overall COPs are recorded for the month of July, mainly because of the low solar irradiation values experienced during this month. The low irradiation values in July, most possibly caused by haze, result in a comparatively low output from the PTSC, while the absorption system has to meet a large cooling load due to the high summer ambient temperatures. Since the PTSC is sized to satisfy the absorption system's heating power needs, the combined effect of the high evaporative load $\dot{Q}_e$ and the low heating power $\dot{Q}_{PTSC}$ resulted in the highest energetic and exergetic COP for the month of July.
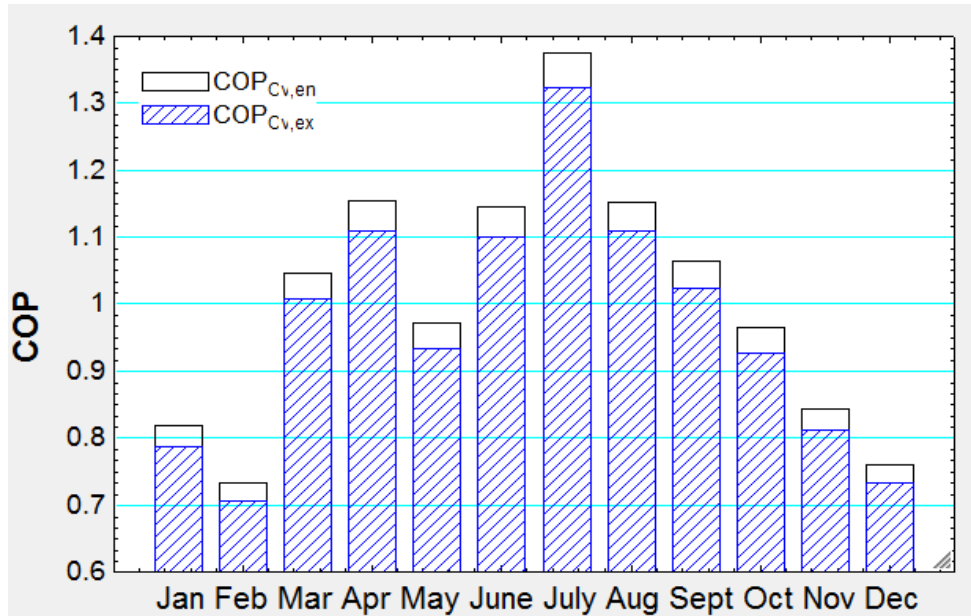
Figure 37: Monthly energetic and exergetic COP of integrated PTSC –DEAS

3.6   Integrated PTSC-TEAS System Results For Case 3

Given in Figure 38 are the monthly generator input requirements and the corresponding heating power produced by the PTSC for Case 3. As can be seen from Figure 38, the PTSC more than met the input requirements of the highest generator of the triple effect absorption system for most of the months. The only exception was the month of July where 57.7 kW of heating were produced in comparison to 62.2 kW of heating required by the absorption machine. This was a result of a low solar irradiation value in July. Given that this exception occurred during the month of July, when cooling loads and ambient temperatures are at a sweltering peak, it was decided that the 55m length of collector was too conservative and a 60 m length collector would be modeled. This would allow the heat requirements to be met, and would offer comfort at all times during the year. Accordingly, the model was modified and run again, this time showing satisfactory performance across the board. Figure 39 puts this into perspective. It helps us to understand what percentage of the heating power produced by a PTSC of length 55m, is in excess of the amount that is required, showing that a considerable factor of safety is met in terms of provision of ample cooling annually with the exception of July, where for a length of 60m, the $\dot{Q}_{gen}$ produced marginally exceeds the required amount required.
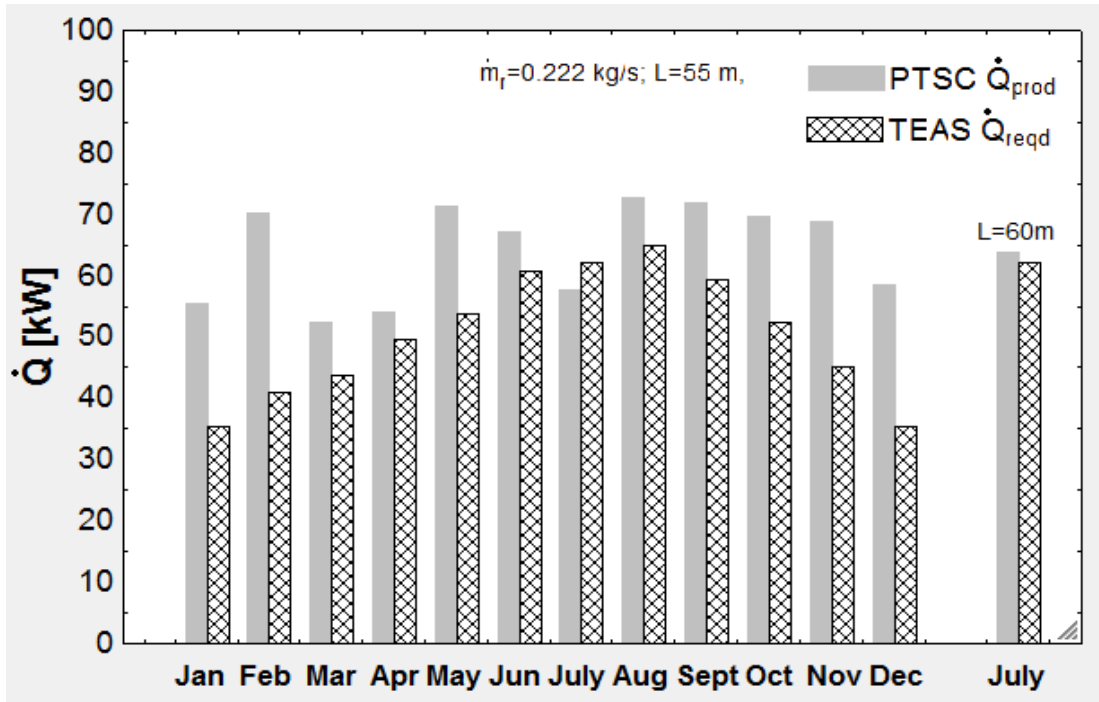
Figure 38: Monthly $\dot{Q}$ required by TEAS generator and produced by the PTSC
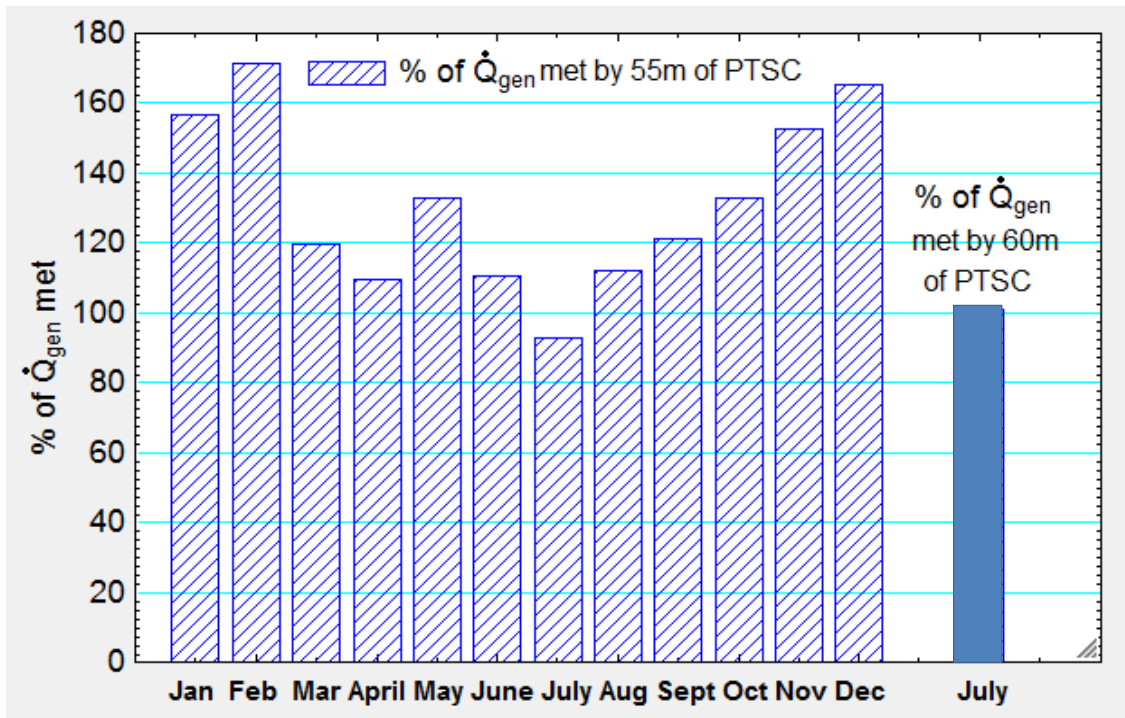

Figure 39: Monthly % of highest generator requirement met by PTSC

Figure 40 shows us the COP produced monthly by the PTSC integrated with the triple effect absorption system. As was the case with the PTSC-DEAS system, the highest overall COPs are recorded for the month of July, mainly because of the low solar irradiation values experienced during this month.
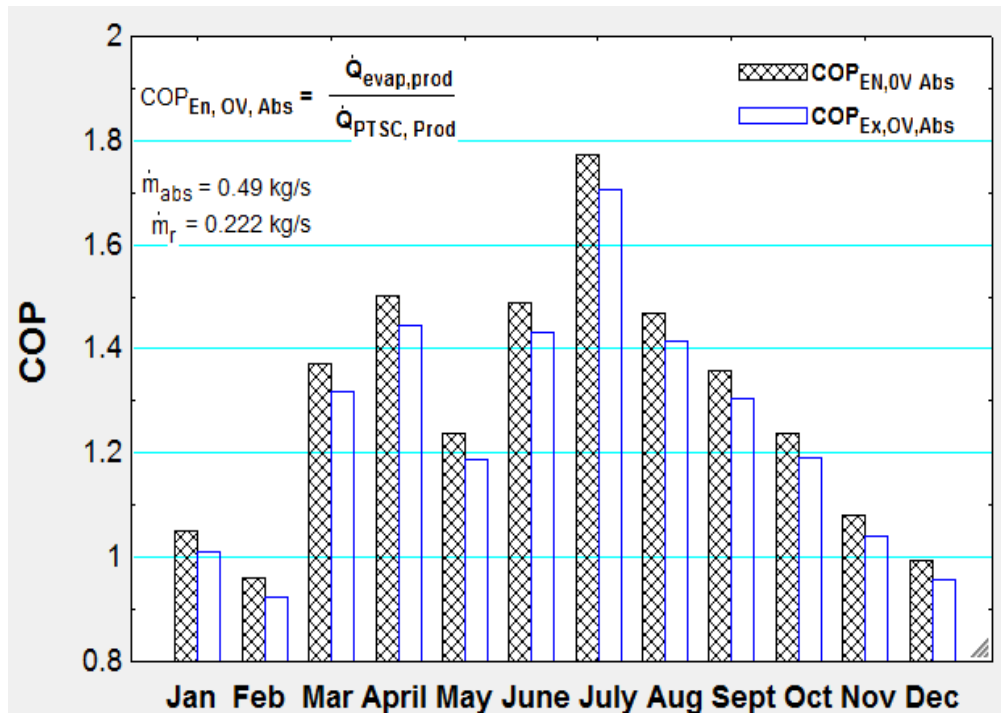
Figure 40: Monthly energetic and exergetic COP of PTSC integrated with Triple Effect Absorption System (TEAS)

The low irradiation values in July, most possibly caused by haze, result in a comparatively low output from the PTSC, while the absorption system has to meet a large cooling load due to the high summer ambient temperatures. Since the PTSC is sized to satisfy the absorption system's heating power needs, the combined effect of the high evaporative load $\dot{Q}_e$ and the low heating power $\dot{Q}_{PTSC}$ resulted in the highest energetic and exergetic COP for the month of July. Also, because of the relatively higher COP of the TEAS compared to the DEAS, it is expected that the combined PTSC-TEAS system should perform better than the combined PTSC-DEAS system. In order to verify this, data was compared and Figures 41 and 42 demonstrate the result of this comparison. As can be seen, the PTSC-TEAS system had a higher energetic

and exergetic COP than the PTSC-DEAS throughout the year, suggesting that thermodynamically the PTSC-TEAS is a more viable option.

Figure 41: Comparison of integrated system energetic COP between the PTSC-DEAS and PTSC-TEAS systems

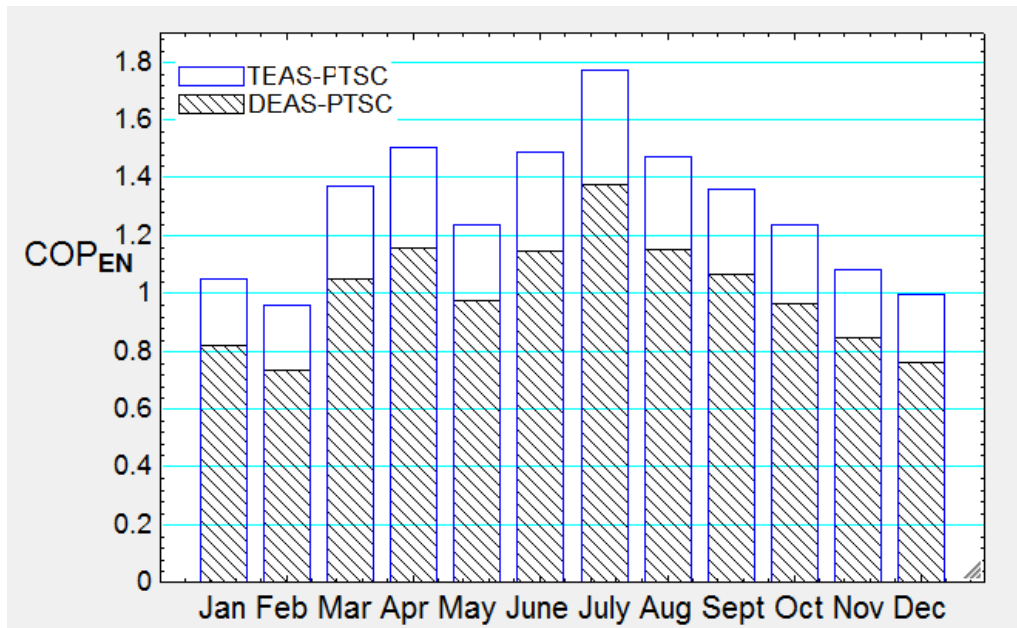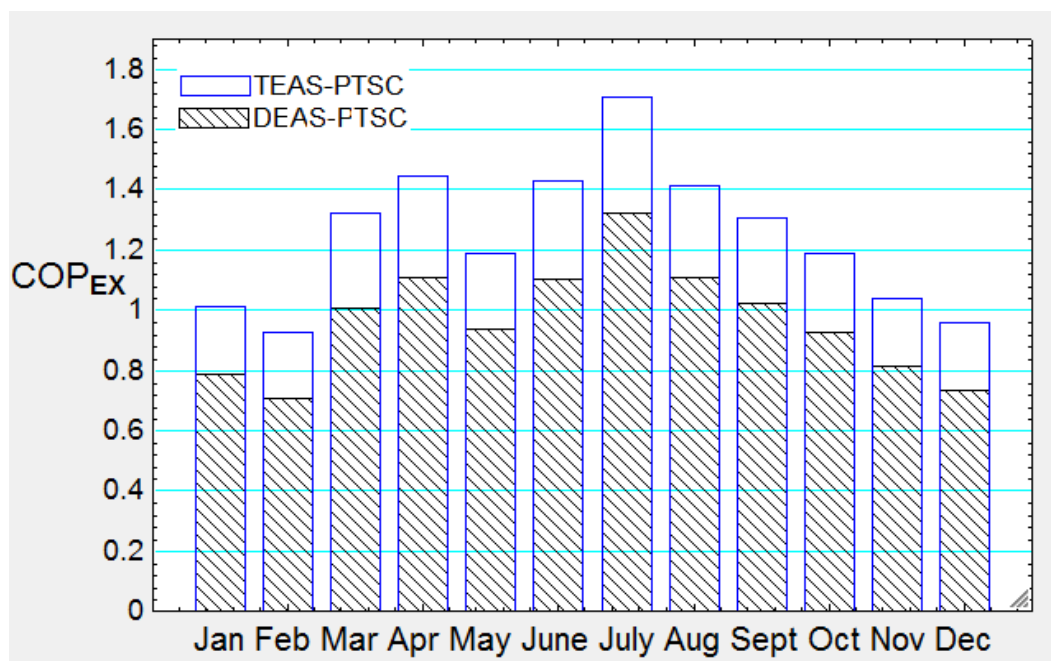Figure 42: Comparison of integrated system exergetic COP between the PTSC-DEAS and PTSC-TEAS systems

Lastly, other measures of performance could be a variation in the definition of overall COP and exergetic efficiency of the PTSC-integrated with the TEAS. Figures 43 and 44 are self-explanatory, and show us how the overall energetic COP and exergetic COP (referred to as the exergetic efficiency in the figure as values for it are below 1.0) respectively would vary monthly for the PTSC-TEAS were they to be defined differently.
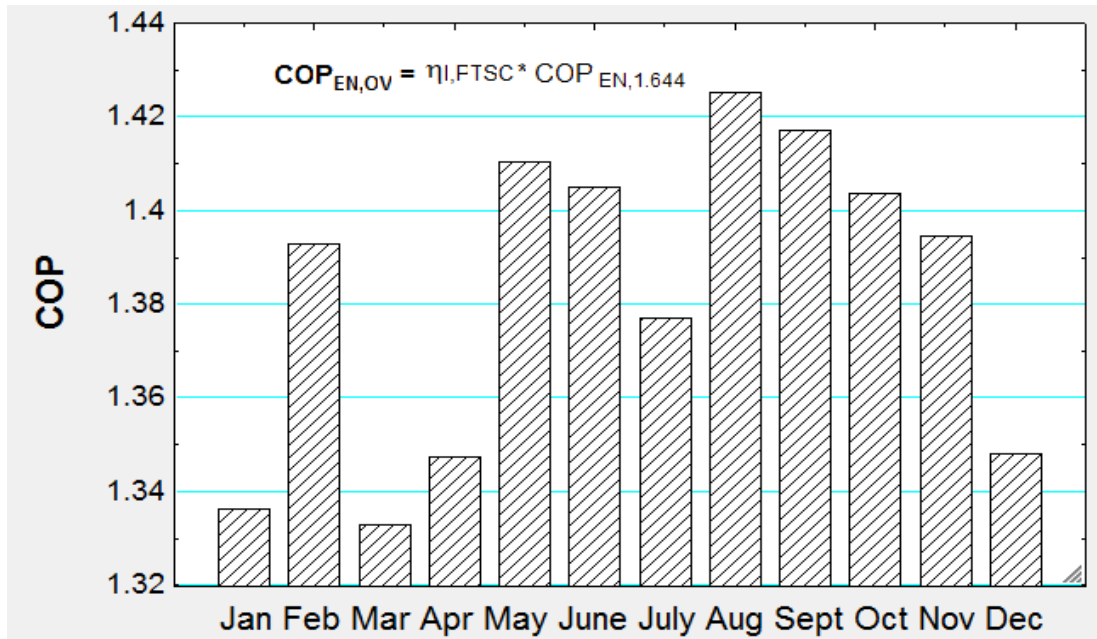
Figure 43: Monthly variation of overall energetic COP using alternate definition

These COP charts tend to follow the effect of the variation in irradiation intensities more closely mainly because the energetic and exergetic COPs of the absorption system were held constant at 1.644 and 1.588 respectively while making these calculations monthly.

These COPs were those obtained for a fixed set of inputs which defined the originally developed absorption system for an average ambient temperature of 25^0C.

The fixed set of system inputs mentioned above include a High Generator temperature T_{gen} of 180^0C, a Low Condenser temperature T_c of 30^0C, an evaporator temperature T_e of 5^0C, Intermediate Heat Exchanger effectiveness values of 0.5 each, and a pinch-point temperature between the intermediate generator-condensers of 5^0C.
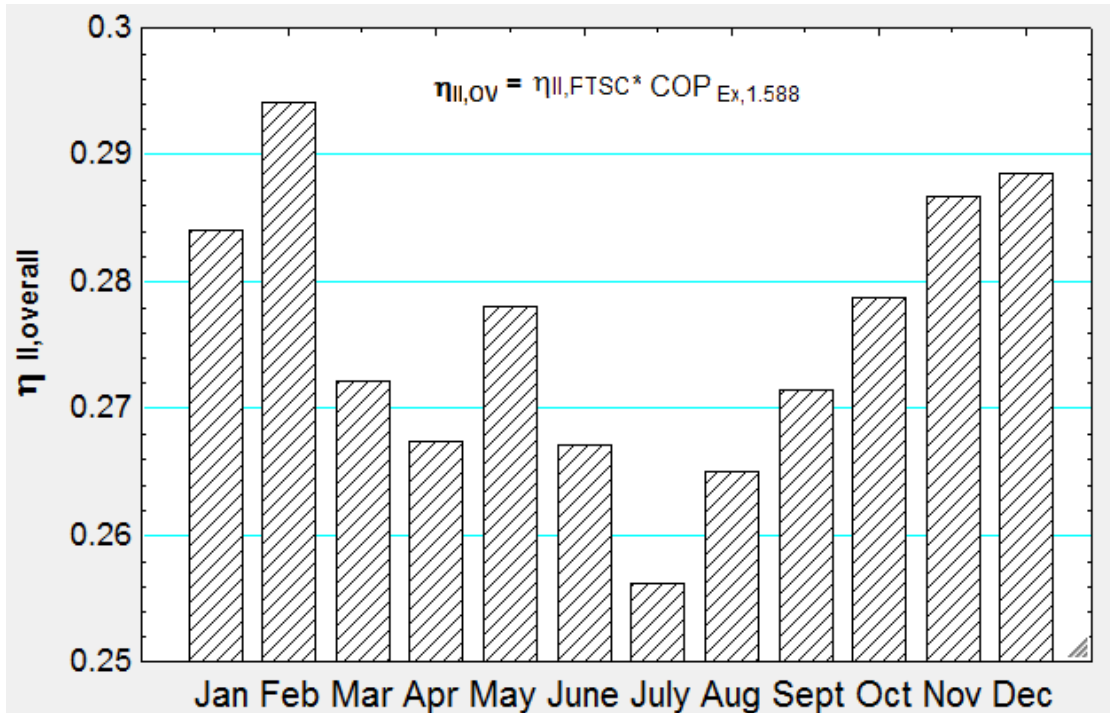
Figure 44: PTSC-TEAS monthly variation of overall exergetic COP using alternate definition

3.7   Wind Turbine

In order to study the thermodynamic performance of the wind turbine, the approach taken by Gadalla et al. [40] is adopted. Northern Power 100, a 100 kW wind turbine supplied by Northern Power Systems [125] is chosen to supply the four residential units with electricity. This particular wind turbine has a low cut-in speed of 3.5 m/s and has higher standards of safety than other wind turbines in the same category such as the WES 18.

Figure 45 shows the power output of the turbine at various wind-speeds up to 25 m/s, which is the cut-out speed of the turbine.

Energetic and exergetic efficiencies for the wind turbine at the earlier assumed yearly average wind-speed of 6.7 m/s were calculated to be 41.19 % and 34.05 % respectively, while power produced by the wind turbine at the same speed is 15kW. The wind turbine is modeled using EES, and the various key inputs and outputs of the model are given in Table 9. The air density is taken to be 1.225 kg/m^3 for the model.

Table 9: Wind turbine simulation parameters

Parameter	Value	Unit
Area	346.4	m^2
P_{atm}	101.3	kPa
T_0	313.0	K
C_p	1.005	kJ/kg.K
ρ_{air}	1.225	kg/m^3
V_1	6.7	m/s
V_2	5.14	m/s
T_1	318.4	K
T_2	318.1	K
$\eta = P_{w.e} / \dot{W}_w$	0.4119	dimensionless
$P_{w.e}$	26.28	kW
$\dot{E}_{K.E.} = \dot{W}_w$	63.81	kW
$\dot{E}_{ph}$	13.37	kW
$\dot{E}_{flow} = \dot{E}_{K.E} + \dot{E}_{ph}$	77.18	kW
$\varepsilon_x = P_{w.e} / \dot{E}_{flow}$	0.3405	dimensionless

These preliminary results of the wind turbine simulation showed that the performance of the wind turbine was quite encouraging at the average wind speeds cited by previous studies for the site selected (Fujairah, U.A.E.) and that the WT at first glance seemed thermodynamically very feasible.

However, as mentioned before, the obtained wind profile for the whole year, i.e., obtained hourly data of wind speeds were not as promising as expected, with March being the only really feasible month for the operation of the turbine (average wind speed above 6.5 m/s).
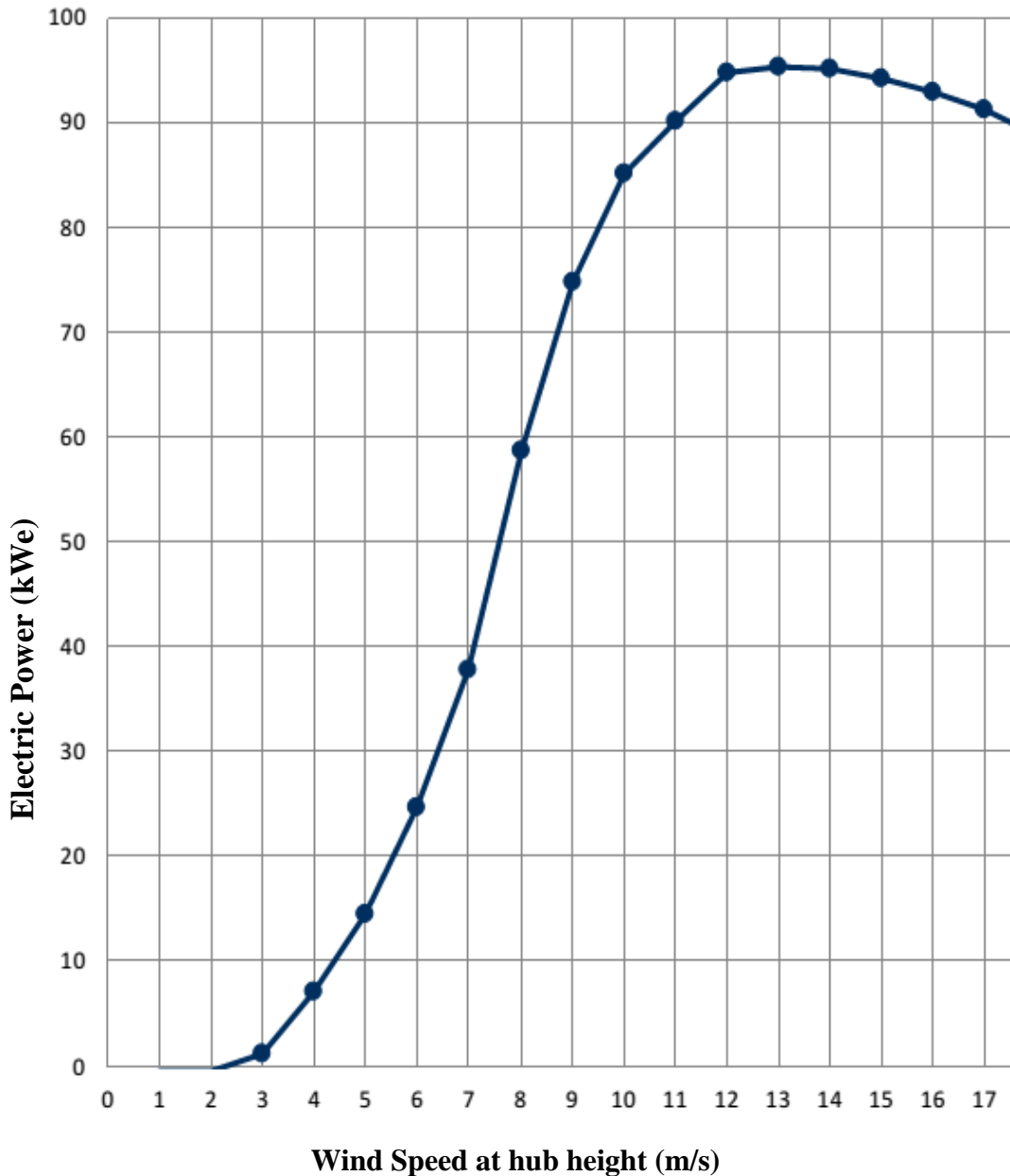
Figure 45: Power curve of WT: electrical power output (kW_e) versus wind-speed [125]

It is again reiterated that these wind speeds were for a measuring location offshore and onshore values may greatly vary. For academic purposes, the daily data obtained shall be used to gauge the wind turbine's performance over the year. The curve in Figure 46 displays the power produced by the model developed for the wind turbine. It is verified against the manufacturer's provided power curve which is given above in Figure 45. Figure 46 shows sufficient agreement between the commercial

performance and the model performance for the range of wind speeds (V_1) practical for power production and frequented in the U.A.E., showing that the model is accurate in the range of interest. This range is between 3 m/s and 7 m/s. Given in Figure 47 are the energetic and exergetic efficiencies of the wind turbine over the same range.
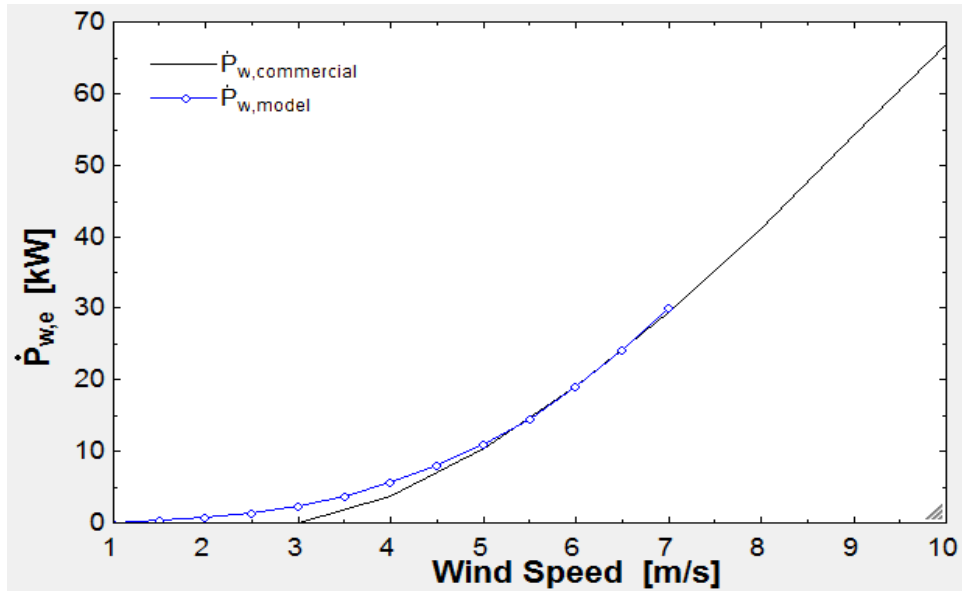
Figure 46: Model verification: variation of $\dot{P}_{w,e}$ generated with wind speed
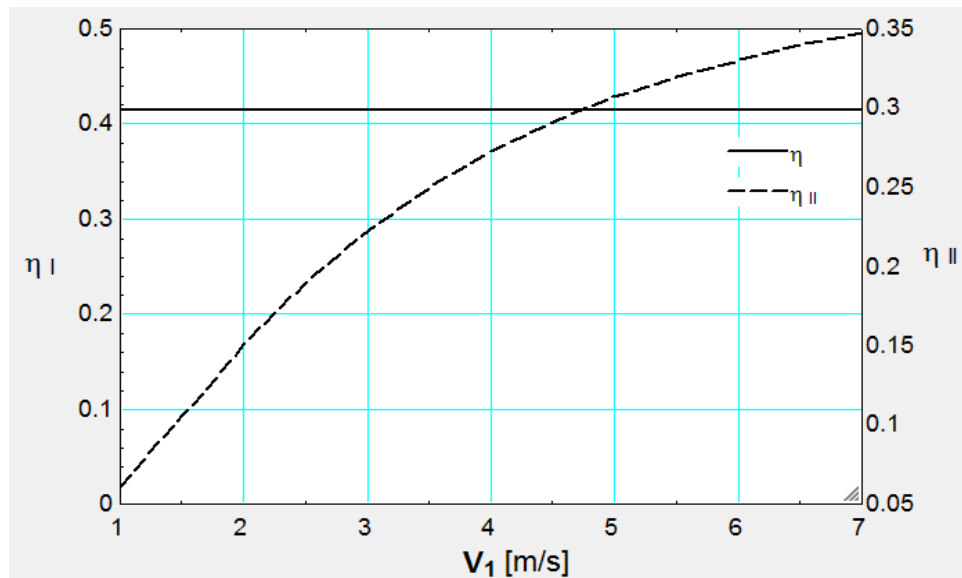
Figure 47: Variation of WT energetic and exergetic efficiency with wind speed

Figure 47 shows us that the wind turbine energetic efficiency is constant for the range of wind speeds considered. This is because the model was developed such that a constant efficiency was assumed so as to allow for a range of power outputs over different wind speeds.

Since there was no such restriction in the development of the equations governing the exergetic efficiency of the turbine, it was possible to plot the latter versus wind speeds to gauge the exergetic performance, which is the actual performance, of the wind turbine. The exergetic efficiency of the wind turbine is seen to increase almost linearly until 3 m/s and then slow down. Since power production only occurs after 3 m/s, we are interested in the shape of the curve beyond that point. The reason for the slowing trend after 3 m/s is that increasing wind speeds are accompanied by increasing irreversibilities due to a number of factors including turbulence, increased friction between moving parts and in mechanical to electrical power conversion. The overall effect of these irreversibilities is to overcome the power production rate is such a way as to slow it down.

Figure 48 gives the monthly power production for the wind turbine at the average monthly wind speeds determined by the data collection process for 2012.
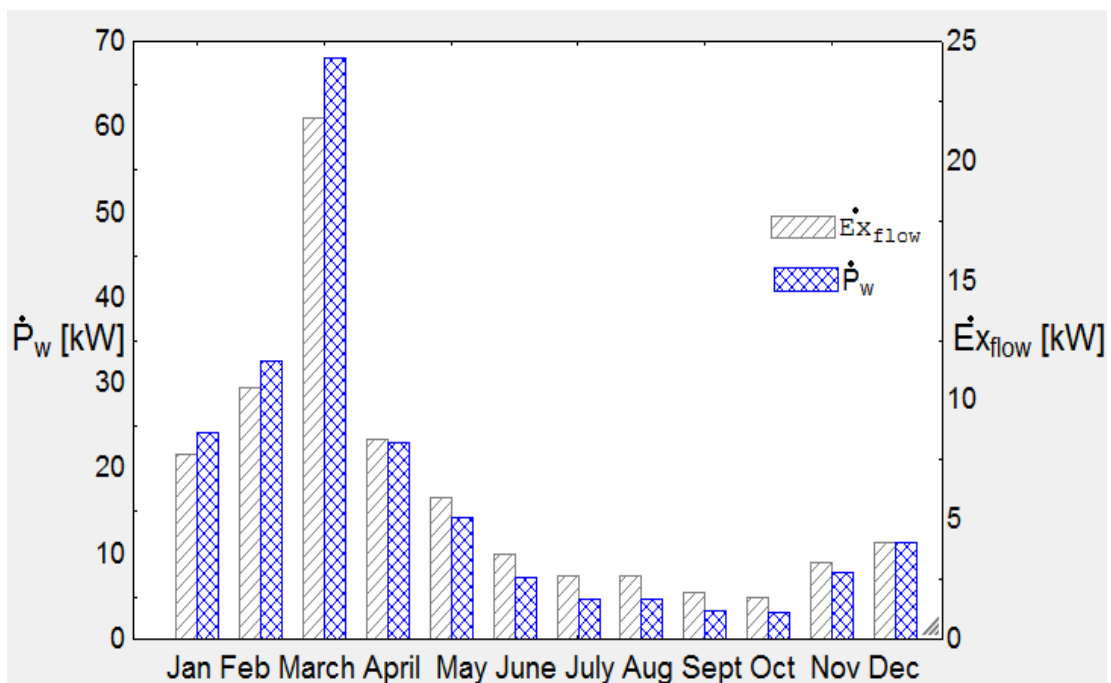
Figure 48: Monthly WT power production and flow exergy, Fujairah, 2012

As can be seen from Figure 48, the highest power production and flow exergies are experienced during the month of March, when wind speeds are highest. The lowest power production is during October, with only 1.12 kW generated on average for a wind speed of 2.335 m/s, the lowest throughout year. Since a yearly average of 15 kW is required from the wind turbine, it being the sole power source for the houses, the wind turbine is seen to not meet the power requirements of the villas in any month except March.

It only partially meets the electrical loads of the houses for the months of January, February, April and May, when average wind speeds are 4.619 m/s, 5.1 m/s, 4.536 m/s and 3.865 m/s respectively. The flow exergy pattern is closely related to the wind speed pattern as flow work is effectively exergy, and is calculated based on wind speed. Monthly exergetic efficiencies show more deviation from wind speed patterns than the monthly flow exergy as can be seen in Figure 49.This is because the exergetic efficiency was plotted by taking not just wind speeds, but also monthly ambient temperatures into consideration, which strongly affect the performance of the wind turbine due to changes in the specific heat of the air at different temperatures.
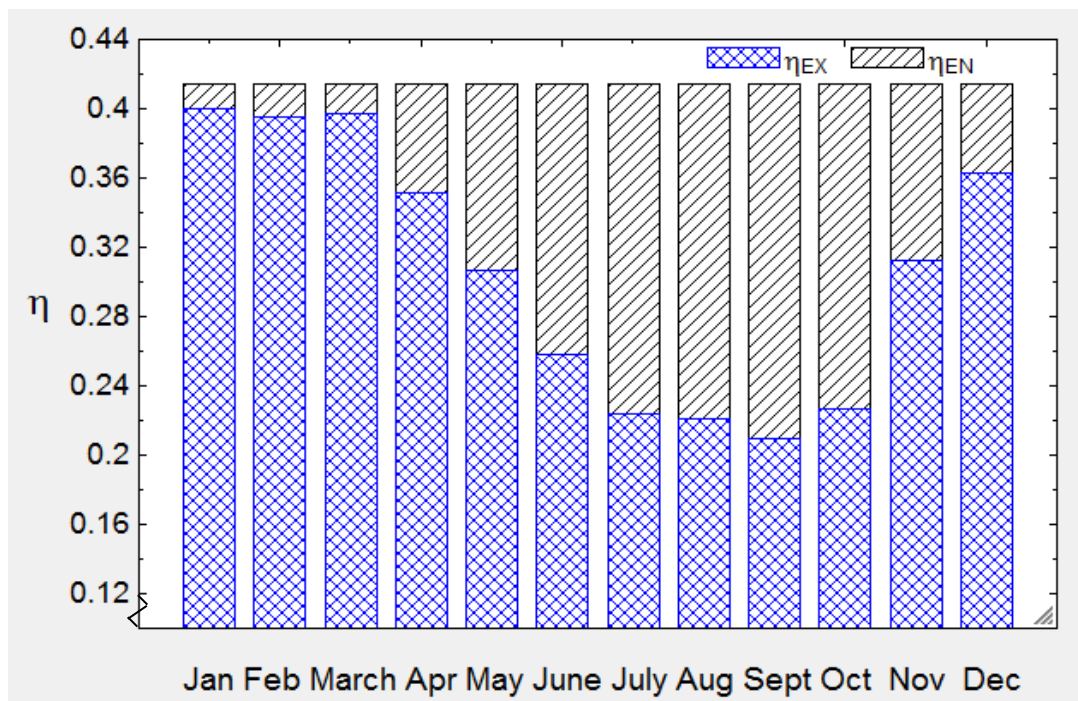
Figure 49: Monthly variation of WT exergetic efficiency

Higher exergetic efficiencies are seen for the cooler months than for hotter ones, with low temperatures resulting in lower entropy generation and maximum exergetic efficiencies approaching 0.4 in January through March.

3.8   Photovoltaic Thermal Collector (PV/T)

The PV/T system was designed as part of this work so that it could be integrated into the solution for providing uninterrupted power and cooling to the group of four households. A PV/T system, the schematic for which is shown in Figure 50, is designed in this study to charge the latent heat storage system that shall cool the homes during the night.
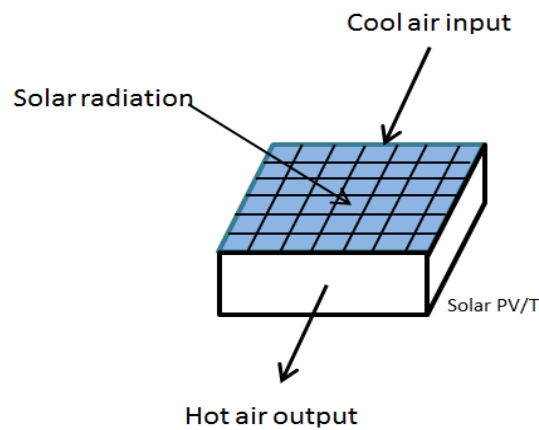
Figure 50: Solar Photovoltaic/Thermal collector (PV/T)

The PV/T system is multi-purpose in that it generates both electrical power and heat. It produces electrical power by using the solar irradiation incident on the panel to break the bonds within the photovoltaic (PV) panel, thus separating protons and electrons.

Then, electrons pass through the circuit, thus producing an electric current. Air passing through the duct placed below this PV panel, gets heated up as a result of the heat generated by the solar energy absorbed by the PV, and is used to provide usable heat to any heat powered process such as that of an absorption system or a domestic solar water heater.

For our system, the primary purpose of the PV/T system is to produce electrical current to run the various electrical appliances and cooling equipment for the

villas. The cooling equipment would include the pumps of the absorption systems, and the compressor for the vapor compression cycle that produces the thermal storage medium, also known as clathrate. A single module (building block) of the PV/T system of area 11 m^2 is initially modeled, and parametric studies are conducted on the model to determine its performance.

The model is later sized as per the needs of the different integrated RES options studied herein. The PV/T system modeled is the glass to glass system developed using the equation and parameters presented in [51], [1], [121] and [44], with model verification carried out with [1].

Parametric studies were performed with variations in solar irradiation intensity and ambient temperature, and monthly performance was determined. It was found that both, electrical and heating power produced, increased linearly with an increase in solar irradiation. This is because a higher irradiation value results in a higher bond-breaking rate as well as a higher rate of heating of the panel, which subsequently leads to a higher heat output from the PV/T. This can be seen in Figure 51.

Figure 51: Variation of PV/T outputs with solar irradiation

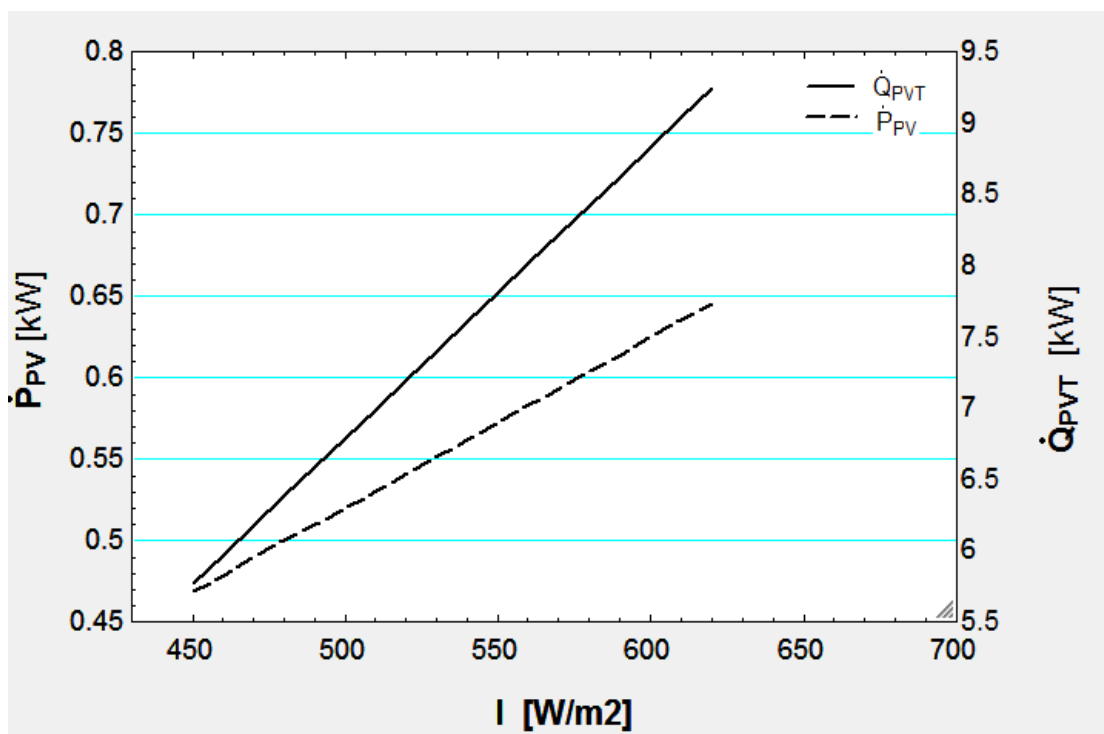Figure 52 shows us the variation of the electrical and thermal efficiencies with solar irradiation '*I*'. Electrical efficiency is seen to drop whereas thermal efficiency is seen to increase.
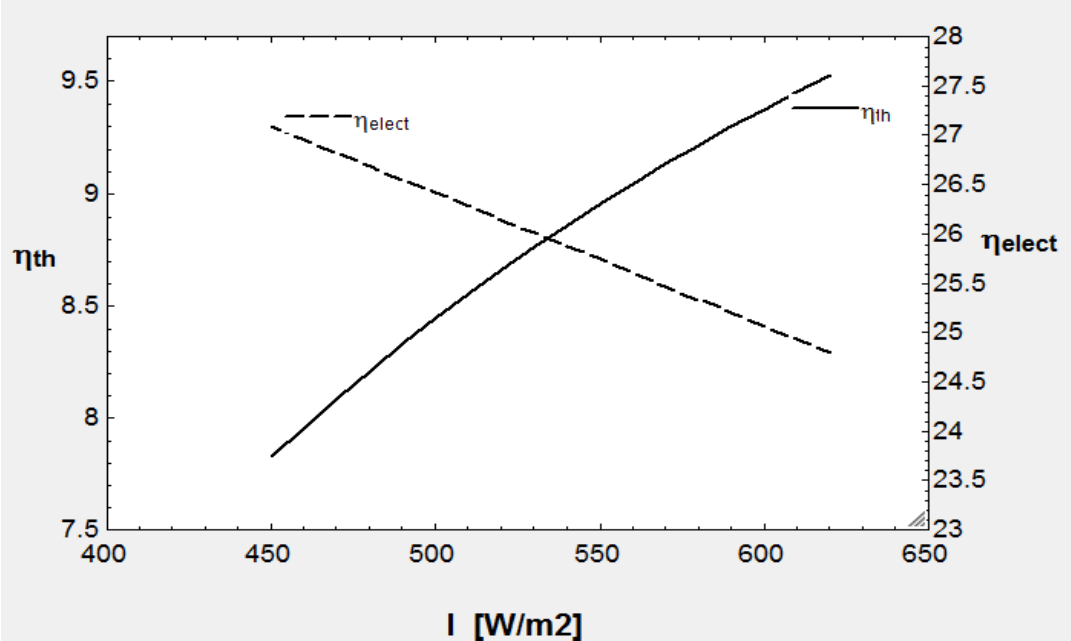

Figure 52: Variation of PV/T electrical and thermal efficiencies with I.
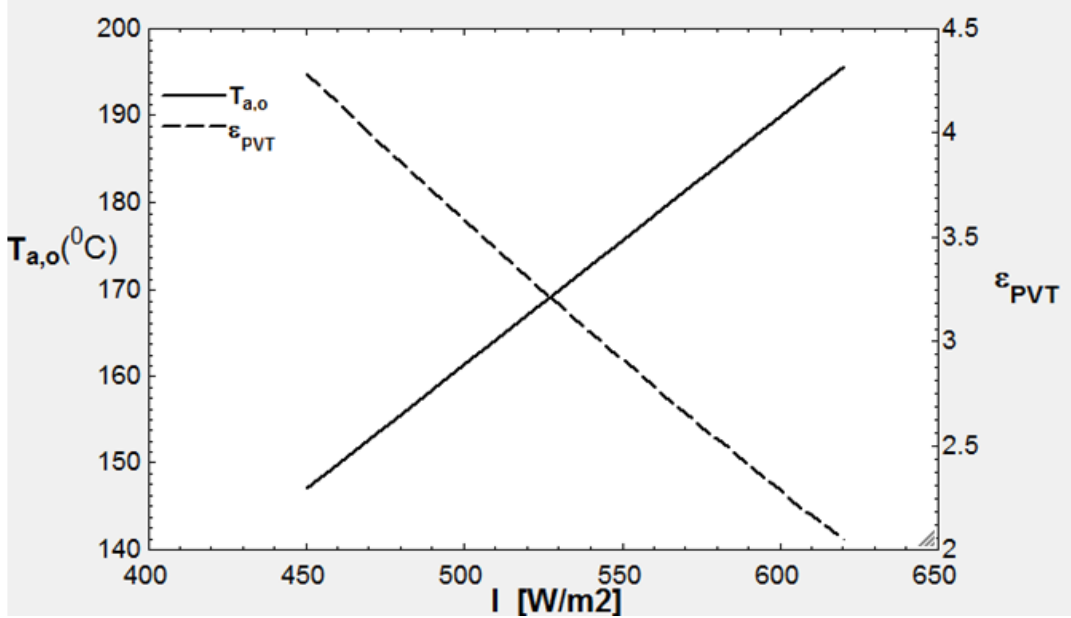
Figure 53: PV/T exergetic efficiency and air outlet temperature vs solar irradiation

These opposing trends are observed because PV performance drops with increasing temperature which occurs with increasing irradiation, and the increasing temperature enhances the thermal performance of the PV/T. Figure 53 below shows the relation between solar irradiation and the exergetic efficiency and air outlet temperature of the PV/T.

There is only one exergetic efficiency which combines the effects of the electrical and thermal irreversibility in one term, according to the analysis conducted by [121]. In Figure 53, this exergetic efficiency is seen to decrease linearly and sharply due to the significant effect of the irreversibility due to high temperatures that are associated with higher values of solar irradiation.

As for outlet air temperature, this is seen to increase because of the higher PV temperatures that the air encounters at larger irradiation (I) values.

The performance of the PV/T is also studied with reference to the ambient temperature. Increasing ambient temperatures results in, as one can tell from intuition, increasing thermal efficiency and reduced electrical efficiency, as seen from Figure 54.

As for the trends in exergetic efficiency for increasing ambient temperatures, the exergetic efficiency is seen to decrease with increasing T_0, as can be observed in Figure 55.

The same causal analysis that is applicable to increasing irradiation applies here, with higher temperatures resulting in higher degrees of irreversibility.
From Figure 54 and Figure 55, we can intuitively deduce that increasing the mass flow rate of the air through the PV/T would not only increase the heating capacity, but also raise the electrical efficiency of the same, albeit at the cost of air outlet temperature.

To confirm this deduction, Figure 56 is produced, where it can be seen that the reduction in the rate of increase of the energetic and exergetic efficiencies is minimal, thus making it preferential to use higher mass flow rates.

Figure 57 shows the variation of exergetic efficiency and air outlet temperatures with increasing mass flow rates. While air outlet temperatures decrease with increasing mass flow rates, exergetic efficiency shows a desirable trend and can be explained by the reduced irreversibility at reduced PV temperatures due to high mass flow rates.
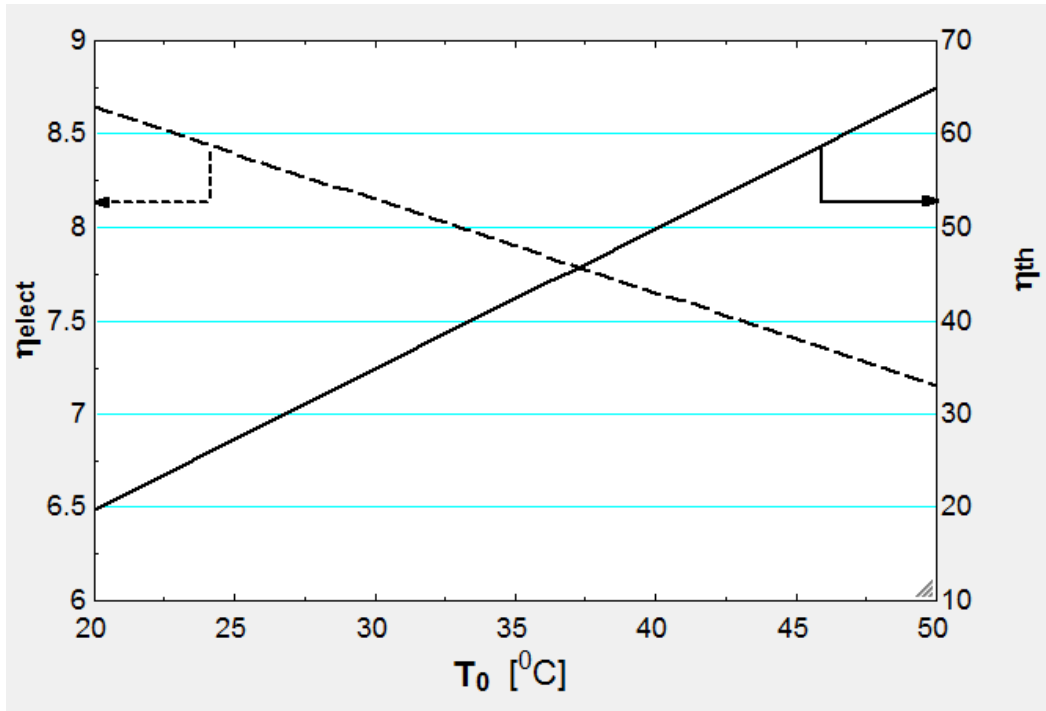
Figure 54: Variation of PV/T electrical and thermal energetic efficiencies with ambient temperature
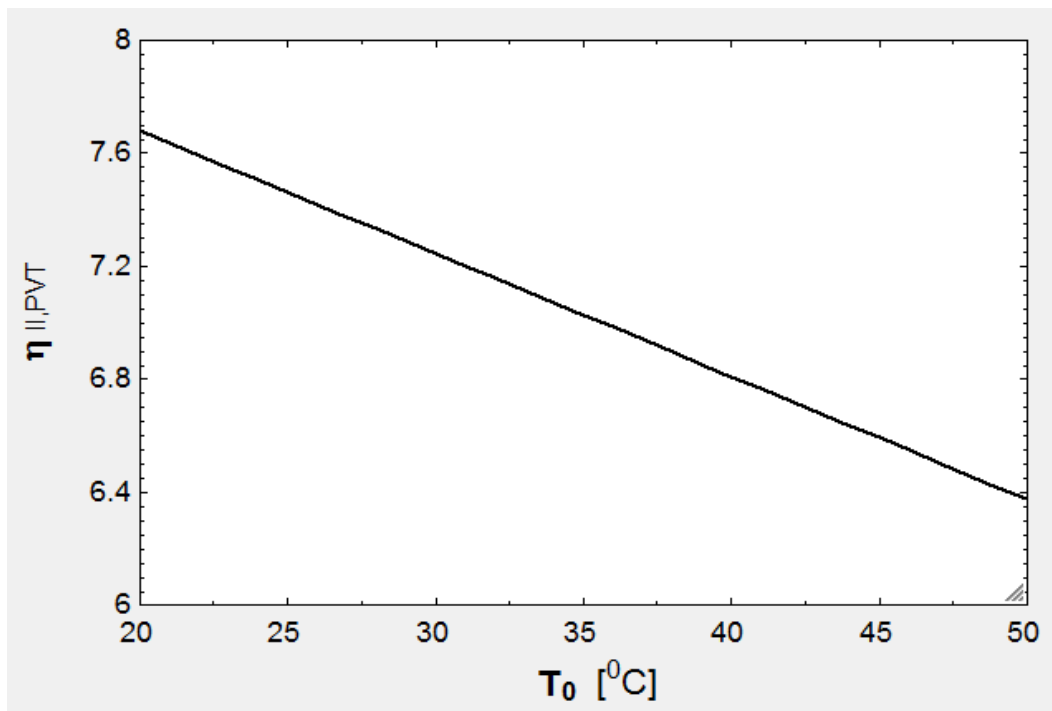
Figure 55: Change in PV/T exergetic efficiency with ambient temperature
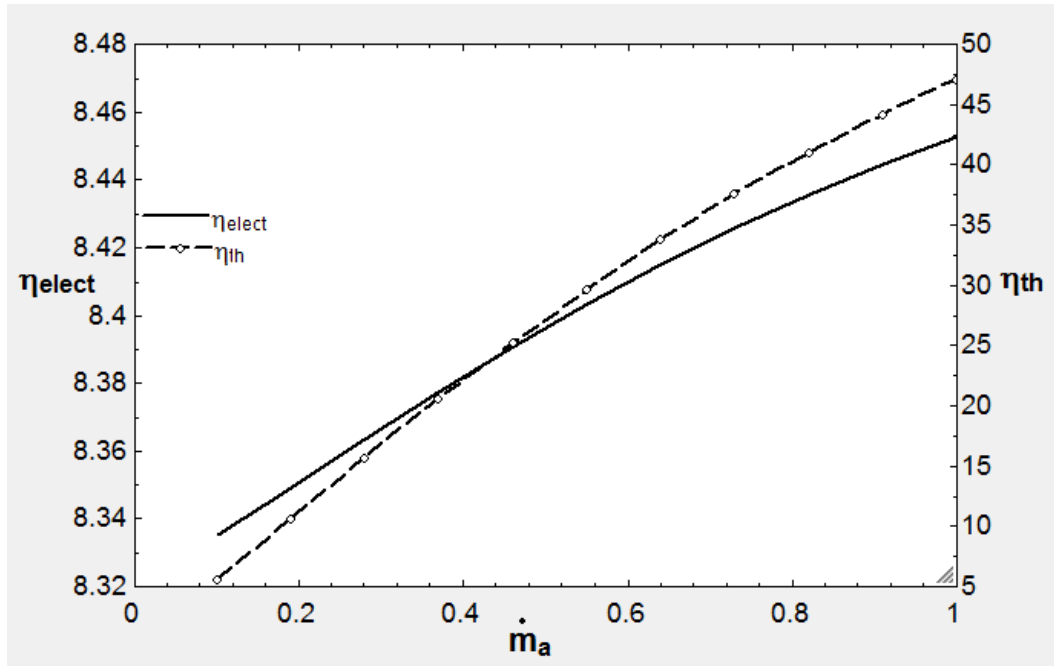
Figure 56: Variation of PV/T electrical and thermal energetic efficiencies with mass flow rate of air
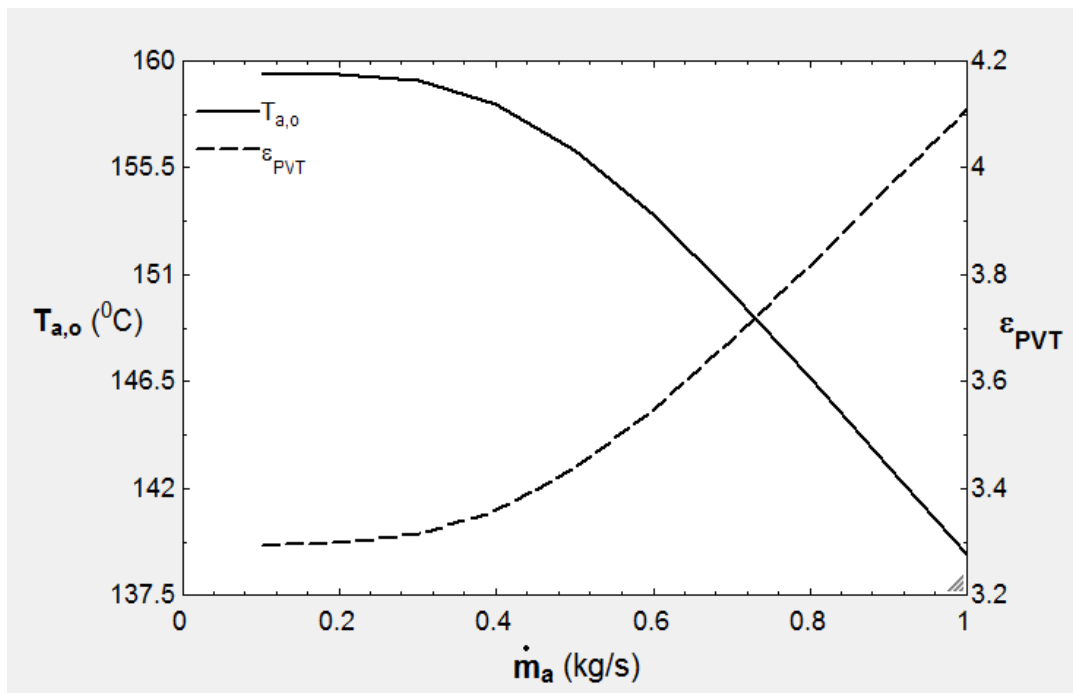
Figure 57: Variation of PV/T exergetic efficiency and air outlet temperature with mass flow rate

The monthly performance of the model of the PV/T module was also determined. Figure 58 shows the monthly electrical power produced, which is highly related to the monthly solar irradiation. The power output is found using both, monthly average ambient temperatures and monthly solar irradiation.
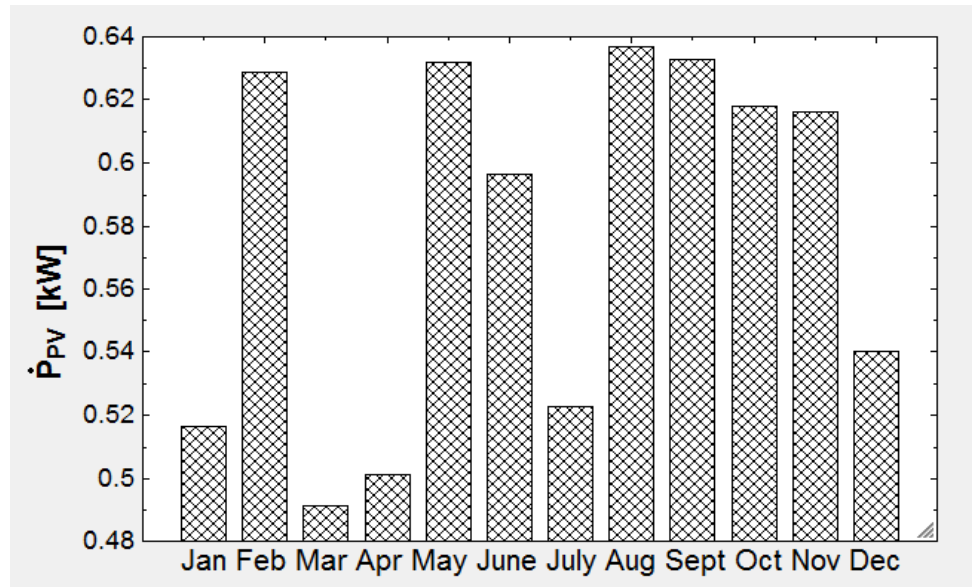
Figure 58: Monthly PV/T electrical power production
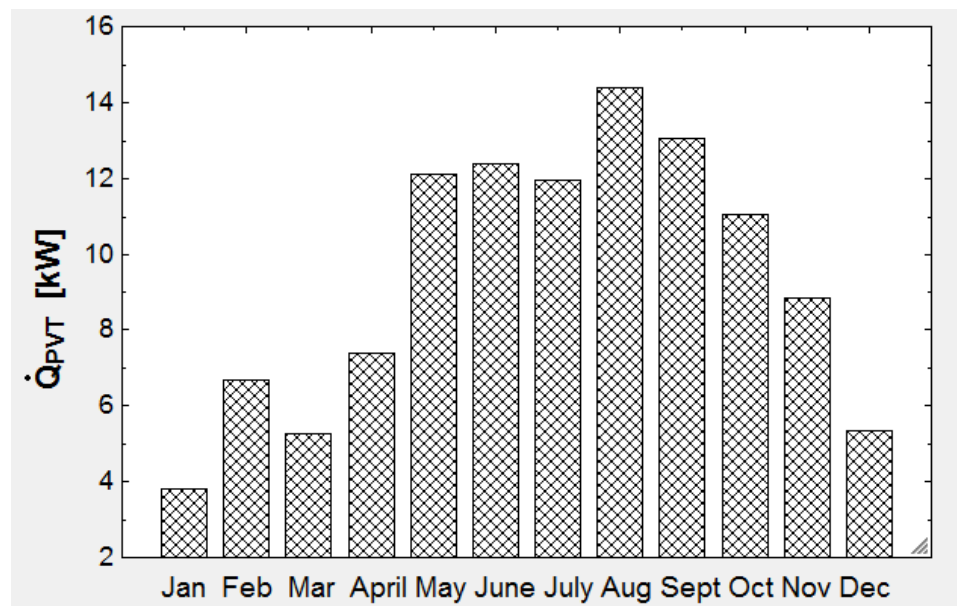
Figure 59: Monthly PV/T thermal production

From Figure 58, it can be determined that monthly performance fluctuates a little, with lows in the months of January, March, April and July. While the power production values are seen to closely follow the solar irradiation intensity pattern, the lows during the cooler months can be attributed to cloud cover, while the dip in power production in July can be attributed to haze. Also studied is the monthly rate of heat produced by the PV/T module, as shown in Figure 59.

Lastly, the monthly energetic and exergetic efficiencies are portrayed in Figures 60 and 61. In Figure 60, it can be seen that thermal efficiency is strongly affected by the ambient temperatures, hence reflecting the trends in T_0, with the highest thermal efficiencies being encountered during the hot summer months. Electrical efficiency, on the other hand varies comparatively little, with the variations being mostly due to fluctuations in solar intensity and ambient temperature, the efficiency dropping with increased solar intensity and ambient temperature.
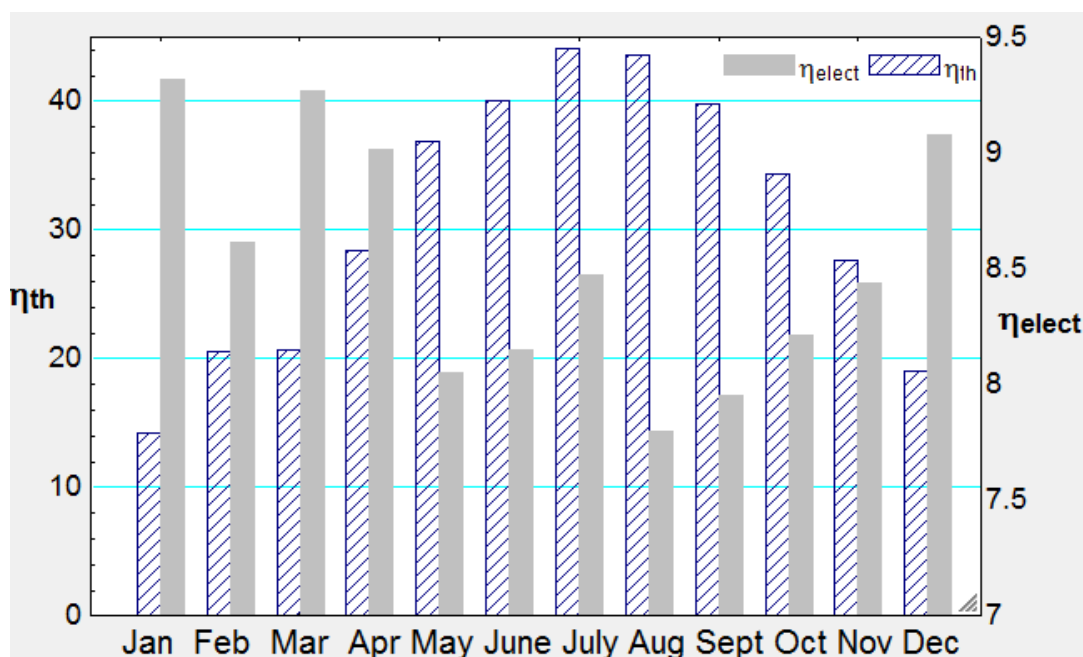
Figure 60: Monthly PV/T electrical and thermal efficiencies

Exergetic efficiency is seen to be mostly affected by solar irradiation, with low irradiation values resulting in higher exergetic efficiencies, as shown in Figure 61.
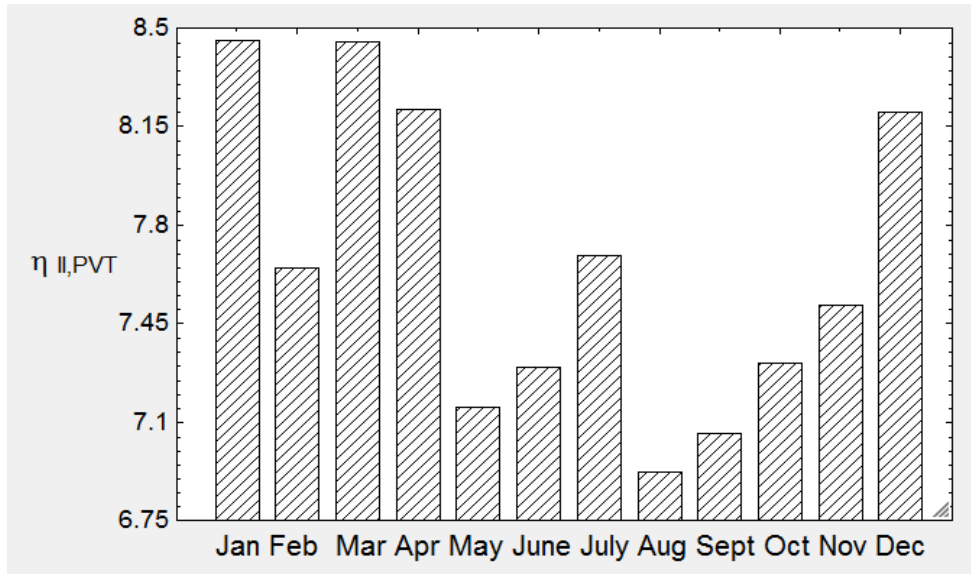
Figure 61: Monthly PV/T exergetic efficiency

3.9   Thermal Latent Storage (Clathrate)

The warm climate of the U.A.E. often necessitates the use of air conditioning, even during the night. With temperatures reaching as high as 35^0C at night, it is often impossible to stay without cooling. This is why a latent heat storage system such as the one shown in Figure 62, is necessary when a well-rounded sustainable system is developed to power and cool homes.

Absorption technology can only work when a heat source is available, and for domestic purposes, solar power is the only option for this source. With the absence of sunlight after the afternoon or early evening hours, no heat is available to run the absorption unless the heat is stored. The other option is to generate ice or a cooling medium during the daytime and store it for later at night. This cold storage can be in the form of clathrate.

Clathrate, as mentioned earlier, is a phase change material, more specifically a refrigerant hydrate that is formed with host molecules of water that clump around the refrigerant molecule. It forms at low temperatures in the range of 5^0C by bubbling refrigerant through a tank of water, hence bringing the refrigerant and water into direct contact, the refrigerant under consideration being R-134a, a refrigerant commonly used for space cooling (see Figure 62).

148
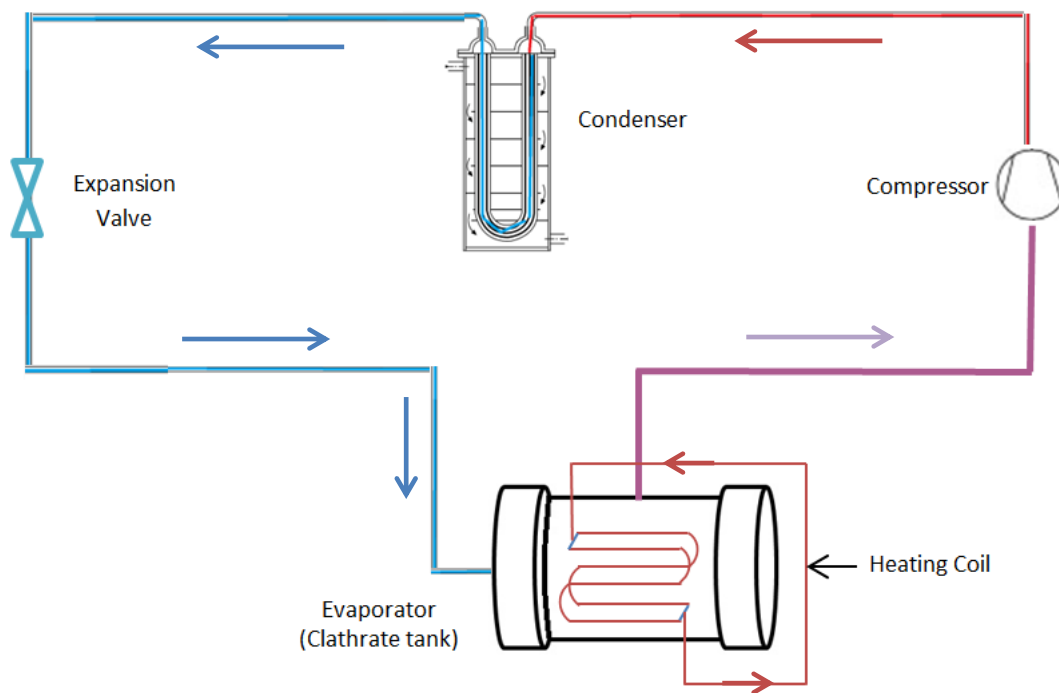
Figure 62: Vapor Compression Cycle for generating R-134a Clathrate during the
daytime

Clathrate is a thermal latent storage medium, which means that during its generation process, most of its latent heat is lost, allowing it to become cold. It remains more or less in this state until a warming stream that needs to be cooled is passed through or in close proximity with it.

The scope of this work with regards to clathrate is determining how much clathrate is needed on average every month, and determining the COP of the system used to generate clathrate. The system is to be modular, with multiple identical units charging simultaneously in parallel. The average amount of clathrate required monthly is given in Table 10.

Determination of the COP is through using two approaches. The first approach, the enthalpy approach, involves estimating the difference in enthalpies of the refrigerant across the evaporator and compressor of the vapor compression cycle used to generate the clathrate, since the refrigerant also serves as the working fluid for the cycle.

Table 10: Mass of R-134a clathrate needed monthly for post-sunset cooling

Month	Mass of Clathrate needed (kg x10^2)
January	9.272
February	9.013
March	9.097
April	12.729
May	15.924
June	17.022
July	18.412
August	19.802
September	18.788
October	16.282
November	12.586
December	9.552

The second approach, involves estimating the COP of the system using the electrical power consumed by the compressor, with $\dot{P}_{ele,comp} = V.I$. Since voltage is more or less constant at 220 V, it is mainly the current which fluctuates with fluctuating compressor loads.

Both types of COP are determined for varying mass ratios of the initial 'charge' to the evaporator, i.e. the charge is the initial amount of refrigerant and water that is fed into the system before the system is sealed and the cycle operated, and the ratio is the ratio of the mass of initial water to the mass of refrigerant.

Clathrate always forms in the Mass Ratio (M.R.) of 2.23, although excess refrigerant is often charged to maximize consumption of the water in the formation of clathrate and to leave a little extra in the system for circulation and super-cooling.

Figure 63 and Figure 64 show the temperature curves for a charging process where the clathrate is generated. The curves are for mass ratios of 2.166 and 2.33.
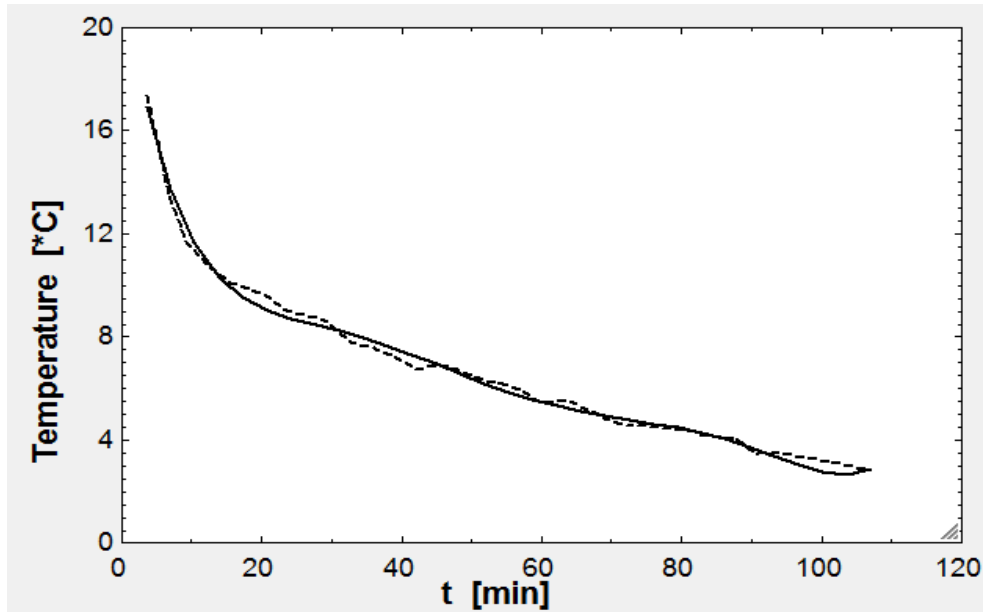
Figure 63: Temperature data and curve fit for charging process of R-134a-Clathrate with a mass ratio of 2.166

Using these curves, a charging temperature curve for a mass ratio of 2.23 is determined, a polynomial is fit through the resulting curve, and a sixth order equation for the polynomial is developed.

The curve in Figure 63 helps us to understand how the temperature would behave during the charging (clathrate formation) process when a refrigerant-water mixture is fed into the system in a mass ratio of 2.166.

The equation of the curve fit for the charging temperature curve for a mass ratio of 2.166 is given in equation 3.1 :

$$T_{2.166} = 21.7487 - 1.6526(t) + 0.0865642(t^2) - 0.00235351(t^3) + 0.0000333119(t^4) - (2.34554(10^{-7}))(t^5) + (6.48498(10^{-10}))(t^6) \qquad (3.1)$$

The agreement of the fit with the curve shows that it can be used to represent the temperature charging process for a mass ratio of 2.166 accurately.

Similarly, the equation of the curve fit for the charging temperature curve for a mass ratio of 2.33 is as follows, with the curve for this equation in Figure 64.

$$T_{2.33} = 21.2265 - 1.71353(t) + 0.104191(t^2) - 0.00332205(t^3) + 0.0000555239(t^4) - (4.70260(10^{-7})(t^5)) + (1.60313(10^{-9}))(t^6) \tag{3.2}$$
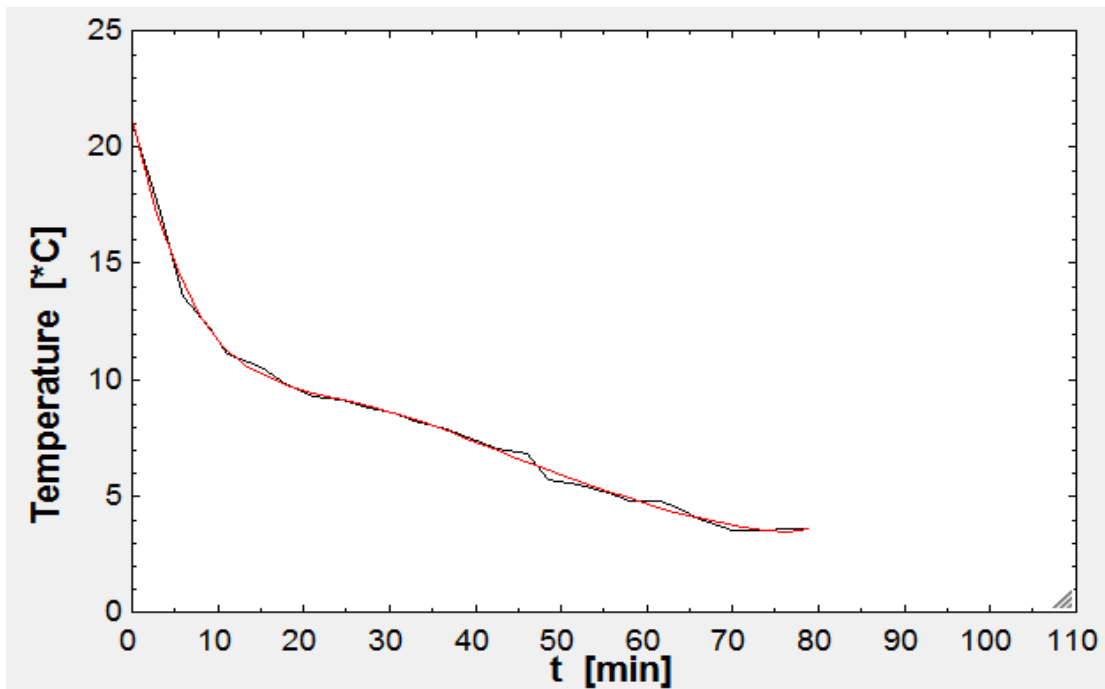
Figure 64: Temperature data and curve fit for charging process of R-134a clathrate with a mass ratio of 2.33

The curves are for mass ratios of 2.166 and 2.33. Once the curve fits are produced, a third curve for a mass ratio of 2.33 is plotted through the actual temperature data, and an approximate plot for the temperature during the charging process is obtained, as shown in Figure 65.

A curve is fitted through this raw data curve and predicted through a sixth order polynomial, which is given by:

$$T_{2.23} = 23.3960703 - 1.90281729(t) + 0.102141777(t^2) - 0.00281201365(t^3) + 0.000040061903(t^4) - 2.82912333(10^{-7})(t^5) + 7.82569077(10^{-10})(t^6) \tag{3.3}$$
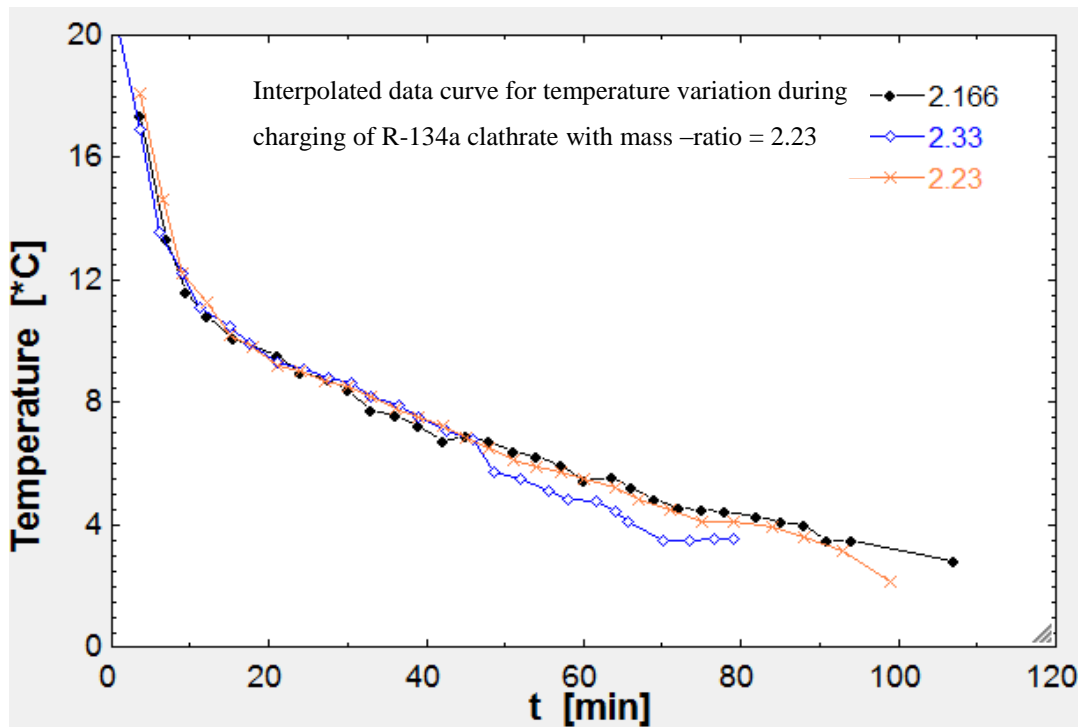
Figure 65: Temperature for charging process of a mass ratio of 2.23
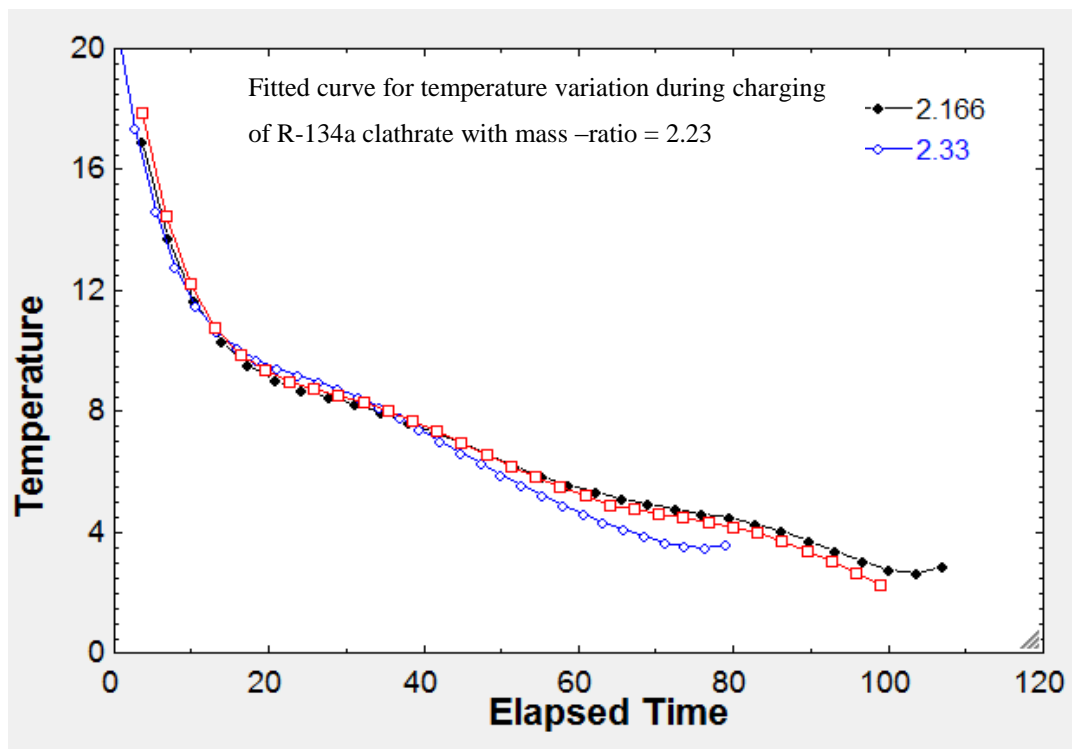
Figure 66: Fitted curve for temperature, charging process; mass ratio 2.23

153

The fitted curve is shown in Figure 66. It is seen to be closer to the 2.166 curve than the 2.33 curve because of the relative difference between the three mass ratios. Also, the difference in temperatures of the tank between the mass ratios is seen to increase mostly after the clathrate is generated. Figure 67 and Figure 68 show the curves obtained for the instantaneous rates of energy absorbed by the evaporator and consumed by the compressor with time, i.e. $\dot{Q}_{e,clathrate}$ and $\dot{Q}_{c,clathrate}$.
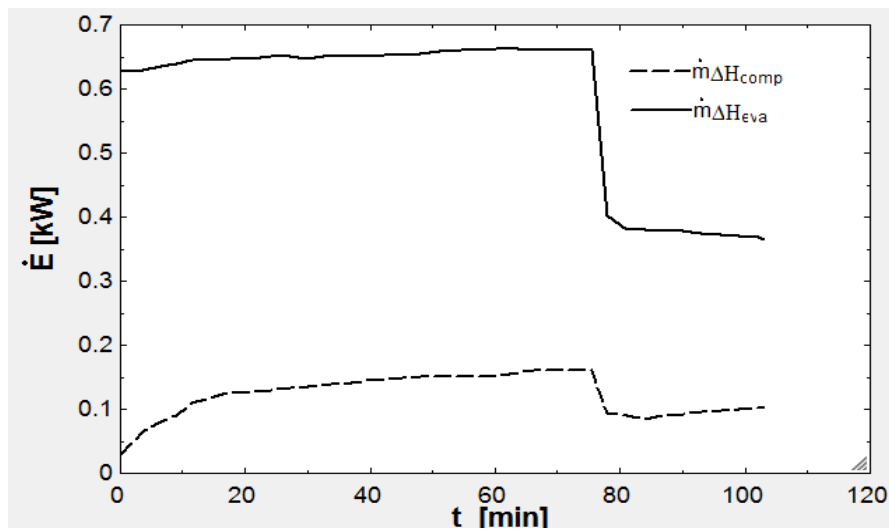
Figure 67: Energy rates across evaporator and compressor during charging of R-134a clathrate with a mass ratio of 2.166
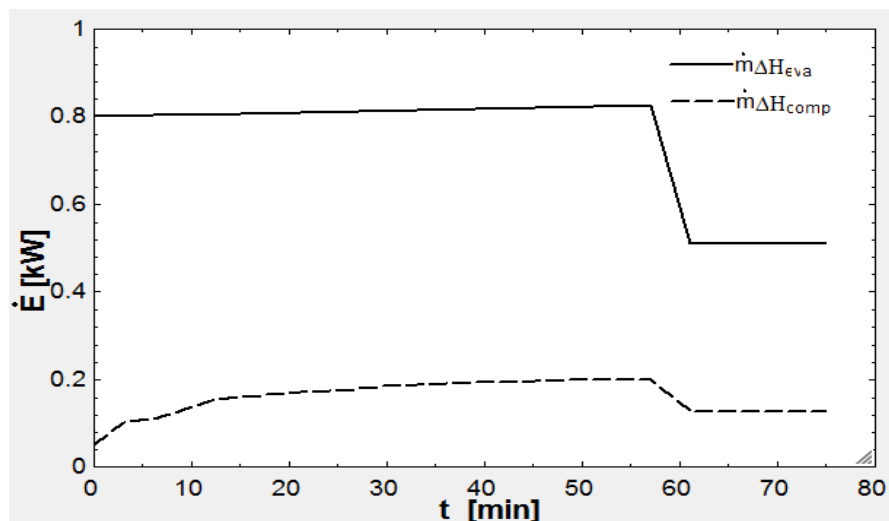
Figure 68: Energy rates across evaporator and compressor during charging of R-134a clathrate with a mass ratio of 2.33

The rates are given by $\dot{m}\Delta h$; Δh is the difference in enthalpies across the respective components. Figure 67 is for a mass ratio of 2.166, whereas Figure 68 is for a mass ratio of 2.33. In order to get a better idea of the effect of different mass ratios, the two curves in Figures 67 and 68 are superimposed on the same set of axes, resulting in Figure 69.
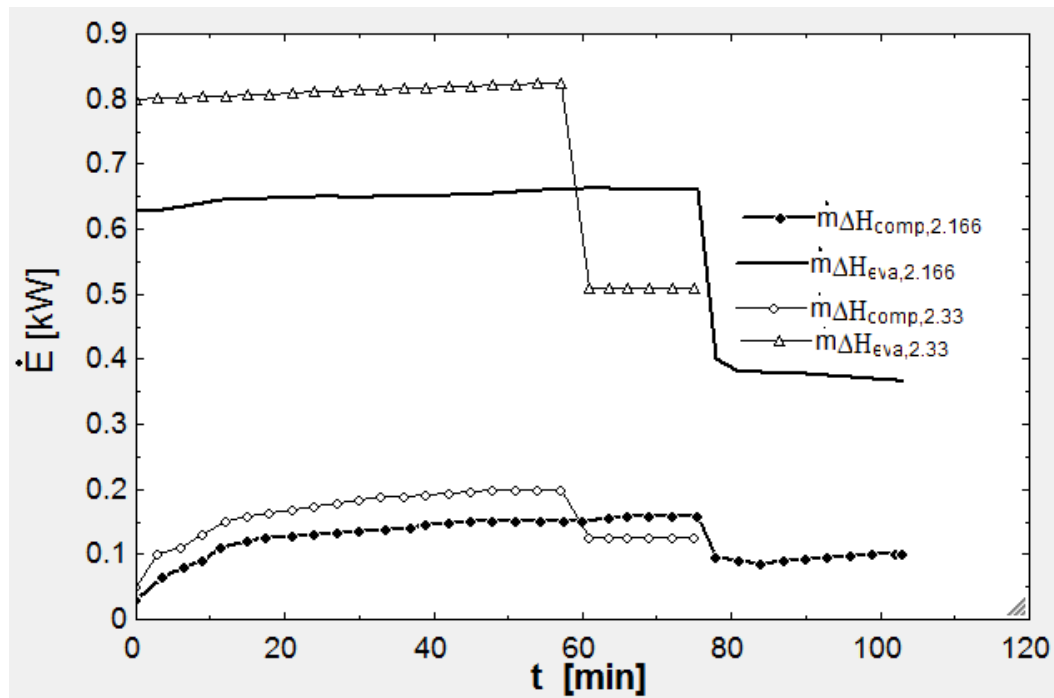
Figure 69: Energy rate comparison across evaporator and compressor during the charging process for different mass ratios of R-134a clathrate

Based on Figure 69, the curves of enthalpy difference for a mass ratio of 2.23 are developed to allow the COP to be calculated for that mass ratio. This is shown in Figure 70. Figure 70 shows the M.R. 2.23 enthalpy curves super imposed on Figure 69. From the comparison, it can be seen that higher mass ratios result in higher heat transfer rates and power consumption. This thus means that the system experiences shorter charging times.

Next, the COP curves obtained when calculating the COP using the difference in enthalpies across the evaporator and compressor are given in Figure 71. The curves are for mass ratios of 2.166 and 2.33.
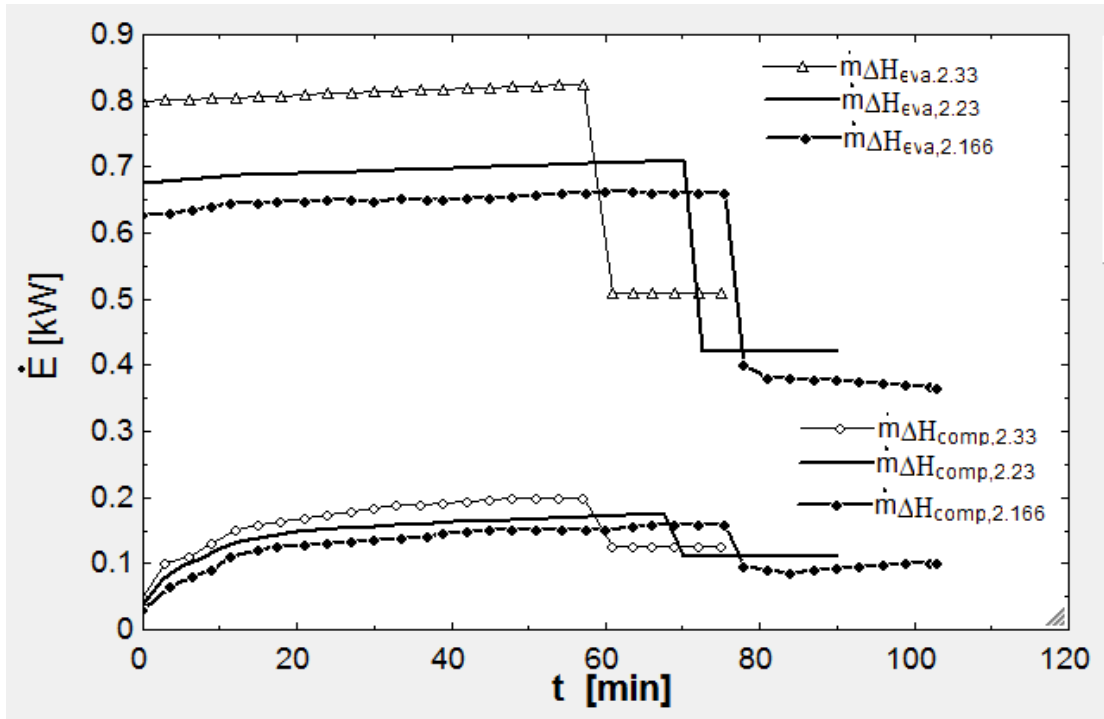
Figure 70: Enthalpy difference curves for evaporator and compressor during the charging process, for different mass ratios of R-134a clathrate
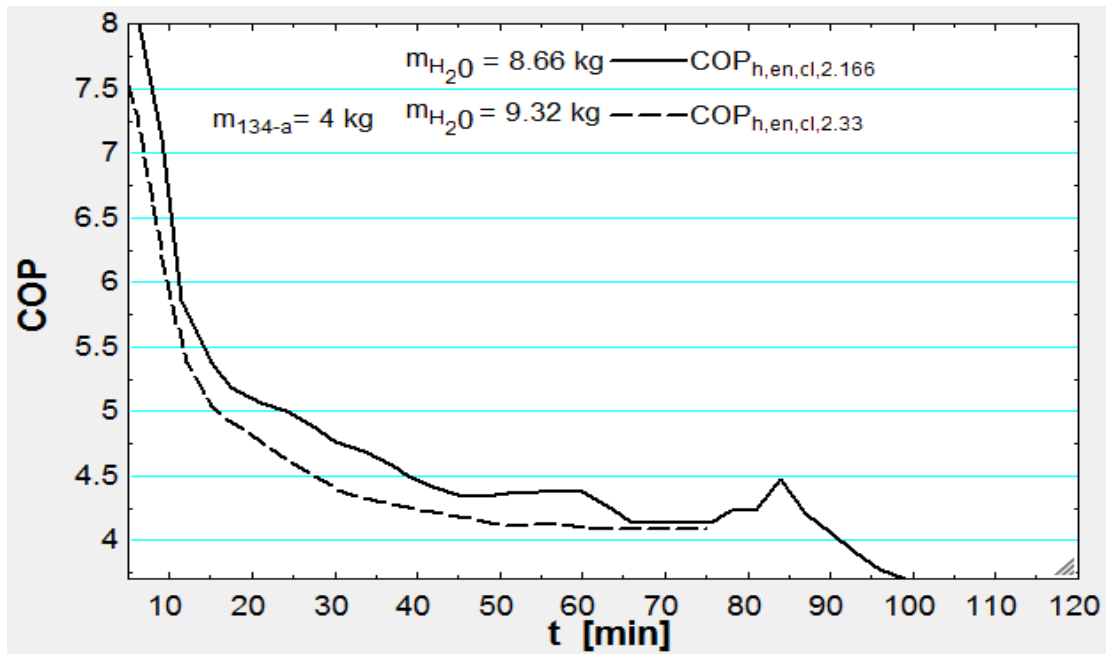
Figure 71: R-134a clathrate COP curves based on enthalpy for charging process; mass ratios 2.166 and 2.33

156

The COP curve for M.R. 2.23 is calculated using the enthalpy curves, and it is superimposed onto Figure 71 to show the relative difference in COPs for the different mass ratios for a charging process, thus resulting in Figure 72.
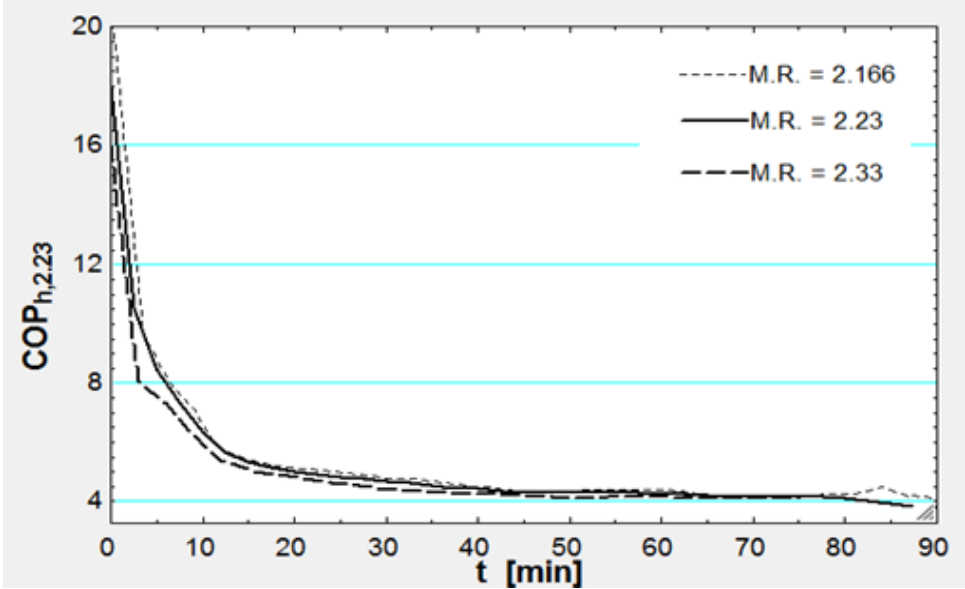
Figure 72: Variation of COP based on enthalpy for various R-134a clathrate mass ratios
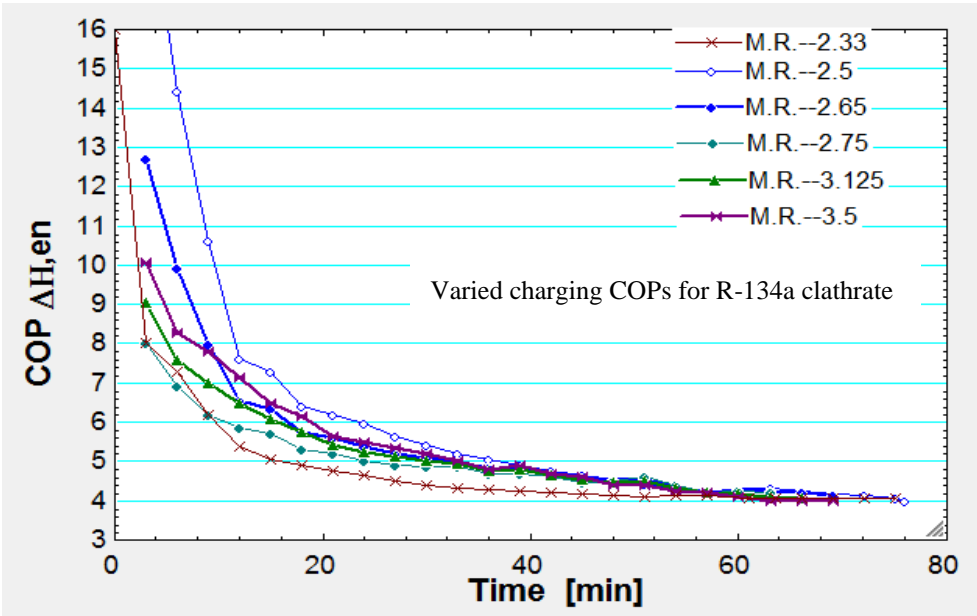
Figure 73: Variation of COP during the charging process for various R-134a clathrate mass-ratios

Similarly, more COP curves were obtained for various mass ratios (see Figure 73), all with 4 kg of water. In figure 73, the curves are for the enthalpy based COP. It can be seen that higher mass ratios don't necessarily result in higher COPs, and thus a mass ratio of 2.33 is preferable for this system as it provides the highest COP during charging before, during and after formation of clathrate. Based on the results obtained and plotted for the enthalpy-based COP, the COP_{el} for M.R. 2.23, being closer to the curve for M.R. 2.166 than M.R. 2.33, seems to be accurate in predicting the COP el for M.R. 2.23, as seen in Figure 74.

The COP curves obtained so far were found using the first approach that uses the enthalpy difference across the evaporator divided by the enthalpy difference across the compressor. An alternate approach would be to calculate the COP using the electrical power consumed by the compressor. Figure 74 and Figure 75 show the COP calculated in this way for different mass ratios. As can be seen from Figure 74, values for the COP_{el} for M.R. 2.23 are about 2.22 for the initial stage (clathrate formation) and about 1.32 after the clathrate is fully formed.
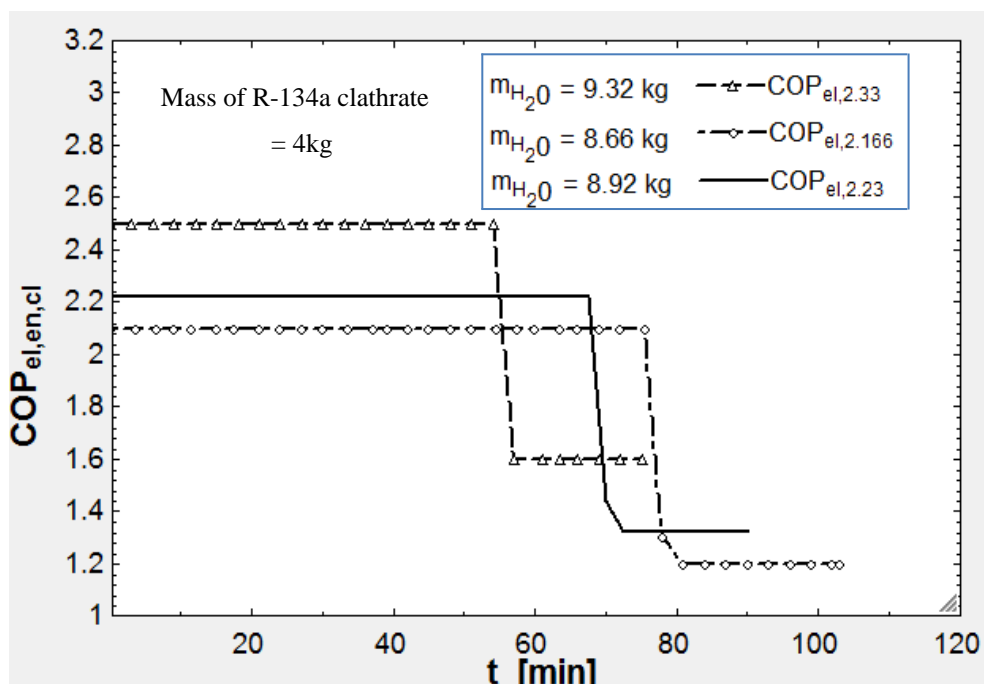
Figure 74: Variation of COP based on electrical power during the charging process for various R-134a clathrate mass ratios
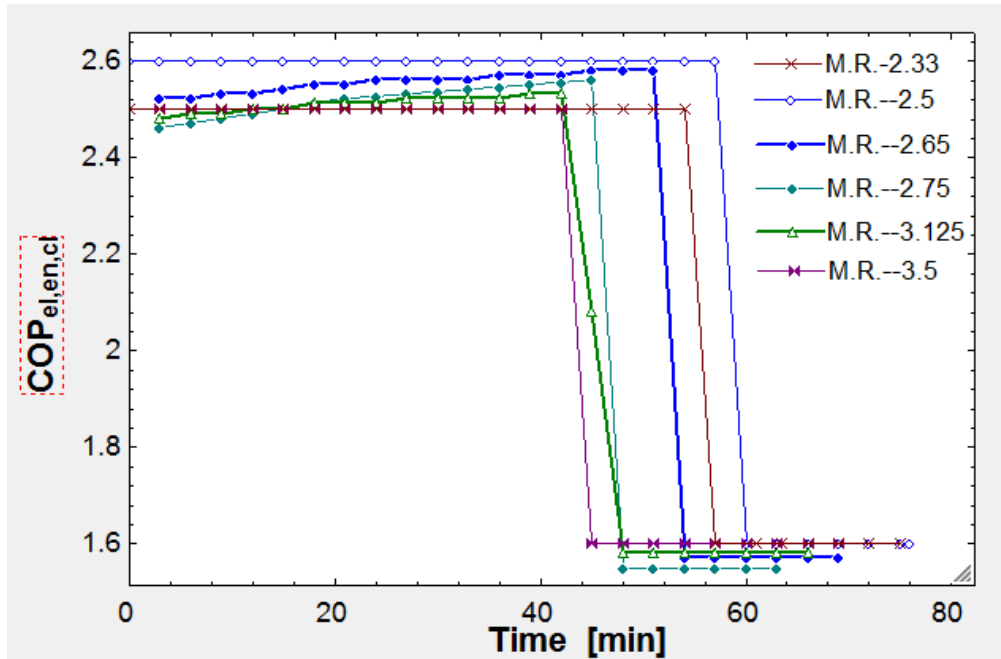
Figure 75: Variation of COP_{el} during the charging process for various operating R-134a clathrate mass ratios

The reasoning behind the drop in COP is that current drawn by the compressor motor increases due to the increased load on it when it has to push the refrigerant to bubble through the formed clathrate to complete the cycle. It can also be seen that a mass ratio of 2.5 takes a marginally longer time for charging, i.e. approximately 10 minutes longer than the shortest charging period which is 70 minutes for a mass ratio of 3.5 and 4 kg of water, although this is insignificant compared to the ample hours for which sun is available in this region as multiple units can be charged simultaneously. The electrical COP curves show us similar results, with the mass ratio of 2.5 being the most suitable in terms of charging performance.

3.10 Hot Thermocline Storage

In order to provide night-time cooling, many alternatives to conventional air-conditioning exist. One of these is to use a sensible heat storage mechanism that can store heat to run a heat driven system such as an absorption system. The most common sensible heat storage mediums include solids such as concrete, and liquids such as water and oil.

159

In this work, water is decided upon as the medium because of its low cost, moderately high specific heat capacity, ease of obtainment and transport, and safety. In order to store this water, a storage tank has to be sized, and accordingly it is determined that a cylindrical tank of height 5m and radius 2.563m will suffice our needs. These dimensions correspond to an area of 121.79m^2, and with an overall heat transfer coefficient of 16 Wm^{-2}K^{-1}, the tank experiences average heat losses of 2.953 kW and 3.147 kW during daytime and nighttime respectively, as shown in the below calculations. Taking worst case scenarios for heat loss, the average daytime temperature is taken to be 35^{0}C, and the average rate of heat loss from the tank during the daytime is calculated to be:

$$\dot{Q}_{l,hst} = 0.00016 \cdot (121.79) \cdot (186.5 - 35)$$
$$= 2.953 \; kW$$

This corresponds to 10,628 kJ/hr and thus 106,279 kJ or 29.53 kWh over the 10 hours of daylight. During the night, the heat loss is estimated to be:

$$\dot{Q}_{l,hst} = 0.00016 \cdot (121.79) \cdot (186.5 - 25)$$
$$= 3.147 \; kW$$

which corresponds to 11,329 kJ/hr and 158,612 kJ or 31.47 kWh over 14 hours of insufficient/absent sunlight. Together, the average loss per day amounts to 70 kWh. Table 11 provides an idea of how much heat is required on average to heat the storage daily. As can be seen from column 7 of Table 11, the heat produced daily to charge the tank more than compensates for this daily loss in every month, and thus there is no need to refine the design. Thus, both, the PTSC charging the tank, and the tank itself, are designed to more than meet the heating requirements of the absorption systems during night, and possibly during periods of no availability of sunlight.

The PTSC length required for simultaneously charging the tank and running the TEAS during the day is determined to be 93m (as opposed to the 65m required for only running the TEAS). The sufficiency of this length and the heating process can also be seen in Table 11. All quantities are for an average night each month.

While it might seem that based on the results in Table 11, the length added to the PTSC (93m − 65m = 28m) for charging the storage tank is not justified and that a smaller length would have been sufficient, the length is chosen because we had to

ensure that not only did the required heating rate be met, but also that the total heat requirement of the absorption system is met by the storage. The reason these two approaches, i.e. sufficiency for heating rate and sufficiency for total heat required, would differ, is given after Table 11.

Table 11: Monthly performance of hot thermal storage for night cooling

	1	2	3	4	5	6	7
Jan	13.25	6.959	4.2	57.93	55.65	818.98	763.33
Feb	12.67	7.076	4.3	77.3	54.481	727.921	673.44
Mar	12	7.538	4.6	44.71	55.2	373.413	318.213
Apr	11.25	11.25	6.8	41.75	76.5	294.508	218.008
May	10.75	14.73	9	66.7	96.75	500.5	403.75
June	10.35	16.36	9.9	52.4	102.46	299.125	196.66
July	10.5	17.44	10.6	35.03	111.3	196.78	85.48
Aug	11	17.9	10.9	57.7	119.9	388.66	268.76
Sept	11.7	15.97	9.7	61.9	113.49	480.47	366.98
Oct	12.5	12.95	7.9	65	98.75	570.67	471.92
Nov	13	9.628	5.9	70.9	76.7	665.27	588.57
Dec	13.4	7.089	4.3	63.11	57.62	613.495	555.875

where the columns 1 through 5 represent:

1   Average length of night (hours)

2   Average cooling rate (kW) required to be produced by TEAS during the night

3   Average heating rate (kW) required to be input to the TEAS highest generator

4   Average heating rate (kW) produced by the PTSC

5   Average heat required by TEAS (kWh)

6   Average heat produced (kWh) by PTSC (93m) for TEAS and heating storage

7   Heat produced to only heat storage (i.e., difference between columns 5 and 6)

As mentioned earlier, to suffice the simultaneous requirements of charging the tank and running the absorption system, a PTSC of length 93m is found to be needed. As can be seen from columns 3 and 4, the average required rate of heat supply to the storage tank is much lower than the average rate of heat produced by the PTSC for supply to the tank. The average rates (required and produced) are calculated using an arithmetic mean of the hourly rates during daylight, which means the rates are

161

calculated by summing the hourly rates and dividing by the number of hours. The hourly rate is the average rate of heating or cooling required for that hour of an average day during that month. This means that only the number of hours for which the sunshine is sufficient for heating and their corresponding rates of heat produced are taken into consideration. However, calculating the mean in this way might lead to an overestimation of the effectiveness of the tank heating process since we only consider hours of significant sunshine for the charging rates, while during sunrise and sunset, heating rates required are actually higher than the heating rates produced, the latter being close to nil. Therefore, this makes it necessary to calculate not just the heating rates required and produced, but also the absolute amounts of heat required and produced to ensure that the *total* amount of heat required is met too. Hence columns 5 and 6 are developed, and it can be seen that particularly during the month of July, when cooling loads are close to peak, the discrepancy between the amount of heat required and produced is quite small. This justifies the lengthening of the PTSC to suffice the simultaneous loads of the TEAS and the charging of the storage tank.

Also determined is the hourly charging process for the tank during the worst-case scenario for solar irradiation. This is during the month of July as the cooling requirements are second to highest during this month while solar insolation values are quite low. The charging process is detailed in steady-state by considering the hourly heat addition to the tank from the PTSC, as well as the hourly losses from the tank, based on the temperature changes the tank undergoes due to these and the hourly changes in ambient temperature. The losses are due to the difference between the temperatures of the tank and the surroundings. It is seen that for a full cycle of 24 hours, the heat added during the day is more than sufficient to charge the tank to enable it to overcome its heat delivery requirements and losses to the environment. It can be inferred from Table 12 and Table 13 that after a full 24 hours of a charging-discharging cycle, the tank is at a higher temperature than it was at the start of the cycle, suggesting that it is possible to charge the tank sufficiently every day without having to worry about the energy stored falling short of requirements.

Table 12 and Table 13 give the details of the 24-hour charging-discharging cycle for the worst case scenario, an average day in the month of July. Summing the net heat added every hour, it can be noted that the charging time required to deliver a net

amount of 111.3 kWh, the amount of heat required to run the absorption at night during an average night in July, is roughly 4.75 hours, which means that the tank is charged by 11:45am. Any surplus heat supplied thereafter can be carried over to the next day or can be used to counter any additional losses.

Table 12: Parameters of charging cycle for HTS

Time	T_{tank} (^{0}C)	T_0 (^{0}C)	Heat addition (kW)	Losses (kW)	Net Heat added (kW)	Charging Efficiency (%)
07:00	192.0102	35	4.28	3.0594	1.2206	28.52
08:00	192.0650	37	9.64	3.0596	6.5804	68.26
09:00	192.1771	40	16.47	3.0217	13.4483	81.65
10:00	192.3596	43	24.87	2.9654	21.9046	88.08
11:00	192.6034	46	32.16	2.9105	29.2495	90.95
12:00	192.8691	48	34.74	2.8568	31.8832	91.78
13:00	193.1374	47	35.03	2.8230	32.2070	91.94
14:00	193.4042	45	34.86	2.8477	32.0123	91.83
15:00	193.6480	44	32.15	2.8919	29.2581	91.01
16:00	193.8396	43	25.91	2.9161	22.9939	88.75
17:00	193.9374	41	14.67	2.9393	11.7307	79.96
18:00	193.9560	40	5.21	2.9802	2.2298	42.80

Table 13: Parameters of discharging cycle for HTS

Time	T_{tank} (^{0}C)	T_0 (^{0}C)	Heat drawn (kW)	Losses (kW)	Total Heat loss (kW)
19:00	193.8226	39	13	3.0000	16.0000
20:00	193.6925	38	12.6	3.0169	15.6169
21:00	193.5689	37	11.8	3.0339	14.8339
22:00	193.4468	36	11.6	3.0510	14.6510
23:00	193.3262	35	11.4	3.0681	14.4681
0:00	193.2072	34	11.2	3.0852	14.2852
1:00	193.0897	33	11	3.1024	14.1024
2:00	192.9737	32	10.8	3.1196	13.9196
3:00	192.8592	31	10.6	3.1368	13.7368
4:00	192.7446	30	10.6	3.1541	13.7541
5:00	192.6298	32	10.6	3.1713	13.7713
6:00	192.4987	34	12.6	3.1301	15.7301
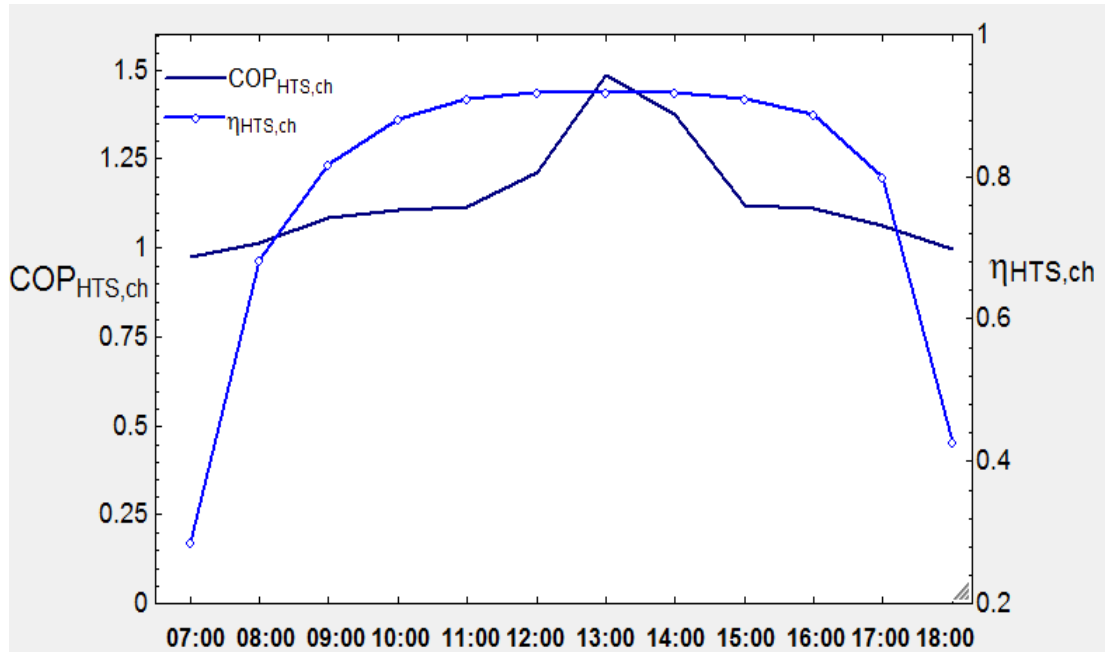
Figure 76: Charging COP curve for the hot water thermocline tank for July

Also Figure 76 displays the daytime charging COP of the HTS-TEAS night-time cooling system and the daytime charging efficiency of the HTS, as defined in the modeling section. Both, charging efficiency and COP are seen to peak at approximately 13:00 hours.

3.11 Comparison of Thermal Storage Technologies

Since both, the CGVCS and the thermal storage tank are a means of allowing cooling during periods of non-availability of sunshine, it is imperative that we compare the effectiveness of both methods. The two technologies are compared on the basis of their merits in the following criteria:

- Thermal Efficiency
- Charging times
- Size
- Cost
- Feasibility of installation
- Environmental friendliness

164

3.11.1 Thermal efficiency.

The thermal efficiencies of the two technologies are determined slightly differently because of their modes of operation. While the CGVCS generates clathrate that can provide direct cooling at night by means of a secondary cooling loop, the HTS stores heat that is used to run the absorption system at night. Hence, the only common performance indicator between the two is the COP. The COP for the CGVCS is calculated using the amount of cooling stored in the clathrate and the electrical power consumed by the compressor, while the COP for the HTS-TEAS is calculated using the heat delivered by the HTS to the TEAS's highest generator and the cooling produced by the evaporator. As was seen earlier, while COPs for the CGVCS during charging are in the 2.4-2.6 range, it can be seen from Figure 75 and Figure 76 that COPs for the HTS-TEAS combined system range between 1 and 1.5 during charging. Though effective cooling produced by the CGVCS might be slightly lower than the amount of cooling stored in the clathrate because of losses incurred through the use of the secondary loop, these numbers go to show that the CGVCS is superior in delivering cooling performance.

3.11.2 Charging times.

For the CGVCS, a mass ratio of 2.5 delivers the best performance with a COP of 2.6. Although clathrate at this mass ratio also takes the longest time to form, the total charging cycle, with sub-cooling takes approximately 77mins. The water in the HTS on the other hand, needs to be heated initially to 190^0C initially, before it can start storing heat that can be used to run the absorption systems. This can take a few days. However, this is a one-time event for the first-time that the tank is used, and additional charging per day needs to only store enough heat for that same night. This daily charging cycle is displayed in Figure 76, and for the worst case scenario of the month of July, takes approximately 4 hours and 45 minutes. Since charging takes place throughout the day for as many hours as there is sunshine, any additional heat charged to the tank is either stored for successive nights, or compensate for losses during the daytime and keep the tank fully charged for hours of insufficient/absent sunlight.

Nevertheless, charging time for the CGVCS is nearly a quarter of that required to charge the HTS, hence showing that the former is more feasible than the latter. Moreover, the CGVCS can be built as modules which can charge simultaneously,

hence offering additional time savings as well as flexibility of use, as some modules might be used for peak-load reduction, while others charge for night-time cooling.

3.11.3   Size.

Size is also an important aspect of any equipment. Smaller units allow for ease of transportation and installation, and can be fitted / placed more conveniently. The HTS, in this respect, is again at a disadvantage compared to the CGVCS. The HTS requires a tank of height 5 m and radius 2.563 m, whereas the CGVCS requires a tank of height 1 m and radius 0.66m for a mass of 1980 kg which has a volume of 1.367 m^3 (volume of clathrate is approximately the same as the volume of water as clathrate is formed of host molecules which clump around the refrigerant molecule.

3.11.4   Cost.

The calculation of the costs for both systems shows us that a custom CGVCS would cost us 70,400 AED. This cost figure is determined based on quotes from well-established air-conditioning companies for manufacturing the system, as well as common market costs for equipment. In comparison, the specific cost of a HTS is 1540 US\$/m^3 [126], which gives us a total figure of 158,892 US\$ (583,135 AED) for 103.177 m^3 of capacity. Once again, it is seen that the CGVCS is much more feasible than the HTS, this time economically.

3.11.5   Feasibility of installation.

The CGVCS, while smaller than the HTS, is a much more sophisticated piece of equipment, making it harder to manufacture and install. However, it does not require any additional equipment to provide cooling, as does the HTS, which supplies heat to the absorption systems so that the latter can provide cooling. Both systems can be run using a renewable source of energy. The heat for the HTS can be supplied by either 28 m of additional PTSC, or through the existing 14 kW_e of PV/T which supply the houses with electrical energy for the appliances and heat for a hot water supply. Alternatively, electrical power generated by the PV/T or WT can also be used to run an electric heater. The CGVCS compressor on the other hand, requires 7 kW_e which can be obtained from the grid (this can be done at night to offset peak daytime loads), or obtained from either the WT or the PV/T.

3.11.6   Environmental friendliness.

Since the purpose of this work is to design a 'green' system, environmental friendliness is a key aspect. While both the CGVCS and the HTS can obtain their energy from renewable sources as stated above, at first sight the CGVCS, compared to the HTS, can be seen to be slightly less friendly to the environment because it has a global warming potential (GWP) of 1300 compared to a GWP of 1 for CO_2.

However, given that the HTS is much larger in size, manufacturing the HTS might have a larger carbon footprint than would manufacturing the CGVCS. Since determination of this footprint for both technologies is beyond the scope of this work, it cannot be said which technology is more environmentally friendly.

Based on the above comparison criteria, from the first four criteria it can be seen that the CGVCS is far more practical as a thermal storage technology than the HTS, and should be implemented in preference to the latter, which is why the three integration options included the CGVCS and not the HTS.

3.12   Integrated System Results

And last but not least, the monthly performance of the remaining integrated systems is obtained. These include the integrated PV/T-WT system, the integrated PV/T-Clathrate Generation Vapor Compression System (CGVCS), and the overall integrated system performance for the three integrated solution cases.

The performance of the PV/T-WT combined system is considered for the case where the PV/T is sized to make up for the deficiency in wind availability so that together, the PV/T and the WT satisfy the villas' electricity requirements, and thus make the villas completely independent of the grid (refer to Figure 77). This combined system would see energetic efficiency varying from a maximum of 14.8% during July to a minimal 5.57% in January, and exergetic efficiency varying from 5.0% during August to a minimum of 1.5% in January, as shown in Figure 78 and Figure 79 respectively. The trend of overall efficiencies for the combined system is seen to more or less follow the solar irradiation intensity pattern even though wind speeds are highest during the first four months. This occurs because the overall system has been sized to meet the 14 kW electrical load of the four villas throughout the year, as can be seen in Figure 77, and thus the PV/T also affects the efficiency of the system.
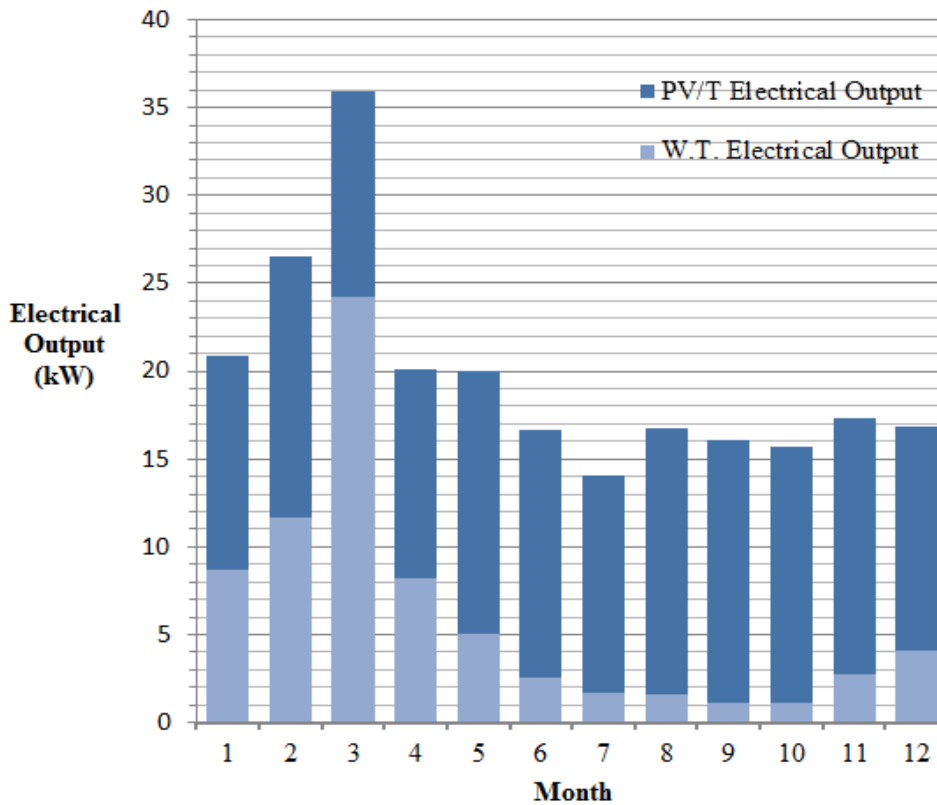
Figure 77: Electrical output of integrated PV/T-WT system

It is to be noted that in Figure 77, the bars representing the PV/T start where those representing the WT end rather than starting at the horizontal axis, and thus the length of a bar representing each month gives us the total electrical output of both technologies. This means that the portion of the total load met by the PV/T increases during the hotter times of the year when wind speeds are much lower. Since the thermal output of the PV/T is much greater than its electrical output, a PV/T system sized as such would have a strong impact on the overall efficiency, and hence the contribution of the PV/T-related factors significantly outweigh those of the WT in the calculation of the overall PV/T-WT energetic efficiency, resulting in the efficiency distribution seen in Figure 78 and Figure 79. Also obtained is the energetic efficiency of the combined PVT-clathrate generation system. Figure 80 shows us that performance is highest during the summer months, particularly during the hottest months of July and August, and hence gives credence to the use of the combined system as a suitable substitute to conventional systems for night-time cooling.
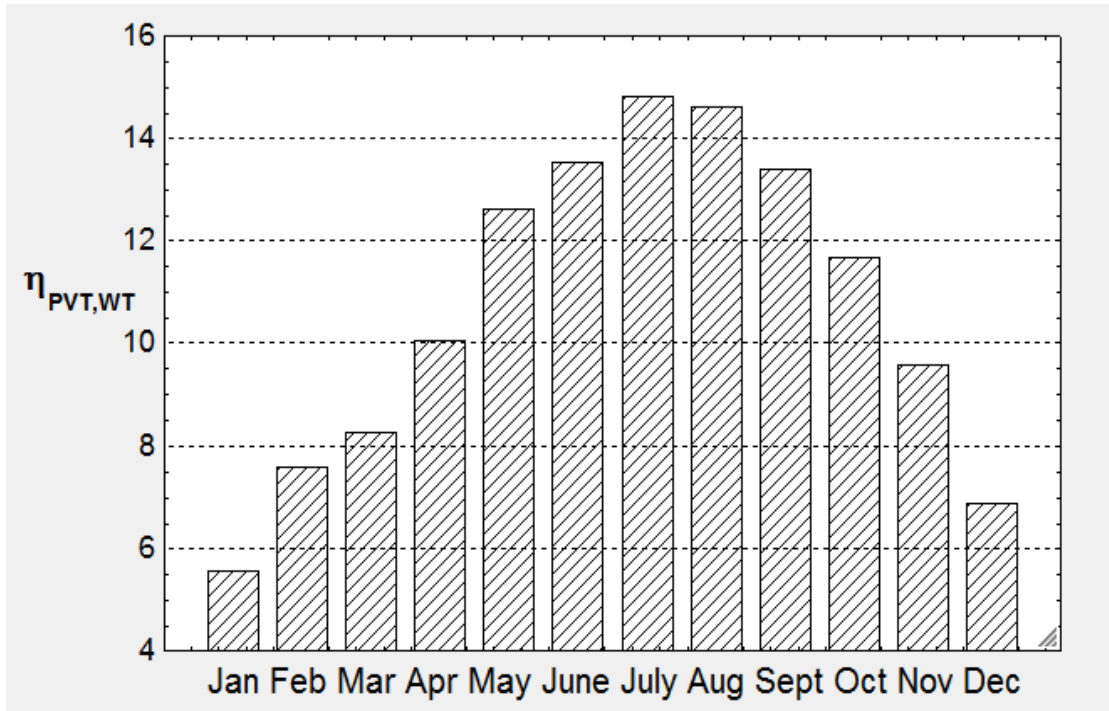
Figure 78: Monthly energetic efficiency of integrated PV/T -WT system
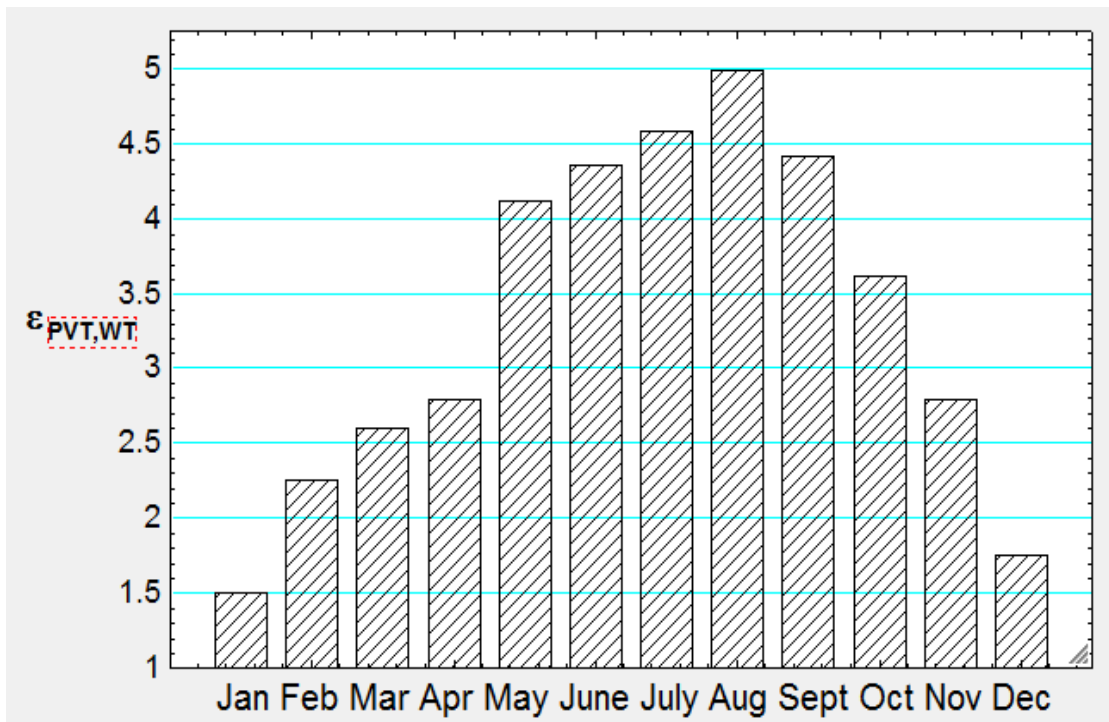
Figure 79: Monthly exergetic efficiency of integrated PV/T -WT system
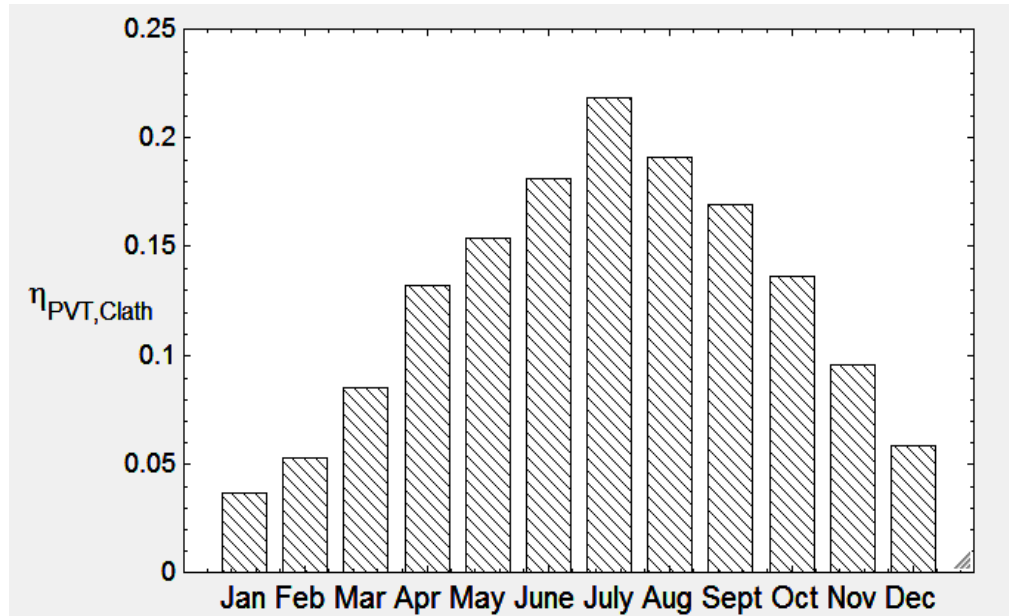
Figure 80: Monthly energetic efficiency of integrated PV/T-clathrate system

Next, a comparison is made between the performances of each integrated case. The energetic and exergetic efficiencies are calculated for all three integrated cases, taking into the account the outputs and inputs to the energy producing and cooling systems. Figures 81 and 82 show us the results of the efficiency comparisons between the three integrated configuration cases considered in this thesis.

Note that because of the transient nature of dynamic loads, battery and CGVCS inputs and outputs were not included in the calculation of these efficiencies which were based on monthly averages.

As can be seen from Figure 81 and Figure 82, Case 3, which provided a comprehensive solution to the homeowners, demonstrated the most efficient performance out of the three integrated options. With the exception of its exergetic efficiency in the months of January and March, Case 3 had the highest overall energetic and exergetic efficiencies, reaching peaks of 0.38 for the energetic efficiency and 0.2 for the exergetic efficiency, both in July. This makes Case 3 the most viable system thermodynamically, not only because it has the highest efficiencies, but also because it provides the most safety for the consumers in terms of uninterrupted supply of electricity and cooling.
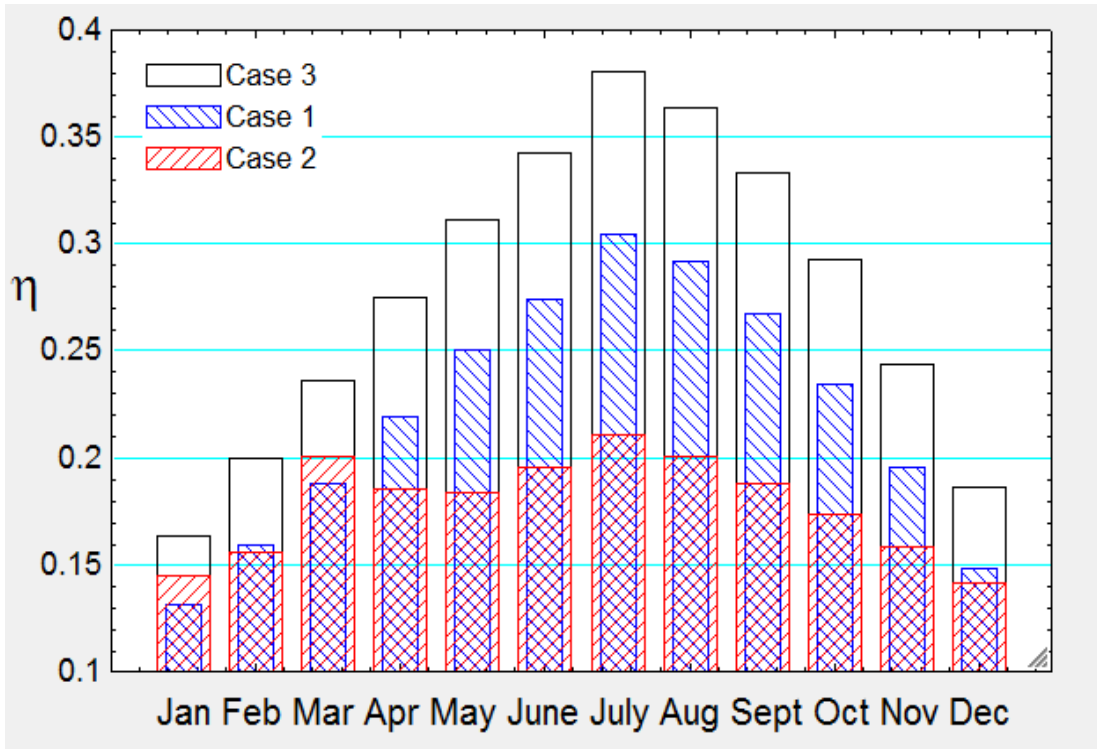
Figure 81: Energetic efficiencies comparison for Case 1, Case 2 and Case 3
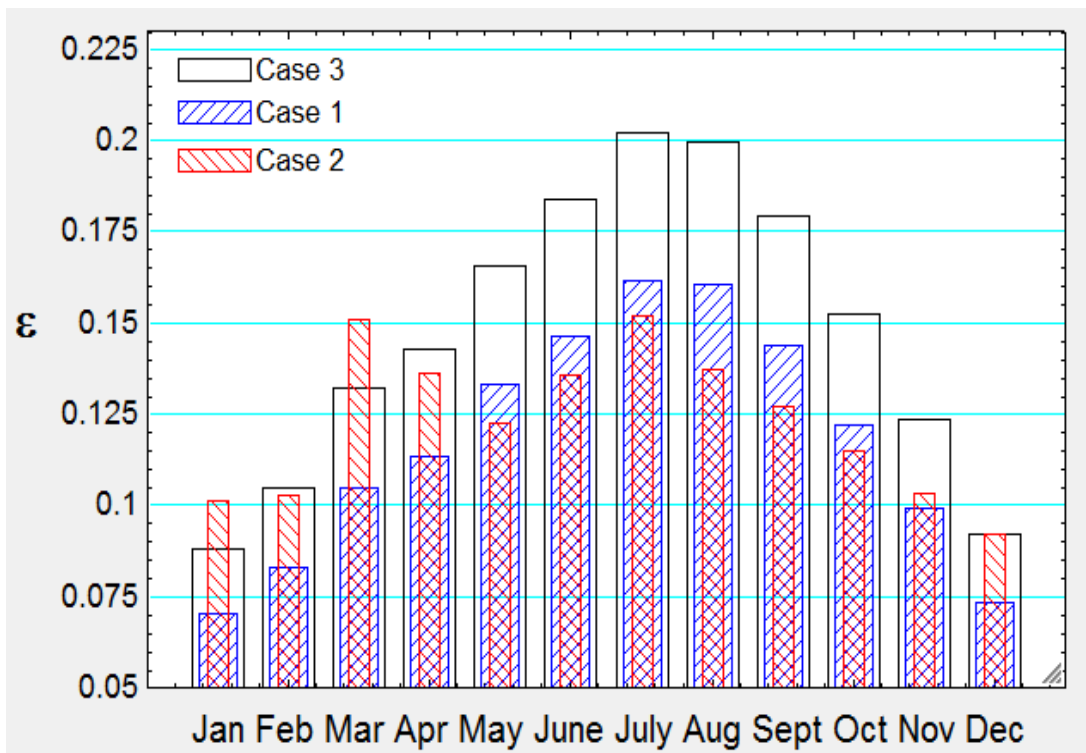
Figure 82: Exergetic efficiencies comparison for Case 1, Case 2 and Case 3

As for Case 2, the deviation from the norm of the exergetic efficiencies for Case 2 is because of the configuration of the system. Half the thermal load required by the TEAS H.G. was assigned to each, the PV/T and the PTSC, and from previous results we see that the exergetic performance of the PV/T was highest during the months of March and January. This resulted in Case 2 having higher exergetic efficiencies during those months than the other two cases.

3.13 Thermo-economic Analysis

In order for the overall system that makes the villas standalone to be profitable, the costs incurred through the installation and operation of the overall system should be less than the cost of electricity for the home owners over a period equal to the 25 year lifecycle of the system.

These costs are calculated through the use of the Present Value method. The present value method determines if a project is economically feasible by allowing the comparison of the long term cash flows in and out of a project, i.e. it compares the present worth of the returns to the present worth of the various costs of the project. If the present worth of the returns is more than the present worth of the costs incurred, then the project is feasible.

3.13.1 Electricity cost to the consumer.

In order to determine the financial feasibility of each RES configuration, the savings obtained through the use of each configuration must be compared to the initial cost of the same. These savings can be calculated as follows. Firstly, the amount that consumers are charged for electricity needs to be determined. This is done by:

- approximating the households' consumption of electricity in kWh and,
- using the electricity rates charged by the government for the various consumption slabs to find out the amount that would be charged to the consumers over a time-period equal to the life of the integrated system.

Using power ratings for various common household appliances, the approximate annual use of electricity by the household's amounts to 365,000 kWh per annum for the 4 households:

Average Electricity Consumption /villa/day   = 250 kWh

Consumption for 4 villas/day = 250*4   = 1000 kWh

Consumption for 4 villas per year = 1000*365 days   = 365,000 kWh/yr. = 30,417 kWh/ month

As for the amount charged to the consumers, it is charged based on consumption slabs, and is governed by the subsidized electricity slab rates, which are given in Table 14 and have been taken from [127].

Table 14: Electricity consumption slab rates

Consumption slab (kWh)	Slab rate charged (AED/kWh)
1 to 2000	23 fils (US ¢ 6.27)
2001 to 4000	28 fils (US ¢ 7.63)
4001 to 6000	32 fils (US ¢ 8.72)
6001 and above	38 fils (US ¢ 10.35)

Secondly, to determine the savings from each RES, it is assumed that by installing, operating and maintaining the integrated system, the owners save an amount equal to the subsidized cost of electricity charged by the power distributor for its services to the owners. This cost of electricity is calculated by summing the cost of electricity over 25 years.

Since electricity is generated for the grid using fossil fuels, it is assumed that the cost of generating electricity increases by a certain percentage year on year due to the limited quantity of fossil fuels, i.e. costs increase as supplies become more rare. This percentage can be calculated based on historical trends of price data, and is found to be 2.38% annually.

Based on this, the slab rates, and the consumption per year of the four villas, the total cost of electricity over 25 years, was calculated to be AED 4,402,408 for Case 1.

This figure was obtained by applying the consumption slab rates to the average electrical consumption of 4 households which is as below:

Consumption per villa/month = $30417/4 = 7604$ kWh/month

Slab tariff for consumption of more than 6000 kWh/month/villa =

(2000 kWh*0.23 AED/kWh) + (2000 kWh*0.28 AED/kWh) + (2000 kWh*0.32 AED/kWh) + [(Consumption-6000)*0.38] + (0.06*consumption) + 60

= 130,900 AED/4villas/year for year 1

Total Cost of electricity to villa owners over 25 years (CS_{elect}) = AED 4,402,408

In order to determine the feasibility of each RES configuration, the savings obtained through the use of each configuration must be compared to the initial cost of the same. These savings can be calculated in the following manner. Since each configuration produces enough electricity to meet some or all of the villas' electrical needs, electricity bills that the owners don't have to pay can be considered to be money saved by the owners. For example, the total cost of electricity (AED 4,402,408) calculated above would be considered as savings for cases 1 and 3 where the systems are villas are entirely independent of the grid. On the other hand, money spent on maintaining, operating and replacing components of the RES, can be considered as expenses for the owners. Any amount that is saved after these costs of operation, maintenance and replacement have been accounted for, is thus considered to be net savings generated by the installation of the RES. Therefore:

$$AS = CS_{elect} - C_{elect} - \Sigma(C_{maint}) - \Sigma(C_{repl})$$

where *AS* are the 'Annual Savings', CS_{elect} is the cost of electricity saved by the owners annually through the use of the system, C_{elect} is the cost of electricity taken from the grid (only applicable to Case 2), $\Sigma(C_{maint})$ is the sum of the maintenance costs of the individual components and $\Sigma(C_{repl})$ is the sum of the replacement costs of the individual components.

Now if one is to compare the savings to the costs of the RES, the savings accumulated over 25 years cannot be compared to the cost of investing in the RES as the latter is paid lump-sum at the beginning of the project. Hence, the present-worth analysis is used to determine how much the savings accumulated over 25 years would amount to were they to be obtained at a single point in time. Calculating the present

worth of the savings each year at the return rate of 5.12, and calculating the sum of these, will give us the present value of the savings. And if this present value is smaller than the capital costs, then it's not economically feasible to invest in the system.

The present worth of the savings is calculated for every year of the lifespan of the system by:

$$PVS(j) = \frac{AS}{(1+i)^j}$$

where *PVS* is the present worth of the system every year, 'j' is the number of years the system has spent in service, and *i* is the nominal interest rate. The sum of the *PVS* for every year of the lifespan is taken to be the present value of the savings. If this sum is smaller than the initial capital costs of the system, the system is economically feasible. This is therefore done next for the three different integrated Cases.

3.13.2 Case 1.

As outlined earlier, this option comprises the DEAS, the clathrate generation VCS, the wind turbine, the PTSC, 21 kW of PV/T and a battery system with a storage capacity of 7 days or 14.7 kAh. Previous analysis on the main components of the overall system has shown us that a WT of 80 kW capacity is required as the average consumption of a villa in the U.A.E. is 250 kWh/day.

Since 65% of power needs are attributed to space cooling this leaves a sole power requirement of 87.5 kWh/day/villa which amounts to 350kWhrs/day for 4 villas. Assuming that peak demand needs to be met 24 hours a day, a WT that produces (350 / 24) = 15kW at average wind speeds of 6.7 m/s, needs to be installed. Cost analysis on the WT shows us that at capital costs of 1675 US$/kW and maintenance costs of 11.68 US$/kW-yr over a wind turbine lifetime of 25 years [35, 128], the 80 kW turbine will cost us:

Initial capital cost (1675 US$/kW for 80 kW)   = 134,000 US$ = AED 493,120

Fixed Maintenance Cost (11.68 US$/kW-yr. for 80 kW)   = 23,360 US$ = AED 85,964

Variable Maintenance Cost (7.11 US$/MWh)   = 383.94 US$ = AED 1,412

Next, the DEAS is taken into account.

Cooling required for 4 villas: (8 tons /villa) x 4 villas =   32 tons   =   112.544 kW$_c$

Cost of 32 ton DEAS   = 30,000 US$ =   AED 110,400

Cost of heat rejection equipment for DEAS   = 6,566 US$ =   AED 24,160

Initial Cost of DEAS = AED 134,560

Next, the cost of the PTSCs required to supply the necessary heat is calculated:

Area of PTSC (aperture area for 75 m with 3.5m aperture width) required to produce

sufficient heat for DEAS   = 255.8m^2

Cost of PTSC / m^2 [129]   = 206 € /m^2

Initial Cost of PTSC   = 52,694 €   = AED 264,000

Also, if the WT is supplemented by a PV/T array that can supply 14kW to the houses and about 7 kW to the VCS generating the clathrate, then over a 25 year period, the PV/T's cost would amount to [128]:

Initial capital cost (4000 US$/kW for 21 kW [130-132] = 84,000 US$ = AED 308,280

Maintenance Cost (65 US$/kW/yr for 21 kW) [128]   = 34,125 US$ = AED 125,580

Next, it would cost us AED 70,400 for a custom clathrate generation system, although mass production would see the price drop to prices comparable to conventional air conditioners in the market. This is because most current air-conditioning machines have complicated indirect contact heat exchangers for the evaporator whereas the direct contact heat exchangers used in a clathrate generation VCC are in effect, just pressure vessels, and are generally easier to manufacture and thus are cheaper [133]. The savings obtained from using a direct contact heat exchanger would probably be offset by the cost added for a more complex controller to control the clathrate generation process, hence making the prices more or less comparable to those of conventional VCCs in the future. Note that, since the PV/T and the wind turbine would barely be making enough power to satisfy the villas' electrical needs, chances are the clathrate system would need to be charged using electricity off the grid.

Lastly, the cost of a battery system that can store power for up to 7 days is calculated. This is to smooth out any non-availability of wind or sun that might occur.

The size of the battery required for a 240 V and 21 kW supply is 14.7 kAh. Note that the life of the battery system is 5 years, and thus the batteries will need replacement five times over the course of the 25 year lifespan of the integrated system.

Initial capital cost (1500 US$/kAh for 14.7 kAh) = 22,050 US$ = AED 80,923

Replacement cost (initial cost *4)   = 88,200 US$ = AED 323,694

Maintenance Cost (50 US$/kAh/yr. for 14.7 kAh) = 18,375 US$ = AED 67,435

Note that theoretically, the houses would be powered solely by renewable energy even if there was no wind blowing. Deduction of the initial costs (shown in bold above) of the various components of the RES from the savings will show us that the project is feasible if the resulting value is positive, and vice versa. However, in order to be able to do this, we have to determine the present value of the savings for every year of the 25 year lifespan, and then sum these present values so that we have the present value of the amount, today, that we would have saved had we invested in the project. Accordingly, it is seen that:

Sum of present value of savings over 25 years= AED 1,394,601

Total Capital Costs = 493,120 + 134,560 + 264,000 + 308,280 + 80,923 + 70,400
                     = AED 1,351,283

Net savings = Savings - Total Capital Costs = AED 43,318

Thus it can be seen that over a period of 25 years, the comprehensive sustainability option is economically viable as the owners will collectively save AED 113,718.

Also note that were the WT to be replaced by another 14 kW of PV/T, not only would the home owners save another AED 287,600, but they would also have access to a more reliable source of energy, except that it would not be available throughout the day. However, the excess produced during the day could be stored in the battery system for periods of non-availability of sun.

3.13.3   Case 2.

This integration option is the sustainability-assisted option where the electrical and cooling loads for the four villas are partially met by the integrated system. This system comprises the TEAS, the clathrate generation VCS, the wind turbine, 30 m of PTSC and 1.5 kW of PV/T with an optional battery bank. The PTSC and the PV/T are sized such that each provides half the heat required to operate the absorption system.

The costs of the various components are as follows. From previous analysis, we know that the WT has a capacity of 80 kW and would cost:

Initial capital cost (1675 US$/kW for 80 kW)   = 134,000 US$ = AED 493,120

Fixed Maintenance Cost (11.68 US$/kW-yr. for 80 kW =23,360US$ = AED 85,964

Variable Maintenance Cost (7.11 US$/MWh   = 383.94 US$ = AED 1,412

Next, the TEAS is taken into account. Given the fact that this technology still hasn't thoroughly permeated the market, prices for the triple effect have to be extrapolated from data on more commonly available single and double effect absorption chillers such as the one in [13].

Cost of 32 ton TEAS   = 34,000 US$ = AED 126,250

Cost of heat rejection equipment for TEAS   = 5,888 US$ = AED 21,700

Initial Cost of TEAS = AED 147,950

For case 2, the size of the PTSCs will be approximately half those required in case 1 as the PTSC shall provide half the heat required to power the TEAS. Thus the cost of the PTSCs required to supply the necessary heat is calculated to be:

Cooling required for 2 villas: (8 tons /villa) x 2 villas = 16 tons   = 56.272 kW_c

Area of PTSC (aperture area for 30 m with 3.5m aperture width)   = 102.3m^2

Cost of PTSC / m^2 [129]   = 206 € /m^2

Initial Cost of PTSC   = 21,115 € = 27,153 US$ = AED 99,925

As mentioned above, for Case 2, the PV/T array is sized such that it provides the remaining half of the heat required to be input to the TEAS HTG. This results in a required area of PV/T of 25.2m^2 which subsequently produces an electric output of 1.5kW.

Initial capital cost (4000 US$/kW for 1.5 kW)   = 6,000 US$ = AED 22,080

Maintenance Cost (65 US$/kW/yr. for 1.5 kW)   = 2,438 US$ = AED 8,970

As for the custom clathrate generation system, it would set us back AED 70,400. However, since not enough electricity is generated to power the homes, let alone charge the system, the clathrate system will not be included, and instead

electricity from the grid will be used to provide cooling to the homes during night-time.

Similarly, during some months the electrical needs of the villas are barely satisfied by even 21kW of PV/T and the WT combined, hence a battery system would mostly be redundant in the case 2 scenario and can be eliminated entirely. In fact, it is found that for the case 2 scenario, the PV/T with the WT would, on average, annually produce only 49.6% of the required electrical load of the houses (not including the load taken by the CGVCS), and thus the remaining electrical load (not met through renewable energy) can/would be met by the grid, in which case the battery system need not be installed.

Conducting the present cost analysis in the same way as was done for case 1, we determine the present value of the savings for every year of the 25 year lifespan, and then sum these present values so that we have the present value of the amount that we would have saved had we invested in the project. Deducting this from the initial cost of the system, we see that:

Present value of savings (PVS) = AED 1,405,220

Total Capital Costs (TCC) = 493,120 + 147,950 + 99,925 + 22,080 =AED 763,075

Net savings = PVS - TCC = AED 642,145

Thus it can be seen that over a period of 25 years, the sustainability-assisted option is economically viable as the owners will collectively save AED 642,145. Note that were the WT to be replaced by 15 kW of PV/T, not only would the home owners save another AED 287,600, but they would also have access to a more reliable source of energy, except that it would not be available throughout the day.

3.13.4 Case 3.

This is the most comprehensive integration option and possibly the most sustainable of the three systems integration options considered in this thesis; it comprises the TEAS, the clathrate generation VCS, the 80 kW wind turbine, the PTSC, 21 kW of PV/T and a battery system with a storage capacity of 7 days or 14.7 kAh, and offers complete independence from reliance on the grid. At capital costs of 1675 US$/kW and maintenance costs of 11.68 US$/kW-yr over a wind turbine lifetime of 25 years [35, 128], the 80 kW turbine will cost us:

Initial capital cost (1675 US$/kW for 80 kW)   = 134,000 US$ = AED 493,120

Fixed Maintenance Cost (11.68 US$/kW-yr.)   = 23,360 US$ = AED 85,964

Variable Maintenance Cost (7.11 US$/MWh   = 383.94 US$ = AED 1,412

Next, the TEAS is taken into account. Given the fact that this technology still hasn't thoroughly permeated the market, prices for the triple effect have to be extrapolated from data on more commonly available single and double effect absorption chillers such as the one in [13].

Cooling required for 4 villas: (8 tons /villa) x 4 villas = 32 tons   = 112.544 kW_c

Cost of 32 ton TEAS   = 34,000 US$ =AED 126,250

Cost of heat rejection equipment for TEAS   = 5,888 US$ = AED 21,700

Initial Cost of TEAS   = AED 147,950

The cost of the PTSCs required to supply the necessary heat is calculated to be:

Area of PTSC (aperture area for 60 m with 3.5m aperture width)   = 204.64m^2

Cost of PTSC / m^2 [129]   = 206 € /m^2

Initial Cost of PTSC = 42,230 € = 54,307 US$ = AED 200,000

Also, if the WT is supplemented by a PV/T array that can supply 14kW to the houses and about 7 kW to the VCS generating the clathrate, then over a 25 year period, the PV/T's cost would amount to [128]:

Initial capital cost (4000 US$/kW for 21 kW [130] = 84,000 US$ = AED 308,280

Maintenance Cost (65 US$/kW/yr. for 21 kW)   = 34,125 US$ = AED 125,580

For a custom clathrate generation system, it would cost us AED 70,400. Lastly, the cost of a battery system that can store power for up to 7 days is calculated. This is to smooth out any non-availability of wind or sun that might occur. The size of the battery required for a 240 V and 21 kW supply is 14.7 kAh. Note that the life of the battery system is 5 years, and thus the batteries will need replacement five times over the course of the 25 year lifespan of the integrated system.

Initial capital cost (1500 US$/kAh for 14.7 kAh)   = 22,050 US$ = AED 80,923

Replacement cost (initial cost *4)   = 88,200 US$ = AED 323,694

Maintenance Cost (50 US$/kAh/yr. for 14.7 kAh)   = 18,375 US$ = AED 67,435

Note that the houses would be powered solely by renewable energy even if there was no wind blowing. Thus it can be seen that over a period of 25 years, the comprehensive sustainability option is economically viable as the owners will collectively save:

Present value of savings (PVS) =AED 1,469,330

Total Capital Costs (TCC) = (493,120 + 147,950 + 200,000 + 308,280

+ 70,400 + 80,923)   = AED 1,300,673

Net savings = PVS - TCC = AED 168,657

Again, replacing the WT by another 14 kW of PV/T, not only would the home owners save another AED 287,600, but they would also have access to a more reliable source of energy, except that it would not be available throughout the day. However, the excess produced during the day could be stored in the battery system for periods of non-availability of sun.

We see that when implemented, all three cases are economically feasible. However, they offer varied degrees of value for money. Since all three integrated configurations that can guarantee the required supply of power and cooling in one way or another, the configuration that offers the most savings is naturally taken to be the most cost-efficient option.

Accordingly, we see that Case 2 is most economically feasible with estimated savings of AED 642,145 over the lifetime of the system. However, Case 2 does not offer complete independence from the grid, and if the location is remote and grid connectivity would prove expensive or impractical, Case 3 would be optimal rather than Case 2 for implementation.

Thus it can be seen that while Case 2 is the most economically competitive of the three integrated cases, case 3 is the most viable solution both thermodynamically and economically. This is because Case 3 makes better thermodynamic sense than Case 2, and offers better performance, safety and value for money than Case 1 which offers identical safety in terms of uninterrupted supply of power and cooling to the homeowners.

Chapter 4: Conclusions and Recommendations

4.1   Conclusions

The core objective of this work was the development of a renewable-energy-powered holistic integrated system that could provide uninterrupted power and cooling to four residential units (villas) in the U.A.E. to make them independent of the grid. Aside from studying the individual behavior of various renewable energy technologies and storage systems, the integration of these systems and the analysis of the resulting systems was conducted. Based on the results obtained through modeling of, and conducting parametric studies on, the integrated systems that would power and cool the villas sustainably, the following main conclusions can be drawn.

- The integrated PTSC-TEAS system performs better than the integrated PTSC-DEAS system.

- The highest energetic and exergetic COPs of the overall PTSC-DEAS system are achieved during July, and are 1.7 and 1.31 respectively.

- The highest energetic and exergetic COPs of the overall PTSC-TEAS system are also achieved during July, and are 1.78 and 1.39 respectively.

- Electrical output of the integrated PV/T-WT system is seen to meet the required electrical load of 14kW throughout the year with the integrated option case 3, with a maximum combined output during March of 36 kW.

- Maximum energetic efficiency of the integrated PV/T-WT system is 14.8% during July whereas the maximum exergetic efficiency is 4.99% during August.

- The CGVCS is a more feasible storage option than the HTS in terms of size, cost, thermal efficiency and charging times.

- The highest energetic efficiency of the combined PV/T-CGVCS system is 0.22, and is experienced during the month of July.

- The best integrated option, thermodynamically, out of the three cases considered, is Case 3, for supplying uninterrupted supply of power and cooling throughout the year. It is also the most economical option in terms of service delivered. In addition, it is considered to be a comprehensive integrated solution comprising of 21 kW$_e$ of PV/T, an 80 kW WT, 60m of PTSC, a 32 RT TEAS, a 5.1 RT CGVCS

and a 14.7 kAh battery bank. The highest energetic efficiency of the Case 3 integrated option is in July at 0.38 while the highest exergetic efficiency is also in July, and amounts to 0.201. Using present worth analysis, it is determined that minimum savings of AED 168,657 can be made if this integrated option is implemented instead of consuming electricity from the grid for power and cooling.

- However, if cost is the most important factor in choosing a solution, Case 2 is the most feasible option. Using present worth analysis, it is determined that Case 2 is the most economically feasible integrated option out of the three options studied, and offers savings of AED 642,145 at the cost of dependence on the grid.

Every effort was made to model the system as close to real-life conditions as possible to give an accurate idea of the feasibility of such a system. However, a model can never be accurate enough as many factors are at play simultaneously which can affect system performance. While the above results are thermodynamically attractive and show that the system has promise for the future, experimental data is necessary for verifying the claims of this thesis.

4.2   Recommendations

Further work, both theoretical and practical, is necessary to determine the feasibility of such a system for real-life implementation. It is suggested that the following topics be further explored:

- Performance of the wind turbine based on actual data collected on site.
- Performance and feasibility of using small wind turbine systems which activate at lower wind speeds and thus suggest greater potential for local application for U.A.E.
- Performance evaluation of the TEAS as a base model using different working pairs and operating conditions.
- Use of hourly electricity consumption data collected over a year to estimate consumption more accurately and optimize system size and cost.
- Potential of connecting this system to the grid so as to benefit home owners during periods of excess consumption.
- Integration of additional varied cold and hot storage systems to find the optimum overall trigeneration solution for homes in the middle-east.

References

[1]   T. A. H. Ratlamwala, M. A. Gadalla, and I. Dincer, "Performance assessment of an integrated PV/T and triple effect cooling system for hydrogen and cooling production," *International Journal of Hydrogen Energy,* vol. 36, no. 17, pp. 11282-11291, 2011.

[2]   T. Qazi. "Abu Dhabi Municipality's Energy Efficiency Programme: Demand Side Management in Existing Buildings -Comprehensive Energy Study." 2012 [Jul. 7, 2013].

[3]   C. D. Moné, D. S. Chau, and P. E. Phelan, "Economic feasibility of combined heat and power and absorption refrigeration with commercially available gas turbines," *Energy Conversion and Management,* vol. 42, no. 13, pp. 1559-1573, 2001.

[4]   T. A. H. Ratlamwala, I. Dincer, and M. A. Gadalla, "Thermodynamic analysis of an integrated geothermal based quadruple effect absorption system for multigenerational purposes," *Thermochimica Acta,* vol. 535, pp. 27-35, 2012.

[5]   F. A. Al-Sulaiman, I. Dincer, and F. Hamdullahpur, "Exergy modeling of a new solar driven trigeneration system," *Solar Energy,* vol. 85, no. 9, pp. 2228-2243, 2011.

[6]   M. Mazloumi, M. Naghashzadegan, and K. Javaherdeh, "Simulation of solar lithium bromide–water absorption cooling system with parabolic trough collector," *Energy Conversion and Management,* vol. 49, no. 10, pp. 2820-2832, 2008.

[7]   M. Qu, H. Yin, and D. H. Archer, "A solar thermal cooling and heating system for a building: Experimental and model based performance analysis and design," *Solar Energy,* vol. 84, no. 2, pp. 166-182, 2010.

[8]   M. Calderón, A. J. Calderón, A. Ramiro, and J. F. González, "Weather data and energy balance of a hybrid photovoltaic-wind system with hydrogen storage," *International Journal of Hydrogen Energy,* vol. 35, no. 15, pp. 7706-7715, 2010.

[9]   M. R. Elkinton, J. G. McGowan, and J. F. Manwell, "Wind power systems for zero net energy housing in the United States," *Renewable Energy,* vol. 34, no. 5, pp. 1270-1278, 2009.

[10]   J.-I. Yoon, K.-H. Choi, C.-G. Moon, Y. J. Kim, and O.-K. Kwon, "A study on the advanced performance of an absorption heater/chiller with a solution preheater using waste gas," *Applied Thermal Engineering,* vol. 23, no. 6, pp. 757-767, 2003.

[11]   R. D. Misra, P. K. Sahoo, and A. Gupta, "Thermoeconomic evaluation and optimization of a double-effect H_2O/LiBr vapour-absorption refrigeration system," *International Journal of Refrigeration,* vol. 28, no. 3, pp. 331-343, 2005.

[12]   W. M. Worek, D. Ludovisi, and M. Meckler, "Enhancement of a double-effect absorption cooling system using a vapor recompression absorber," *Energy,* vol. 28, no. 12, pp. 1151-1163, 2003.

[13]   A. Elsafty and A. J. Al-Daini, "Economical comparison between a solar-powered vapour absorption air-conditioning system and a vapour compression

system in the Middle East," *Renewable Energy,* vol. 25, no. 4, pp. 569-583, 2002.

[14] S. C. Kaushik and A. Arora, "Energy and exergy analysis of single effect and series flow double effect water–lithium bromide absorption refrigeration systems," *International Journal of Refrigeration,* vol. 32, no. 6, pp. 1247-1258, 2009.

[15] K. Cheung, Y. Hwang, J. F. Judge, K. Kolos, A. Singh, and R. Radermacher, "Performance assessment of multistage absorption cycles," *International Journal of Refrigeration,* vol. 19, no. 7, pp. 473-481, 1996.

[16] L. Jiang, Z. Gu, X. Feng, and Y. Li, "Thermo-economical analysis between new absorption–ejector hybrid refrigeration system and small double-effect absorption system," *Applied Thermal Engineering,* vol. 22, no. 9, pp. 1027-1036, 2002.

[17] J.-S. Kim, F. Ziegler, and H. Lee, "Simulation of the compressor-assisted triple-effect H_2O/LiBr absorption cooling cycles," *Applied Thermal Engineering,* vol. 22, no. 3, pp. 295-308, 2002.

[18] D. M. Manole and J. L. Lage, "Thermodynamic optimization method of a triple effect absorption system with wasted heat recovery," *International Journal of Heat and Mass Transfer,* vol. 38, no. 4, pp. 655-663, 1995.

[19] K. E. Herold, R. Radermacher, and S. A. Klein, *Absorption chillers and heat pumps.* Boca Raton, FL: CRC Press, 1996.

[20] A. N. Celik, "Techno-economic analysis of autonomous PV-wind hybrid energy systems using different sizing methods," *Energy Conversion and Management,* vol. 44, no. 12, pp. 1951-1968, 2003.

[21] S. K. Nandi and H. R. Ghosh, "Prospect of wind–PV-battery hybrid power system as an alternative to grid extension in Bangladesh," *Energy,* vol. 35, no. 7, pp. 3040-3047, 2010.

[22] M. Eroglu, E. Dursun, S. Sevencan, J. Song, S. Yazici, and O. Kilic, "A mobile renewable house using PV/wind/fuel cell hybrid power system," *International Journal of Hydrogen Energy,* vol. 36, no. 13, pp. 7985-7992, 2011.

[23] I. Dincer and M. A. Rosen, "Thermodynamic aspects of renewables and sustainable development," *Renewable and Sustainable Energy Reviews,* vol. 9, no. 2, pp. 169-189, 2005.

[24] V. Abate, General Electric Company. *Deutsche Bank Securities 2011 Alternative Energy, Utilities and Power Conference*, 2011.

[25] I. Dincer, "Renewable energy and sustainable development: a crucial review," *Renewable and Sustainable Energy Reviews,* vol. 4, no. 2, pp. 157-175, 2000.

[26] G. D. W. Rueter. "Calculating the true cost of electricity." Internet: http://www.dw.de/dw/article/, 2012 [Sept. 18, 2012].

[27] S. Kalogirou, *Solar energy engineering : processes and systems.* Burlington, MA: Elsevier/Academic Press, 2009.

[28] O. Ozgener and L. Ozgener, "Exergy and reliability analysis of wind turbine systems: A case study," *Renewable and Sustainable Energy Reviews,* vol. 11, no. 8, pp. 1811-1826, 2007.

[29] E. P. I. A. "Key facts and figures."Internet: http://www.epia.org/solar-pv/faq.html, 2010 [Mar. 8, 2013].

[30]   W. Zhou, C. Lou, Z. Li, L. Lu, and H. Yang, "Current status of research on optimum sizing of stand-alone hybrid solar–wind power generation systems," *Applied Energy,* vol. 87, no. 2, pp. 380-389, 2010.

[31]   M. T. Iqbal, "A feasibility study of a zero energy home in Newfoundland," *Renewable Energy,* vol. 29, no. 2, pp. 277-289, 2004.

[32]   J. K. Kaldellis, P. Koronakis, and K. Kavadias, "Energy balance analysis of a stand-alone photovoltaic system, including variable system reliability impact," *Renewable Energy,* vol. 29, no. 7, pp. 1161-1180, 2004.

[33]   P. Bajpai and V. Dash, "Hybrid renewable energy systems for power generation in stand-alone applications: A review," *Renewable and Sustainable Energy Reviews,* vol. 16, no. 5, pp. 2926-2939, 2012.

[34]   G. K. Singh, "Modeling and analysis of six-phase synchronous generator for stand-alone renewable energy generation," *Energy,* vol. 36, no. 9, pp. 5621-5631, 2011.

[35]   B. E. Türkay and A. Y. Telli, "Economic analysis of standalone and grid connected hybrid energy systems," *Renewable Energy,* vol. 36, no. 7, pp. 1931-1943, 2011.

[36]   Siemens. "Siemens to decisively strengthen its position in the growth market solar thermal power." Internet: http://www.siemens.com/press/en/pressrelease/, [Sept. 18, 2012].

[37]   S. Electric. "Schneider Electric to Showcase SmartCity Solution at Fifth World Future Energy Summit in Abu Dhabi."Internet: http://www.schneider-electric.ae/uae/en/company/news/, Jan. 19, 2012 [Sept. 20, 2012].

[38]   L. E. Saad. "Averting Crisis: Managing Energy Use in Abu Dhabi." Internet: http://www.carboun.com/energy/averting-crisis-managing-energy-use-in-abu-dhabi/, 2012 [Sept. 16, 2012]

[39]   I. J. Bachellerie. "Renewable Energy in the GCC countries- Resources, Potential and Prospects. " Internet: http://library.fes.de/pdf-files/bueros/amman /09008.pdf, 2012 [Mar. 14, 2012].

[40]   A. M. Redha, I. Dincer, and M. Gadalla, "Thermodynamic performance assessment of wind energy systems: An application," *Energy,* vol. 36, no. 7, pp. 4002-4010, 2011.

[41]   A. Kazmi, "Abu Dhabi perfect for wind farming." *Gulf News* (July, 2009), U.A.E., environment.

[42]   R. Luna-Rubio, M. Trejo-Perea, D. Vargas-Vázquez, and G. J. Ríos-Moreno, "Optimal sizing of renewable hybrids energy systems: A review of methodologies," *Solar Energy,* vol. 86, no. 4, pp. 1077-1088, 2012.

[43]   EWS-WWF.   "EWS-WWF-Conducts-Three-Household-Carbon-Audits-and-Retrofits ."   Internet: http://uae.panda.org/?204616/EWS-WWF-Conducts-Three-Household-Carbon-Audits-and-Retrofits, 2012 [Sept. 15, 2012].

[44]   Kalogirou, *Solar Energy Engineering: Processes and Systems*: Elsevier Science & Technology, 2009.

[45]   R. Lizarte, M. Izquierdo, J. D. Marcos, and E. Palacios, "An innovative solar-driven directly air-cooled LiBr–H_2O absorption chiller prototype for residential use," *Energy and Buildings,* vol. 47, pp. 1-11, 2012.

[46]   A. Paurine, G. G. Maidment, and I. W. Eames, "Development of a packed bed regenerative solution heat exchanger (R-SHX) for a single stage LiBr–H_2O

vapour absorption refrigeration (VAR) system," *Applied Thermal Engineering,* vol. 60, no. 1-2, pp. 182-187, 2013.

[47]   T. Avanessian and M. Ameri, "Energy, exergy, and economic analysis of single and double effect LiBr–H_2O absorption chillers," *Energy and Buildings,* vol. 73, pp. 26-36, 2014.

[48]   N. Ketjoy, R. Yongphayoon, and K. Mansiri, "Performance Evaluation of 35kW LiBr–H_2O Solar Absorption Cooling System in Thailand," *Energy Procedia,* vol. 34, pp. 198-210, 2013.

[49]   J. Wonchala, M. Hazledine, and K. Goni Boulama, "Solution procedure and performance evaluation for a water–LiBr absorption refrigeration machine," *Energy,* vol. 65, pp. 272-284, 2014.

[50]   A. S. Joshi, A. Tiwari, G. N. Tiwari, I. Dincer, and B. V. Reddy, "Performance evaluation of a hybrid photovoltaic thermal (PV/T) (glass-to-glass) system," *International Journal of Thermal Sciences,* vol. 48, no. 1, pp. 154-164, 2009.

[51]   S. Dubey and G. N. Tiwari, "Thermal modeling of a combined system of photovoltaic thermal (PV/T) solar water heater," *Solar Energy,* vol. 82, no. 7, pp. 602-612, 2008.

[52]   A. S. Joshi, I. Dincer, and B. V. Reddy, "Thermodynamic assessment of photovoltaic systems," *Solar Energy,* vol. 83, no. 8, pp. 1139-1149, 2009.

[53]   E. Saloux, A. Teyssedou, and M. Sorin, "Analysis of photovoltaic (PV) and photovoltaic/thermal (PV/T) systems using the exergy method," *Energy and Buildings,* vol. 67, pp. 275-285, 2013.

[54]   S. Dubey, G. S. Sandhu, and G. N. Tiwari, "Analytical expression for electrical efficiency of PV/T hybrid air collector," *Applied Energy,* vol. 86, no. 5, pp. 697-705, 2009.

[55]   Q.-Y. Li, Q. Chen, and X. Zhang, "Performance analysis of a rooftop wind solar hybrid heat pump system for buildings," *Energy and Buildings,* vol. 65, pp. 75-83, 2013.

[56]   M. Rabbani, I. Dincer, and G. F. Naterer, "Thermodynamic assessment of a wind turbine based combined cycle," *Energy,* vol. 44, no. 1, pp. 321-328, 2012.

[57]   D. Buhagiar and T. Sant, "Steady-state analysis of a conceptual offshore wind turbine driven electricity and thermocline energy extraction plant," *Renewable Energy,* vol. 68, pp. 853-867, 2014.

[58]   L. M. Al-Hadhrami, "Performance evaluation of small wind turbines for off grid applications in Saudi Arabia," *Energy Conversion and Management,* vol. 81, pp. 19-29, 2014.

[59]   E. Oró, A. de Gracia, A. Castell, M. M. Farid, and L. F. Cabeza, "Review on phase change materials (PCMs) for cold thermal energy storage applications," *Applied Energy,* vol. 99, pp. 513-533, 2012.

[60]   I. Dincer, "On thermal energy storage systems and applications in buildings," *Energy and Buildings,* vol. 34, no. 4, pp. 377-388, 2002.

[61]   M. Hänchen, S. Brückner, and A. Steinfeld, "High-temperature thermal storage using a packed bed of rocks – Heat transfer analysis and experimental validation," *Applied Thermal Engineering,* vol. 31, no. 10, pp. 1798-1806, 2011.

[62]   G. Zanganeh, A. Pedretti, S. Zavattoni, M. Barbato, and A. Steinfeld, "Packed-bed thermal storage for concentrated solar power – Pilot-scale demonstration

and industrial-scale design," *Solar Energy,* vol. 86, no. 10, pp. 3084-3098, 2012.

[63] H. Bindra, P. Bueno, J. F. Morris, and R. Shinnar, "Thermal analysis and exergy evaluation of packed bed thermal storage systems," *Applied Thermal Engineering,* vol. 52, no. 2, pp. 255-263, 2013.

[64] N. G. Barton, "Simulations of air-blown thermal storage in a rock bed," *Applied Thermal Engineering,* vol. 55, no. 1-2, pp. 43-50, 2013.

[65] S. Kuravi, J. Trahan, D. Y. Goswami, M. M. Rahman, and E. K. Stefanakos, "Thermal energy storage technologies and systems for concentrating solar power plants," *Progress in Energy and Combustion Science,* vol. 39, no. 4, pp. 285-319, 2013.

[66] A. Modi and C. D. Pérez-Segarra, "Thermocline thermal storage systems for concentrated solar power plants: One-dimensional numerical model and comparative analysis," *Solar Energy,* vol. 100, pp. 84-93, 2014.

[67] H. Yin, J. Ding, and X. Yang, "Experimental research on thermal characteristics of a hybrid thermocline heat storage system," *Applied Thermal Engineering,* vol. 62, no. 1, pp. 293-301, 2014.

[68] M. Wu, M. Li, C. Xu, Y. He, and W. Tao, "The impact of concrete structure on the thermal performance of the dual-media thermocline thermal storage tank using concrete as the solid medium," *Applied Energy,* vol. 113, pp. 1363-1371, 2014.

[69] P. L. W. Karaki, J. V. Lew, M. M. Valmiki, C. Chan and J. Stephens. "Experimental Investigation of Thermal Storage Processes in a Thermocline Storage Tank," in *Proceedings of the ASME 2011 5th International Conference on Energy Sustainability ES 2011,* 2011.

[70] S. Khare, M. Dell'Amico, C. Knight, and S. McGarry, "Selection of materials for high temperature latent heat energy storage," *Solar Energy Materials and Solar Cells,* vol. 107, pp. 20-27, 2012.

[71] S. Wu, G. Fang, and Z. Chen, "Discharging characteristics modeling of cool thermal energy storage system with coil pipes using n-tetradecane as phase change material," *Applied Thermal Engineering,* vol. 37, pp. 336-343, 2012.

[72] H. El Qarnia, "Theoretical study of transient response of a rectangular latent heat thermal energy storage system with conjugate forced convection," *Energy Conversion and Management,* vol. 45, no. 9-10, pp. 1537-1551, 2004.

[73] L. F. Cabeza, M. Ibáñez, C. Solé, J. Roca, and M. Nogués, "Experimentation with a water tank including a PCM module," *Solar Energy Materials and Solar Cells,* vol. 90, no. 9, pp. 1273-1282, 2006.

[74] P. Principi and R. Fioretti, "Thermal analysis of the application of pcm and low emissivity coating in hollow bricks," *Energy and Buildings,* vol. 51, pp. 131-142, 2012.

[75] A. Castell, I. Martorell, M. Medrano, G. Pérez, and L. F. Cabeza, "Experimental study of using PCM in brick constructive solutions for passive cooling," *Energy and Buildings,* vol. 42, no. 4, pp. 534-540, 2010.

[76] N. H. S. Tay, M. Belusko, and F. Bruno, "Designing a PCM storage system using the effectiveness-number of transfer units method in low energy cooling of buildings," *Energy and Buildings,* vol. 50, pp. 234-242, 2012.

[77]	W. A. Qureshi, N.-K. C. Nair, and M. M. Farid, "Impact of energy storage in buildings on electricity demand side management," *Energy Conversion and Management,* vol. 52, no. 5, pp. 2110-2120, 2011.

[78]	A. H. Mosaffa, C. A. Infante Ferreira, F. Talati, and M. A. Rosen, "Thermal performance of a multiple PCM thermal storage unit for free cooling," *Energy Conversion and Management,* vol. 67, pp. 1-7, 2013.

[79]	T. Kousksou, P. Bruel, G. Cherreau, V. Leoussoff, and T. El Rhafiki, "PCM storage for solar DHW: From an unfulfilled promise to a real benefit," *Solar Energy,* vol. 85, no. 9, pp. 2033-2040, 2011.

[80]	E.-B. S. Mettawee and G. M. R. Assassa, "Experimental study of a compact PCM solar collector," *Energy,* vol. 31, no. 14, pp. 2958-2968, 2006.

[81]	A. Lecuona, J.-I. Nogueira, R. Ventas, M.-d.-C. Rodríguez-Hidalgo, and M. Legrand, "Solar cooker of the portable parabolic type incorporating heat storage based on PCM," *Applied Energy,* vol. 111, pp. 1136-1147, 2013.

[82]	H. M. S. Hussein, H. H. El-Ghetany, and S. A. Nada, "Experimental investigation of novel indirect solar cooker with indoor PCM thermal storage and cooking unit," *Energy Conversion and Management,* vol. 49, no. 8, pp. 2237-2246, 2008.

[83]	H. Weinläder, A. Beck, and J. Fricke, "PCM-facade-panel for daylighting and room heating," *Solar Energy,* vol. 78, no. 2, pp. 177-186, 2005.

[84]	G. Evola, L. Marletta, and F. Sicurella, "A methodology for investigating the effectiveness of PCM wallboards for summer thermal comfort in buildings," *Building and Environment,* vol. 59, pp. 517-527, 2013.

[85]	K. Azzouz, D. Leducq, and D. Gobin, "Performance enhancement of a household refrigerator by addition of latent heat storage," *International Journal of Refrigeration,* vol. 31, no. 5, pp. 892-901, 2008.

[86]	B. Gin and M. M. Farid, "The use of PCM panels to improve storage condition of frozen food," *Journal of Food Engineering,* vol. 100, no. 2, pp. 372-376, 2010.

[87]	E. Oró, L. Miró, M. M. Farid, and L. F. Cabeza, "Improving thermal performance of freezers using phase change materials," *International Journal of Refrigeration,* vol. 35, no. 4, pp. 984-991, 2012.

[88]	A. Waqas and Z. Ud Din, "Phase change material (PCM) storage for free cooling of buildings—A review," *Renewable and Sustainable Energy Reviews,* vol. 18, pp. 607-625, 2013.

[89]	M. Kenisarin and K. Mahkamov, "Solar energy storage using phase change materials," *Renewable and Sustainable Energy Reviews,* vol. 11, no. 9, pp. 1913-1965, 2007.

[90]	G. Li, Y. Hwang, R. Radermacher, and H.-H. Chun, "Review of cold storage materials for subzero applications," *Energy,* vol. 51, pp. 1-17, 2013.

[91]	I. Chatti, A. Delahaye, L. Fournaison, and J.-P. Petitet, "Benefits and drawbacks of clathrate hydrates: a review of their areas of interest," *Energy Conversion and Management,* vol. 46, no. 9-10, pp. 1333-1343, 2005.

[92]	L. F. Cabeza, "3.07 - Thermal Energy Storage," in *Comprehensive Renewable Energy*, 1st Ed., A. Sayigh, Ed. Oxford: Elsevier, 2012, pp. 211-253.

[93]	T. Nomura, N. Okinaka, and T. Akiyama, "Waste heat transportation system, using phase change material (PCM) from steelworks to chemical plant," *Resources, Conservation and Recycling,* vol. 54, no. 11, pp. 1000-1006, 2010.

[94]   D. Mondieig, F. Rajabalee, A. Laprie, H. A. J. Oonk, T. Calvet, and M. Angel Cuevas-Diarte, "Protection of temperature sensitive biomedical products using molecular alloys as phase change material," *Transfusion and Apheresis Science,* vol. 28, no. 2, pp. 143-148, 2003.

[95]   M. Almajali, K. Lafdi, and P. H. Prodhomme, "Effect of copper coating on infiltrated PCM/foam," *Energy Conversion and Management,* vol. 66, pp. 336-342, 2013.

[96]   A. J. Gallego, A. Ruíz-Pardo, A. Cerezuela-Parish, J. Sánchez, C. Martín-Macareno, L. F. Cabeza, E. F. Camacho, and E. Oró, "Mathematical modeling of a PCM storage tank in a solar cooling plant," *Solar Energy,* vol. 93, pp. 1-10, 2013.

[97]   K. Ermis, A. Erek, and I. Dincer, "Heat transfer analysis of phase change process in a finned-tube thermal energy storage system using artificial neural network," *International Journal of Heat and Mass Transfer,* vol. 50, no. 15-16, pp. 3163-3175, 2007.

[98]   Y. Zhang, G. Zhou, K. Lin, Q. Zhang, and H. Di, "Application of latent heat thermal energy storage in buildings: State-of-the-art and outlook," *Building and Environment,* vol. 42, no. 6, pp. 2197-2209, 2007.

[99]   N. Soares, J. J. Costa, A. R. Gaspar, and P. Santos, "Review of passive PCM latent heat thermal energy storage systems towards buildings' energy efficiency," *Energy and Buildings,* vol. 59, pp. 82-103, 2013.

[100]   M. Pomianowski, P. Heiselberg, and Y. Zhang, "Review of thermal energy storage technologies based on PCM application in buildings," *Energy and Buildings*, vol. 67, pp. 56-59, 2013.

[101]   "06/00760 Dynamics of energy storage in phase change drywall systems: Darkwa, K. and Kim, J.-S. International Journal of Energy Research, 2005, 29, (4), 335–343," *Fuel and Energy Abstracts,* vol. 47, no. 2, pp. 113-114, 2006.

[102]   K. Darkwa, P. W. O'Callaghan, and D. Tetlow, "Phase-change drywalls in a passive-solar building," *Applied Energy,* vol. 83, no. 5, pp. 425-435, 2006.

[103]   G. Li, Y. Hwang, and R. Radermacher, "Review of cold storage materials for air conditioning application," *International Journal of Refrigeration,* vol. 35, no. 8, pp. 2053-2077, 2012.

[104]   H. Tajima, T. Nagata, A. Yamasaki, F. Kiyono, and T. Masuyama, "Formation of HFC-134a hydrate by static mixing," *Journal of Petroleum Science and Engineering,* vol. 56, no. 1-3, pp. 75-81, 2007.

[105]   J. Li, D. Liang, K. Guo, R. Wang, and S. Fan, "Formation and dissociation of HFC134a gas hydrate in nano-copper suspension," *Energy Conversion and Management,* vol. 47, no. 2, pp. 201-210, 2006.

[106]   Y. H. Mori and N. Komae, "A note on the evaluation of the guest-gas uptake into a clathrate hydrate being formed in a semibatch- or batch-type reactor," *Energy Conversion and Management,* vol. 49, no. 5, pp. 1056-1062, 2008.

[107]   H. Tajima, A. Yamasaki, and F. Kiyono, "Energy consumption estimation for greenhouse gas separation processes by clathrate hydrate formation," *Energy,* vol. 29, no. 11, pp. 1713-1729, 2004.

[108]   T. Ogawa, T. Ito, K. Watanabe, K.-i. Tahara, R. Hiraoka, J.-i. Ochiai, R. Ohmura, and Y. H. Mori, "Development of a novel hydrate-based refrigeration system: A preliminary overview," *Applied Thermal Engineering,* vol. 26, no. 17-18, pp. 2157-2167, 2006.

[109] M. Sugaya and Y. H. Mori, "Behavior of clathrate hydrate formation at the boundary of liquid water and a fluorocarbon in liquid or vapor state," *Chemical Engineering Science,* vol. 51, no. 13, pp. 3505-3517, 1996.

[110] N. E. Wijeysundera, M. N. A. Hawlader, C. W. B. Andy, and M. K. Hossain, "Ice-slurry production using direct contact heat transfer," *International Journal of Refrigeration,* vol. 27, no. 5, pp. 511-519, 2004.

[111] Y. Xie, G. Li, D. Liu, N. Liu, Y. Qi, D. Liang, K. Guo, and S. Fan, "Experimental study on a small scale of gas hydrate cold storage apparatus," *Applied Energy,* vol. 87, no. 11, pp. 3340-3346, 2010.

[112] Y. Bi, T. Guo, L. Zhang, L. Chen, and F. Sun, "Entropy generation minimization for charging and discharging processes in a gas-hydrate cool storage system," *Applied Energy,* vol. 87, no. 4, pp. 1149-1157, 2010.

[113] R. Ohmura, S. Kashiwazaki, and Y. H. Mori, "Measurements of clathrate-hydrate film thickness using laser interferometry," *Journal of Crystal Growth,* vol. 218, no. 2-4, pp. 372-380, 2000.

[114] J. Wu and S. Wang, "Research on cool storage and release characteristics of R134a gas hydrate with additive," *Energy and Buildings,* vol. 45, pp. 99-105, 2012.

[115] P. Zhang and Z. W. Ma, "An overview of fundamental studies and applications of phase change material slurries to secondary loop refrigeration and air conditioning systems," *Renewable and Sustainable Energy Reviews,* vol. 16, no. 7, pp. 5021-5058, 2012.

[116] P. Zhang, Z. W. Ma, and R. Z. Wang, "An overview of phase change material slurries: MPCS and CHS," *Renewable and Sustainable Energy Reviews,* vol. 14, no. 2, pp. 598-614, 2010.

[117] Z. Youssef, A. Delahaye, L. Huang, F. Trinquet, L. Fournaison, C. Pollerberg, and C. Doetsch, "State of the art on phase change material slurries," *Energy Conversion and Management,* vol. 65, pp. 120-132, 2013.

[118] X. Wang, M. Dennis, and L. Hou, "Clathrate hydrate technology for cold storage in air conditioning systems," *Renewable and Sustainable Energy Reviews,* vol. 36, pp. 34-51, 2014.

[119] R. Petela, "Exergy analysis of the solar cylindrical-parabolic cooker," *Solar Energy,* vol. 79, no. 3, pp. 221-233, 2005.

[120] A. Hepbasli and Z. Alsuhaibani, "Exergetic and exergoeconomic aspects of wind energy systems in achieving sustainable development," *Renewable and Sustainable Energy Reviews,* vol. 15, no. 6, pp. 2810-2825, 2011.

[121] A. S. Joshi, I. Dincer, and B. V. Reddy, "Performance analysis of photovoltaic systems: A review," *Renewable and Sustainable Energy Reviews,* vol. 13, no. 8, pp. 1884-1897, 2009.

[122] J. F. Krieder, A. Rabl, and P. S. Curtiss, *Heating and cooling of buildings : design for efficiency*. New York: McGraw-Hill, 1942.

[123] J. V. L. P. W. Li, W. Karaki, C. L. Chan, J. Stephens and J. E. O'Brien "Transient Heat Transfer and Energy Transport in Packed Bed Thermal Storage Systems," in *Developments in Heat Transfer*, M. A. D. S. Bernardes, Ed.: InTech, 2011, pp. 373-416.

[124] A. Al-Alili, M. D. Islam, I. Kubo, Y. Hwang, and R. Radermacher, "Modeling of a solar powered absorption cycle for Abu Dhabi," *Applied Energy,* vol. 93, pp. 160-167, 2012.

[125] N.P. Systems. "Northern Power 100." Internet: http://www.northernpower.com /products/nps100/, 2014 [Jun. 3, 2014].

[126] Y.-D. Kim, K. Thu, H. K. Bhatia, C. S. Bhatia, and K. C. Ng, "Thermal analysis and performance optimization of a solar hot water plant with economic evaluation," *Solar Energy,* vol. 86, no. 5, pp. 1378-1395, 2012.

[127] W. B. S. D. D. M. M. E. a. N. A. R. (MNA). "Exploring the Potential for Electricity Trade and Interconnection among Yemen and GCC countries." Internet: https://open knowledge.worldbank.org/, 2009 [Sept. 13, 2012].

[128] H. Yang, Z. Wei, and L. Chengzhi, "Optimal design and techno-economic analysis of a hybrid solar–wind power generation system," *Applied Energy,* vol. 86, no. 2, pp. 163-169, 2009.

[129] M. J. Montes, A. Abánades, J. M. Martínez-Val, and M. Valdés, "Solar multiple optimization for a solar-only thermal power plant, using oil as heat transfer fluid in the parabolic trough collectors," *Solar Energy,* vol. 83, no. 12, pp. 2165-2176, 2009.

[130] PTLSOLAR. Internet: http://www.ptlsolar.com/ [Jan. 4, 2014]

[131] A. Buonomano, F. Calise, G. Ferruzzi, and L. Vanoli, "A novel renewable polygeneration system for hospital buildings: Design, simulation and thermo-economic optimization," *Applied Thermal Engineering,* vol. 67, no. 1-2, pp. 43-60, 2014.

[132] G. Kosmadakis, D. Manolakos, and G. Papadakis, "Simulation and economic analysis of a CPV/thermal system coupled with an organic Rankine cycle for increased power generation," *Solar Energy,* vol. 85, no. 2, pp. 308-324, 2011.

[133] H. R. Jacobs. "Direct Contact Heat Exchangers." Internet: http://www. thermopedia.com/content/700/, 2013 [Apr.10, 2013]

VITA

Emaduddin Iqbal Akhtar was born on December 20, 1986, in Jeddah, Saudi Arabia. He was brought up in the U.A.E. since, and attended a British curriculum school, where he passed his GCE O-levels with distinction in 7 subjects. He completed his GCE A levels in four subjects before joining the American University of Sharjah in 2005 for his undergraduate studies in Mechanical Engineering. He was awarded and granted a Merit scholarship and financial aid respectively throughout the program, and made it into the Dean's List in 2008. He graduated from A.U.S. in 2009 with a Bachelor of Science in Mechanical Engineering.

Mr. Emaduddin then attended A.U.S. for a Master of Science in Mechanical Engineering and was awarded a full scholarship. He worked in the Mechanical Engineering Department as a Graduate Teaching Assistant for one semester wherein he was assigned the duties of conducting labs. He then left his position in A.U.S. to work with the Abu Dhabi Transmission and Dispatch Company (TRANSCO) in Abu Dhabi, U.A.E. while he continued his studies. During his M.Sc., Mr. Emaduddin has worked on 3 papers which are awaiting review in reputed journals.